SAPIENZA
UNIVERSITÀ DI ROMA

DOTTORATO DI RICERCA IN BIOCHIMICA

CICLO XXVI (A.A. 2010-2013)

Membrane-active derivatives of the frog skin peptide Esculentin-1 against relevant human pathogens

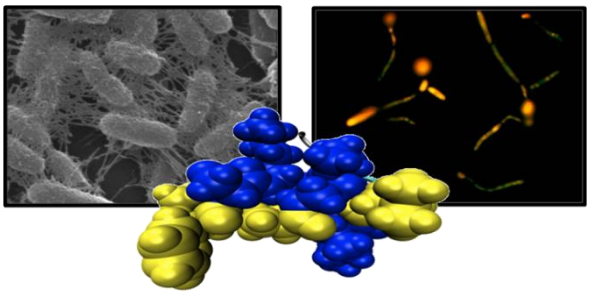

Docente guida

Prof.ssa Maria Luisa MANGONI

Prof.ssa Donatella BARRA

Coordinatore

Prof. Francesco MALATESTA

Dottorando

Vincenzo LUCA

Dicembre 2013

SAPIENZA
UNIVERSITÀ DI ROMA

DOTTORATO DI RICERCA IN BIOCHIMICA

CICLO XXVI (A.A. 2010-2013)

Membrane-active derivatives of the frog skin peptide Esculentin-1 against relevant human pathogens

Dottorando

Vincenzo LUCA

Docente guida

Prof.ssa Maria Luisa MANGONI

Prof.ssa Donatella BARRA

Coordinatore

Prof. Francesco MALATESTA

Dicembre 2013

To my brother

INDEX

List of papers relevant for this thesis

1. **Luca V**, Olivi M, Di Grazia A, Palleschi C, Uccelletti D, Mangoni ML (2013a) **Anti-*Candida* activity of 1-18 fragment of the frog skin peptide esculentin-1b: *in vitro* and *in vivo* studies in a *Caenorhabditis elegans* infection model**. Cell Mol Life Sci. IN PRESS.

2. **Luca V**, Stringaro A, Colone M, Pini A, Mangoni ML (2013b) **Esculentin(1-21), an amphibian skin membrane-active peptide with potent activity on both planktonic and biofilm cells of the bacterial pathogen *Pseudomonas aeruginosa***. Cell Mol Life Sci 70, 2773-2786.

List of other papers

1. Coccia C, Rinaldi AC, **Luca V**, Barra D, Bozzi A, Di Giulio A, Veerman ECI, Mangoni ML (2011) **Membrane interaction and antibacterial properties of two mildly cationic peptide diastereomers, bombinins H2 and H4, isolated from *Bombina* skin**. Eur Biophys J 40:577-88.

2. Grieco P, **Luca V**, Auriemma L, Carotenuto A, Saviello MR, Campiglia P, Barra D, Novellino E, Mangoni ML (2011) **Alanine scanning analysis and structure-function relationships of the frog-skin antimicrobial peptide temporin-1Ta**. J Pept Sci 17:358-65.

3. Grieco P, Carotenuto A, Auriemma L, Saviello MR, Campiglia P, Gomez-Monterrey IM, Marcellini L, **Luca V**, Barra D, Novellino E, Mangoni ML (2012) **The effect of D-amino acid substitution on the selectivity of temporin L towards target cells: identification of a potent anti-*Candida* peptide**. Biochim Biophys Acta 1828:652-60.

4. Falciani C, Lozzi L, Pollini S, **Luca V**, Carnicelli V, Brunetti J, Lelli B, Bindi S, Scali S, Di Giulio A, Rossolini GM, Mangoni ML, Bracci L, Pini A (2012) **Isomerization of an antimicrobial peptide broadens antimicrobial spectrum to Gram-positive bacterial pathogens**. PLos One 7:e46259.

5. Grieco P, Carotenuto A, Auriemma L, Limatola A, Di Maro S, Merlino F, Mangoni ML, **Luca V**, Gatti S, Campiglia P, Gomez-Monterrey I, Novellino E, Catania A (2013) **Novel α-MSH peptide analogues with broad spectrum antimicrobial activity**. PLos One 8:e61614.

1. INTRODUCTION

1.1 Antimicrobial peptides and innate immunity

Antimicrobial peptides (AMPs) are important components of the non-specific innate immunity and form a first line of defense against infection by pathogenic microorganisms. They are widespread in nature, being produced at all levels of the evolutionary scale: in bacteria and fungi, as well as in higher eukaryotes as reported below [Brown and Hancock, 2006].

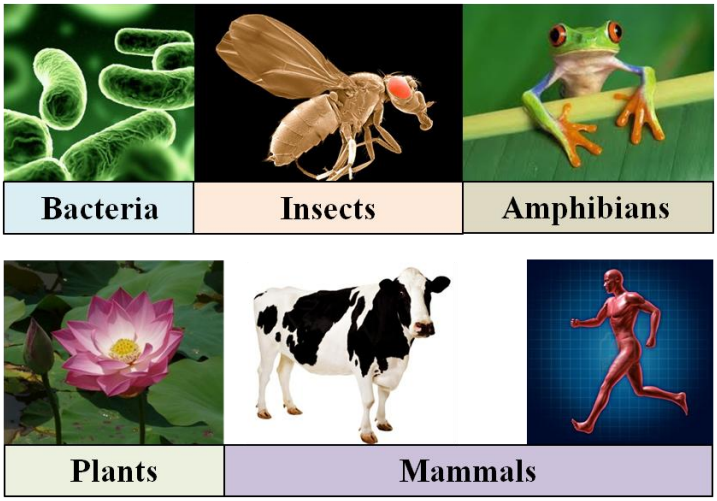

Schematic representation of some living organisms producing AMPs

In animals, AMPs are located at those anatomical sites that easily come into contact with microorganisms, such as the skin and the mucosal or epithelial surfaces of the respiratory, genitourinary and gastrointestinal tracts [Bals, 2000]. They are also mostly found in circulating granulocytic leukocytes.

AMPs are promptly synthesized at low metabolic cost, stored in large amounts into granules for extracellular secretion. Peptide antibiotics differ from the classical antibiotics, which are synthesized by microorganisms and made stepwise, with different enzymes at each step [Boman, 1995]. Indeed, AMPs are encoded by genes and ribosomally synthesized as pre-propeptides. The synthesis of AMPs can be constitutive or inducible by microbial components. However, it depends on the cell type and differentiation state.

In animals, including humans, normal flora of bacteria exists on the skin, in the mouth, in the intestine, in the reproductive organs and in the air ways. It is likely that the control of the natural flora is due to a continuous production of peptide antibiotics.

The main advantage of AMPs as factors of the innate immunity is that they can function without high specificity and memory. The innate immune system can respond in a matter of hours before the adaptive immunity is activated. The time needed to synthesize and process a pre-propeptide with 100-150 residues is certainly shorter than the time required to produce two heavy and two light immunoglobulin chains, the production of which also requires the differentiation of a memory cell to a plasma cell. This is a very important aspect considering the difference in the growth rate between a bacterium (generation time 20-30 min) and a lymphocyte (24-48 hours of doubling time). Thus, a primary bacterial infection can never be eliminated by a clonally-based mechanism, because this response is not fast enough. Even in a secondary microbial infection (when memory cells are present), it would likely take too long time to mobilize antibodies and/or specific effector

cells to curb a bacterial infection without the help of innate immune components [Boman, 1995].

Overstimulation of innate immunity, however, leads to a syndrome termed sepsis. Innate immunity is triggered when bacterial molecules (for example lipopolysaccharide, LPS) interact with host pattern recognition receptors including Toll-like receptors (TLRs). After TLRs binding, effector mechanisms that assist the prevention or resolution of infections are stimulated. Stimulation of innate immunity by natural mechanisms, for example using TLR agonists, creates the risk of inducing or exacerbating potentially harmful pro-inflammatory responses [Hancock and Sahl, 2006].

AMPs are known to play an important role in both innate and adaptive immunity [Zasloff, 2002]. AMPs from higher eukaryotes also act as intracellular signaling molecules and coordinate the innate and adaptive host defense responses, influencing processes like cytokine release, cell proliferation, angiogenesis, wound healing, chemotaxis, control and resolution of the inflammatory response (Fig. 1.1). Some of these properties would be considered pro-inflammatory, but AMPs actually suppress TLR signaling responses, by blocking the LPS-stimulated production of cytokines, like tumor necrosis factor-alpha (TNF-α), and therefore, the emergence of septic shock syndrome in animal models [Hancock and Sahl, 2006]. Note that the LPS-binding properties of many AMPs are believed to play an important role in detoxifying LPS during infection (Rosenfeld et al, 2006b). In addition, some AMPs, like human defensins and LL-37, are chemoattractive peptides for leukocytes. Specifically, they can have a dual role: (i) killing microorganisms, at high concentrations, and (ii) attracting leukocytes to the

site of infection, at low concentrations [Dürr and Peschel, 2002], thus providing a link between the innate and adaptive immunity.

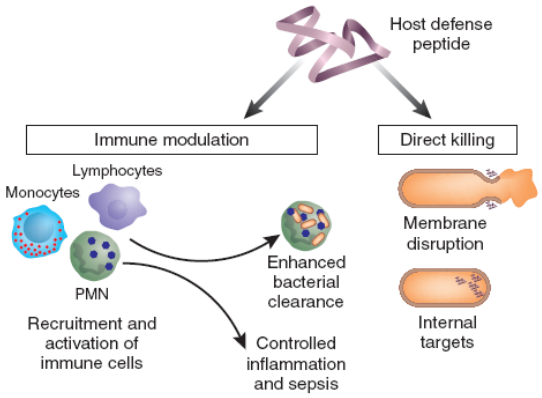

Figure 1.1 Biological roles of host defense peptides. Both direct antimicrobial killing and innate immune modulation occur for the majority. Although certain peptides have one or the other activity, preferentially.

1.2 AMPs: structural features and mechanism of action

AMPs vary significantly in their sequences, suggesting that a specific sequence is not crucial for their biological activity. Despite substantial variations in chain length (8-50 amino acids), sequence and conformation, most AMPs share some important features: i) a net positive charge at neutral pH, due to the presence of basic amino acids; ii) a composition of approximately 30% of hydrophobic residues in their primary structure; iii) a random coil conformation in water solution; iv) the possibility to adopt in a hydrophobic environment an amphipathic structure with a hydrophobic side facing a hydrophilic one. The cationic character of AMPs, which can be reinforced by a C-terminal amidation, as well as the tendency to adopt an

amphipathic conformation are crucial factors for their antimicrobial activity. AMPs have a preferential selectivity for prokaryotic and transformed eukaryotic cell membranes (such as virally infected and tumor cells) that depends on the different lipid composition of bacterial and transformed cell membranes with respect to normal eukaryotic membranes [Nikaido and Vaara, 1985; Utsugi et al, 1991]. In particular, before reaching the target cytoplasmic membrane, which has a high transmembrane potential (-140 mV), peptides must traverse, by electrostatic interactions, the surface of the outer bacterial membranes that are negatively charged because they are composed of LPS, in Gram-negative bacteria [Nikaido and Nakae, 1979] or of teichoic acids-rich peptidoglycan layer, in Gram-positive ones.

After this self-promote uptake in the periplasmic space, a common step for the killing mechanism of cationic AMPs is their electrostatic interaction with the negatively-charged microbial inner membrane that is composed predominantly of phosphatidylethanolamine (PE), phosphatidylglycerol (PG) and cardiolipin (CL). The membrane can be a means for the peptide to reach internal targets or can be lysed (Fig. 1.1), depending on the target, the biophysical peptide's properties and its concentration [Brogden, 2005].

In the first case, AMPs exert their activity selectively against bacteria through an apparently non-membranolytic mode of action. An interaction with the plasma membrane or with a hypothetical transporter/receptor protein allows their translocation into the cytosol. Once inside the cell, the AMP binds to one or more macromolecular target(s) and alters its/their activity affecting various vital cells processes: for example, the arrest of DNA synthesis, the breakage of single-strand DNA, the inhibition of chaperone-

assisted protein folding, the production of hydrogen peroxide, the activation of apoptosis in eukaryotic cells or autolysis in bacterial targets.

In the second case, the electrostatic binding is followed by membrane destabilization (i.e. transmembrane channels formation) [Lehrer et al, 1993; Boman, 1995] with release of metabolites. Some general mechanisms have been proposed to describe the molecular events taking place during the membrane-permeation process.

In the **barrel-stave model** [Ehrenstein and Lecar, 1977], after the initial electrostatic binding to the outer leaflet of the membrane, the peptide adopts an amphipathic alpha-helical structure, self associates on the surface of the membrane and then inserts into the phospholipid bilayer to form transmembrane bundles/channels (Fig. 1.2). In this structure, the hydrophobic peptide region aligns with the lipid core region of the bilayer, while the hydrophilic surface points inward, producing an aqueous pore. A minimum number of peptide molecules (at least 6) is thought to be necessary for the formation of a channel. Because peptides insert into the hydrophobic core of the membrane, their interaction with the target membrane is driven predominantly by hydrophobic interactions.

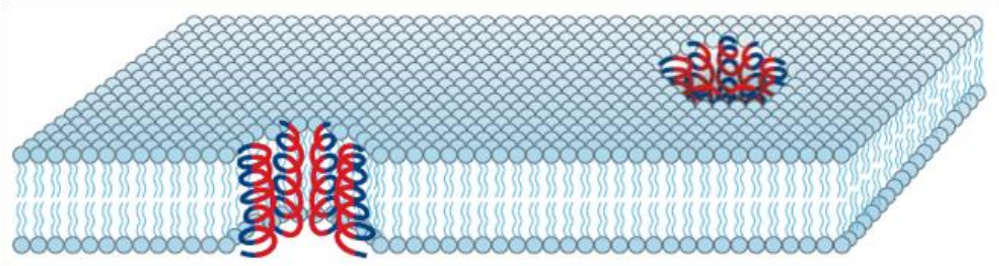

Figure 1.2 Scheme of the barrel-stave model. Hydrophilic regions of the peptide are shown coloured red, hydrophobic regions of the peptide are shown coloured blu [Brogden, 2005].

The **toroidal-pore model** [Ludtke et al, 1996; Matsuzaki et al, 1996] differs from the barrel-stave model in that the peptides are always associated with the phospholipid head-groups, even when they are perpendicularly inserted into the lipid bilayer. This model predicts no peptide aggregation. The polar faces of the peptides associate with the polar head groups of the lipids. The lipids in these openings then tilt from the normal position and connect the two leaflets of the membrane, forming a continuous bend from the top to the bottom in the fashion of a toroidal hole. The pore is lined by both the peptides and the lipid head groups, which are likely to screen and mask cationic peptide charges (Fig. 1.3). In contrast with the barrel-stave model, toroidal pores are short-lived and reversible structures which can leak water-soluble substances.

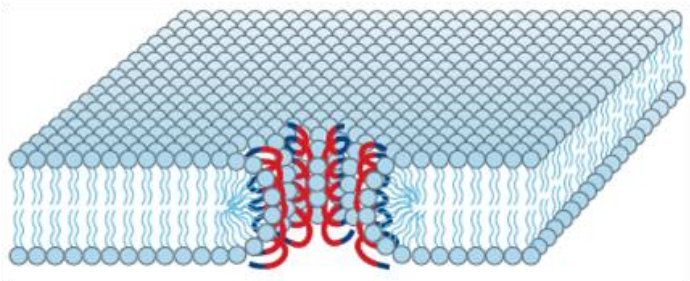

Figure 1.3 Scheme of the toroidal-pore model. Hydrophilic regions of the peptide are shown coloured red, hydrophobic regions of the peptide are shown coloured blu [Brogden, 2005].

The **carpet model** [Shai, 2002] proposes that peptides adsorb to the membrane surface interacting with the anionic phospholipid head groups and cover the membrane in a carpet-like manner (Fig. 1.4). Subsequently, peptides orient their hydrophobic surface towards the membrane and the hydrophilic one towards the solvent. When a threshold concentration of

peptide monomers is reached, they cause membrane permeation and transient pores can be formed. Holes like these may allow the passage of low molecular weight molecules. Higher peptide concentrations can lead to the membrane disintegration in a detergent-like manner eventually leading to the formation of micelles (Fig. 1.4). Contrary to the barrel-stave model, in the carpet-like model, peptide interaction with the target membrane is electrostatically driven and peptide molecules are not inserted into the hydrophobic core of the membrane, neither they do assembly with their hydrophilic surfaces facing each other.

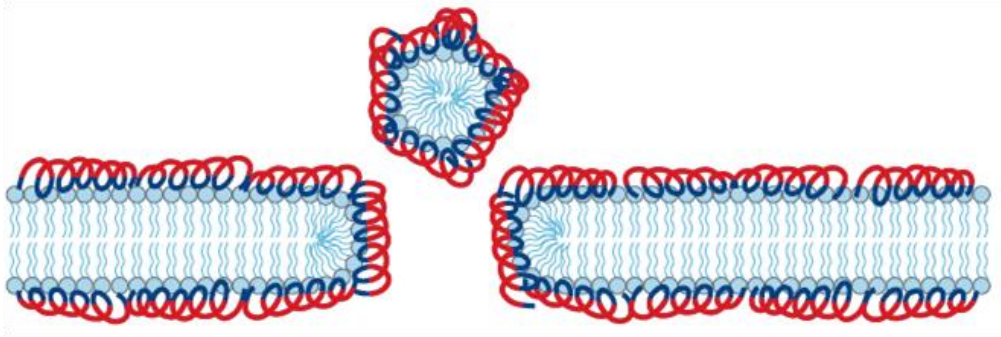

Figure 1.4 Scheme of the carpet-like model. Hydrophilic regions of the peptide are shown coloured red, hydrophobic regions of the peptide are shown coloured blu [Brogden, 2005].

The **sinking raft model** [Pokorny et al, 2002] proposes a side-by-side aggregation of peptides on the membrane, with the peptide helices parallel to the surface, creating a mass imbalance across the lipid bilayer with a consequent increase in local curvature. The peptide aggregate behaves as a "raft" that sinks deeper into the outer leaflet of the membrane (sinking raft) inducing the formation of a transient pore and peptide translocation across the lipid bilayer (Fig. 1.5).

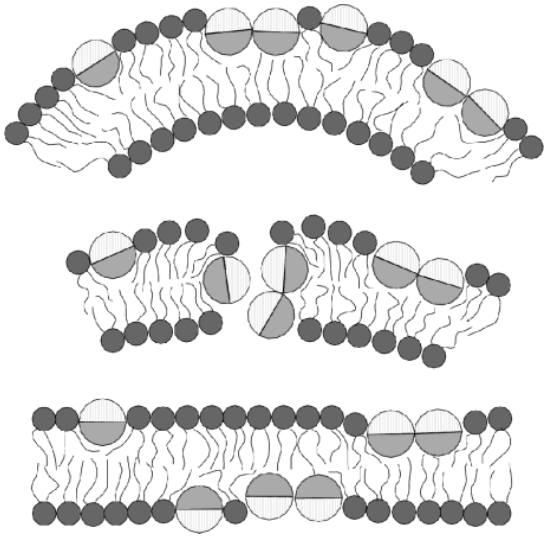

Figure 1.5 Sinking raft model for peptide-induced transient pore formation and peptide translocation across the bilayer. The alpha-helices are shown as cross section, the darker half circles representing the hydrophobic faces and the lighter half circles the polar faces.

The **Shai-Matsuzaki-Huang (SMH) model** proposes a common mechanism which agrees with the various models. In the SMH model, peptides interact first with the outer leaflet of the membrane in a carpet-like fashion (Fig. 1.6 A). Subsequently, they insert into the membrane and thin its outer leaflet generating a displacement of lipids, because of an expansion of the surface area relative to the inner leaflet (Fig. 1.6 B). This leads to an alteration of the membrane structure with "wormhole" formation, as in the toroidal-pore model (Fig. 1.6 C). Transport of lipids and peptides into the inner leaflet (Fig. 1.6 D) and diffusion of peptides inside the cells (Fig. 1.6 E) or a collapse of the membrane (Fig. 1.6 F) can then occur.

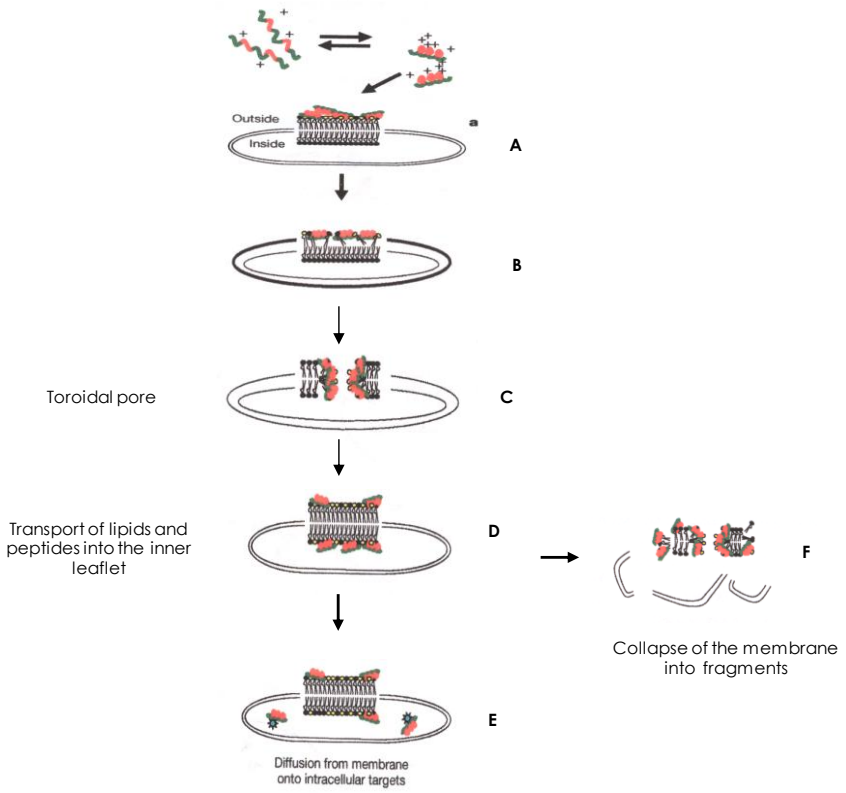

Figure 1.6 The Shai-Matsuzaki-Huang model.

The selectivity of many cationic AMPs toward bacteria is generally attributed to their membranes composition that is organized in such a way that the outermost leaflet of the bilayer is heavily populated by lipids with negatively charged phospholipid headgroups. In contrast, the outer leaflet of the membranes of plants and animals is composed principally of lipids with no net charge (such as phosphatidylcholine and sphingomyelin); most of the lipids with negatively charged headgroups are segregated into the inner

leaflet, facing the cytoplasm. The presence of cholesterol in the target membrane in general reduces the activity of the AMP, due either to stabilization of the lipid bilayer or to interactions between cholesterol and the peptide [Sood and Kinnunen, 2008; Torrent et al, 2011]. Generally, studies on the interaction of AMPs with model phospholipid membranes have revealed a lower affinity to zwitterionic phospholipids compared to acidic phospholipids [Williams et al, 1990; Pouny et al, 1992; Gazit et al, 1994; Strahilevitz et al, 1994; Gazit and Shai, 1995; Oren and Shai, 1996; Latal et al, 1997; Matsuzaki et al, 1999; Oren et al, 1999a; Oren et al, 1999b; Hetru et al, 2000].

1.3 AMPs and resistance

AMPs kill rapidly a broad spectrum of microorganisms, inducing a damage hard to fix rather than acting via a receptor-mediated mechanism. This makes it difficult for the bacteria to develop resistance, which would require a change in membrane composition, a very expensive solution for the majority of microbes [Zasloff, 2002]. Commonly used drugs operate on specific intracellular targets and do not modify the bacterial morphology, making it easy for the microorganisms to become resistant to those drugs [Yeaman and Yount, 2003]. The rate of acquisition of resistance to AMPs by a sensitive microbial strain is several orders of magnitude lower than that needed to conventional antibiotics [Kraus and Peschel, 2006]. However, it has been shown that *in vivo* exposure of bacteria to slowly increasing AMP concentrations, over several hundred generations, can result in reversible physiological adaptation and/or spontaneous, inheritable resistance to the peptide used [Rosenfeld et al, 2006a]. For example, it was recently observed

the existence of variants of *Enterococcus faecalis* that are resistant to different doses of the fungal AMP alamethicin [Mehla and Sood, 2011]. However, it remains unclear how fast such adaptation can occur *in vivo* - where the presence of a cocktail of defense agents will create a selection pressure that differs greatly from that present in an *in vitro* experiment, using just one AMP -, how specific these adaptations might be and what the fitness costs are.

An AMP-resistance strategy used by microorganisms is based on reducing the net anionic charge of the bacterial cell envelope. This decrease reduces the affinity of AMPs for the bacterial membrane, and contributes to bacteria resistance to various cationic antimicrobial molecules [Ernst et al, 2001; Peschel, 2002]. Bacterial cell-envelope contains anionic molecules such as peptidoglycan, teichoic acids, lipid A (the conserved highly hydrophobic and toxic region of LPS) or phospholipids. They are formed by complex biosynthesis processes, and it is unlikely that microorganisms can replace these essential macromolecules with novel structures that would be less favorable for AMP interactions. However, many bacteria can acquire protection against AMPs by reducing the net negative charge of their surface. The teichoic acid polymers found in the cell walls of Gram-positive bacteria have a strong anionic character, due to the phosphate groups in their glycerophosphate repeating units [Neuhaus and Baddiley, 2003]. Many bacteria can partially neutralize this negative charge by modifying teichoic acid with D-alanine residues that bear positively charged amino groups. *Staphylococcus aureus* uses a similar concept to change the net negative charge of the major membrane lipid phosphatidylglycerol into a net positive charge by inserting L-lysine residues [Peschel et al, 2001]. Several Gram-

negative bacteria incorporate positively charged aminoarabinose into lipid A, which contains anionic phosphate groups, thereby reducing its affinity to AMPs [Ernst et al, 2001; Miller et al, 2005]. However, even bacteria which are capable of these modifications can be inactivated by many AMPs at high concentrations, as the neutralization of the cell envelope remains incomplete. The bacterial capacity to reduce the anionic net charge of their surface seems to have certain limits and some AMPs preserve activity against this type of strains [Midorikawa et al, 2003; Weidenmaier et al, 2004]. Several bacterial pathogens have evolved mechanisms to interfere with some specific activity of certain AMPs. This is because they rely on the recognition and extracellular extrusion of AMPs from the bacterial membrane. *S. aureus* produces the exoprotein staphylokinase which, in addition to its fibrinolytic activity, can bind and inactivate alpha-defensins from human neutrophils [Jin et al, 2004]. *Streptococcus pyogens* produces two inhibitors of complement, SIC [Frick et al, 2003], and the cell-wall-anchored M1 proteine [Nizet, 2005] that bind AMPs with high affinity, preventing them from accessing to the bacterial cytoplasmic membrane. In addition, AMPs are substrate for the mtrCDE multiple drug resistance exporter of *Neisseria gonorrhoeae* [Shafer et al, 1998] and *Neisseria meningitides* [Tzeng, 2005]. AMP-capturing and AMP-extruding molecules depend on the direct recognition of certain AMP sequences or structural motifs. Accordingly, the SIC proteins of *S. pyogens* mediate resistance to the human beta-defensins 2 and 3 (hBD2 and hBD3), but not to human beta-defensin 1 (hBD1). Another strategy used by bacteria to inactivate AMPs is to produce peptidases and proteases that degrade these peptides. Therefore, making peptide structures more rigid, for example through the introduction of disulphide bridges, renders AMPs considerably

more resistant to proteolysis. In addition to disulphide bridges, the introduction of proline residues and the C-terminal amidation might render AMPs more resistant to proteases. However, despite the virtues of disulphide bridges and structural stabilization they afford, linear AMPs have not disappeared during the course of evolution. Notably, only a small number of amino acid positions in most AMP sequences are essential for antimicrobial activity, while many other residues can be exchanged without loss of function. In conclusion, it can be assumed that most AMP-resistant mechanisms do not provide complete protection and do result in a reduced susceptibility to AMPs. The simultaneous presence of many variants of AMPs makes it considerably more difficult for microorganisms to develop AMP resistance. Indeed, AMPs have been effective for billions of years [Hancock and Sahl, 2006].

1.4 Amphibian AMPs

Amphibians are a kind of animals forced to survive in various habitat full of pathogenic microbes. Therefore, they are endowed with an excellent chemical defense system composed of peptides with pharmacological and antimicrobial activities. Among the several sources of natural peptide antibiotics, amphibian skin is the richest [Simmaco et al, 1998; Rinaldi, 2002], especially that of frogs of the genus *Rana*, which has a worldwide distribution with approximately 250 different species [Conlon et al, 2004]. Frog skin AMPs are produced by dermal serous glands, which are mainly located in the dorsal region of the animal and are controlled by sympathetic axons. The cytoplasm of the cells is rich in granules, where AMPs are stored, and the lumen is reduced to a small empty cavity. Contraction of myocytes

surrounding the glands, as a reaction to stress or injury, causes a synchronous discharge of their content, in a holocrine mechanism.

1.5 The esculentin family

Each species of ranid frog produces its own specific set of peptides [Conlon et al, 2004]. From skin secretions of *Pelophylax lessonae/ridibundus* (previously classified as *Rana esculenta* [Conlon, 2008]), a large variety of AMPs have been isolated [Simmaco et al, 1993; Simmaco et al, 1994; Ali et al, 2003]. Among them, the esculentin-1 family represents the most potent one, being active against Gram-positive and Gram-negative bacteria as well as fungi (lethal concentration values ranging from 0.1 to 1.5 μM), with negligible effects on eukaryotic cells. All members of this family are 46-amino acid residues long and contain a C-terminal hepta-membered ring stabilized by a disulfide bridge. They have a net charge of +5 at neutral pH and adopt an amphipathic alpha-helical structure in membrane mimetic environments (i.e. 30% trifluoroethanol, TFE). Their sequences are reported below (basic residues in red, acid residues in blue; identical residues marked with an asterisk).

```
         ******  **  ********* ********** ********** ******
Esc-1    GIFSKLGRKK IKNLLISGLK NVGKEVGMDV VRTGIDIAGC KIKGEC
Esc-1a   GIFSKLAGKK IKNLLISGLK NVGKEVGMDV VRTGIDIAGC KIKGEC
Esc-1b   GIFSKLAGKK LKNLLISGLK NVGKEVGMDV VRTGIDIAGC KIKGEC
```

Since a little amount of esculentin-1 can be recovered from frog skin secretions, analogues of this peptide were produced by recombinant expression in *E. coli* of a fusion protein which is sequestered in inclusion

bodies [Ponti et al, 1999]. The peptide was inserted at the N-terminus of the protein GABA transaminase, from which it could be released by cyanogen bromide (CNBr) cleavage. Two esculentin analogues of 47-amino acid residues were produced: the esculentin-C, a cyclic analogue carrying the substitution Met28Leu and an additional Met at position 47, for CNBr cleavage of the recombinant fusion protein; the esculentin-L, a linear esculentin analogue, which had the same structure of esculentin-C but carried also the substitutions Cys40Ser and Cys46Ser. It was demonstrated that the antimicrobial activity of these analogues, tested *in vitro* against a number of bacterial strains, was very similar to that of the natural peptide. This indicates that the presence of a disulfide bridge at the C-terminal region is not essential for antimicrobial and cytolytic properties of the peptide.

Esculentin-1 and its analogues displayed a strong activity *in vitro* against plant pathogens [Ponti et al, 1999]. They shared the N-terminal sequence Gly-Ile-Phe-Ser with a defensin subfamily from spinach [Segura et al, 1998]. These findings reinforced the possibility that esculentin can be properly processed in plants, thus conferring an enhancement of the physiological response to infections. Ponti et al, [2003] reported the transgenic expression of esculentin-C in *Nicotiana tabacum*. The peptide was detected in the intercellular fluid, as secretion product, and then tested against phytopathogens. The results of this study showed the absence of peptide toxicity to the plants and a resistance enhancement of transformed plants toward bacteria (*Pseudomonas syringae* pv *tobaci* and *Pseudomonas aeruginosa ATCC 15692*) and yeast (*Phytophthora nicotianae*) infections [Ponti et al, 2003]. From the HPLC purification of esculentin in the intercellular fluid, a degradation of the C-terminal region was found to occur

and all the shorter peptides (1-35, 1-34, 1-23, 1-22) were found to retain the antimicrobial activity.

Note that the 19-46 fragment, common to all esculentin-1 family molecules, was also isolated from skin secretions: it was devoid of antimicrobial activity, possibly due to its low net positive charge (+1 versus +5 of the whole molecule) at neutral pH [Simmaco et al, 1994]. These data suggested that the antimicrobial properties of esculentin-1 are mainly exerted by its N-terminal region.

1.6 The 1-18 fragment of esculentin-1b, Esc(1-18)

Since no antimicrobial activity was detected for the 19-46 fragment of esculentin-1, it was investigated whether this activity was retained in the N-terminal portion of the molecule. The 1-18 fragment was not found in the HPLC fractionation of the secretion, possibly because of its proteolytic degradation. Therefore, its antimicrobial activity was analyzed in detail on a synthetic peptide (Esc1-18), amidated at the C-terminus to maintain a net charge of +5 at neutral pH and to increase its stability [Mangoni et al, 2003]. Note that the amidation at the carboxyl-end is a very common post-translational modification in linear AMPs from frog skin [Mangoni et al, 2000; Mangoni, 2006; Nicolas and El Amri, 2009].

The biological activity on bacteria (either Gram-positive or Gram-negative strains), yeasts and human erythrocytes of this peptide was compared to that of the full-length recombinant peptide, esculentin-C [Mangoni et al, 2003]. This study showed that the antimicrobial activity of Esc(1-18) was quite similar to that of the esculentin-C (with lethal

concentration values ranging from 0.1 to 1.5 μM) and that the activity of the 18-mer was greater than that of the full-length peptide against the filamentous fungus *P. nicotianae*. Moreover, Esc(1-18) showed a lower hemolytic capacity compared to esculentin-C. Since no activity was found for the 1-15 N-terminal segment of esculentin-1 [Roice et al, 2001], which contains the same number of positive charges as Esc(1-18), we can assume that the three C-terminal amino acids of Esc(1-18) (Ile-Ser-Gly) contribute to either stability of the amphipathic structure and/or hydrophobicity of the molecule. These data indicated that the antibiotic activity of esculentin-C was located in its N-terminal portion, and that the first 18 residues are required to display antimicrobial properties.

1.7 The 1-21 fragment of esculentin-1a, Esc(1-21)

To better investigate the antibacterial activity of the esculentin family, an analogue containing 21 amino acids was synthesized and tested against different *P. aeruginosa* ATCC strains and clinical isolates. This peptide was named esculentin-1a (1-21), Esc(1-21), since it shares the first 20 residues with the natural esculentin-1a. Differently from Esc(1-18), Esc(1-21) carries the substitution Leu-11-Ile and three additional C-terminal residues (Leu-Lys-Gly) which give it a higher net positive charge at neutral pH (+6), a feature that is important for the electrostatic interaction with the negatively-charged membranes of Gram-negative bacteria.

1.8 *Candida albicans* pathogen

Candida albicans is a widespread opportunistic fungal pathogen capable of growing as unicellular budding yeast or as filamentous hyphae, a trait termed fungal dimorphism.

Candida species are normally harmless commensal of the gastro-intestinal and urinary tracts of human beings. However, under some circumstances, e.g., when the immune system is weakened or competing bacterial flora is eliminated following a broad-spectrum antibiotic treatment, *Candida* cells can switch from yeast, more suited for dissemination in the bloodstream [Gow et al, 2002; Saville et al, 2003; Huang et al, 2012], to hyphae responsible for promoting tissue penetration [Kumamoto and Vinces, 2005; Berman, 2006; Sudbery, 2011], during superficial (e.g., oral and vaginitis) and systemic invasive candidoses (Fig. 1.7) [Mayer et al, 2013].

The capability to produce hyphae confer a greater resistance to phagocytosis compared with yeast and the ability to invade epithelial layers. In particular, the hyphal state is essential for adhesion to mucosal surfaces and initiation of clinical infectious diseases [Odds, 1987; Berman and Sudbery, 2002]. *Candida* cells defective in the formation of hyphae (e.g. mutations that block the transition to both forms [Kohler and Fink, 1996; Sharkey et al, 1999]) are both avirulent in animal models [Lo et al, 1997] and more sensitive to macrophage engulfment and growth inhibition [Marcil et al, 2002].

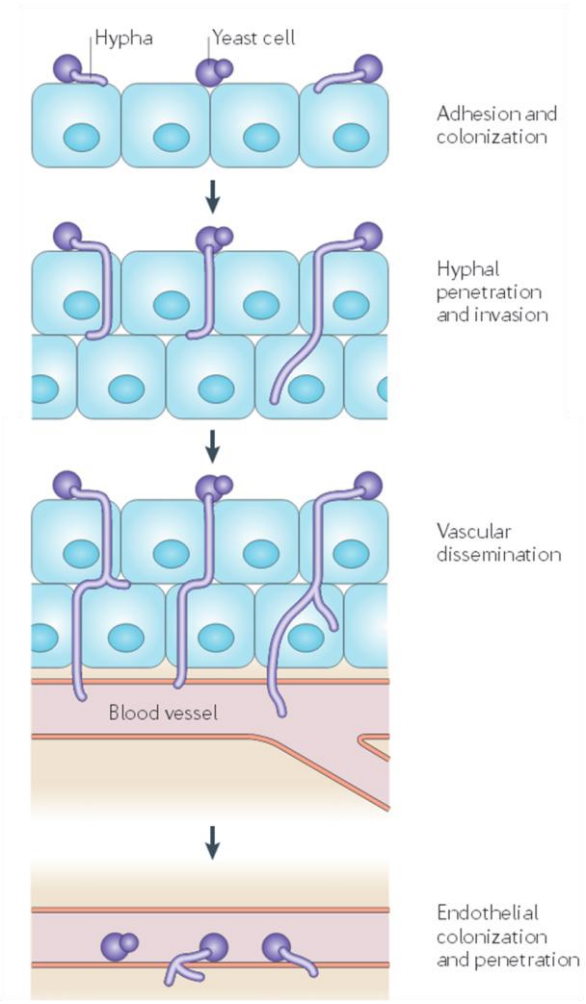

Figure 1.7 Steps in invasion by *Candida albicans* of an epithelial cell surface [Gow et al, 2011].

1.9 *Pseudomonas aeruginosa* pathogen

Pseudomonas aeruginosa is an opportunistic bacterial pathogen capable of causing life-threatening infections, including ocular keratitis, burn wound infections, and lung infections in cystic fibrosis (CF) patients [Hassett et al, 2002; Bjarnsholt et al, 2009; Brugha and Davies, 2011; Bjarnsholt, 2013]. A major reason for its prominence as a pathogen is its high intrinsic resistance to antibiotics due in part to many elaborate virulence factors and the formation of biofilm matrices. Biofilms are sessile communities of bacteria [Costerton et al, 1999; Fux et al, 2005; Hoiby et al, 2011] that are very difficult to eradicate (Fig. 1.8).

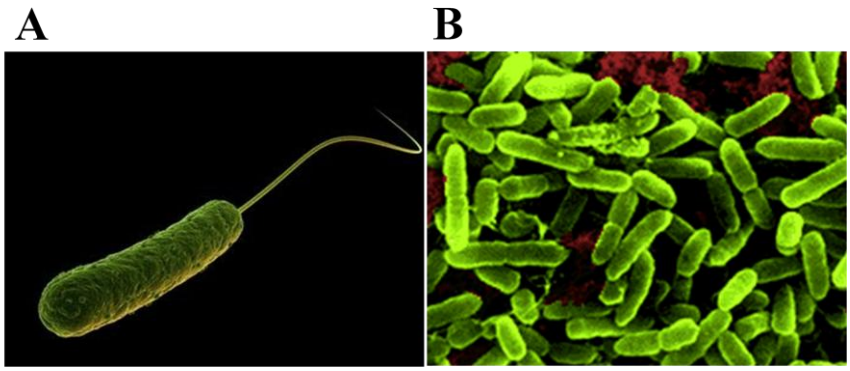

Figure 1.8 *Pseudomonas aeruginosa* bacterium. (A) Planktonic form. (B) Biofilm form.

The formation of *Pseudomonas* biofilms is very common in the lungs of cystic fibrosis patients with chronic infections. The colonization of the respiratory tract by this pathogen usually starts with the tissue adhesion of non-mucoid and motile strains. Subsequently, motility is repressed and bacteria frequently evolve a mucoid phenotype forming thicker biofilms.

Bacterial biofilms are a structured consortium of embedded cells into a self-promoted polymeric matrix consisting of anionic polysaccharides (mainly alginate), proteins, and extracellular DNA [Moreau-Marquis et al, 2008; Flemming and Wingender, 2010]. These confer bacterial population protection from antibiotics, chemicals, as well as opsonization and phagocytosis by host immune cells [Kuchma and O'Toole, 2000; Stephens, 2002; Mah et al, 2003].

1.10 *Caenorhabditis elegans*: a simple infection model

C. elegans is a convenient infection model for its simple, transparent body, invariant cell lineage, small size (1 mm in length), and rapid generation cycle [Brenner, 1974]. The two sexes of *C. elegans* are males (XO) and self-fertilizing hermaphrodites (XX) producing both sperm and eggs.

The *C. elegans* tissues that are in regular contact with microbes are the hypodermis and the intestine. The hypodermis is a single layer epithelium that surrounds the animal and is a multinucleate syncytium that secretes collagen to form a tough outer cuticle [Chisholm and Hardin, 2005]. *C. elegans* feeds on microbes that are ingested by the pharynx, which helps degrade food sources before they reach the intestine. The intestine is comprised of 20 epithelial cells that are mostly in pairs of cells that form a tube that runs the length of the animal [McGhee, 2007]. The intestinal cells share many morphological similarities with human intestinal epithelial cells, including actin-rich microvilli on the apical side of cells that absorb nutrients from the lumen (Fig. 1.9).

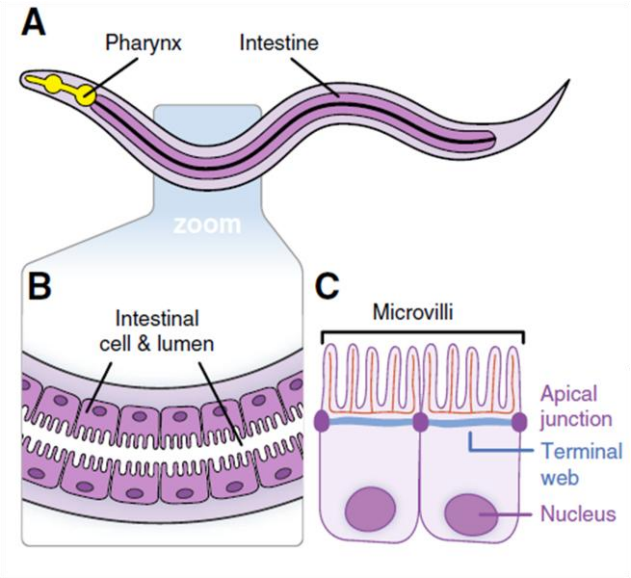

Figure 1.9 Features of the *C. elegans* intestine. (A) Simplified body plan of *C. elegans*. (B-C) Close-up of the intestinal cells [Balla and Troemel, 2013].

Feeding-based infections of *C. elegans* are relatively straight forward to perform, which aids studies of intestinal infections in this host. The primary food source in a laboratory setting is the *E. coli* strain *OP50*, but other bacteria and fungi also support growth and reproduction [Brenner, 1974; Mylonakis et al, 2002]. In our experiments, a feeding-based infection model has been developed, which involves simply substituting a microbial pathogen in place of the normal food source of *E. coli*. Interestingly, many virulence factors used by yeasts and bacteria to kill *C. elegans* play important roles in inducing pathogenesis in mammals, as well [Sifri et al, 2003; Mylonakis and Aballay, 2005; Sifri et al, 2005]. The lifespan of *C. elegans* on *E. coli* is only about 2 weeks, which makes it easy to assess whether pathogens cause a

shortening of lifespan. Because *C. elegans* nematodes are transparent, these infections provide the opportunity to visualize both intestinal and microbial cells *in vivo* during the course of infection.

C. elegans does not appear to have adaptive immune system, such as phagocytes [Irazoqui et al, 2010]. It responds to bacterial and fungal pathogens by a vast repertoire of genes that could provide defense. Indeed, about 17% of the genes in the *C. elegans* genome are predicted to encode secreted proteins, and a third of those are upregulated by exposure to pathogens [Suh and Hutter, 2012]. These factors are part of expanded gene families and include some proteins conserved with mammals, e.g. the secreted C-type lectins endowed with antimicrobial activity. Furthermore, *C. elegans* produces its own AMPs, such as nlps or neuropeptide-like proteins and caenacins.

2. AIM OF THE STUDY

The aim of this work was to evaluate the antimicrobial activity and the mechanism of action of two N-terminal derivatives of esculentin-1 peptide: Esc(1-18) and Esc(1-21) with the purpose to develop them as new anti-infective agents. The first one was assayed against the yeast and hyphal forms of the human pathogen *C. albicans* under both *in vitro* and *in vivo* conditions using a *C. elegans* infection model. The second one was utilized against the planktonic and biofilm forms of another relevant human pathogen, such as *P. aeruginosa*.

3. MATERIALS AND METHODS

3.1 Materials

Synthetic all-L and all-D Esc(1-18), the rhodamine-labelled form of the all-L peptide [rho-Esc(1-18)] and Esc(1-21) were purchased from Selleck Chemicals (Houston, TX, USA). The purity of the peptides, their sequences and concentrations were determined as described in [Mangoni et al, 2003]. Sytox Green was from molecular probes (Invitrogen, Carlsbad, CA, U.S.A.); 3-(4,5-dimethylthiazol-2-yl)-2,5-diphenyltetrazolium bromide (MTT), poly-L-lysine (150,000-300,000 mol wt), 2',7'-dichlorofluorescein diacetate (DCFHDA), crystal violet (CV) and 2-nitrophenyl β-D-galactoside (ONPG) were all purchased from Sigma (St. Louis, MO, U.S.A.). All other chemicals were reagent-grade.

3.2 Microorganisms and nematode strains

The following *C. albicans* strains were used: the reference ATCC 10231, ATCC 90028 and the clinical isolates *C. albicans* n. 1s and *C. albicans* n. 1r. The wild-type *C. elegans* strain N2 was used in all experiments and propagate on nematode grow medium (NGM) plates containing *E. coli* OP50 as a food fource [Stiernagel, 2006]. *C. albicans* ATCC 10231 was used for all the experiments with *C. elegans*.

The strains of *P. aeruginosa* used for the antimicrobial assays were: the standard non-mucoid ATCC 27853 [Li J. Turnidge et al, 2001] and PAO1, the clinical multidrug resistant (MDR) isolates MDR1, MDR2, and MDR3 and the following strains from Cystic Fibrosis (CF) patients: the mucoid

AA11 and non-mucoid TR1 isolated at the onset of chronic lung colonization; both mucoid AA43 and TR67 isolated after years of chronic colonization, according to what was reported in [Bragonzi et al, 2005; Bragonzi et al, 2009]. These CF strains were chosen from the strains collection of the CF clinic Medizinische Hochschule of Hannover, Germany [Bragonzi et al, 2009]. Mode of action studies and β-galactosidase activity measurements were carried out with *P. aeruginosa* PAO1 carrying plasmid pPrsal190 [Rampioni et al, 2007], kindly provided by Prof. Livia Leoni (Roma Tre University, Rome, Italy).

3.3 Circular dichroism (CD) analysis

CD experiments were performed using a JASCO J-600 spectropolarimeter with a 1 mm path length cell. The CD spectra of the peptides were recorded at 25°C at 0.2 nm wavelength intervals in the 195-250 nm range. CD spectra were collected for Esc(1-18) at a concentration of 100 μM in water and in different mixtures with increasing the TFE/water volume ratio. Esc(1-21) was used at a concentration of 5 μM in 10 mM sodium phosphate buffer pH 7.4 (NaPB) or in a suspension of lipid vesicles composed of phosphatidylethanolamine (PE)/phosphatidylglycerol (PG) (7:3, w:w) to mimic the Gram-negative cell membranes. CD data from eight scans were averaged.

3.4 Hemolytic activity

The hemolytic peptide activity was determined using fresh human erythrocytes. The blood was centrifuged and the erythrocytes were washed three times with 0.9% NaCl. Peptide solutions were incubated with the

erythrocyte suspension ($1x10^7$ cells/ml) at 37°C for 2 h. Then, the extent of hemolysis was measured on the supernatant, from the optical density at 540 nm. Hypotonically lysed erythrocytes were used as a standard for 100% hemolysis.

3.5 Determination of the minimal peptide concentration inhibiting the growth of free-living microorganisms

(i) Yeasts: susceptibility testing was performed by the microbroth dilution method according to the procedures outlined by the National committee for Clinical Laboratory Standards (2001) using sterile 96-well plates. Serial 2-fold dilutions of Esc(1-18) in 50 μl of Wing broth (WB) were prepared through the wells of a microtiter plate. Afterwards, aliquots (50μl) of yeast cells grown to the mid-log phase at 28°C, at a concentration of $7x10^4$ colony forming units (CFU)/ml in WB, were added to each well. The range of peptide concentration used was 0.5-32 μM. Minimal inhibitory concentration (MIC) was determined as the lowest peptide concentration at which 100% inhibition of growth was observed after 16-18 h at 37°C.

(ii) Bacteria: Aliquots (50 μl) of bacteria at a concentration of $2x10^6$ (CFU)/ml in Mueller Hinton broth (MH) were added to 50 μl of MH containing the peptide in serial two-fold dilutions. The MIC was determined as above-mentioned.

(iii) To evaluate the potential peptide-induced resistance, multiple exposures of the bacterial suspension to serial two-fold dilutions of the peptide or a conventional antibiotic (ciprofloxacin) were performed using a diluted inoculum (1:10.000), from the bacterial culture grown at ½ MIC. After 15

MIC cycles (total duration 30 days), the drug/peptide was removed and bacteria were grown for two passages in antibiotic-free medium (20 h each). Afterwards, the MIC assay was carried out as described above.

3.6 Anti-biofilm activity

Biofilm formation was performed by adapting the procedure described in [Ceri et al, 2001; Falciani et al, 2012] using the Calgary Biofilm Device (Innovotech, Innovotech Inc. Edmonton, Canada). Briefly, 96-well plates, each well containing 150 µl of the bacterial inoculum ($1x10^7$ cells/ml) in Luria-Bertani (LB) medium, were sealed with 96 pegs-lids on which biofilm cells can build up. Afterwards, the plates were placed in a humidified orbital incubator at 35°C for 20 h under agitation at 125 rpm. Once the biofilms were allowed to form, the pegs were rinsed twice with phosphate buffered saline (PBS) to remove planktonic cells. Each peg-lid was then transferred to a "challenge 96-well microtiter plate", each well containing 200 µl of a twofold serial dilution of Esc(1-21) in PBS. The "challenge plate" was incubated at 37°C for 2 h. Peptide activity on preformed biofilm was evaluated by three independent methods:

(i) Visual observation of bacterial growth. The peg-lid was removed from the "challenge plate", rinsed with PBS, and used to cover a 96-well "recovery microtiter plate", each well containing 200 µl LB. The "recovery plate" was sealed, incubated at 37°C for 4 h, and then observed for detection of any visible growth of bacteria detached from the peptide-treated biofilm. Growth of bacteria in a particular well indicates re-growth of planktonic cells from surviving biofilm. Minimum biofilm eradication concentration

(MBEC) was defined as the minimum peptide concentration preventing re-growth of bacteria from the treated biofilm, within 4 h.

(ii) Numbering of living bacterial cells after peptide treatment. To determine viable cell counts after peptide treatment, pegs were broken from the lid and each peg was transferred into an Eppendorf tube containing 500 µl of PBS. After sonication to remove bacterial cells from the peg, aliquots of bacterial suspension were plated on LB-agar plates for counting. CFU were expressed as a percentage with respect to the control (peptide-untreated biofilms). The minimum bactericidal concentration (MBCb) was definied as the lowest peptide concentration required to reduce the number of viable biofilm cells of ≥ 3 $\log_{10}$ (99.9 % killing) after 2 h [Harrison et al, 2010]. Viable biofilm cells were also determined by the reduction of MTT to its insoluble formazan (Fig. 3.1) MTT is a tetrazolium salt which is reduced to an insoluble formazan product, by mitochondrial reductases, giving a purple color. The intensity of the color is directly proportional to the number of viable cells.

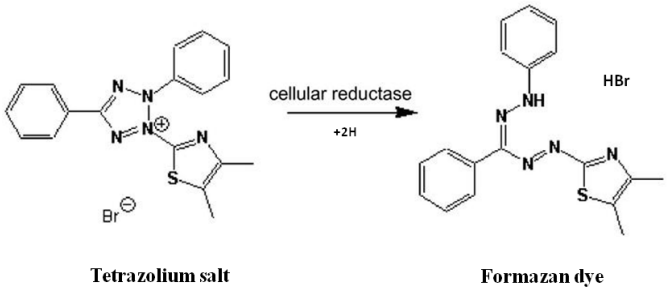

Figure 3.1 Reduction of the yellow tetrazole to purple insoluble formazan, by metabolically active cells.

Briefly, after peptide treatment, the peg lid was washed with PBS and used to close another 96-well microtiter plate, each well containing 200 µl of 0.5 mg/ml MTT in PBS. The plate was incubated at 37°C for 4 h. Afterwards,

50 μl of 25% sodium dodecyl sulphate (SDS) were added to each well to dissolve formazan crystals. Bacterial viability was determined by absorbance measurements at 595 nm [Mangoni et al, 2005] and calculated with respect to control cells (bacteria not treated with the peptide).

(iii) Evaluation of biomass. To determine the biofilm biomass, peptide-treated pegs were washed in PBS, fixed in 99% methanol for 15 min at room temperature, and air-dried. Then, by using a 96-well microtiter plate, pegs were stained with 200 μl of a CV solution (0.05 % in water). After 20 min, the excess CV was removed by washing the pegs with water. Finally, bound CV was released from pegs by adding 200 μl of 33 % acetic acid. The absorbance was measured at 600 nm.

3.7 Time-killing of free-living microorganisms (yeasts and bacteria)

(i)Yeasts: The peptide's effect on the viability of yeast cells was determined by the MTT colorimetric method. Briefly, about $1x10^6$ CFU of *C. albicans* ATCC 10231 in 100 μl of 10 mM sodium phosphate buffer (NaPB), pH 7.4, were incubated at 37°C with Esc(1-18) at different concentrations. At different time intervals, samples were centrifuged for 5 min (1,4 x g) and resuspended in 100 μl RPMI 1640 medium (Sigma) supplemented with 0.5 mg/ml MTT. After 2 h incubation at 37°C, formazan crystals were solubilized by adding 100 μl of 10 % SDS. The absorbance at 590 nm of triplicate samples was measured spectrophotometrically with a microplate reader (Infinite M200; Tecan, Salzburg, Austria). Cell viability was expressed as percentage of survival with respect to the control (yeast cells not treated with the peptide).

(ii) Bacteria: about $1x10^5$ or $1x10^6$ CFU in 100 µl PBS (as indicated in the Results section) were incubated at 37°C with Esc(1-21) at 0.5 or 1 µM. Aliquots of 10 µl were withdrawn at different intervals, diluted in MH, and spread onto LB-agar plates. After overnight incubation at 37°C, the number of CFU was counted. Controls were run without peptide and in the presence of peptide solvent (water). Bactericidal activity was defined as the peptide concentration necessary to cause a reduction in the number of viable bacteria of $\geq \log_{10}$ CFU/ml.

3.8 Peptide's effect on the viability of hyphae

RPMI supplemented with 2 mM L-glutamine and 0.165 M morpholinepropanesulfonic acid (pH 7.0) was used as the hyphal growth-promoting (HP) medium for *C. albicans* [Hawser et al, 1996; Cleary et al, 2011]. Yeast-form cells of *C. albicans* ATCC 10231 were collected from fresh cultures on Sabouraud agar plates and suspended in HP medium at $3x10^5$ or $1x10^5$ cells/ml. Each well of a 96-well flat-bottom poly-L-lysine-coated microplate received 100 µl of *Candida* suspension. The plate was incubated at 37°C for 3 h (Fig. 3.2) or a longer time (12 h and 18 h), respectively.

Figure 3.2 Phase-contrast image of *C. albicans* ATCC 10231 hyphae. Hyphae were obtained after 3 h growth of $3x10^4$ yeast cells in 100 µl HP medium at 37°C. Scale bar is 10 µm long.

The medium in the wells was then discarded and the adhesive *Candida* hyphae were treated with different concentrations of Esc(1-18) (100 µl in NaPB) at different time intervals at 37°C. The peptide's effect on hyphae

viability was determined by the MTT method [Islas-Rodriguez et al, 2009]. Briefly, peptide-containing NaPB was removed; 100 µl of MTT solution (0.5 mg/ml in HP medium) were added and the plate was incubated at 37°C for 4 h. Afterwards, formazan crystals were solubilized by adding 100 µl of 10% SDS. The absorbance at 590 nm of triplicate samples was measured. The minimal fungicidal concentrations (MFC_{50} and MFC_{90}) were defined as the minimal peptide concentrations causing a reduction in hyphae viability by 50% and 90%, respectively, within 60 min, compared with the control (cells not treated with the peptide).

3.9 Inhibition of hyphal development

The peptide's ability to inhibit hyphal development from yeast budding cells was evaluated on *C. albicans* ATCC 10231. Briefly, $1x10^5$ yeast cells in WB were transferred into poly-L-lysine-coated wells of a 96-well plate and incubated at 37°C for 3 h in the presence of different concentrations of Esc(1-18). The inhibition of hyphal development was visualized microscopically under an inverted microscope (Olympus CKX41) at x 40 magnification and photographed with a Color View II digital camera.

3.10 Membrane permeabilization of *C. albicans* and *P. aeruginosa*

(i) Sytox Green assay

a. To asses the ability of Esc(1-18) to alter the membrane permeability of yeast cells of *C. albicans* ATCC 10231, $1x10^6$ CFU in 95 ul of NaPB supplemented with 1 µM Sytox Green were loaded into the wells of a 96-microtiter plate. After 20 min in the dark, 5 ul of peptide were added [Marcellini et al, 2009]. The increase in fluorescence, owing to the binding

of the dye to intracellular DNA, was measured every 10 min at 37°C in the microplate reader (excitation and wavelengths were 485 and 535 nm, respectively). Controls were cells without peptide.

b. In the case of 3 h-grown hyphae, HP medium was removed from each well and replaced by 95 µl of NaPB supplemented with 1 µM Sytox Green, as above. Also in this case, controls were given by hyphae without peptide.
c. To assess the ability of Esc(1-21) to alter the bacterial membrane permeability of planktonic cells of *Pseudomonas*, $1x10^6$ cells in 100 µl of PBS were mixed with 1 µM Sytox Green for 5 min in the dark. After adding the peptide, the increase in fluorescence was measured every 5 min as described above. Controls were cells without peptide, whereas the maximal membrane perturbation was obtained after treating bacteria with the highest peptide concentration used (32 µM) followed by the addition of 1 mM ethylenediaminetetraacetic acid (EDTA) + 0,5% Triton X-100 (final concentration) to completely destabilize the lipopolysaccharide-outer membrane and solubilize the phospholipid bilayer of the cytoplasmic membrane [Uccelletti et al, 2010]. Note that the addition of EDTA + Triton X-100 to the bacteria with the highest peptide concentration did not induce any change in the fluorescence intensity, thus excluding any possible interference between the peptide and the detergent used.
d. In the case of 20-h preformed biofilm, after 2-h peptide treatment in the "challenge microtiter plate" (each well containing 200 µl of a twofold serial dilution of Esc(1-21) in PBS supplemented with 1 µM Sytox Green), pegs were broken from the lid and each peg was transferred into an Eppendorf tube together with the corresponding 200 µl from the "challenge well". After sonication to detach bacterial cells from the peg,

the cell suspension of each sample (200 µl volume) was transferred into wells of another microtiter plate for fluorescence measurement as described above. Also in this case, controls were given by cells without peptide, whereas the maximal membrane perturbation was obtained after treating biofilm cells with the highest peptide concentration (48 µM), followed by the addition of 1 mM EDTA + 0.5% Triton X-100 to dissolve the extracellular matrix [Baillie and Douglas, 2000] and make the bacterial membranes fully permeable [Uccelletti et al, 2010].

(ii) β-galactosidase assay.

The ability of Esc(1-21) to cause more pronounced damage to the cytoplasmic membrane of *Pseudomonas* was determined by measuring the extracellular release of β-galactosidase, using ONPG as a substrate [Marcellini et al, 2009]. For the planktonic form, *P. aeruginosa* PAO1 that constitutively expresses the β-galactosidase (see 3.2 section) was grown at 37°C in LB to an $OD_{590\ nm}$ of approximately 0.8, washed twice, centrifuged for 10 min (1,4 x g) and resuspended in PBS at the same OD. About $1x10^6$ cells (in 100 µl PBS) were incubated with different concentrations of Esc(1-21) for 30 min at 37°C. Controls were bacteria without peptide, whereas the maximal membrane perturbation was obtained as described for the Sytox Green assay on planktonic cells (see 3.10 (i)c section). At the end of the incubation time, 2-µl aliquots were withdrawn, diluted 1:100 in LB, and spread on LB plates for counting. Afterwards, 450 µl of PBS was added to the remaining bacterial suspension, which was passed through a 0.2-µm filter. The hydrolysis of 2 mM ONPG, added to the culture filtrate, was recorded at 420 nm (Fig. 3.3) using a spectrophotometer (UV-1700 Pharma Spec Shimadzu).

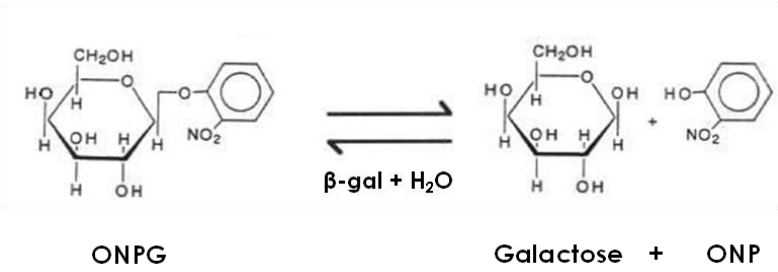

Figure 3.3 β-galactosidase hydrolysis of the colourless ONPG to produce galactose and the yellow o-nitrophenol, which absorbs light at 420 nm.

In the case of preformed biofilm, pegs were broken from the lid of the "challenge plate", transferred into Eppendorf tubes together with the corresponding 200 µl from the wells of the "challenge plate", and then sonicated. Then, 2-µl aliquots of the cell suspension were withdrawn and diluted as described above, for counting. One ml of PBS was added to the sonicated cell suspension, which was filtered; hydrolysis of 2 mM ONPG was followed as described above. Controls and maximal membrane perturbation were obtained as for the Sytox Green assay on biofilm cells (see 3.10 (i)d section).

3.11 Scanning electron microscopy (SEM) on planktonic and biofilm cells

Approximately $1x10^6$ bacterial cells in PBS were treated with the peptide at different concentrations for 30 min at 37°C and then fixed with 2.5% glutaraldehyde in 0.2 M cacodylate buffer (pH 7.2). The samples were deposited on glass coverslips of 12-mm diameter. Afterwards, they were washed three times in cacodylate buffer, post-fixed with 1% (w/v) osmium tetroxide for 1 h, and dehydrated using a graded ethanol series (70; 85; 95%). After the passage in 100% ethanol, the samples were air-dried (overnight)

and gold coated by sputtering (SCD 040 Balzers device, Bal-Tec). The samples were examined with a scanning electron microscope (SEM) (FEI Quanta Inspect FEG, USA).

To visualize biofilm-colonized pegs, after 20 h of biofilm formation by *P. aeruginosa* on Calgary microtiter plates, pegs were broken from the lid, washed with PBS and fixed with 2.5% glutaraldehyde in 0.2 M cacodylate buffer. Pegs were placed in this solution at 4°C for 16 h. Following this fixing step, the pegs were washed in 0.2 M cacodylate buffer for approximately 10 min. Then, they were post-fixed, dehydrated, and gold coated as described above. The pegs were examined under the same scanning electron microscope and those portions containing bacterial cells were photographed.

3.12 Measurement of reactive oxygen species (ROS) in *C. albicans*

The formation of endogenous ROS in *C. albicans* yeast and hyphal forms was measured by a fluorometric assay with DCFH-DA according to [Bland et al, 2001; François et al, 2006].

After diffusion into the cell, DCFH-DA is deacetylated by cellular esterases to a non-fluorescent compound, 2', 7'-dichlorodihydrofluorescein (DCFH) which is rapidly oxidized by ROS to the highly fluorescent 2', 7'-dichlorofluorescein (DCF) (Fig. 3.4). The fluorescence intensity is proportional to the ROS levels within the cell cytosol.

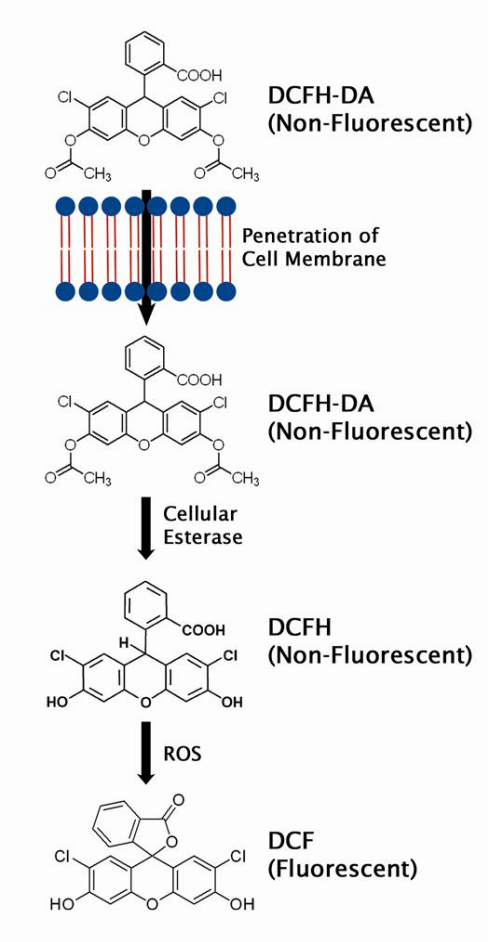

Figure 3.4 Detection of ROS production using DCFH-DA. DCFH-DA enters the cells and is cleaved by intracellular esterases to DCFH and oxidized by ROS to the highly fluorescent molecule DCF.

Briefly, yeast culture in Sabouraud was centrifuged and resuspended in NaPB containing 20 μM DCFH-DA. After 30 min incubation at 37°C in the darkness, the cell culture was centrifuged, washed once with NaPB to remove DCFH-DA and then resuspended in NaPB. About $1x10^6$ cells in 95 μl were transferred into wells of a microtiter plate and mixed with 5 μl of peptide at

different concentrations or water (in control samples) and incubated at 37°C. In the case of hyphal cells, after their formation on poly-L-lysine-coated wells (as described above), 20 μM DCFH-DA in NaPB was added (100 μl volume). After 30 min incubation at 37°C, the probe was removed and the cells were washed with NaPB. Then, 100 μl of peptide solution in NaPB at different concentrations or NaPB without peptide (in control samples) were added to each well. Fluorescence emitted by the cells was measured with the microplate reader (excitation and emission wavelengths were 485 and 535 nm, respectively) after 10, 20, 30, 60, 120 and 180 min of incubation. As a positive control for ROS production, both yeast and hyphal cells were treated with 2 mM H_2O_2 [Phillips et al, 2003] and the results were read after 30, 60, 120 and 180 min incubation time.

3.13 Apoptosis assay on *C. albicans*

Apoptosis in *Candida* cells was assessed by using the HT TiterTACS kit (Trevigen, Gaithersburg, MD) which allows quantitative colorimetric analysis in both adherent and suspension cell cultures. This assay is based on the incorporation of biotinylated nucleotides by the terminal deoxynucleotidyl transferase at the 3' OH end of the DNA fragments that are formed during apoptosis. The biotinylated nucleotides were detected by using a streptavidin-horseradish peroxidase with a specific colorimetric substrate. TACS-Nuclease was used to generate DNA breaks in every cell, providing an appropriate positive control. Briefly, both yeast and hyphal cells were treated or not with 16 μM of Esc(1-18) in NaPB for 20 and 60 min. Afterwards, cells were washed twice in PBS and fixed in 3.7% formaldehyde, post-fixed in methanol and stored at +4°C until required. Cell permeabilization and

TUNEL (terminal dUTP Nicked End Labelling) reaction were carried out according to the kit's manufactures.

3.14 Staining protocols: fluorescent probes for microscopic assessment of peptide's distribution and fungal membrane integrity

To visualize, in a single preparation, the distribution of Esc(1-18) and to detect, at the same time, the membrane permeabilization induced by the peptide on both yeast and hyphal forms of *Candida*, we used rho-Esc(1-18) and the two following fluorochromes: (i) the double-stranded DNA-binding dye DAPI, to stain the nuclei of all cells and (ii) the green fluorescent probe Sytox Green, which is unable to traverse the cytoplasmic membrane of intact cells. After exposure of yeast cells ($1x10^6$ CFU in NaPB) to 16 μM rho-Esc(1-18) (100 μl as a final volume in a 1.5 ml eppendorf tube) for 30 min at 37°C, the microbial culture was centrifuged, washed three times with NaPB and incubated with 100 μl of 1 μM Sytox Green (in NaPB) for 15 min at room temperature. The sample was centrifuged as described above and washed three times with NaPB. Afterwards, 100 μl of DAPI solution (10 μg/ml in NaPB) were added [Mangoni et al, 2004]. After 15 min at room temperature, the sample was centrifuged to remove DAPI solution, and washed three times. The pellet was resuspended in a drop of NaPB and poured onto a glass slide which was further covered with a round cover glass. The slide was then examined by phase-contrast and fluorescence microscopy. Both phase-contrast and fluorescence images were recorded using the Olympus optical microscope equipped with an oil-immersion objective (x100).

In the case of hyphae, 96-well glass bottom microplates (MGB096-1-2-LG-L, Matrical Bioscience Spokane WA, USA) were used and coated with poly-L-lysine. More precisely, $3x10^4$ yeast cells in HP medium were added to each single well and the plate was incubated at 37°C for 3 h to permit hyphal development. Incubation with 16 μM of rho-Esc(1-18) (100 μl final volume in NaPB) was carried out for 30 min at 37°C. The peptide solution was then removed and the wells were washed three times with NaPB. Afterwards, Sytox Green solution in NaPB was added to single wells (100 μl final volume). After 15 min at room temperature, Sytox Green was removed, and each well was washed three times before adding 100 μl of DAPI solution. After 15 min at room temperature and appropriate washings, 50 μl of NaPB were added to each well before observation under the inverted microscope at x 100 magnification. In all cases, controls were run in the absence of peptide.

3.15 *C. elegans* infection

Freshly grown *Candida* cells were picked from a single colony and inoculated into 2 ml of yeast extract-peptone-dextrose (YPD) broth. Cells were grown overnight with agitation at 28°C. Fungal lawns used for *C. elegans* infection assays were prepared by spreading 100 μl of the overnight culture of *C. albicans* (diluted 1:100 in distilled water) on brain heart infusion (BHI) agar plates. The plates were then incubated for approximately 20 h at 28°C before being seeded with adult hermaphrodite nematodes from a synchronized culture grown at 16°C [Stiernagel, 2006]. About 100-200 worms were washed with M9 buffer [Stiernagel, 2006] and placed in the middle of *C. albicans* lawns. The infection was performed at 25°C for 20 minutes.

3.16 Worm survival assay

The infected worms were washed several times with M9 buffer to remove *C. albicans* cells from their surface. Twenty worms were then transferred into plates (3-cm diameter) containing 2 ml of liquid medium (79% M9, 20% BHI, 10 μg/ml cholesterol and 90 μg/ml kanamycin) according to [Breger et al, 2007]. The peptide was either added to the plates, or omitted as indicated. The plates were incubated at 25°C and examined for worm survival after 24 h. Plates were hand shaken and worms were considered to be dead if they did not respond to being touched by a platinum wire pick. Living nematodes maintain a sinusoidal shape, whereas dead nematodes appear as straight, rigid rods as the corpses become filled with fungal cells [Moy et al, 2006]. The experiments were done in triplicate.

3.17 Peptide's effect on the number of yeast cells and their switch to the hyphal form, within the nematode intestine

Twenty infected nematodes in triplicate were treated (or not in case of controls) with the peptide at 25°C for 24 h. afterwards, for each replicate, worms were broken with 50 μl of M9 buffer-1% Triton X-100. Appropriate dilutions of whole-worm lysates were plated on YPD agar plates for colony counts after two days of incubation at 30°C. The experiments were performed a minimum of three times. In parallel, to evaluate the effect of Esc(1-18) on the morphology of fungal cells, peptide-treated and untreated infected worms were mounted onto pads of 3% agarose in M9 buffer supplemented with 20 mM sodium azide to paralyze them. Animals were then observed under a Zeiss AXIOVERT25 microscope and photographed with a Zeiss AxioCam camera using Axiovision 4.6 (Zeiss) software.

In another set of experiments, infected nematodes were treated with 25 μM rho-Esc(1-18) for 3 h and then observed by fluorescence microscopy as reported above.

3.18 Statistical analysis

Data are presented as mean ± SD, and the Student's test (GraphPad Prism 4.0 software) was used to determine the statistical significance between experimental groups. The difference was considered significant if the p-value was less than 0.05.

4. RESULTS

4.1 Structural properties of the Esc(1-18) and Esc(1-21) fragments

Table 1 Primary structure of the fragments.

Peptide	Sequence
Esc(1-18)	**GIFSKLAGKKLKNLLISG-NH_2**
Esc(1-21)	**GIFSKLAGKKIKNLLISGLKG-NH_2**

CD spectra of Esc(1-18) (whose amino acidic sequence is indicated in Table 1) dissolved in water and in different water/TFE solutions are shown in Fig. 4.1. The helicity degree increased with increasing the TFE content. The maximum helicity was achieved in the 40% v/v TFE/water solution [Manzo et al, 2012].

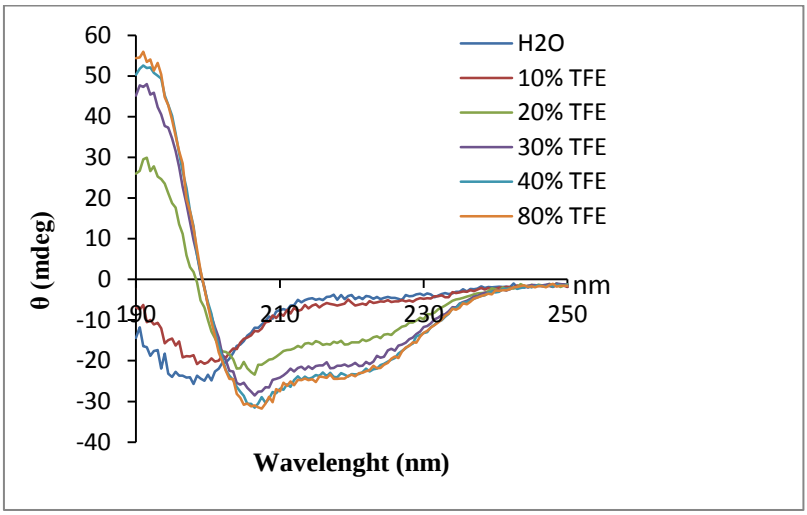

Figure 4.1 Circular dichroism spectra of Esc(1-18) in water and in different TFE/water (v/v) mixtures.

NMR analysis showed that in 50% TFE solution, the N-terminal part of the peptide, encompassing the first 11 residues, displayed a right-handed helical conformation, whereas the C-terminal portion was basically unfolded [Manzo et al, 2012]. This peptide conformation is clearly amphipathic, with the hydrophobic and hydrophilic residues neatly arranged on the opposite sides. The only interruption of this global amphipathicity occurs right at the end of the helical region, where the residues K10 and L11 appears to be dislocated (Fig. 4.2).

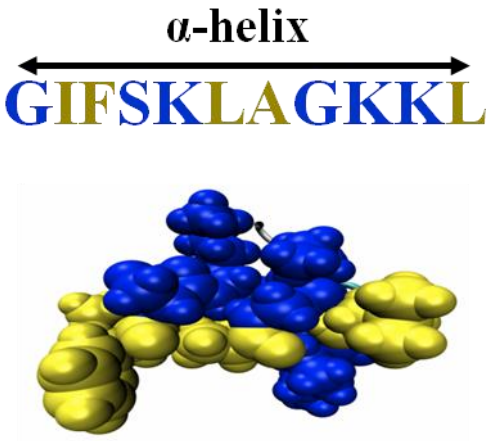

Figure 4.2 3D NMR structure of the first 11 amino acids of the N-terminal Esc(1-18) peptide in a 50% v/v TFE/water solution. Hydrophilic and hydrophobic residues are represented in blue and yellow, respectively [Manzo et al, 2012].

Preliminary data about the structural properties of Esc(1-21) (whose amino acid sequence is showed in Table 1) were also obtained by means of CD analysis. While the peptide was disordered in solution (NaPB), it adopted an α-helical structure when associated with PE/PG vesicles mimicking the

Gram-negative cell membrane (data not shown). Similarly to the Esc(1-18) peptide, the side chains are oriented in an amphiphilic arrangement, with all charged residues segregated to one face of the helix (data not shown).

4.2 Anti-*Candida* activity of Esc(1-18)

4.2.1 *In vitro* activity

4.2.1.1 Anti-*Candida* activity of all-L/all-D Esc(1-18) enantiomers

The activity of Esc(1-18) against *C. albicans* yeast cells was evaluated by the microdilution broth assay using a standard inoculum of 3.5 x 10^4 CFU/ml. Against all the strains tested, the MIC value was 4 μM with the exception of *C. albicans* n.1r strain. Note that the same MIC value was obtained when samples were incubated at 28°C instead of 37°C (data not shown). In our experiments the reference strain ATCC 10231 was selected as a representative strain to perform further additional studies, since it is a well-characterized standard strain with the ability to grow under both yeast and hyphal forms under the experimental conditions. As most of the experiments described below required a higher number of yeast cells, an inoculum of $1x10^6$ and $1x10^7$ CFU/ml was also used to determine the MIC which was found to be directly related to cell number: 16 and 64 μM, respectively.

In order to confirm a fungicidal activity of Esc(1-18), a killing kinetics study was carried out on the 3 h-grown hyphae after peptide treatment at different concentrations, by the MTT colorimetric assay. A dose-dependent candidacidal activity was observed, with approximately 80% reduction in cell survival within the first 20 min at 16 μM (Fig. 4.3A), whereas approximately

90% killing of hyphal population was recorded after a longer incubation time (60 min) at the same concentration of 16 μM (MFC_{90}).

Furthermore, to find out whether the killing activity was a stereospecific mechanism mediated by recognition of chiral targes, we also used the all-D enantiomer of Esc(1-18). Interestingly, it was found to display the same MIC (4 μM) of the all-L isoform, as well as a similar fungicidal activity (Fig. 4.3B).

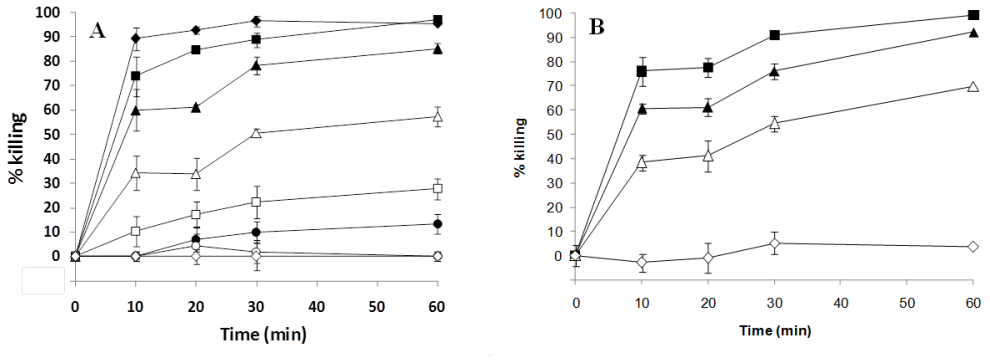

Figure 4.3 killing kinetics of all-L Esc(1-18) (panel A) and all-D Esc(1-18) (panel B) on *C. albicans* ATCC 10231 hyphal cells in NaPB. Hyphae, obtained after 3 h growth of $3x10^4$ yeast cells, were incubated with different peptide concentrations at 37°C. Data points represent the mean of triplicate samples ± SD from a single experiment, representative of three independent experiments. The killing activity was determined by the colorimetric MTT assay and is expressed as percentage with respect to the control sample (cells not treated with the peptide) at the corresponding time intervals. Peptide concentrations used are the following: 0.25 μM (◊); 0.5 μM (○); 1 μM (●); 2μM (□); 4 μM (Δ); 8 μM (▲); 16 μM (■); 32 μM (♦).

Note also that both all-L and all-D Esc(1-18) showed similar killing kinetics also against the yeast cells of this pathogen (see Luca et al, 2013a. Fig. 1a). Interestingly, when the peptide was tested on the fungal biofilm obtained after 12 h or 18 h growth of hyphae (Fig. 4.4 upper panels), its efficacy to cause 50% and 90% fungal killing was found to be only 4-fold or 8-fold lower than that recorded against 3h-grown hyphae (see Luca et al,

2013a. Table 2). Phase-contrast images of *Candida* biofilm treated or not treated with the peptide at its MFC_{90} (64 μM), after MTT colorimetric assay, are reported in Fig. 4.4 (lower panels).

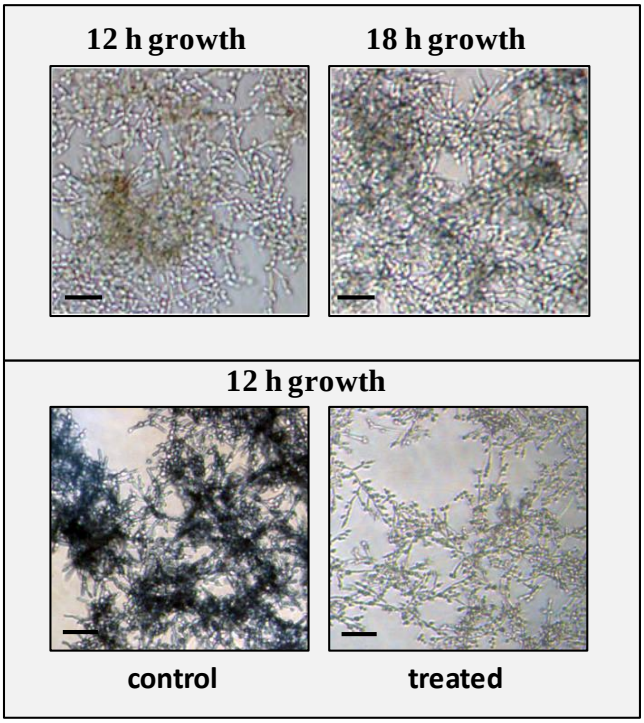

Figure 4.4 Phase-contrast images of *Candida* biofilm obtained after 12 h and 18 h growth of yeast cells at 37°C (upper panels). The peptide's effect on the viability of 12 h-grown biofilm is shown after the MTT colorimetric assay (lower panels). The black color in the peptide-untreated (control) sample indicates viable cells, whereas the transparency in the peptide-treated sample, indicates the presence of dead yeast and hyphal cells. Scale bar is 20 μm long.

4.2.1.2 Membrane perturbation of both yeast and hyphal forms

We have analyzed whether Esc(1-18) was able to alter the membrane permeability of *Candida* hyphae by monitoring the intracellular influx of Sytox Green upon peptide's addition. Sytox Green (MW 900 Da) is a cationic dye which is not able to enter intact cells, but only those having membrane breakages whose size is enough to allow its entrance.

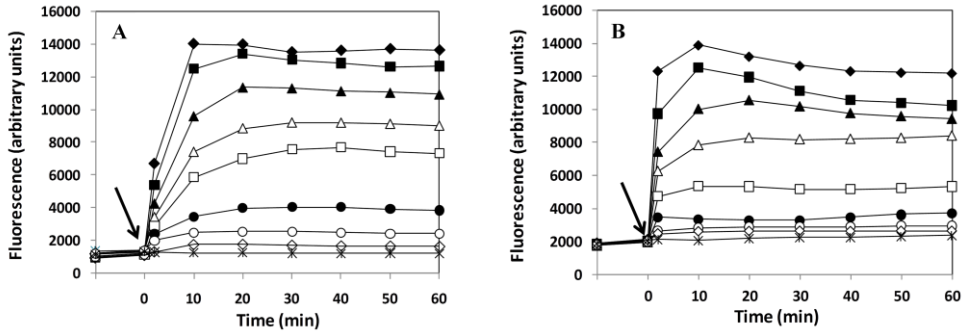

Figure 4.5 Membrane permeabilization of *C. albicans* ATCC 10231 hyphae obtained after 3 h growth of yeast cells ($3x10^4$ cells per well). Samples were incubated with 1 μM Sytox Green in NaPB. Once basal fluorescence reached a constant value, the all-L Esc(1-18) (panel A) or all-D Esc(1-18) (panel B) was added (arrow, t = 0) and changes in fluorescence (λ_{exc} = 485 nm, λ_{ems} = 535 nm) were monitored for 60 min at different intervals. Peptide concentrations used are the following: 0.25 μM (◊); 0.5 μM (○); 1 μM (●); 2μM (□); 4 μM (Δ); 8 μM (▲); 16 μM (■); 32 μM (♦). Control (*) is given by cells without peptide. Data points represent the mean of triplicate samples from a single experiment, representative of three independent experiments.

The all-L Esc(1-18) peptide disturbed the structural organization of the membrane of the filamentous form of *Candida* in a concentration-dependent manner (Fig. 4.5A) which directly correlates with its killing activity. Likewise to the results found for the all-L peptide, a dose-dependent membrane perturbation was detected for the all-D enantiomer, with a kinetic overlapping that of the all-L peptide (Fig. 4.5B), thus excluding the involvement of specific/chiral components of the lipid membrane in the peptide-induced membrane perturbation process.

A very similar outcome for both Esc(1-18) enantiomers was also obtained on the yeast cells (data not shown).

In our experiments, the polyene antifungal drug amphotericin B was also used for comparison. This drug has the ability to interact with membrane constituents and to induce pore formation [Hong et al, 1999; Younsi et al, 2000] causing a fungicidal activity in 2-3 h, depending on the strain [Canton

et al, 2004]. We have obtained only a modest increase in fluorescence intensity within the first 20 min after the addition of amphotericin B, even when used at a concentration 64-fold higher the MIC. However, it gradually increased with time reaching its maximum value, which was found to be identical to that obtained with 16 μM Esc(1-18), within 3 h (data not shown).

ROS determination – We evaluated whether the membrane perturbation was the final result of more complex intracellular signaling events, such as the production of reactive oxigen species (ROS) whose accumulation would rapidly lead to oxidation of phospholipids and other macromolecules leading to membrane damage. For that purpose, we analyzed the peptide's ability to induce ROS formation by using the cell permeant fluorigenic dye DCFH-DA (see 3.12 section).

As illustrated in Fig. 4.6, a very low level of fluorescence intensity was recorded in yeast (Fig. 4.6A) and hyphal cells (Fig. 4.6B) only after a long incubation time with the peptide (120 and 180 min) compared to the results found when these cells were exposed to the ROS-inducer H_2O_2, whose fungicidal effect was previously found to occur after ~3 h incubation [Phillips et al, 2003]. Overall, our results indicate a lacking production of ROS by Esc(1-18)-treated *Candida*, at the killing time (10-20 min) and only a rather weak production of ROS when yeast cells are treated with the peptide for a much longer time (3h).

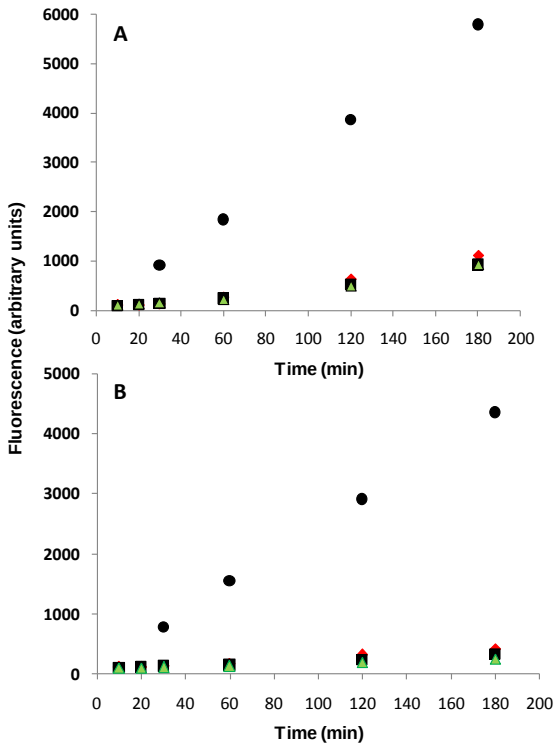

Figure 4.6 Effect of Esc(1-18) on the production of ROS by yeasts (panel A) and hyphal cells (panel B).
(A) Logarithmically growing *C. albicans* cells ($1x10^6$) were suspended in NaPB, preincubated with 20 μM DCFHDA at 37°C and then treated with the peptide at different concentrations: 16 μM (red rhomb); 8 μM (black square) and 4 μM (green triangle) for 3 h. Fluorescence emitted by the cells was recorded as reported in 3.12 section. As a positive control for ROS production, cells were treated with 2 mM H_2O_2 (black circle) and the results were read after 30, 60, 120 and 180 min incubation time. Fluorescence of control samples (cells pre-incubated with the probe, but without any treatment) at any time was subtracted from all values.
(B) Hyphal cells were incubated with DCFHDA in NaPB for 30 min. Afterwards, the probe was removed and cells were treated with the peptide or H_2O_2, as above. The results are the mean of triplicate samples from a single experiment representative of three independent experiments.

Cell apoptosis – To know if Esc(1-18) treatment of *Candida* cells induced a programmed cell-death, both yeast and hyphal cells were assessed for apoptotic markers i.e. DNA fragmentation, detected by TUNEL assay (see 3.13 section). As shown in Fig. 4.7 (panels A and B), no significant differences were found between peptide-treated and untreated cells. We chose 16 μM Esc(1-18), because this concentration was found to cause approximately 80% killing of both yeast and hyphal cells within 20 min. Note that similar results were obtained after a longer incubation time with the peptide (60 min, data not shown), hence excluding apoptosis as a possible cell death mechanism caused by Esc(1-18).

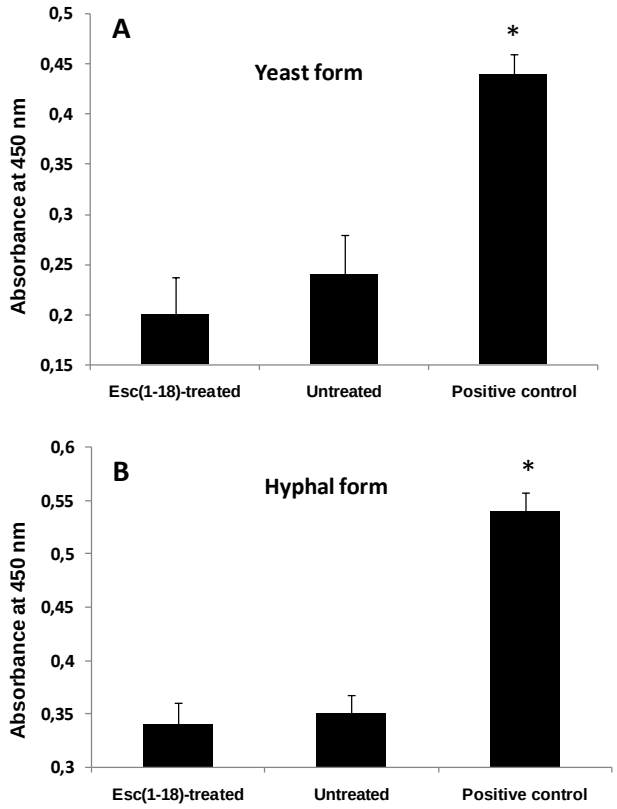

Figure 4.7 Quantitation of apoptosis in yeast (panel A) and hyphal (panel B) cells after treatment with 16 μM Esc(1-18) at 37°C for 20 min using the HT-TiterTACS kit. Cells were fixed and labeled according to the protocol prior to colorimetric analysis. Afterwards, they were incubated with TACS-SapphireTM substrate and the colorimetric reaction was stopped with 0.2N HCl after 30 min and measured at 450 nm. Untreated cells were those not treated with the peptide; positive control was given by nuclease treated cells. The results are the mean of triplicates ± SD from a single experiment, representative of three independent experiments. (*) indicates $p < 0.01$ versus untreated cells. Note that no statistical significance was found between peptide-treated and untreated samples.

Importantly, these results are in line with the lacking production of ROS, whose accumulation is one of the phenotypical markers of yeast cells undergoing apoptosis [Madeo et al, 1999].

4.2.1.3 Fluorescence studies

To visualize both the peptide's distribution and alteration of the cell membrane integrity, either yeast or hyphal forms were treated with 16 μM of rho-Esc(1-18), followed by DAPI (for nuclei detection) and Sytox Green staining. We noted that rhodamine did not affect the anti-*Candida* activity of Esc(1-18) since the MIC value of rho-Esc(1-18) was equal to that of the

unlabelled peptide. As shown in Fig. 4.8, rho-Esc(1-18) appeared to be distributed evenly over the yeast cells and hyphae, and the membrane perturbation (as detected by the green fluorescence of Sytox Green) occurred in a similar manner along the entire cell structure.

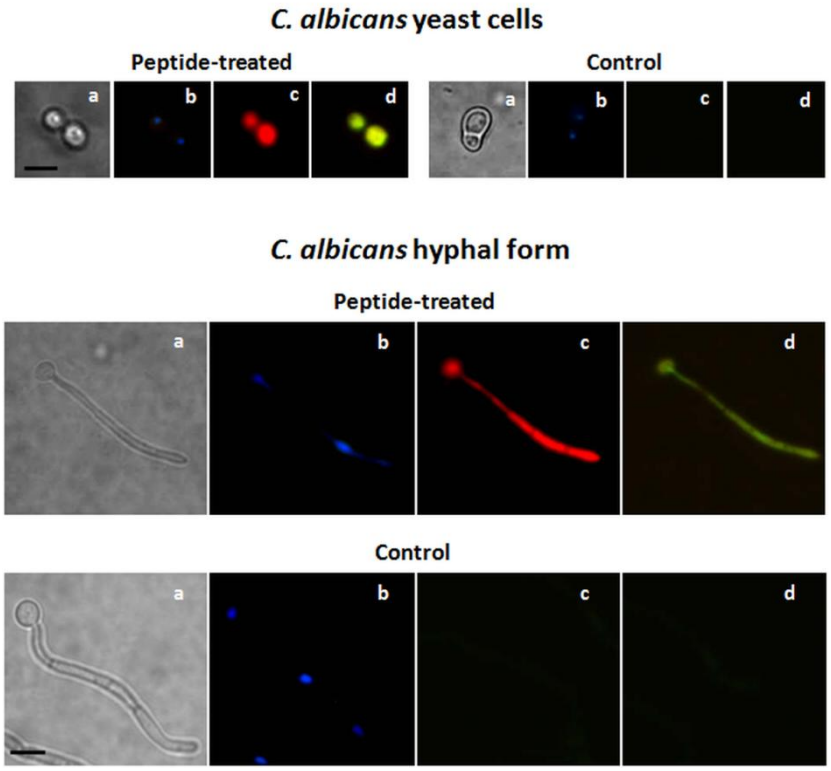

Figure 4.8 Detection of peptide distribution and membrane perturbation of both *C. albicans* ATCC 10231 yeast cells and hyphae. Cells were treated with 16 μM of rho-Esc(1-18) for 30 min and then stained with DAPI and Sytox Green as described in 3.14 section. In all cases, controls were run in the absence of peptide. Samples were then examined by light (a) and fluorescence microscopy (b, c, d) at x 100 magnification. Blu (b), red (c) and green (d) fluorescence indicate the distribution of DAPI, the labeled-Esc(1-18) and Sytox-Green, respectively. Scale bars are 5 μm long and apply to all images.

4.2.1.4 Inhibition of hyphal development

It is largely known that *C. albicans* hyphae represent the most virulent phenotype of this pathogen and that the ability of a drug to prevent the morphological change of fungal cells from their budding shape into the filamentous form would be extremely advantageous. We therefore studied the capability of Esc(1-18) to block hyphal formation and found out that this effect was more pronounced when $1x10^6$ CFU/ml were used. Indeed, a clear inhibition of germ tubes was detected after a 3 h treatment of yeast cells with sub-inhibitory concentrations of Esc(1-18) (Fig. 4.9). More precisely, the minimal peptide concentration causing such inhibition was found to be 4 μM, corresponding to ¼ the MIC (16 μM with $1x10^6$ CFU/ml). Importantly, this effect was maintained up to 24 h, despite the achieved high cell density, due to cell proliferation (data not shown).

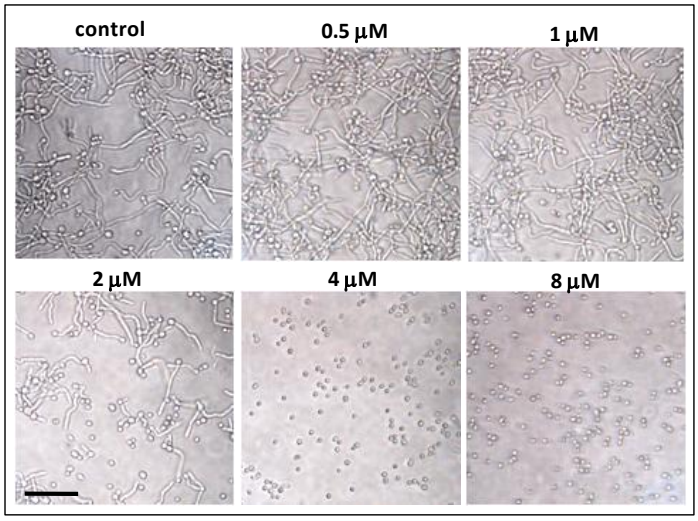

Figure 4.9 Effect of Esc(1-18) on the development of *C. albicans* hyphae. Freshly grown yeast cells ($1x10^5$ in 100 μl WB) were put into the wells of a 96-well microtiter plate and incubated with different concentrations of peptide at 37°C. After 3 h, samples were observed under an inverted microscope at 40 x magnification and photographed. Scale bar is 20 μm long and applies to all images.

Interestingly, when the all-D enantiomer of Esc(1-18) was used, no inhibition of hyphae formation was detected at concentrations below its MIC

(Fig. 4.10) which was equal to that of the all-L peptide, 4 μM. This suggests that a specific mechanism (i.e. inhibition of a unique pathway) is presumably subtending such event, rather than being the result of a global insult to the cells.

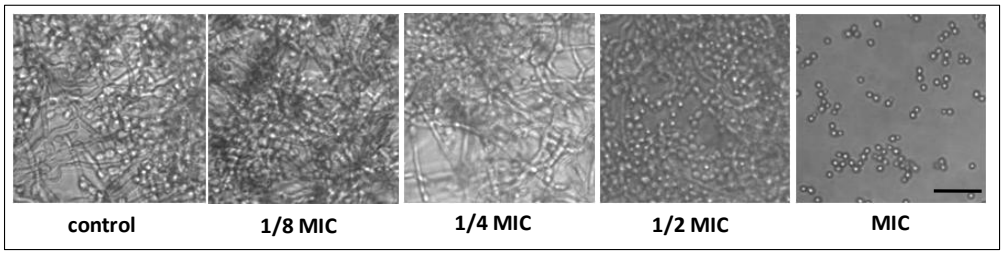

Figure 4.10 Effect of all-D Esc(1-18) on the development of hyphal form of *C. albicans* ATCC 10231. Freshly grown yeast cells ($1x10^5$ in 100 μl WB) were put into the wells of a 96-well microtiter plate and incubated with different concentrations of the peptide at 37° C. After 24 h, samples were observed under an inverted microscope at 40 x magnification and photographed. Scale bar is 20 μm long and applies to all images.

4.2.2 *In vivo* activity

4.2.2.1 Peptide effect on *C. elegans* survival

When infected wild-type nematodes were transferred to liquid medium (see 3.16 section), yeast cells underwent hyphal development, presumably induced by environmental factors of the animal's intestine. This usually results in a very aggressive infection leading to worm lethality in about 40 h. Indeed, hyphae penetrate and destroy the cuticle to finally pierce through the body (Fig. 4.11). In our case, Esc(1-18) was added to the worms, at 50 μM, after 20 min of their exposure to *Candida*. Interestingly, the peptide increased *C. elegans* survival by more than 50% within 24 h (Fig. 4.12A), causing

approximately 40% reduction in the number of CFU within the nematode's intestine (Fig. 4.12B).

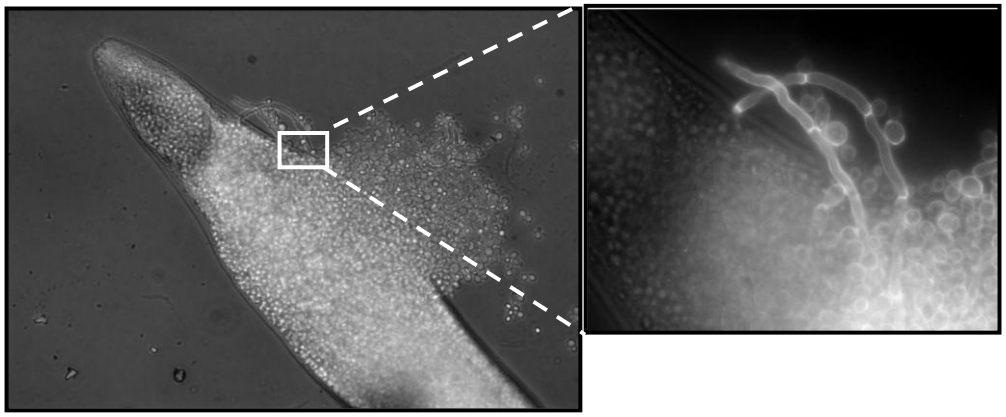

Figure 4.11 A representative nematode, 40 h after infection with *C. albicans* ATCC 10231. The sample was stained for 5 min with 5 mM Calcofluor White which is a specific cell-wall probe. Hyphae protruding from the cuticle are clearly visible in the zoom.

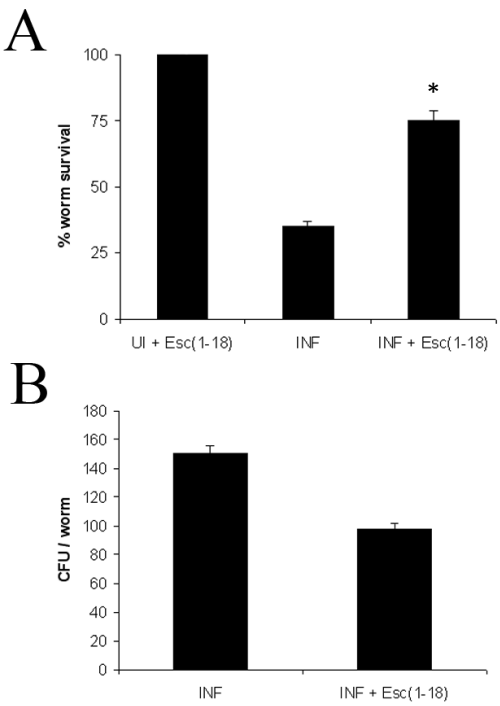

Figure 4.12 Effect of Esc(1-18) on the survival of nematodes (panel A) and the number of live *Candida* cells within the worm's gut (panel B).

(A) Survival of infected *C. elegans* upon peptide treatment at 50 μM [INF+Esc(1-18)] was analyzed after 24 h in comparison with untreated infected nematodes (INF). Control uninfected worms treated with the peptide [UI+Esc(1-18)] exhibited 100% viability. (*) indicates $p < 0.05$ compared to values from INF. (B) CFU were determined in the gut of 20 live worms after 24 h of peptide treatment. Infected nematodes not treated with the peptide (INF) were included for comparison. The reported values represent the means of at least three independent experiments; the error bars indicate SD.

4.2.2.2 *In vivo* inhibition of hyphal development and peptide localization

In line with our *in vitro* results, Esc(1-18) dramatically hampered hyphae formation within the worm's gut, in 3 h (Fig. 4.13A). In order to accurately assess the *in vivo* distribution of the peptide, the rho-Esc(1-18) analog was used. As illustrate in Fig. 4.13B, the peptide was homogeneously confined to the worm's intestinal lumen and uniformly associated with the cell perimeter of *Candida* cells.

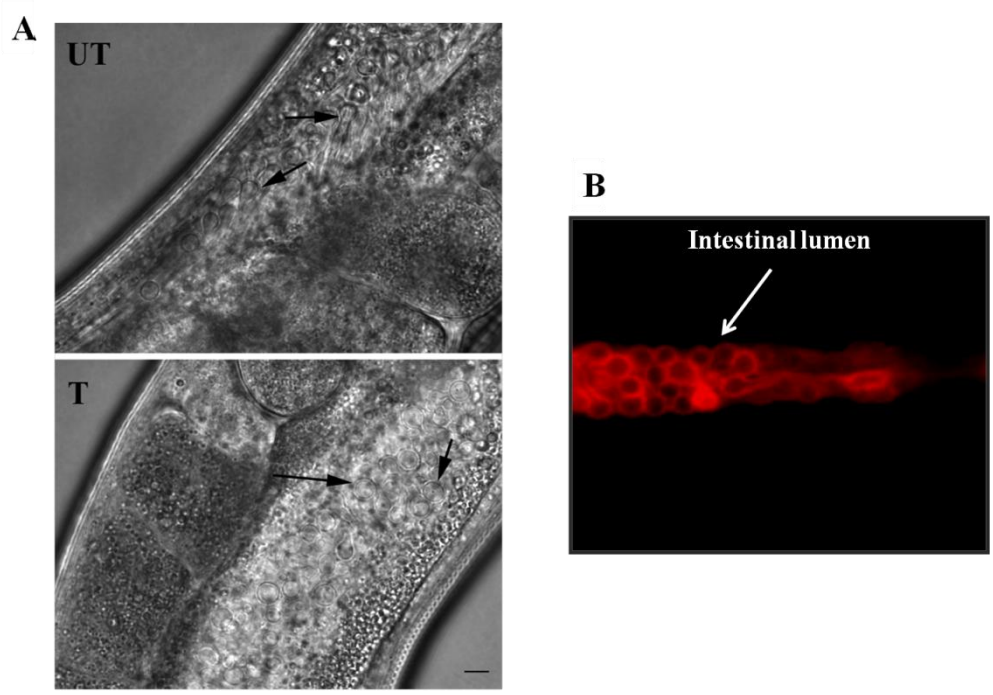

Figure 4.13 Panel A: morphology of *Candida* cells within the gut of a representative infected animal, after 3 h treatment with 50 μM Esc(1-18) (T). A representative infected nematode not treated with the peptide (UT) is included for comparison. Arrows indicate germ tube formation or yeast budding cells in the untreated or peptide-treated sample, respectively. Scale bar is 8 μm long. Panel B: *in vivo* distribution of rho-Esc(1-18). Nematodes were infected with *C. albicans* ATCC 10231 yeast cells for 20 min and then treated with 25 μM of the labeled peptide. Fluorescence photomicrograph of a representative worm, 3 h after the addition of the peptide at 25°C. The red fluorescence indicates the peptide distribution within the worm's intestinal lumen around the fungal cells.

4.3 Anti-*pseudomonas* activity of Esc(1-21)

4.3.1 Antimicrobial activity on planktonic cells

First of all, we evaluated the possible tendency of Esc(1-21) to induce resistance against *P. aeruginosa* (see 3.5 (iii) section), a bacterial species that frequently develops resistance against different conventional antibiotics. To this end, we performed multiple exposures of the bacterial suspension to serial two-fold dilutions of the peptide or a conventional antibiotic, i.e. ciprofloxacin, that is normally used against *P. aeruginosa* human infections and that is known to induce resistance.

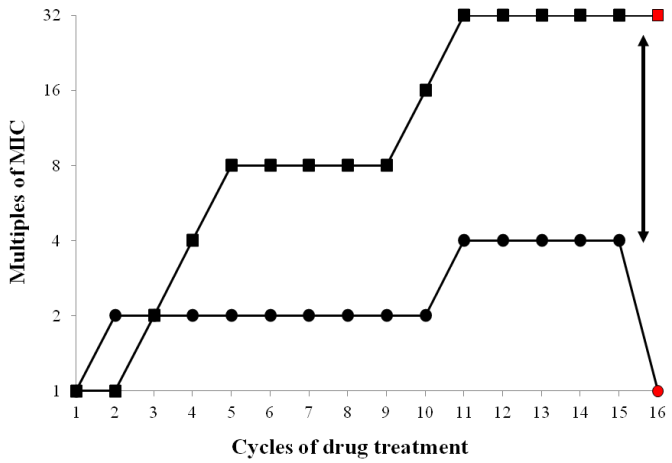

Figure 4.14 *P. aeruginosa* PAO1 resistance induced by Esc(1-21) (●) and ciprofloxacin (■). The double arrow indicates drug removal. (●) and (■) indicate MIC values after drug removal.

Interestingly, after 11 cycles of exposure to ciprofloxacin, the MIC of this antibiotic was found to be 32-fold higher than the initial value, whereas the MIC of Esc(1-21) increased by only 4-fold (Fig. 4.14). Moreover, if, after

15 cycles, drugs were removed, bacteria were grown in the absence of them and subsequently re-exposed to ciprofloxacin or Esc(1-21), the MIC remained 32-fold higher or went back to the initial value, respectively, indicating that Esc(1-21) does not induce resistance.

The activity of Esc(1-21) in inhibiting bacterial growth in liquid medium was tested on reference *P. aeruginosa* strains (ATCC 27853 and PAO1), MDR-clinical isolates, and strains from CF patients. The peptide had the same activity against all the microorganisms tested, with a MIC value of 4 μM except for MDR2 (8 μM).

We then performed killing kinetics experiments in PBS. The peptide caused approximately 99.9% killing of the reference PAO1 strain (Fig. 4.15) within 15 min, at a concentration of 1 μM. Similar results were obtained with all the other strains under study (data not shown) thus excluding the inhibition of intracellular processes (e.g. DNA, protein or cell wall synthesis) as the major mechanisms underlying the bactericidal activity of Esc(1-21).

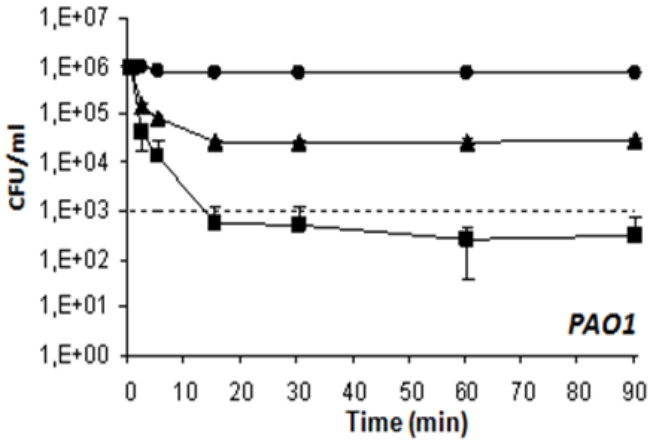

Figure 4.15 Time-kill curves of Esc(1-21) on *P. aeruginosa* PAO1 strain. Bacteria ($1x10^6$ CFU/ml) were incubated with 0.5 μM (▲) or 1 μM (■) of peptide in PBS at 37°C. The control (●) is given by bacteria without peptide. Data points represent the mean of triplicate samples ± SD from a single experiment, representative of three independent experiments. The dotted line indicates 99.9% bacterial killing.

4.3.2 Anti-Biofilm activity

The activity of Esc(1-21) on 20-h pre-formed biofilm of *P. aeruginosa* ATCC 27853 was tested by using three different methods (see 3.6 section): (i) visual observation of bacterial growth; (ii) evaluation of living bacterial cells after peptide treatment, and (iii) estimation of the peptide's effect on the bacterial biomass.

The minimum peptide concentration able to inhibit re-growth of bacteria from peptide-treated biofilm (MBEC) was found to be 6 μM. Moreover, as indicated by the results of colony counts of biofilm cells or the MTT reduction assay (see 3.6 (ii) section) the peptide was found to cause a 3-$\log_{10}$ reduction in the number of viable biofilm cells at 12 μM, a concentration 2-fold higher the MBEC. However, when CV staining was performed, we obtained from 15 to 32% biofilm biomass at those peptide concentrations giving rise to almost total microbial death (from 48 to 12 μM, respectively), suggesting that such a percentage was only related to the presence of lifeless biological material (see Luca et al, 2013b. Table 3 and Table 4).

4.3.3 Mode of action

4.3.3.1 Membrane perturbation assays and SEM

The capability of Esc(1-21) to perturb the cytoplasmic membrane of planktonic cells of *P. aeruginosa* PAO1 was monitored by the Sytox Green assay. The data revealed that the membrane perturbation occurs in a dose-dependent manner and within the first 15 min from peptide addition, with a kinetic overlapping that of the microbial killing (Fig. 4.16).

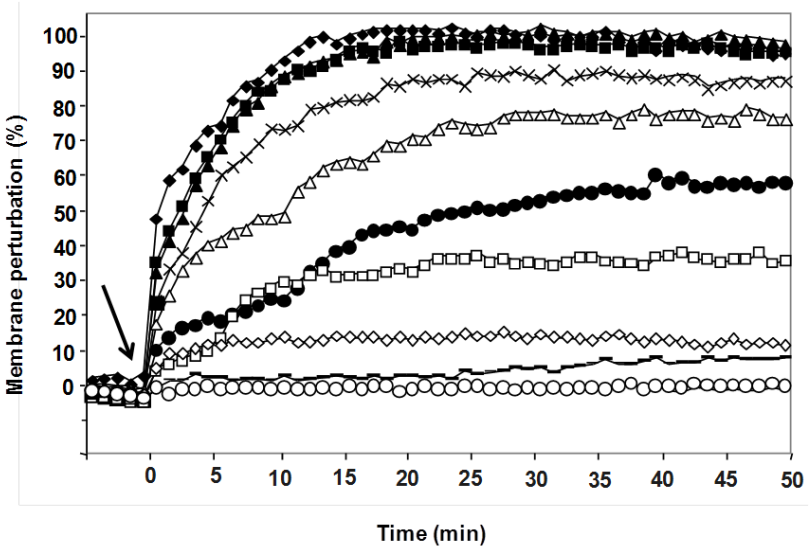

Figure 4.16 Effect of Esc(1-21) on the membrane-perturbation of the planktonic form of *P. aeruginosa* PAO1. Cells ($1x10^7$ CFU/ml) were prepared as described before (see 3.10 (i)c section). After peptide addition (arrow, t = 0) changes in fluorescence were monitored and plotted as the percentage of the maximal membrane perturbation. Data points represent the average values of three independent experiments, with SD not exceeding 2.5%. Peptide concentrations used were the following: 0.125 μM (hyphen); 0.25 μM (diamond); 0.5 μM (square); 1 μM (filled circle); 2 μM (triangle); 4 μM (cross); 8 μM (filled triangle); 16 μM (filled square); 32 μM (filled diamond). Control (circle) is given by bacteria without peptide.

Note that in order to get an optimal detection of membrane-perturbation by the Sytox Green assay a higher number of bacterial cells ($1x10^7$ CFU/ml) was needed compared to the regular amount ($1x10^6$ CFU/ml) used for MIC and killing kinetic assays.

However, to directly compare the killing and the membrane-perturbation activities of Esc(1-21), we performed both assays using the same number of cells ($1x10^7$ CFU/ml) and incubation time (Fig. 4.17A).

As reported in Fig. 4.17A, the percentage of cell viability gradually decreased at increasing peptide concentrations, in parallel with an increasing membrane perturbation. Moreover, to expand our knowledge on the extent of membrane lesions induced by the peptide, we assessed the release of large intracellular compounds, such as the cytoplasmic β-galactosidase, from peptide-treated cells. To this end, a recombinant *Pseudomonas* strain constitutively expressing this enzyme, was used (see 3.10 (ii) section). Esc(1-21) provoked ~50-60% enzyme leakage at those concentrations (from 8 to 32 μM) causing the complete microbial death (Fig. 4.17A). Hereafter, to directly observe the peptide's effect on the morphology of bacterial cells, we used scanning electron microscopy. Untreated bacteria appeared smooth, whereas cells treated with Esc(1-21) elicited a remarkable modification of the cell shape with the formation of blebs (pustules) and cell debris arising from them (Fig. 4.17B).

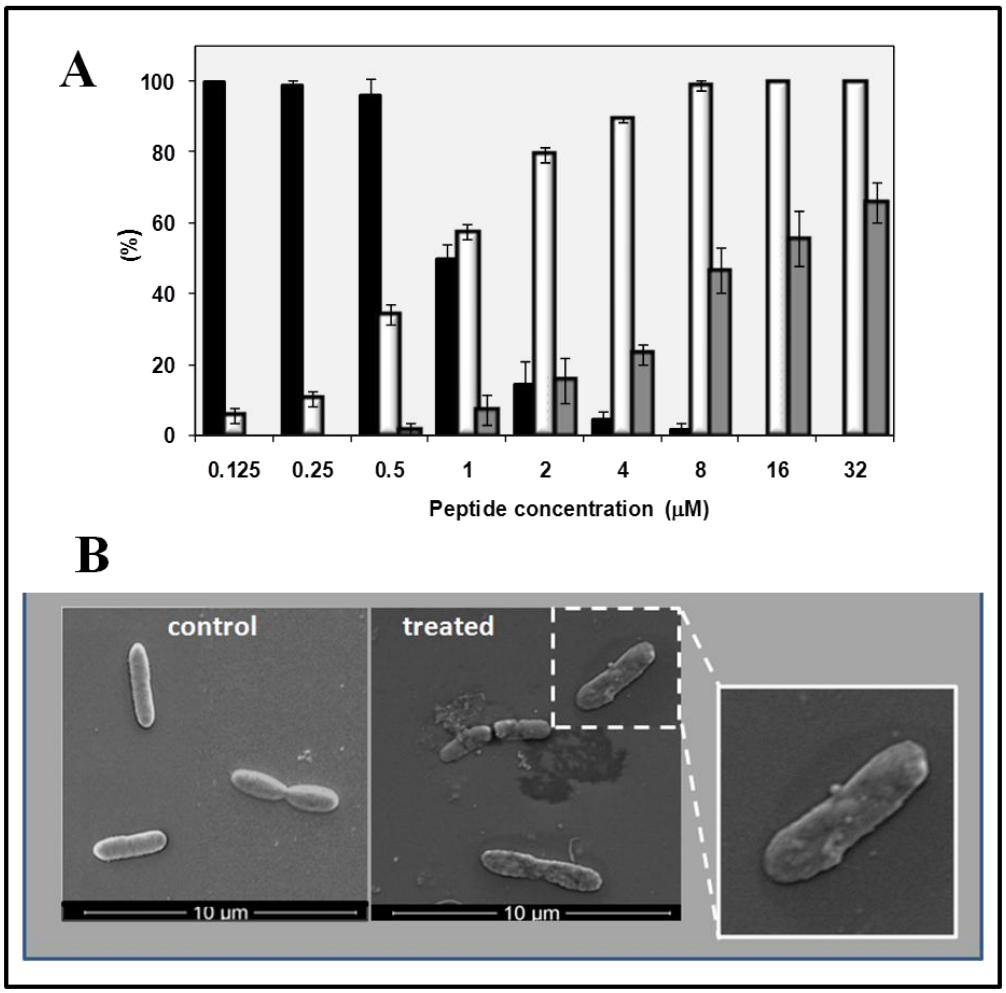

Figure 4.17 Effect of Esc(1-21) on the viability, membrane perturbation and morphology of the planktonic form of *P. aeruginosa* PAO1. Planktonic cells ($1x10^7$ CFU/ml in PBS) were incubated with the peptide at different concentrations for 30 min at 37°C. (A) The percentage of surviving CFU (black bars) is given with respect to the control (bacteria not treated with the peptide). Membrane perturbation was evaluated by the Sytox Green (white bars) and β-galactosidase (gray bars) assay. The Sytox Green fluorescent signal and the β-galactosidase enzymatic activity were expressed as percentage with respect to the maximal membrane perturbation obtained after cell lysis (see 3.10 (i)c section). All data points represent the means of three independent measurements ± SD. (B) Scanning electron microscopy of cells treated at 8 μM (causing ~100% killing, as shown in A). Controls are cells not treated with the peptide.

The ability of Esc(1-21) to cause damages on 20-h biofilm cells was also studied by both the Sytox Green and β-galactosidase assays, after 2 h peptide treatment (Fig. 4.18A). Interestingly, we obtained similar results to those found for the free living form, although a weaker damage to the cell membrane was recorded, as demonstrated by the minor leakage of β-galactosidase at those peptide concentrations causing ~100% microbial killing. Moreover, as evinced from electron microscopy analysis (Fig. 4.18B) protrusions from the cells surface were observed, with an evident disintegration of the extracellular matrix, becoming less packed and thinner, confirming the results obtained by the CV staining (see 4.3.2 section).

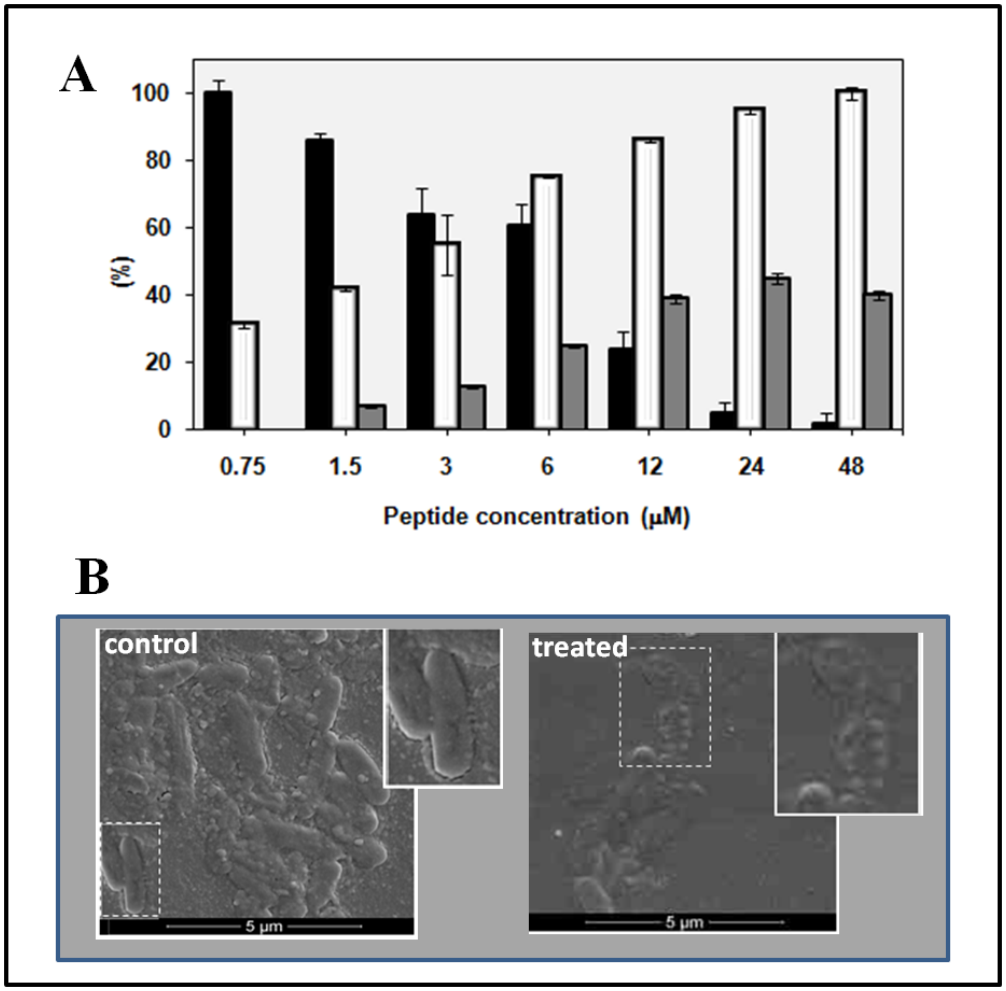

Figure 4.18 Effect of Esc(1-21) on the viability, membrane perturbation and morphology of the 20-h biofilm growth of *P. aeruginosa* PAO1. Bacterial biofilms grown on pegs were treated with the peptide at different concentrations for 2 h at 37°C. (A) The percentage of surviving biofilm cells (black bars) and membrane perturbation measured by using Sytox Green (white bars) and β-galactosidase (gray bars) assays were expressed as described for the planktonic cells. All data points represent the means of three independent measurements ± SD. (B) Scanning electron microscopy of biofilm cells treated at 24 μM (causing ~95% killing, as shown in A). Controls are cells not treated with the peptide.

4.4 Hemolytic activity

The ratio between antimicrobial and hemolytic activity is defined as the therapeutic index. It is necessary for AMPs to have a high therapeutic index, which indicates a high antimicrobial potency but low citotoxicity.

Both Esc(1-18) and Esc(1-21) peptides showed a very weak activity against human erythrocytes, causing approximately 10% hemolysis at a concentration 16-fold higher the MIC (64 μM) and were practically not hemolytic at lower concentrations.

As mentioned above, the selectivity of AMPs towards microbial cells with respect to mammalian ones mainly depends of the different lipid composition between their membranes. Specifically, microbial membranes are much richer in anionic phospholipids which favor electrostatic interaction with the cationic AMPs.

5. DISCUSSION

C. albicans and *P. aeruginosa* are two human commensal microorganisms. In certain circumstances they can give rise to opportunistic infections at different human anatomical regions such as oral, systemic infections and vaginitis (in the case of *C. albicans*) or otitis, keratitis infections associated with burns, wounds, pulmonary epithelium (especially in patients with cystic fibrosis) or with colonization of medical devices e.g. catheters and implants (in the case of *P. aeruginosa*).

Both of these microorganisms can hardly be eradicated when, under certain conditions, they become pathogenic. *C. albicans* is capable of reaching the bloodstream, colonizing different tissues, penetrating them and switching from the yeast to the hyphal form. *P. aeruginosa* strains can colonize lungs, repress motility and adhere to the lung-tissue evolving a mucoid phenotype able to secrete anionic polysaccharides and to produce sessile communities, with a protective layer around the cells that confers more resistance to antibiotic therapy.

Conventional antibiotics/antimycotics are frequently ineffective mainly because of their undesiderable side effects, emergence of resistant strains or because their lacking activity against pathogenic forms (i.e. hyphae, biofilms). Due to these reasons, novel anti-infective agents are of great interest to the medical community. In this context, we have studied two derivatives of a frog skin AMP: Esc(1-18) and Esc(1-21) and focused our attention mainly on their antimicrobial efficacy and mechanism of action.

Both of them are cationic and have an N-terminal amphipathic α-helical structure, as confirmed by CD spectra and/or by NMR analysis. More specifically, the C-terminal part of Esc(1-18) appears to be unfolded and the hydrophobic cluster of residues (L14-L15-I16), which is located in the middle of this region, may act as an anchoring tail favoring the peptide's incorporation into the phospholipid bilayer.

Our natural microbial flora consists of nearly 2 kg microbes (mainly bacteria) in the digestive tract and about 200 g microbes on the outer surfaces. Importantly, when the host's immune system is compromised, these bacteria (most of which double in number every 20 min) can take over. Therefore, for a surviving host, an effective defense system must be faster than the growth rate of an invading microorganism.

Here, we have shown that both peptides display a MIC around 4 μM against reference strains and clinical isolates of both *C. albicans* and *P. aeruginosa* pathogens and have a good therapeutic index, being slightly hemolytic at a concentration 16-fold greater the MIC. They have a fast microbicidal activity causing approximately 85-99% fungal/bacterial killing at 1-16 μM within 15-20 min (Figs. 4.3 and 4.15), with a concomitant membrane perturbation process.

The membrane perturbation process caused by Esc(1-18) on yeast and hyphal cells of *Candida* is not a consequence of intracellular signaling events, such as apoptosis (Fig. 4.7) and/or production of ROS (Fig. 4.6), but is presumably the result of a direct interaction of the peptide with the membrane. Moreover, we can also exclude that the membrane perturbation is the consequence of a binding-site mediated insertion of Esc(1-18) into the

fungal membrane, as supported by the same results of the all-L and all-D enantiomers of Esc(1-18) in terms of membrane perturbation (Fig. 4.5) and MIC.

Esc(1-21) is able to perturb the membrane of planktonic and sessile *Pseudomonas* cells where the degree of injury enhances in parallel with the peptide dosage, presumably enlarging the size of membrane breakages that lead to an increasing loss of bulky intracellular compounds, such as the β-galactosidase (Figs. 4.17A and 4.18A). Note that such membrane damage is also supported by SEM images of the peptide-treated cells.

As mentioned above, in Cystic Fibrosis patients, the two major problems during chronic lung infections are the development of antibiotic-resistant strains and the formation of bacterial biofilm, both difficult to eradicate. Esc(1-21) does not induce resistant strains *in vitro* (Fig. 4.14) even after multiple exposure to the peptide. This peptide is also able to inhibit re-growth of cells from *Pseudomonas*-treated biofilm and to eliminate biofilm cells within 2 h at a concentration 3-fold higher the MIC.

In vivo experiments, conducted on *Candida*-infected *C. elegans*, demonstrate that Esc(1-18) is able to prolong worm survival by 2-fold within 24 h and to hinder hyphal development from the yeast form. Presumably, these findings are due to a direct effect of Esc(1-18) on *Candida* cells, reducing their number (Fig. 4.12) and avoiding their shift to the more virulent and toxic phenotype (Fig. 4.13A). Even if this mini-host model cannot substitute for mammalian models, it offers a number of advantages over vertebrates, including the possibility to infect the *C. elegans* gastrointestinal tract upon cells ingestion by the nematode, which is an accurate

representation of what physiologically takes place in susceptible human hosts, where fungal cells in the intestinal mucosa can disseminate to other organs.

6. REFERENCES

Ali MF, Knoop FC, Vaudry H, Conlon JM (2003) **Characterization of novel antimicrobial peptides from the skins of frogs of the *Rana esculenta* complex**. Peptides 24:955-961.

Baillie GS, Douglas LJ (2000) **Matrix polymers of *Candida* biofilms and their possible role in biofilm resistance to antifungal agents**. J Antimicrob Chemother 46:397-403.

Balla KM, Troemel ER (2013) ***Caenorhabditis elegans* as a model for intracellular pathogen infection**. Cell Microbiol 15:1313-1322.

Bals R (2000) **Epithelial antimicrobial peptides in host defense against infection**. Respir Res 1:141-150.

Bechinger B, Zasloff M, Opella SJ (1993) **Structure and orientation of the antibiotic peptide magainin in membranes by solid-state nuclear magnetic resonance spectroscopy**. Protein Sci 2:2077-2084.

Berman J (2006) **Morphogenesis and cell cycle progression in *Candida albicans***. Curr Opin Microbiol 9:595-601.

Berman J, Sudbery PE (2002) ***Candida albicans*: a molecular revolution built on lessons from budding yeast**. Nat Rev Genet 3:918-930.

Bjarnsholt T (2013) **The role of bacterial biofilms in chronic infections**. APMIS Suppl (136):1-51.

Bjarnsholt T, Jensen PO, Fiandaca MJ, Pedersen J, Hansen CR, Andersen CB, Pressler T, Givskov M, Hoiby N (2009) ***Pseudomonas aeruginosa*** **biofilms in the respiratory tract of cystic fibrosis patients**. Pediatr Pulmonol 44:547-558.

Bland EJ, Keshavarz T, Bucke C (2001) **Using 2',7'-dichlorodihydrofluoresceindiacetate to assess polysaccharides as immunomodulating agents**. Mol Biotechnol 19:125-131.

Boman HG (1995) **Peptide antibiotics and their role in innate immunity**. Annu Rev Immunol 13:61-92.

Bragonzi A, Paroni M, Nonis A, Cramer N, Montanari S, Rejman J, Di Serio C, Doring G, Tummler B (2009) ***Pseudomonas aeruginosa*** **microevolution during cystic fibrosis lung infection establishes clones with adapted virulence**. Am J Respir Crit Care Med 180:138-145.

Bragonzi A, Worlitzsch D, Pier GB, Timpert P, Ulrich M, Hentzer M, Andersen JB, Givskov M, Conese M, Doring G (2005) **Non-mucoid *Pseudomonas aeruginosa* expresses alginate in the lungs of patients with cystic fibrosis and in a mouse model**. J Infect Dis 192:410-419.

Breger J, Fuchs BB, Aperis G, Moy TI, Ausubel FM, Mylonakis E (2007) **Antifungal chemical compounds identified using a *C. elegans* pathogenicity assay**. PLoS Pathog 3:e18.

Brenner S (1974) **The genetics of *Caenorhabditis elegans***. Genetics 77:71-94.

Brogden KA (2005) **Antimicrobial peptides: pore formers or metabolic inhibitors in bacteria?** Nat Rev Microbiol 3:238-250.

Brown KL, Hancock RE (2006) **Cationic host defense (antimicrobial) peptides**. Curr Opin Immunol 18:24-30.

Brugha RE, Davies JC (2011) ***Pseudomonas aeruginosa* in cystic fibrosis: pathogenesis and new treatments**. Br J Hosp Med 72:614-619.

Canton E, Peman J, Gobernado M, Viudes A, Espinel-Ingroff A (2004) **Patterns of amphotericin B killing kinetics against seven *Candida* species**. Antimicrob Agents Chemother 48:2477-2482.

Ceri H, Olson M, Morck D, Storey D, Read R, Buret A, Olson B (2001) **The MBEC Assay System: multiple equivalent biofilms for antibiotic and biocide susceptibility testing**. Methods Enzymol 337:377-385.

Chisholm AD, Hardin J (2005) **Epidermal morphogenesis**. WormBook 1 December: 1-22.

Cleary IA, Reinhard SM, Miller CL, Murdoch C, Thornhill MH, Lazzell AL, Monteagudo C, Thomas DP, Saville SP (2011) ***Candida albicans* adhesion Als3p is dispensable for virulence in the mouse model of disseminated candidiasis**. Microbiology 157:1806-1815.

Conlon JM (2008) **Reflections on a systematic nomenclature for antimicrobial peptides from the skins of frogs of the family *Ranidae***. Peptides 29:1815-1819.

Conlon JM, Kolodziejek J, Nowotny N (2004) **Antimicrobial peptides from ranid frogs: taxonomic and phylogenetic markers and a potential source of new therapeutic agents**. Biochim Biophys Acta 1696:1-14.

Costerton JW, Stewart PS, Greenberg EP (1999) **Bacterial biofilms: a common cause of persistent infections**. Science 284:1318-1322.

Dürr M, Peschel A (2002) **Chemokines meet defensins: the merging concepts of chemoattractants and antimicrobial peptides in host defens**. Infect Immun 70:6515-6517.

Ehrenstein G, Lecar H (1977) **Electrically gated ionic channels in lipid bilayers**. Q Rev Biophys 10:1-34.

Ernst RK, Guina T, Miller SI (2001) ***Salmonella typhimurium*** **outer membrane remodeling: role in resistance to host innate immunity**. Microbes infect 3:1327-1334.

Falciani C, Lozzi L, Pollini S, Luca V, Carnicelli V, Brunetti J, Lelli B, Bindi S, Scali S, Di Giulio A, Rossolini GM, Mangoni ML, Bracci L, Pini A (2012) **Isomerization of an antimicrobial peptide broadens antimicrobial spectrum to Gram-positive bacterial pathogens**. PLoS ONE 7:e46259.

Flemming HC, Wingender J (2010) **The biofilm matrix**. Nat Rev Microbiol 8:623-633.

François IE, CB, Borgers M, Ausma J, Dispersyn GD, KT (2006) **Azoles: mode of antifungal action and resistance development: effect of miconazole on endogenous reactive oxygen species production in *Candida albicans***. Anti-Infective Agents in Med Chem 5:3-13.

Frick IM, Akesson P, Rasmussen M, Schmidtchen A, Björck L (2003) **SIC, a secreted protein of *Streptococcus pyogenes* that inactivates antibacterial peptides**. J Biol Chem 278:16561-16566.

Fux CA, Costerton JW, Stewart PS, Stoodley P (2005) **Survival strategies of infectious biofilms**. Trends Microbiol 13:34-40.

Gazit E, Lee WJ, Brey PT, Shai Y (1994) **Mode of action of the antibacterial cecropin B2: a spectrofluorometric study**. Biochemistry 33:10681-10692.

Gazit E, Shai Y (1995) **The assembly and organization of the alpha 5 and alpha 7 helices from the pore-forming domain of *Bacillus thuringiensis* delta-endotoxin. Relevance to a functional model**. J Biol Chem 10:2571-2578.

Ghannounm MA, Janini G, Khamis L, Radwan SS (1986) **Dimorphism-associated variations in the lipid composition of *Candida albicans***. J Gen Microbiol 132:2367-2375.

Gow NA, Brown AJ, Odds FC (2002) **Fungal morphogenesis and host invasion**. Curr Opin Microbiol 5:366-371.

Gow NA, van der Veerdonk FL, Brown AJ, Netea MG (2011) ***Candida albicans* morphogenesis and host defence: discriminating invasion from colonization**. Nat Rev Microbiol 10:112-122.

Hancock RE, Sahl HG (2006) **Antimicrobial and host-defense peptides as new anti-infective therapeutic strategies**. Nat Biotechnol 24:1551-1557.

Harrison JJ, Stremick CA, Turner RJ, Allan ND, Olson ME, Ceri H (2010) **Microtiter susceptibility testing of microbes growing on peg lids: a miniaturized biofilm model for high-throughput screening**. Nat Protoc 5:1236-1254.

Hassett DJ, Cuppoletti J, Trapnell B, Lymar SV, Rowe JJ, Yoon SS, Hillard GM, Parvatiyar K, Kamani MC, Wozniak DJ, Hwang SH, McDermott TR, Ochsner UA (2002) **Anaerobic metabolism and quorum sensing by *Pseudomonas aeruginosa* biofilms in chronically infected cystic fibrosis airways: rethinking antibiotic treatment strategies and drug targets**. Adv Drug Deliv Rev 54:1425-1443.

Hawser S, Francolini M, Islam K (1996) **The effects of antifungal agents on the morphogenetic transformation by *Candida albicans in vitro***. J Antimicrob Chemother 38: 579-587.

Hetru C, Letellier L, Oren Z, Hoffmann JA, Shai Y (2000) **Androctonin, a hydrophilic disulphide-bridged non-haemolytic anti-microbial peptide: a plausible mode of action**. Biochem J 345:653-664.

Hitchcock CA, Barrett-Bee KJ, Russell NJ (1989) **The lipid composition and permeability to the triazole antifungal antibiotic ICI 153066 of serum-grown mycelia cultures of *Candida albicans***. J Gen Microbiol 135:1949-1955.

Hoiby N, Ciofu O, Johansen HK, Song ZJ, Moser C, Jensen PO, Molin S, Givskov M, Tolker-Nielsen T, Bjarnsholt T (2011) **The clinical impact of bacterial biofilms**. Int J Oral Sci 3:55-65.

Hong SY, Oh JE, Lee KH (1999) ***In vitro*** **antifungal activity and cytotoxicity of a novel membrane-active peptide**. Antimicrob Agents Chemother 43:1704-1707.

Huang G (2012) **Regulation of phenotypic transition in the fungal pathogen *Candida albicans***. Virulence 3:251-261.

Irazoqui JE, Urbach JM, Ausubel FM (2010) **Evolution of host innate defence: insights from *Caenorhabditis elegans* and primitive invertebrates**. Nat Rev Immunol 10:47-58.

Islas-Rodriguez AE, Marcellini L, Orioni B, Barra D, Stella L, Mangoni ML (2009) **Esculentin 1-21: a linear antimicrobial peptide from frog skin with inhibitory effect on bovine mastitis-causing bacteria**. J Pep Sci 15:607-614.

Jin T, Bokarewa M, Foster T, Mitchell J, Higgins J, Tarkowski A (2004) ***Staphylococcus aureus*** **resists human defensins by production of staphylokinase, a novel bacterial evasion mechanism**. J Immunol 172:1169-1176.

Kohler JR, Fink GR (1996) ***Candida albicans*** **strains heterozygous and homozygous for mutations in mitogen-activated protein kinase signaling components have defects in hyphal development**. Proc Natl Acad Sci USA 93:13223-13228.

Kraus D, Peschel A (2006) **Molecular mechanisms of bacterial resistance to antimicrobial peptides**. Curr Top Microbiol Immunol 306:231-250.

Kuchma SL, O'Toole GA (2000) **Surface-induced and biofilm-induced changes in gene expression**. Curr Opin Biotechnol 11:429-433.

Kumamoto CA, Vinces MD (2005) **Contributions of hyphae and hypha-co-regulated genes to *Candida albicans* virulence**. Cell Microbiol 7:1546-1554.

Latal A, Degovics G, Epand RF, Epand RM, Lohner K (1997) **Structural aspects of the interaction of peptidyl-glycylleucine-carboxyamide, a highly potent antimicrobial peptide from frog skin, with lipids**. Eur J Biochem 248:938-946.

Lehrer RI, Lichtenstein AK, Ganz T (1993) **Defensins: antimicrobial and cytotoxic peptides of mammalian cells**. Annu Rev Immunol 11:105-128.

Li J. Turnidge J, Milne R, National RL, Coulthard K (2001) ***In vitro* pharmacodynamic properties of colistin and colistin methanesulfonate against *Pseudomonas aeruginosa* isolates from patients with cystic fibrosis**. Antimicrob Agents Chemother 45:781-785.

Luca V, Olivi M, Di Grazia A, Palleschi C, Uccelletti D, Mangoni ML (2013a) **Anti-*Candida* activity of 1-18 fragment of the frog skin peptide esculentin-1b: *in vitro* and *in vivo* studies in a *Caenorhabditis elegans* infection model**. Cell Mol Life Sci. IN PRESS.

Luca V, Stringaro A, Colone M, Pini A, Mangoni ML (2013b) **Esculentin(1-21), an amphibian skin membrane-active peptide with**

potent activity on both planktonic and biofilm cells of the bacterial pathogen *Pseudomonas aeruginosa*. Cell Mol Life Sci 70, 2773-2786.

Ludtke SJ, He K, Heller WT, Harroun TA, Yang L, Huang HW (1996) **Membrane pores induced by magainin**. Biochemistry 35:13723-13728.

Lo HJ, Kohler JR, DiDomenico B, Loebenberg D, Cacciapuoti A, Fink GR (1997) **Nonfilamentous *C. albicans* mutants are avirulent**. Cell 90:939-949.

Madeo F, Frohlich E, Ligr M, Grey M, Sigrist SJ, Wolf DH, Frohlich KU (1999) **Oxygen stress: a regulator of apoptosis in yeast**. J Cell Biol 145:757-767.

Mah TF, Pitts B, Pellock B, Walker GC, Stewart PS, O'Toole GA (2003) **A genetic basis for *Pseudomonas aeruginosa* biofilm antibiotic resistance**. Nature 426:306-310.

Mangoni ML (2006) **Temporins, anti-infective peptides with expanding properties**. Cell Mol Life Sci 63:1060-1069.

Mangoni ML, Fiocco D, Mignogna G, Barra D, Simmaco M (2003) **Functional characterisation of the 1-18 fragment of esculentin-1b, an antimicrobial peptide from *Rana esculenta***. Peptides 24:1771-1777.

Mangoni ML, Grovale N, Giorgi A, Mignogna G, Simmaco M, Barra D (2000) **Structure-function relationships in bombinins H, antimicrobial peptides from *Bombina* skin secretions**. Peptides 21:1673-1679.

Mangoni ML, Papo N, Barra D, Simmaco M, Bozzi A, Di Giulio A, Rinaldi AC (2004) **Effects of the antimicrobial peptide temporin L on cell morphology, membrane permeabilità and viability of *Escherichia coli***. Biochem J 380:859-865.

Mangoni ML, Saugar JM, Dellisanti M, Barra D, Simmaco M, Rivas L (2005) **Temporins, small antimicrobial peptides with leishmanicidal activity**. J Biol Chem 280:984-990.

Manzo G, Sanna R, Casu M, Mignogna G, Mangoni ML, Rinaldi AC, Scorciapino MA (2012) **Toward an improved structural model of the frog-skin antimicrobial peptide esculentin-1b(1-18)**. Biopolymers 97:873-881.

Marcellini L, Borro M, Gentile G, Rinaldi AC, Stella L, Aimola P, Barra D, Mangoni ML (2009) **Esculentin-1b(1-18) a membrane-active antimicrobial peptide that synergizes with antibiotics and modifies the expression level of a limited number of proteins in *Escherichia coli***. The FEBS journal 276:5647-5664.

Marcil A, Harcus D, Thomas DY, Whiteway M (2002) ***Candida albicans* killing by RAW 264.7 mouse macrophage cells: effects of *Candida* genotype, infection ratios, and gamma interferon treatment**. Infect Immun 70:6319-6329.

Matsuzaki K, Murase O, Fujii N, Miyajima K (1996) **An antimicrobial peptide, magainin 2, induced rapid flip-flop of phospholipids coupled with pore formation and peptide translocation**. Biochemistry 35:11361-11368.

Matsuzaki K, Sugishita K, Miyajima K (1999) **Interactions of an antimicrobial peptide, magainin 2, with lipopolysaccharide-containing liposomes as a model for outer membranes of gram-negative bacteria**. FEBS Lett 449:221-224.

Mayer FL, Wilson D, Hube B (2013) ***Candida albicans* pathogenicity mechanisms**. Virulence 4:119-128.

McGhee JD (2007) **The *C. elegans* intestine**. WormBook 27 March: 1-36.

Mehla J, Sood SK (2011) **Substantiation in Enterococcus faecalis of dose-dependent resistance and cross-resistance to pore-forming antimicrobial peptides by use of a polydiacetylene-based colorimetric assay**. Appl Environ Microbiol 77:786-793.

Midorikawa K, Ouhara K, Komatsuzawa H, Kawai T, Yamada S, Fujiwara T, Yamazaki K, Sayama K, Taubman MA, Kurihara H, Hashimoto K, Sugai M (2003) ***Staphylococcus aureus* susceptibility to innate antimicrobial peptides, beta-defensins and CAP18, expressed by human keratinocytes**. Infect Immun 71:3730-3739.

Miller SI, Ernst RK, Bader MW (2005) **LPS, TLR4 and infectious disease diversity**. Nat Rev Microbiol 3:36-46.

Moreau-Marquis S, Stanton BA, O'Toole GA (2008) ***Pseudomonas aeruginosa* biofilm formation in the cystic fibrosis airway**. Pulm Pharmacol Ther 21:595-599.

Moy TI, Ball AR, Anklesaria Z, Casadei G, Lewis K, Ausubel FM (2006) **Identification of novel antimicrobials using a live-animal infection model**. Proc Natl Acad Sci 103:10414-10419.

Mylonakis E, Aballay A (2005) **Worms and flies as genetically tractable animal models to study host-pathogen interactions**. Infect Immun 73:3833-3841.

Mylonakis E, Ausubel FM, Perfect JR, Heitman J, Calderwood SB (2002) **Killing of *Caenorhabditis elegans* by *Cryptocossus neoformans* as a model of yeast pathogenesis**. Proc Natl Acad Sci USA 99:15675-15680.

Neuhaus FC, Baddiley J (2003) **A continuum of anionic charge: structures and functions of D-alanyl-teichoic acids in gram-positive bacteria**. Microbiol Mol Biol Rev 67:686-723.

Nicolas P, El Amri C (2009) **The dermaseptin superfamily: a gene-based combinatorial library of antimicrobial peptides**. Biochim Biophys Acta 1788:1537-1550.

Nikaido H, Nakae T (1979) **The outer membrane of Gram-negative bacteria**. Adv Microb Physiol 20:163-250.

Nikaido H, Vaara M (1985) **Molecular basis of bacterial outer membrane permeability**. Microbiol Rev 49:1-32.

Nizet V in **Antimicrobial Peptides in Human Health and Disease** (ed. Gallo RL) 277-304 (Horizon Bioscience, Norfolk, 2005).

Odds FC (1987) ***Candida* infections: an overview**. Crit Rev Microbiol 15:1-5.

Oren Z, Lerman JC, Gudmundsson GH, Agerberth B, Shai Y (1999a) **Structure and organization of the human antimicrobial peptide LL-37 in phospholipid membranes: relevance to the molecular basis for its non-cell-selective activity**. Biochem J 341:501-513.

Oren Z, Hong J, Shai Y (1999b) **A comparative study on the structure and function of a cytolytic alpha-helical peptide and its antimicrobial beta-sheet diastereomer**. Eur J Biochem 259:360-369.

Oren Z, Shai Y (1996) **A class of highly potent antibacterial peptides derived from pardaxin, a pore-forming peptide isolated from Moses sole fish *Pardachirus marmoratus***. Eur J Biochem 237:303-310.

Peschel A (2002) **How do bacteria resist human antimicrobial peptides?** Trends Microbiol 10:179-186.

Peschel A, Jack RW, Otto M, Collins LV, Staubitz P, Nicholson G, Kalbacher H, Nieuwenhuizen WF, Jung G, Tarkowski A, van Kessel KP, van Strijp JA (2001) ***Staphylococcus aureus* resistance to human defensins and evasion of neutrophil killing via the novel virulence factor MprF is based on modification of membrane lipids with l-lysine**. J Exp Med 193:1067-1076.

Phillips AJ, Sudbery I, Ramsdale M (2003) **Apoptosis induced by environmental stresses and amphotericin B in *Candida albicans***. Proc Natl Acad Sci 100:14327-14332.

Pokorny A, Birkbech TH, Almeida PF (2002) **Mechanism and kinetics of delta-lysin interaction with phospholipid vesicles**. Biochemistry 41:11044-11056.

Ponti D, Mangoni ML, Mignogna G, Simmaco M, Barra D (2003) **An amphibian antimicrobial peptide variant expressed in *Nicotiana tabacum* confers resistance to phytopathogens**. Biochem J 370:121-127.

Ponti D, Mignogna G, Mangoni ML, De Biase D, Simmaco M, Barra D (1999) **Expression and activity of cyclic and linear analogues of esculentin-1, an anti-microbial peptide from amphibian skin**. Eur J Biochem 263:921-927.

Pouny Y, Rapaport D, Mor A, Nicolas P, Shai Y (1992) **Interaction of antimicrobial dermaseptin and its fluorescently labeled analogues with phospholipid membranes**. Biochemistry 31:12416-12423.

Rampioni G, Schuster M, Greenberg EP, Bertani I, Grasso M, Venturi V, Zennaro E, Leoni L (2007) **RsaL provides quorum sensing homeostasis and functions as a global regulator of gene expression in *Pseudomonas aeruginosa***. Mol Microbiol 66:1557-1565.

Rinaldi AC (2002) **Antimicrobial peptides from amphibian skin: an expanding scenario**. Curr Opin Chem Biol 6:799-804.

Roice M, Suma G, Kumar KS, Pillai VN (2001) **Synthesis of esculentin-1 antibacterial peptide fragments on 1,4-butanediol dimethacrylate cross-linked polystyrene support**. J Protein Chem 20:25-32.

Rosenfeld Y, Barra D, Simmaco M, Shai Y, Mangoni ML (2006a) **A synergism between temporins towards Gram-negative bacteria overcomes resistance imposed by the lipopolysaccharide protective layer**. 281:28565-28574.

Rosenfeld Y, Papo N, Shai Y (2006b) **Endotoxin (lipopolysaccharide) neutralization by innate immunity host-defense peptides. Peptide properties and plausible modes of action**. J Biol Chem 281:1636-1643.

Saville SP, Lazzell AL, Monteagudo C, Lopez-Ribot JL (2003) **Engineered control of cell morphology *in vivo* reveals distinct roles for yeast and filamentous forms of *Candida albicans* during infection**. Eukaryot Cell 2:1053-1060.

Segura A, Moreno M, Molina A, Garcia-Olmedo F (1998) **Novel defensin sub family from spinach (*Spinacia oleracea*)**. FEBS Lett 435:159-162.

Shafer WM, Qu X, Waring AJ, Lehrer RI (1998) **Modulation of *Neisseria gonorrhoeae* susceptibility to vertebrate antibacterial peptides due to a member of the resistance/nodulation/division efflux pump family**. Proc Natl Acad Sci U S A 95:1829-1833.

Shai Y (2002) **Mode of action of membrane active antimicrobial peptides**. Biopolymers 66:236-248.

Sharkey LL, McNemar MD, Saporito-Irwin SM, Sypherd PS, Fonzi WA (1999) **HWP1 functions in the morphological development of**

Candida albicans **downstream of EFG1, TUP1, and RBF1**. J Bacteriol 181:5273-5279.

Sifri CD, Begun J, Ausubel FM (2005) **The worm has turned-microbial virulence modeled in *Caenorhabditis elegans***. Trends Microbiol 13:119-127.

Sifri CD, Begun J, Ausubel FM, Calderwood SB (2003) ***Caenorhabditis elegans*** **as a model host for *Staphylococcus aureus* pathogenesis**. Infect Immun 71:2208-2217.

Simmaco M, Mignogna G, Barra D (1998) **Antimicrobial peptides from amphibian skin: what do they tell us?** Biopolymers 47:435-450.

Simmaco M, Mignogna G, Barra D, Bossa F (1993) **Novel antimicrobial peptides from skin secretion of the European frog *Rana esculenta***. FEBS Lett 324:159-161.

Simmaco M, Mignogna G, Barra D, Bossa F (1994) **Antimicrobial peptides from skin secretions of Rana esculenta. Molecular cloning of cDNAs encoding esculentin and brevinins and isolation of new active peptides**. J Biol Chem 269:11956-11961.

Sood R, Kinnunen PK (2008) **Cholesterol, lanosterol, and ergosterol attenuate the membrane association of LL-37(W27F) and temporin L**. Biochim Biophys Acta 1778:1460-1466.

Stephens C (2002) **Microbiology: breaking down biofilms**. Curr Biol 12:132-134.

Stiernagel T (2006) **Maintenance of *C. elegans***. Wormbook, ed. The *C. elegans* Research Community, Wormbook. doi/10.895/wormbook.1.101.1. http://www.wormbook.org 11 Feb 2006.

Strahilevitz J, Mor A, Nicolas P, Shai Y (1994) **Spectrum of antimicrobial activity and assembly of dermaseptin-b and its precursor form in phospholipid membranes**. Biochemistry 33:10951-10960.

Sudbery PE (2011) **Growth of *Candida albicans* hyphae**. Nat Rev Microbiol 9:737-748.

Suh J, Hutter H (2012) **A survey of putative secreted and transmembrane proteins encoded in the *C. elegans* genome**. BMC Genomics 13:333.

Torrent M, Valle J, Nogués MV, Boix E, Andreu D (2011) **The generation of antimicrobial peptide activity: a trade-off between charge and aggregation?** Angew Chem Int Ed Engl 50:10686-10689.

Tzeng YL, Ambrose KD, Zughaier S, Zhou X, Miller YK, Shafer WM, Stephens DS (2005) **Cationic antimicrobial peptide resistance in *Neisseria meningitidis***. J Bacteriol 187:5387-5396.

Uccelletti D, Zanni E, Marcellini L, Palleschi C, Barra D, Mangoni ML (2010) **Anti-*Pseudomonas* activity of frog skin antimicrobial peptides in a *Caenorhabditis elegans* infection model: a plausible mode of action *in vitro* and *in vivo***. Antimicrob Agents Chemother 54:3853-3860.

Utsugi T, Schroit AJ, Connor J, Bucana CD, Fidler IJ (1991) **Elevated expression of phosphatidylserine in the outer membrane leaflet of**

human tumor cells and recognition by activated human blood monocytes. Cancer Res 51:3062-3066.

Weidenmaier C, Kokai-Kun JF, Kristian SA, Chanturiya T, Kalbacher H, Gross M, Nicholson G, Neumeister B, Mond JJ, Peschel A (2004) **Role of teichoic acids in *Staphylococcus aureus* nasal colonization, a major risk factor in nosocomial infections**. Nat Med 10:243-245.

Williams RW, Starman R, Taylor KM, Gable K, Beeler T, Zasloff M, Covell D (1990) **Raman spectroscopy of synthetic antimicrobial frog peptides magainin 2a and PGLa**. Biochemistry 29:4490-4496.

Yeaman MR, Yount NY (2003) **Mechanisms of antimicrobial peptide action and resistance**. Pharmacol Rev 55:27-55.

Younsi M, Ramanandraibe E, Bonaly R, Donner M, Coulon J (2000) **Amphotericin B resistance and membrane fluidity in *Kluyveromyces lactis* strains**. Antimicrob Agents Chemother 44:1911-1916.

Zasloff M (2002) **Antimicrobial peptides of multicellular organisms**. Nature 415:389-395.

ACKNOWLEDGMENTS

Voglio ringraziare, innanzitutto, la Prof.ssa Maria Luisa Mangoni per avermi dato l'opportunità di lavorare nel suo gruppo, per avermi fatto crescere scientificamente, per aver riposto in me tanta fiducia e per essere stata un grande maestro.

Vorrei fare un ringraziamento particolare alla Prof.ssa Donatella Barra per aver avuto fiducia in me, spronandomi ad andare sempre avanti senza demoralizzarmi mai.

Ringrazio Antonio, Bruno e Floriana per essere stati parte importante e produttiva del gruppo di lavoro, con i quali ho condiviso momenti belli o difficili di laboratorio e di vita.

Ringrazio i miei genitori e tutta la mia famiglia per la pazienza che hanno sempre avuto e per essere stati comprensivi nei momenti difficili.

Un grazie affettuoso va a Giovanni e Rosalinda, per essere stati sempre presenti, per aver condiviso con me tante emozioni importanti e per essere stati ottimi confidenti di vita.

APPENDIX - REPRINT OF PAPERS

Eur Biophys J (2011) 40:577–588
DOI 10.1007/s00249-011-0681-8

ORIGINAL PAPER

Membrane interaction and antibacterial properties of two mildly cationic peptide diastereomers, bombinins H2 and H4, isolated from *Bombina* skin

Cristina Coccia · Andrea C. Rinaldi · Vincenzo Luca · Donatella Barra · Argante Bozzi · Antonio Di Giulio · Enno C. I. Veerman · Maria Luisa Mangoni

Received: 1 November 2010 / Revised: 11 January 2011 / Accepted: 27 January 2011 / Published online: 17 February 2011

Abstract Bombinins H are mildly cationic antimicrobial peptides isolated from the skin of the anuran genus *Bombina*, the fire-bellied toad. Some members of this peptide family coexist in skin secretions as diastereomers in which a single D-amino acid (alloisoleucine or leucine) is incorporated as a result of the post-translational modification of the respective gene-encoded L-amino acid. Here we report on the antimicrobial properties and membrane interactions of bombinins H2 and H4. The latter differs from H2 by the presence of a D-alloisoleucine at the second N-terminal position. Specifically, we have evaluated the antimicrobial activity of H2 and H4 against a large panel of reference and clinical isolates of Gram-negative and Gram-positive bacteria; performed membrane permeation assays on both intact cells and model membranes (lipid monolayers and liposomes) mimicking the composition of the plasma membrane of Gram-negative/positive bacteria; used biochemical tools, such as trypsin-encapsulated liposomes and capillary electrophoresis, to monitor the peptides' ability to translocate through the membrane of liposomes mimicking *Escherichia coli* inner membrane. The results revealed interesting relationships between the presence of a single D-amino acid in the sequence of an antimicrobial peptide and its target microbial cell selectivity/membrane-perturbing activity.

Keywords Bombinins H · Antimicrobial peptides · Peptide-membrane interaction · Liposomes · Capillary electrophoresis · Frog skin

Abbreviations

AMP	Antimicrobial peptide
CD	Circular dichroism
CFU	Colony-forming units
CL	Cardiolipin
CZE	Capillary zone electrophoresis
FITC-D4/D20/D70	Fluorescein isothiocyanate-dextrans of 4, 20, and 70 kDa average molecular mass, respectively
LPS	Lipopolysaccharide
MHB	Mueller-Hinton broth
MIC	Minimum inhibitory concentration
PBS	Phosphate-buffered saline
PE	L-α-phosphatidylethanolamine
PG	L-α-phosphatidyl-DL-glycerol
SBTI	Soybean trypsin inhibitor
SDS	Sodium-dodecyl sulphate
SPB	Sodium phosphate buffer, pH 7.4 with 0.1 mM EDTA

Membrane-active peptides: 455th WE-Heraeus-Seminar and AMP 2010 Workshop.

C. Coccia · A. Bozzi · A. Di Giulio
Dipartimento di Scienze e Tecnologie Biomediche, Università de L'Aquila, 67010 L'Aquila, Italy

A. Bozzi
Istituto Nazionale di Biostrutture e Biosistemi, Rome, Italy

A. C. Rinaldi
Dipartimento di Scienze e Tecnologie Biomediche, Università di Cagliari, 09042 Monserrato, Italy

V. Luca · D. Barra · M. L. Mangoni (✉)
Istituto Pasteur-Fondazione Cenci Bolognetti, Dipartimento di Scienze Biochimiche, "A. Rossi Fanelli", Università La Sapienza, Piazzale Aldo Moro, 5, 00185 Rome, Italy
e-mail: marialuisa.mangoni@uniroma1.it

E. C. I. Veerman
Department of Dental Basic Sciences, Section Oral Biochemistry, Academic Centre for Dentistry Amsterdam, Amsterdam, The Netherlands

Introduction

Naturally occurring gene-encoded antimicrobial peptides (AMPs) are an extremely diverse group of anti-infective molecules whose function is crucial for the host immune response (Boman 2003; Ganz 2003; Giuliani and Rinaldi 2010; Selsted and Ouellette 2005). Besides being key components of the innate immune system of all living organisms, rapidly killing a broad spectrum of microbes, they interact with the host itself, triggering events (e.g., anti-endotoxin activity, chemotactic activity) that complement their role as antibiotics (Beisswenger and Bals 2005; Hancock and Diamond 2000).

Furthermore, the mechanism of action of the majority of AMPs is based on the permeation of the microbial cell membrane, causing damage that is hard to fix (Mangoni et al. 2007). This limits the induction of microbial resistance to AMPs and makes them attractive molecules for the development of alternative anti-infective agents (Easton et al. 2009). The search for new therapeutics is strongly required because of the growing emergence of resistant pathogens to the commercially available antibiotics/antimycotics, most of which interfere with intracellular processes (Yeaman and Yount 2003). Although AMPs do possess a wide variety of structural and conformational features, many of them share selected properties such as being usually cationic at neutral pH, and displaying the tendency to form amphipathic structures upon interacting with the membrane of the pathogen (Dempsey et al. 2010; Shai 1999).

Among the natural sources for peptide antibiotics, the granular glands of amphibian skin constitute one of the richest storehouses (Rinaldi 2002; Simmaco et al. 1998). An interesting and unique family of AMPs is the short and mildly cationic bombinins H, from the skin secretion of *Bombina* genus, the fire-bellied toad (Simmaco et al. 2009). Their existence was predicted from the sequence of the bombinin precursors, obtained via cDNA cloning (Gibson et al. 1991; Simmaco et al. 1991). Bombinins H are 17–20 residue AMPs with an amidated C-terminus (Mangoni et al. 2000). However, their most surprising feature is the presence of a D-amino acid (alloisoleucine or leucine) at the second N-terminal position in some of them, as a consequence of post-translational modification (there is no codon for a D-amino acid) of the respective gene-encoded L-isoleucine or L-leucine (Kreil 1994; Mor et al. 1992). During this reaction, the chirality of the α-carbon is changed and the enzyme responsible for this L- to D-isomerization has been purified and characterized from the skin secretions of *B. variegata* (Jilek et al. 2005).

The discovery of a D-amino acid in ribosomally synthesized peptides of animal origin first occurred in the opioid skin peptides dermorphins and delthorphins from the South American frogs *Phyllomedusa sauvagei* and *P. bicolour* (Erspamer et al. 1989; Montecucchi et al. 1981), and later in other neuropeptides and toxins from invertebrates (Buczek et al. 2005; Kamatani et al. 1989; Kreil 1997; Kuwada et al. 1994; Torres et al. 2002). However, bombinins H are the first example of natural AMPs with a single D-amino acid in their sequence. Furthermore, in contrast with opioid peptides, the D-amino acid–containing AMPs coexist with their all-L counterparts.

In this paper, we focussed our attention on a pair of bombinins H: the all L-peptide H2 (IIGPVLGLVGS ALGGLLKKI-NH_2) and its diastereomer H4, which differs from H2 by the presence of a D-alloisoleucine in position 2. Both peptides have a +3 net charge at pH 7. Previous studies on their antimicrobial properties in agar medium revealed a stronger activity for the D-amino acid–containing bombinin H4. In addition, mode of action studies pointed out that both peptides are capable of permeating the membrane of Gram-negative bacteria, causing the release of large cytosolic components, such as the *β*-galactosidase, with H4 having a faster killing kinetic (Mangoni et al. 2000). In order to enlarge our knowledge on the anti-infective properties of these two compounds and to explore whether the mechanism underlying their different antimicrobial activity is related to a different ability to permeate the microbial cell membrane, the following experiments were performed: (1) antimicrobial assays to determine the minimum inhibitory concentration (MIC) value on a large panel of reference and clinical isolates of Gram-negative and Gram-positive bacteria; (2) membrane permeation assays on both intact cells and model membranes (lipid monolayers and liposomes) mimicking the composition of the plasma membrane of Gram-negative/positive bacteria; (3) biochemical assays, using trypsin-encapsulated liposomes and capillary electrophoresis, to monitor the peptides' ability to translocate through the membrane of liposomes mimicking the *Escherichia coli* inner membrane.

Although more quantitative information should be obtained in the future, considering simulation of peptide dynamics in lipid membranes as well, an interesting relationship between the target cell selectivity/membrane-perturbing activity and the presence of a single D-amino acid in the sequence of an AMP has emerged from these investigations.

Materials and methods

Materials

Synthetic bombinins H2 and H4 were purchased from GENEPEP (Prades-le-Lez, France). The purity of the

peptides, their sequence and concentrations were determined as previously described (Mangoni et al. 2000). L-α-phosphatidylethanolamine (PE), L-α-phosphatidyl-DL-glycerol (PG), cardiolipin (CL), fluorescein isothiocyanate dextrans of 4, 20, and 70 kDa average molecular mass (FITC-D4/D20/D70), calcein, ammonium thiocyanate, and iron (III) chloride hexahydrate were obtained from Sigma. Trypsin (EC 3.4.21.4, sequencing grade) was purchased from Roche Diagnostics, Mannheim, Germany. Soybean trypsin inhibitor (SBTI) was obtained from ICN Biomedicals (Irvine, CA, USA). Imidazole was purchased from Merck (Whitehouse Station, NJ, USA). SYTOX^{TM} Green was from Molecular Probes (Invitrogen, Carlsbad, CA, USA). All other chemicals used were of reagent grade.

Microorganisms

The following bacteria were used for the microbiological assays. Gram-negatives: *Acinetobacter baumannii* ATCC 19606, *A. baumannii* 1 (clinical isolate), *Escherichia coli* D21, *E. coli* O111:B4, *E. coli* ATCC 25922, *Pseudomonas aeruginosa* 3 (clinical isolate), *P. aeruginosa* ATCC 27853, and *Yersinia pseudotuberculosis* YPIII. Gram-positives: *Staphylococcus aureus* ATCC 29213, *S. aureus* Cowan I, *S. epidermidis* ATCC 12228 and the clinical isolates *S. aureus* 8, *S. aureus* 43300, *S. aureus* 11270, *S. capitis* n.1, *S. epidermidis* 18, and *Enterococcus faecalis* 9546.

Antibacterial activity of the peptides

Susceptibility testing of peptides was performed by adapting the microbroth dilution method outlined by the Clinical and Laboratory Standards Institute (CLSI 2006), using sterile 96-well plates (Falcon, Franklin Lakes, NJ, USA). Stock solutions of peptides were prepared in serial twofold dilutions in 20% ethanol; 5 µl was then added to 45 µl of Mueller-Hinton broth (MHB; Oxoid, Cambridge, UK), previously put into the wells of the microtiter plate. Afterwards, aliquots (50 µl) of bacteria in mid-log phase, at a concentration of 2×10^6 colony-forming units (CFU)/ml, were added to each well. The range of peptide dilutions used was 1.56–50 µM. Inhibition of growth was determined by measuring the absorbance at 595 nm with a microplate reader (Infinite M200, Tecan, Salzburg, Austria) after 18–20 h incubation at 37°C. Antibacterial activities were expressed as MIC, the minimum concentration of peptide causing 100% inhibition of bacterial growth.

Bactericidal activity

The bactericidal activity of H2 and H4 against the Gram-positive *S. aureus* ATCC 29213 and *S. aureus* Cowan I was evaluated as previously described (Mangoni et al. 2008). Briefly, exponentially growing bacteria in MHB were harvested by centrifugation and then resuspended in fresh MHB or phosphate-buffered saline (PBS) to obtain a density of 1×10^7 CFU/ml. Ten µl of the bacterial suspension was incubated at 37°C for 90 min in the presence of different concentrations of peptide (serial twofold dilutions ranging from 6.25 to 50 µM) dissolved in MHB or PBS, to a final volume of 100 µl.

Following incubation, appropriate aliquots were plated onto Luria-Bertani agar plates to accurately determine the 99.9% killing. The number of surviving bacteria was counted after overnight incubation at 37°C. Bactericidal activity was expressed as the peptide concentration necessary to induce a reduction in the number of viable bacteria of ≥ 3 $\log_{10}$ CFU/ml (Maisetta et al. 2006). Controls were run without peptide and in the presence of peptide solvent (20% ethanol) at a final concentration of 1%.

Bacterial membrane permeabilization

To assess the ability of bombinins H to alter the bacterial membrane permeability, 1×10^6 cells in 100 µl of PBS were mixed with 1 µM SYTOX^{TM} Green for 5 min in the dark. After adding peptide, the increase in fluorescence, due to the binding of the dye to intracellular DNA, was measured at 37°C in the microplate reader (excitation and emission wavelengths were 485 and 535 nm, respectively). The peptide concentrations ranged from 3.125 to 50 µM. Controls were given by cells without peptide, whereas the maximum membrane perturbation was obtained after lysing bacteria in 1% (v/v) Triton X-100.

Measurement of penetration of bombinins H2 and H4 in lipid monolayers

Insertion of H2 and H4 into monolayers formed of either PE/PG (7:3, w/w) and PG/CL (6:4, w/w) was evaluated as an indication of the peptides' ability to bind and penetrate microbial targets' plasma membranes. To this end, lipid mixtures in chloroform were spread at an air/buffer (50 mM potassium phosphate, pH 7, with 0.1 mM EDTA) interface, and penetration was monitored by measuring surface pressure (π) with a Wilhelmy wire attached to a microbalance (DeltaPi, Kibron, Helsinki) connected to a PC and using circular glass wells (subphase volume 0.5 ml). After evaporation of lipid solvent and stabilization of monolayers at different initial surface pressures (π_0), the peptide (1 µM, final concentration) was injected into the subphase, and the increment in surface pressure of the lipid film upon intercalation of the peptide dissolved in the subphase was followed for the next 35 min. The difference between the initial surface pressure and the value observed

after the penetration of bombinins H into the film was taken as $\Delta\pi$. Surface activity of H2 and H4 at the air/buffer interface was also evaluated in the absence of lipids, by injecting increasing amounts of the peptide into the subphase and measuring the variation of π_0 with time. All measurements were performed at room temperature.

Preparation of calcein/dextran-loaded liposomes and leakage measurement

Calcein-loaded liposomes of different compositions (PE/PG, 7:3 w/w and PG/CL, 6:4 w/w) were prepared as previously described (Rinaldi et al. 2002). Briefly, phospholipids were dissolved in chloroform and mixed with a calcein solution (60 mM in phosphate buffer, pH 7.0). The mixture was then sonicated until becoming homogeneous.

Liposomes were prepared by reverse phase evaporation (Szoka and Papahadjopoulos 1978). Free calcein was removed through gel filtration (Sephadex G-50), with a 1.5 × 15 cm column, equilibrated and eluted with 50 mM potassium phosphate buffer, pH 7.4 containing 0.1 mM EDTA. The lipid concentration was determined by the Stewart method (Stewart 1980). Calcein loaded in liposomes is self-quenched (Allen 1981) and its leakage was monitored as a relief of quenching (excitation and emission wavelengths were 490 and 517 nm, respectively) with a Perkin-Elmer LS 55B spectrofluorimeter. The maximum fluorescence intensity corresponding to 100% calcein release was determined by addition of Triton X-100 (0.2%, v/v, final concentration), which produced the total destruction of the vesicles. The leakage value was calculated according to the equation:

$$\text{Leakage}\,(\%) = 100 \times (F - F_0)/(F_t - F_0)$$

where F and F_t denote the fluorescence intensity before and after the addition of the detergent, respectively, and F_0 represents the fluorescence of intact vesicles.

Liposomes loaded with FITC-D4/D20/D70 were prepared as reported elsewhere (Rinaldi et al. 2001). The release of dextran from loaded vesicles upon interaction with bombinin H2 and H4 was examined fluorimetrically; excitation and emission wavelengths were 494 and 520 nm, respectively. In a typical experiment, an aliquot of the peptide solution in 20% (v/v) ethanol was incubated with a suspension of dextran-loaded vesicles in 50 mM buffer (sodium phosphate, pH 7.4 with 0.1 mM EDTA, SPB), at a final lipid concentration of 50 μM. The mixture (2 ml, final volume) was stirred gently for 10 min in the dark and centrifuged at 27,000*g* for 30 min. The supernatant was recovered, and its fluorescence intensity was measured. The total dextran release was determined by the addition of 20 μl of 10% (v/v) Triton X-100 to the vesicle suspension. The leakage value was calculated as described above for calcein. All experiments were carried out at room temperature.

Preparation and degradation of peptides by trypsin-loaded liposomes

Trypsin-loaded liposomes were prepared from a 7:3 (w/w) mixture of PE and PG. The lipid mixture in chloroform was vacuum-dried and hydrated with 5 mM SPB containing 100 μg/ml trypsin, to a final lipid concentration of 2.5 mg/ml. After five cycles of freeze-thawing, liposomes were extruded 21 times through two stacked 400 nm filters, as described previously (MacDonald et al. 1991). Free trypsin was removed by gel filtration on a Sephadex G-50, 1.5 × 15 cm column, equilibrated and eluted with 5 mM SPB. Liposomes were stored at 4°C and used within 48 h. Trypsin-loaded liposomes were suspended in 5 mM SPB supplemented with 10 μg/ml of imidazole, an internal standard for capillary zone electrophoresis (CZE), and with or without 20 μg/ml of SBTI, at a lipid concentration of 250 μg/ml. The concentration of SBTI was sufficient to effectively inhibit all trypsin activity after liposomes were lysed by adding an aliquot of Triton X-100 (0.1% v/v, final concentration), as reported in Den Hertog et al. (2004). The suspension of lipid vesicles was subsequently incubated with 60 μM of each bombinin H or 40 μM of the control membrane-inactive peptide cystatin cysS1–15 (SSSKEENRIIPGGIY), corresponding to the first 15 N-terminal amino acids of cystatin S (Den Hertog et al. 2004). At different time intervals, 50 μl aliquots were withdrawn, boiled for 5 min to inhibit all trypsin activity, lysed in 0.1% Triton X-100, and analyzed by CZE. Degradation of peptides implied digestion, by trypsin, of the peptide internalized within the liposome.

Capillary zone electrophoresis

Purity and degradation of peptides was analyzed by CZE on a BioFocus 2000 Capillary Electrophoresis System (Bio-Rad, Hercules, CA, USA) equipped with an uncoated fused silica capillary of 50 μm internal diameter and a length of 24 cm. Samples were loaded by pressure injection at 20 lbf in^{-2} s^{-1} (where 1 lbf in^{-2} = 6.9 kPa), and peptide separation was performed according to the manufacturer's instructions at 10 kV (anode at the detector side) and 20°C, using 0.1 M phosphate buffer, pH 2.5, as the electrolyte. Online UV detection was performed at 200 nm. The running time of the analysis was 20 min, and data were analyzed using BioFocus Integrator software. The level of peptide degradation was quantified in the electropherogram by comparing the relevant peak heights of the sample with that of the internal standard imidazol.

Results

Antimicrobial activity

In our previous studies, the antimicrobial activity of H2 and H4 was tested on standard Gram-negative and Gram-positive bacterial strains using the inhibition zone assay in agar medium (Mangoni et al. 2000). Here, to deepen our understanding of the antibacterial activity of these two peptides, we analyzed their ability to inhibit the microbial growth in liquid medium, employing the commonly used serial twofold dilution method. This allowed us to determine the MIC values, as defined in the "Materials and methods" section. A large panel of standard and clinical isolates of Gram-negative and Gram-positive bacterial strains, most of which have not been studied previously, was investigated. The results are reported in Table 1. They indicated that bombinin H4 had the same or a higher activity than that of H2 against Gram-negative bacteria. In contrast, the opposite behavior was detected toward Gram-positive species, with bombinin H2 having a two- to fourfold lower MIC—and thus a stronger activity—than H4 against almost all of the tested microorganisms. Note that our previous data using the inhibition zone assay had shown a slightly higher activity of H4 than H2 against the Gram-positive *S. aureus* Cowan I (Mangoni et al. 2000).

Table 1 Antibacterial activity of bombinins H2 and H4 on selected bacterial strains

Bacterial strain	MIC (μM)	
	H2	H4
Gram-negative		
A. baumannii ATCC 19606	12.5	12.5
A. baumannii 1	50	12.5
E. coli D21	>50	>50
E. coli O111:B4	>50	50
E. coli ATCC 25922	>50	50
P. aeruginosa 3	>50	>50
P. aeruginosa ATCC 27853	>50	>50
Y. pseudotuberculosis YPIII	12.5	12.5
Gram-positive		
E. faecalis 9546	>50	>50
S. aureus ATCC 29213	12.5	25
S. aureus Cowan I	12.5	50
S. aureus n.8	>50	>50
S. aureus 11270	12.5	50
S. aureus 43300	12.5	50
S. capitis n. 1	12.5	25
S. epidermidis ATCC 12228	12.5	12.5
S. epidermidis n.18	>50	>50

This could be due to a different solubility and diffusion of the peptides through a solid medium.

We next examined the bactericidal activity of the two diastereomers against some representative Gram-positive bacterial strains (i.e., *S. aureus* ATCC 29213 and *S. aureus* Cowan I), by counting the number of viable cells after 90 min of incubation with the peptide, in both MHB and PBS. Specifically, PBS was used to assay the bactericidal activity of bombinins H in a medium whose ionic strength (150 mM sodium salt compared to 100 mM of MHB) was closer to that of biological fluids (Li et al. 2003). Surprisingly, both peptides caused 99.9% killing of the microbial population at the same concentration (Table 2). When tested in MHB, the two diastereomers displayed a bactericidal activity at 50 μM (Table 2), a peptide concentration fourfold higher than the corresponding MICs of H2, and equal or twofold higher the MIC, in the case of H4 (Table 1). When tested in PBS, both peptides were found to be more active, with a bactericidal activity at 12.5 and 25 μM, against *S. aureus* ATCC 29213 and *S. aureus* Cowan I, respectively. Interestingly, these two peptide concentrations were equal or twofold higher than the corresponding MICs of H2 on these two strains, but they were twofold lower than the MICs of H4 (Table 1).

Mode of action studies on intact cells

As mentioned above, previous reports had emphasized the ability of these two bombinins H to permeate the membrane of Gram-negative bacteria with a stronger effect for the D-amino acid–containing peptide H4 (Mangoni et al. 2000).

Here, the activity of the two diastereomers on the membrane permeability of Gram-positive bacteria, such as *S. aureus* ATCC 29213, was studied by measuring the intracellular influx of SYTOX^{TM} Green (Fig. 1). This cationic dye (mw ≈ 600), which is excluded by intact membranes but not by those having lesions of a size large enough to allow its entrance (Marcellini et al. 2009), dramatically increases its fluorescence when bound to

Table 2 Bactericidal activity of bombinins H2 and H4 on two *S. aureus* strains in MHB and PBS

Bacterial strain	Peptide	Bactericidal activity[a]	
		MHB	PBS
S. aureus ATCC 29213	H2	50	12.5
	H4	50	12.5
S. aureus Cowan I	H2	50	25
	H4	50	25

[a] The bactericidal activity is expressed as the concentration of peptide (μM) that is sufficient to reduce the number of viable bacteria of ≥3 $\log_{10}$ CFU/ml after 90 min of incubation

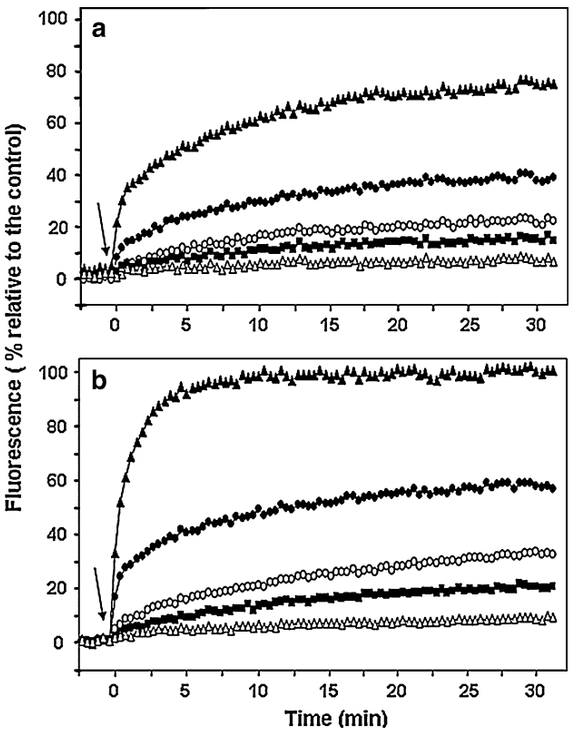

Fig. 1a, b Effect of bombinins H2 and H4 on the membrane permeation of *S. aureus* ATCC 29213. Cells (1×10^7 CFU/ml) were incubated with 1 μM SYTOX™ Green in PBS. Once basal fluorescence reached a constant value, the peptide was added (*arrow*, $t = 0$) and changes in fluorescence were monitored ($\lambda_{exc} = 485$ nm, $\lambda_{ems} = 535$ nm) and plotted as the percentage of fluorescence relative to that of bacteria fully permeated by the addition of Triton X-100 (1%, v/v, final concentration). All readings were normalized by subtracting fluorescence values of control (bacteria without peptide). Data points represent the average values of three independent experiments, with SD not exceeding 5%. Peptide concentrations used for bombinin H2 (**a**) and H4 (**b**) were as follows: 3.125 μM (*open triangle*), 6.25 μM (*filled square*), 12.5 μM (*open circle*), 25 μM (*filled circle*), and 50 μM (*filled triangle*)

intracellular nucleic acids. As indicated in Fig. 1b, bombinin H4 augmented the membrane's permeability to SYTOX™ Green to a larger extent with respect to H2 (Fig. 1a). In addition, H4 caused the complete alteration of the plasma membrane's structure, at 2 × MIC (Fig. 1b). Conversely, in the case of bombinin H2 (Fig. 1a), a peptide concentration fourfold higher than the MIC was not enough to completely disintegrate the membrane.

Mode of action studies on model membranes

Peptide insertion into PE/PG and PG/CL monolayers

Monomolecular lipids have been increasingly used as suitable model systems to analyze the interaction of peptides (and proteins) with biological membranes (Brockman 1999; Maget-Dana 1999; Zhao and Kinnunen 2002). We therefore used PE/PG (7:3, w/w) and PG/CL (6:4, w/w) monolayers to mimic the lipid composition of the bacterial plasma membrane of the Gram-negative *E. coli* and the Gram-positive *S. aureus*, respectively (Epand and Epand 2009).

The surface activity of H2 and H4, recorded in the absence of lipids, is shown in Fig. 2. Both peptides were found to be highly surface active, with surface pressure rising rapidly with increasing peptide concentration. Maximum surface pressure reached 30.4 and 33.9 mN/m for H2 and H4, respectively, at a peptide concentration of 2 μM. Of note, H4 was always found to be more surface active than H2, especially at lower peptide concentrations.

Bombinins H2 and H4 efficiently and readily penetrated into PG/CL and PE/PG monolayers, as demonstrated by the increase in film surface pressure (Fig. 3a, b).

Through analysis of measurements in terms of $\Delta\pi$ versus π_0, the critical surface pressure corresponding to the lipid lateral packing density preventing the intercalation of H2 and H4 into the PG/CL film could be derived by extrapolating the $\Delta\pi - \pi_0$ slope to $\Delta\pi = 0$, giving a value $\approx$43 mN/m for both peptides (Fig. 3a). In the case of the PE/PG monolayer, this value increased to 44 and 47 mN/m for H2 and H4, respectively (Fig. 3b). It is well appreciable that in the case of both PE/PG and PG/CL films, H4 displayed a constantly stronger intercalation activity with respect to H2, although this difference was not dramatic. Such differences were not found when the intercalation of H2 and H4 was tested in neutral dipalmitoylphosphatidylcholine (DPPC) monolayers (data not shown), showing that the lipid composition of the model

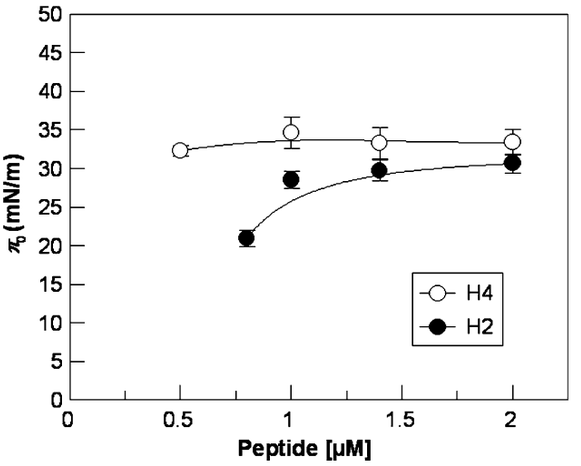

Fig. 2 The surface activity of bombinins H2 and H4. The adsorption of peptides at the air/buffer (potassium phosphate 50 mM, pH 7, with 0.1 mM EDTA) interface was monitored as increasing surface pressure (π_0) over time. The maximum values of these surface pressures were plotted against peptide's final subphase concentration. Values are means ± SD of three independent measurements

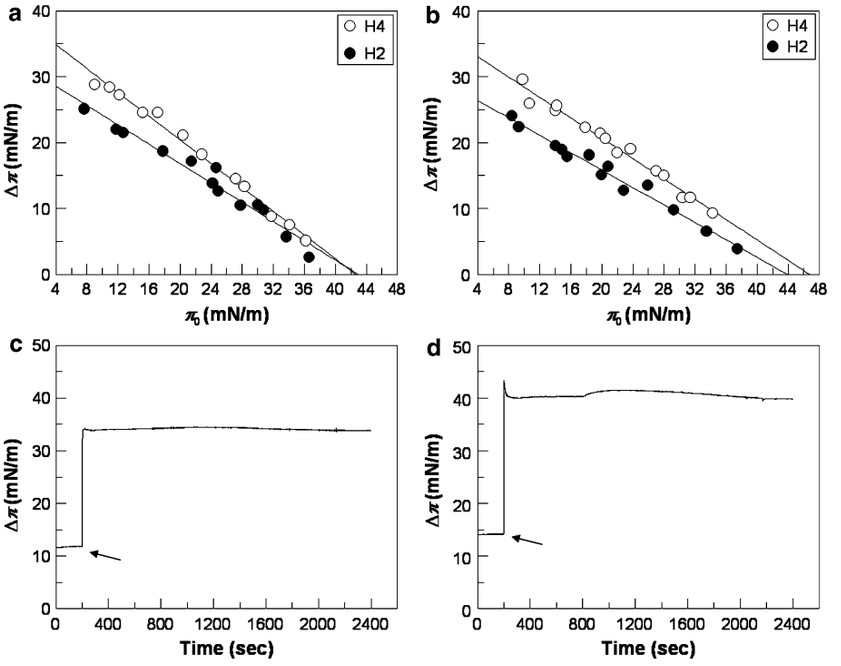

Fig. 3a–d Insertion of H2 and H4 into lipid monolayers. Increments of surface pressure of PG/CL (**a**) and PE/PG (**b**) monolayers due to the addition of 1.0 μM H2 and H4 into the subphase are illustrated as a function of initial surface pressure. Typical kinetics of surface pressure increase related to H2 penetration into a PG/CL film (**c**; $\pi_0 = 11.8$, with 1.0 μM peptide) and of H4 into a PE/PG monolayer (**d**; $\pi_0 = 14.2$, with 1.0 μM peptide) are shown as representative of general trends. *X*-axis shows elapsed time (s). Peptide injection into the subphase took place at ≈200 s (*arrow*)

membrane drove the different behavior of H2 and H4, and that the stronger film intercalation activity detected for H4 was not (only) due to its inherently greater surface activity. The kinetics of the insertion of the peptides into lipid monolayers was also analyzed and found to be comparable for both H2 and H4 and both monolayer compositions (Fig. 3c, d). In general, the kinetics were characterized by a very fast initial peptide intercalation subsequent to the peptide's injection into the subphase, followed by a rather stable value of π, with a few signs of relaxation or peptide's reorganization. This general kinetics pattern was apparently independent from the specific peptide tested and from initial surface pressure (Fig. 3c, d).

The very rapid kinetics of intercalation recorded resembles that found previously for the frog skin-derived AMP temporins (Zhao and Kinnunen 2002) and fits well with the strong surface activity of bombinins H, as discussed above.

Peptide-induced liposome permeabilization

The ability of H2 and H4 to destabilize bacterial membranes by a nonstereospecific process was confirmed by employing calcein-loaded PE/PG and PG/CL liposomes.

Different concentrations of each peptide were added to a suspension of lipid vesicles (50 μM final lipid concentration), and membrane permeabilization was monitored by following fluorescence recovery due to calcein leakage from the liposomes. Figure 4 (panels a and c) shows the kinetics and the dose-response of peptide-induced calcein release from PE/PG liposomes. The data highlighted a comparable membrane-perturbing activity for both bombinins H with a slightly stronger effect for the isoform H4, at a peptide concentration range of 1–2.5 μM. For both peptides, the vesicle-permeabilization activity increased in a concentration-dependent manner and reached the maximum effect at a peptide concentration of 2.5 μM. Similarly to what was seen with calcein-loaded vesicles, when the peptides were analyzed for their ability to cause the release of fluorescently labeled dextrans of different size (4/20/70 kDa) from PE/PG liposomes, both H2 and H4 displayed basically the same activity, with the probe being released in a manner that depended significantly on the size of the solute (Table 3).

The results obtained with PG/CL liposomes are reported in Fig. 4 (panels b and d). Both bombinins H displayed a generally lower activity on this membrane composition than that recorded for PE/PG liposomes. Interestingly, in this case, bombinin H4 appeared to be remarkably more potent than the all-L H2, giving rise to a total membrane permeation at a peptide concentration (3.5 μM) that was approximately fourfold lower than that needed for H2. These observations are in line with the results of the membrane-permeability assay described above, using intact cells (Fig. 1) and are consistent with the suggestion that the two isomers bind and perturb the membrane of Gram-positive bacteria with a different effectiveness.

Peptide translocation through a PE/PG membrane

To get insight into the ability of these two frog skin peptides to translocate through a model of *E. coli* inner

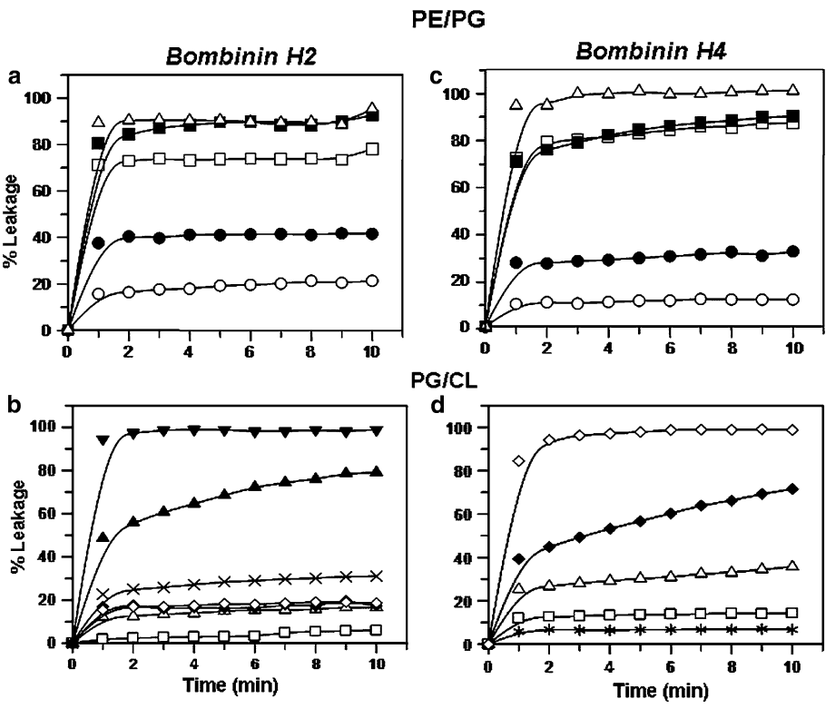

Fig. 4 Calcein leakage from PE/PG (7:3, w/w; panels **a** and **c**) or PG/CL (6:4, w/w; panels **b** and **d**) vesicles, after bombinin H2 (*left panels*) and H4 (*right panels*) treatment. Calcein release from liposomes (50 μM final lipid concentration) was detected fluorimetrically ($\lambda_{exc} = 490$ nm, $\lambda_{ems} = 517$ nm). The percentage of leakage was calculated as described in "Materials and methods". Data points represent the average values of three independent measurements, with SD not exceeding 3%. Peptide concentrations used were as follows: 0.25 μM (*open circle*), 0.5 μM (*asterisk*), 0.75 μM (*filled circle*), 1 μM (*open square*), 1.5 μM (*filled square*), 2.5 μM (*open triangle*), 3 μM (*filled diamond*), 3.5 μM (*open diamond*), 7.5 μM (*cross symbol*), 10 μM (*filled triangle*), 15 μM (*filled inverted triangle*)

Table 3 Effect of bombinins H2 and H4 (5 μM) on the release of FITC-labeled dextrans from PE/PG liposomes

FITC-dextrans	Dextran release (%)	
	H2	H4
FITC-D4	84.1 ± 2.8	85.2 ± 3.1
FITC-D20	57.8 ± 2.6	59.0 ± 3.0
FITC-D70	27.0 ± 1.5	30.0 ± 2.2

Probe release relative to that of controls, where the total liposome disruption was obtained by adding Triton X-100. Values are means ± SD from three independent experiments. The lipid concentration was 50 μM in 50 mM SPB

membrane, an enzyme digestion assay was developed. As described in "Materials and methods," to this end, trypsin-loaded PE/PG liposomes were incubated with peptides. In the absence of liposomes, both bombinins H were susceptible to trypsin action (two trypsin cleavage sites are present at the C-terminal region of each peptide), as proved by the appearance of novel peaks in the electropherograms of the peptide samples upon enzyme treatment (data not shown).

When trypsin-loaded liposomes were used, in the case of bombinin H2, only two very small peaks, at a migration time in capillary electrophoresis (t_m) of approximately 9 and 11 min, could be detected within 2 h of incubation with the peptide (Fig. 5a, gray and white bars, respectively), whereas in the presence of SBTI, no peptide degradation was discerned at all (Fig. 5b). On the other hand, with bombinin H4, a partial degradation of the peptide was detected within the first 60 min of incubation with the liposomes, as indicated by the presence of three peaks at 4, 9, and 11 min t_m (Fig. 5c, light gray, gray and white bars, respectively). Note that the peak at 4 min t_m was not present in the electropherograms of H2. In addition, the amount of one specific degradation product (peak at 9 min t_m) increased with the incubation time, making up to 30% of total digestion products after 2 h (Fig. 5c). In the presence of SBTI, H4 degradation was strongly reduced (Fig. 5d), probably due to the influx of SBTI through the peptide-induced membrane cracks and, therefore, to the inhibition of trypsin activity inside the liposome.

Discussion

The secretory glands of amphibian skin produce a multitude of bioactive peptides, many with antimicrobial activities, thus representing important constituents of the innate immune system of these animals (Boman 2000; Zasloff 2002). In particular, from the *Bombina* genus, several bombinin peptides have been discovered, as well as the structurally unrelated bombinins H, whose peculiar characteristic is the presence of a D-amino acid in the sequence of some of them. Most AMPs are unfolded in solution and acquire their active conformation only upon binding to their target membrane (Bechinger and Lohner 2006). Bombinins H2 and H4 are not an exception to this rule.

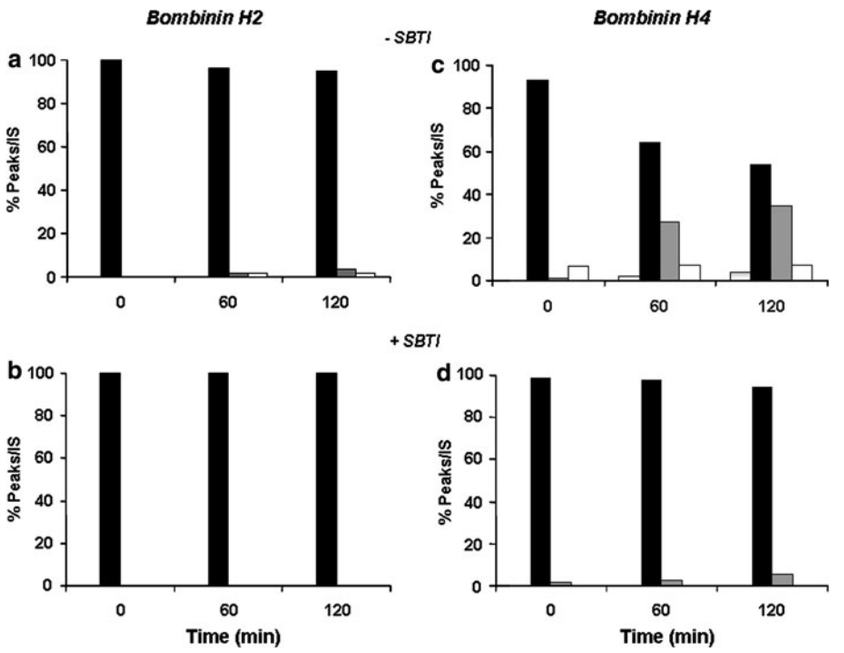

Fig. 5a–d Detection of bombinin H2 (*left panels*) and H4 (*right panels*) translocation into PE/PG (7:3, w/w) liposomes, using the trypsin digestion assay. Trypsin-loaded liposomes (250 μg/ml) were incubated with 60 μM peptides either in the absence (panels **a** and **c**) or in the presence (panels **b** and **d**) of SBTI. At different time points (0, 60, and 120 min), aliquots were taken, boiled for 5 min, and lysed in 0.1% Triton X-100. Samples were analyzed by CZE using imidazole as internal standard. Peptide degradation is indicated by the appearance of peptide fragments with different t_m. *Black bars* indicate the peaks area at 7 min t_m, corresponding to the intact peptides. *Light gray, gray, and white bars* indicate peaks at 4, 9, and 11 min t_m, respectively. All values are the averages of three different experiments with SD not exceeding 2.5% and are expressed as percentages with respect to the internal standard

Molecular dynamic simulations have shown that both peptides have an intrinsic propensity to fold when still in water, with H4 being less constrained and more flexible due to the inability of its D-alloisoleucine in position 2 to establish intramolecular contacts (Bozzi et al. 2008).

Environmental conditions, as well as the composition and the physical state of the phospholipid bilayer may be crucial for the ultimate peptide structure and mechanism of action. Circular dichroism (CD) spectra have shown that in a membrane-mimicking environment, such as trifluoroethanol, both H2 and H4 adopt predominantly an amphiphatic α-helical structure (Bozzi et al. 2008; Mangoni et al. 2000). More detailed CD and FTIR analyses of H2 and H4 structural features in lipid bilayers of different composition have confirmed that both peptides adopt mainly an α-helical structure—with H2 being slightly more helical than H4 in all membranes—and display a β-sheet component ranging from 14 to 33% (Mangoni et al. 2006). The same study also revealed that H2, but not H4, has the tendency to aggregate in membranes, in the form of aggregated strands (Mangoni et al. 2006).

In the present work, we have found that the two diastereomers H2 and H4 do possess different antimicrobial activity, with H4 being generally more active on Gram-negative bacteria (either standard or clinical strains), but less active on the majority of Gram-positive bacteria with respect to H2, when the microbroth dilution method is used to determine the MIC. Presumably, when the peptides are used in a bacterial growth medium at low concentrations, H2 is more potent than H4 in blocking those cellular functions that are involved in the control of the microbial growth, in Gram-positive bacteria, without significantly affecting the integrity of the plasma membrane and hence the bacterial viability. Nevertheless, a different outcome is found when the two peptides are tested for their bactericidal activity against a representative Gram-positive bacterial species, i.e., *S. aureus*. Indeed, when bacteria are incubated in MHB (the same growth medium used for MIC assays), 99.9% killing of the microbial population is caused by H4 at a concentration equal or twofold higher than its MIC (Table 2), while in the case of H2, a peptide concentration fourfold higher the corresponding MIC is necessary to get the same bactericidal effect. This could be due to the formation of larger membrane ruptures by H4, compared to H2, which is in agreement with the higher affinity of H4 towards PG/CL phospholipid monolayers (Fig. 3) and to its higher membrane-perturbing activity for this lipid composition. These latter effects are highlighted by the results of the

permeabilization of PG/CL liposomes when monitoring the calcein release (Fig. 4), and by the results of the permeabilization of *S. aureus* cell membrane when monitoring the intracellular influx of SYTOX Green (Fig. 1).

In the case of Gram-negative bacteria, a higher antimicrobial and membrane-perturbing activity was formerly demonstrated for the D-isoform H4 (Mangoni et al. 2000). However, working with PE/PG liposomes to mimic the lipid composition of *E. coli* inner membrane, we have observed that both bombinins H are similarly capable of injuring this type of membrane (Fig. 4 and Table 3), although a slightly stronger membrane-perturbing activity of H4 with respect to H2 is discernable, and this is also true in the case of the peptides' intercalation into a PE/PG monolayer (Fig. 3). Therefore, the discrepancies found between these two diastereomers when intact bacteria are used might be attributed to differences in their diffusion process through the Gram-negative cell wall before reaching the target cytoplasmic membrane. Note that the outer membrane component of the cell wall of Gram-negative bacteria, the first barrier AMPs are faced with before reaching the plasma membrane, is made by a complex mixture of lipopolysaccharides (LPS), phospholipids, lipoproteins, and proteins.

In addition, our membrane translocation experiments, employing PE/PG trypsin-loaded liposomes, have indicated only a tiny degradation of the all-L H2 in the absence of the trypsin inhibitor SBTI. A possible explanation for this finding is that H2 molecules present in the sample bind the model membrane resembling that of Gram-negative bacteria in a highly aggregated peptide-lipid molecular complex not available for trypsin cleavage, but efficient enough to perturb the membrane causing the leakage of either the low-molecular-weight calcein and of liposome-preincapsulated dextrans of increasing size (Table 3). The aggregation tendency of H2 has been reported before (Mangoni et al. 2006) and discussed above, and both H2 and H4 were shown previously to cause the release of β-galactosidase from *E. coli* cells in a dose-dependent manner (Mangoni et al. 2000).

Thus, as found for other frog-skin AMPs such as temporins (Rinaldi et al. 2001), it is very likely that bombinins H cause marker leakage from lipid vesicles (and possibly from microbial target cells)—not thanks to a total membrane disruption (detergent-like effect), but rather by perturbing the bilayer organization on a local scale. Concerning H4, a partial peptide degradation by trypsin entrapped into PE/PG liposomes was detected. This might be related to a more flexible conformation of H4, compared to the more structured and aggregated H2 (Bozzi et al. 2008; Mangoni et al. 2006), which would make it easier for H4 to traverse the phospholipids bilayer.

Overall, we can conclude that bombinins H2 and H4 are membrane-active peptides whose different bactericidal activity on Gram-negative and Gram-positive bacteria can be assigned to a different behavior in their binding affinity and permeation of the target cytoplasmic membrane, and/or in their translocation through the cell wall/plasma membrane of the target cell. In general, we can state that the D-amino acid–containing bombinin H4 is more efficient than bombinin H2 at disturbing bacterial membranes.

Bombinin H4 was also earlier indicated to be more active against the protozoan pathogen *Leishmania*, binding a model of its membrane with a fivefold greater affinity than bombinin H2 (Mangoni et al. 2006).

In the case of Gram-positive bacteria, such as *S. aureus*, the data reported in this work show a higher ability of bombinin H4 to wreck the structure of phospholipid bilayers of these microorganisms, as supported by the results obtained working with intact cells and model membranes (Figs. 1, 3, and 4).

On the other side, in the case of Gram-negative strains, the higher membrane-perturbing activity of H4 (Mangoni et al. 2000) would reflect its easier partition into the inner cytoplasmic membrane. Furthermore, a partial membrane crossing activity could occur for H4, but not for H2, also in living bacteria. Once having crossed the membrane, H4 might influence the activity of intracellular functions, thus reinforcing the membrane perturbation effect and contributing to killing the microbial cell.

However, we cannot rule out, at this stage, the possibility that additional factors (e.g., interaction with peptidoglycan, LPS layer, and other cell surface components) could induce mechanical stress affecting the cell wall/membrane structure and thus the antimicrobial activity of the two bombinin diastereomers in a different way.

Finally, both bombinins H were also found to preserve their antimicrobial properties in high-ionic strength media resembling physiological environments, which is an important feature for molecules to be used as templates for the development of new drugs.

Importantly, besides getting insight into the molecular mechanism of a pair of natural peptide diastereomers at the level of Gram-positive and Gram-negative bacterial membranes, these studies have expanded our knowledge of the effect of a single L-to-D epimerization on the target cell selectivity of an AMP and its mode of action.

Acknowledgments This work was supported by grants from Università di Roma La Sapienza, MIUR (Italian Ministry of Education, University and Research; PRIN 2008), and Istituto di Biologia e Patologia Molecolari of the Italian National Research Council (CNR).

References

Allen TM (1981) A study of phospholipid interactions between high-density lipoproteins and small unilamellar vesicles. Biochim Biophys Acta 640:385–397

Bechinger B, Lohner K (2006) Detergent-like actions of linear amphipathic cationic antimicrobial peptides. Biochim Biophys Acta 1758:1529–1539

Beisswenger C, Bals R (2005) Functions of antimicrobial peptides in host defense and immunity. Curr Protein Pept Sci 6:255–264

Boman HG (2000) Innate immunity and the normal microflora. Immunol Rev 173:5–16

Boman HG (2003) Antibacterial peptides: basic facts and emerging concepts. J Intern Med 254:197–215

Bozzi A, Mangoni ML, Rinaldi AC, Mignogna G, Aschi M (2008) Folding propensity and biological activity of peptides: the effect of a single stereochemical isomerization on the conformational properties of bombinins in aqueous solution. Biopolymers 89:769–778

Brockman H (1999) Lipid monolayers: why use half a membrane to characterize protein-membrane interactions? Curr Opin Struct Biol 9:438–443

Buczek O, Yoshikami D, Bulaj G, Jimenez EC, Olivera BM (2005) Post-translational amino acid isomerization: a functionally important D-amino acid in an excitatory peptide. J Biol Chem 280:4247–4253

CLSI (2006) Methods for dilution antimicrobial susceptibility tests for bacteria that grow aerobically, approved standard, 7th edn. CLSI document M7–A7, vol. 26, no.2. Clinical and Laboratory Standards Institute, Wayne

Dempsey CE, Hawrani A, Howe RA, Walsh TR (2010) Amphipathic antimicrobial peptides—from biophysics to therapeutics? Protein Pept Lett 17:1334–1344

Den Hertog AL, Wong Fong Sang HW, Kraayenhof R, Bolscher JG, Van't Hof W, Veerman EC, Nieuw Amerongen AV (2004) Interactions of histatin 5 and histatin 5-derived peptides with liposome membranes: surface effects, translocation and permeabilization. Biochem J 379:665–672

Easton DM, Nijnik A, Mayer ML, Hancock RE (2009) Potential of immunomodulatory host defense peptides as novel anti-infectives. Trends Biotechnol 27:582–590

Epand RM, Epand RF (2009) Lipid domains in bacterial membranes and the action of antimicrobial agents. Biochim Biophys Acta 1788:289–294

Erspamer V, Melchiorri P, Falconieri-Erspamer G, Negri L, Corsi R, Severini C, Barra D, Simmaco M, Kreil G (1989) Deltorphins: a family of naturally occurring peptides with high affinity and selectivity for delta opioid binding sites. Proc Natl Acad Sci USA 86:5188–5192

Ganz T (2003) Defensins: antimicrobial peptides of innate immunity. Nat Rev Immunol 3:710–720

Gibson BW, Tang DZ, Mandrell R, Kelly M, Spindel ER (1991) Bombinin-like peptides with antimicrobial activity from skin secretions of the Asian toad, *Bombina orientalis*. J Biol Chem 266:23103–23111

Giuliani A, Rinaldi AC (2010) Antimicrobial peptides. Methods and protocols. Methods in molecular biology, vol 618. Humana Press, New York

Hancock RE, Diamond G (2000) The role of cationic antimicrobial peptides in innate host defences. Trends Microbiol 8:402–410

Jilek A, Mollay C, Tippelt C, Grassi J, Mignogna G, Mullegger J, Sander V, Fehrer C, Barra D, Kreil G (2005) Biosynthesis of a D-amino acid in peptide linkage by an enzyme from frog skin secretions. Proc Natl Acad Sci USA 102:4235–4239

Kamatani Y, Minakata H, Kenny PT, Iwashita T, Watanabe K, Funase K, Sun XP, Yongsiri A, Kim KH, Novales-Li P et al (1989) Achatin-I, an endogenous neuroexcitatory tetrapeptide from *Achatina fulica* Ferussac containing a D-amino acid residue. Biochem Biophys Res Commun 160:1015–1020

Kreil G (1994) Conversion of L- to D-amino acids: a posttranslational reaction. Science 266:996–997

Kreil G (1997) D-amino acids in animal peptides. Annu Rev Biochem 66:337–345

Kuwada M, Teramoto T, Kumagaye KY, Nakajima K, Watanabe T, Kawai T, Kawakami Y, Niidome T, Sawada K, Nishizawa Y et al (1994) Omega-agatoxin-TK containing D-serine at position 46, but not synthetic omega-[L-Ser46]agatoxin-TK, exerts blockade of P-type calcium channels in cerebellar Purkinje neurons. Mol Pharmacol 46:587–593

Li XZ, Poole K, Nikaido H (2003) Contributions of MexAB-OprM and an EmrE homolog to intrinsic resistance of *Pseudomonas aeruginosa* to aminoglycosides and dyes. Antimicrob Agents Chemother 47:27–33

MacDonald RC, MacDonald RI, Menco BP, Takeshita K, Subbarao NK, Hu LR (1991) Small-volume extrusion apparatus for preparation of large, unilamellar vesicles. Biochim Biophys Acta 1061:297–303

Maget-Dana R (1999) The monolayer technique: a potent tool for studying the interfacial properties of antimicrobial and membrane-lytic peptides and their interactions with lipid membranes. Biochim Biophys Acta 1462:109–140

Maisetta G, Batoni G, Esin S, Florio W, Bottai D, Favilli F, Campa M (2006) In vitro bactericidal activity of human beta-defensin 3 against multidrug-resistant nosocomial strains. Antimicrob Agents Chemother 50:806–809

Mangoni ML, Grovale N, Giorgi A, Mignogna G, Simmaco M, Barra D (2000) Structure-function relationships in bombinins H, antimicrobial peptides from *Bombina* skin secretions. Peptides 21:1673–1679

Mangoni ML, Papo N, Saugar JM, Barra D, Shai Y, Simmaco M, Rivas L (2006) Effect of natural L- to D-amino acid conversion on the organization, membrane binding, and biological function of the antimicrobial peptides bombinins H. Biochemistry 45:4266–4276

Mangoni ML, Marcellini L, Simmaco M (2007) Biological characterization and modes of action of temporins and bombinins H, multiple forms of short and mildly cationic anti-microbial peptides from amphibian skin. J Pept Sci 13:603–613

Mangoni ML, Maisetta G, Di Luca M, Gaddi LM, Esin S, Florio W, Brancatisano FL, Barra D, Campa M, Batoni G (2008) Comparative analysis of the bactericidal activities of amphibian peptide analogues against multidrug-resistant nosocomial bacterial strains. Antimicrob Agents Chemother 52:85–91

Marcellini L, Borro M, Gentile G, Rinaldi AC, Stella L, Aimola P, Barra D, Mangoni ML (2009) Esculentin-1b(1–18)–a membrane-active antimicrobial peptide that synergizes with antibiotics and modifies the expression level of a limited number of proteins in *Escherichia coli*. FEBS J 276:5647–5664

Montecucchi PC, de Castiglione R, Piani S, Gozzini L, Erspamer V (1981) Amino acid composition and sequence of dermorphin, a novel opiate-like peptide from the skin of *Phyllomedusa sauvagei*. Int J Pept Protein Res 17:275–283

Mor A, Amiche M, Nicolas P (1992) Enter a new post-translational modification: D-amino acids in gene-encoded peptides. Trends Biochem Sci 17:481–485

Rinaldi AC (2002) Antimicrobial peptides from amphibian skin: an expanding scenario. Curr Opin Chem Biol 6:799–804

Rinaldi AC, Di Giulio A, Liberi M, Gualtieri G, Oratore A, Bozzi A, Schininà ME, Simmaco M (2001) Effects of temporins on molecular dynamics and membrane permeabilization in lipid vesicles. J Pept Res 58:213–220

Rinaldi AC, Mangoni ML, Rufo A, Luzi C, Barra D, Zhao H, Kinnunen PK, Bozzi A, Di Giulio A, Simmaco M (2002) Temporin L: antimicrobial, haemolytic and cytotoxic activities, and effects on membrane permeabilization in lipid vesicles. Biochem J 368:91–100

Selsted ME, Ouellette AJ (2005) Mammalian defensins in the antimicrobial immune response. Nat Immunol 6:551–557

Shai Y (1999) Mechanism of the binding, insertion and destabilization of phospholipid bilayer membranes by alpha-helical antimicrobial and cell non-selective membrane-lytic peptides. Biochim Biophys Acta 1462:55–70

Simmaco M, Barra D, Chiarini F, Noviello L, Melchiorri P, Kreil G, Richter K (1991) A family of bombinin-related peptides from the skin of *Bombina variegata*. Eur J Biochem 199:217–222

Simmaco M, Mignogna G, Barra D (1998) Antimicrobial peptides from amphibian skin: what do they tell us? Biopolymers 47:435–450

Simmaco M, Kreil G, Barra D (2009) Bombinins, antimicrobial peptides from *Bombina* species. Biochim Biophys Acta 1788:1551–1555

Stewart JC (1980) Colorimetric determination of phospholipids with ammonium ferrothiocyanate. Anal Biochem 104:10–14

Szoka F Jr, Papahadjopoulos D (1978) Procedure for preparation of liposomes with large internal aqueous space and high capture by reverse-phase evaporation. Proc Natl Acad Sci USA 75:4194–4198

Torres AM, Menz I, Alewood PF, Bansal P, Lahnstein J, Gallagher CH, Kuchel PW (2002) D-amino acid residue in the C-type natriuretic peptide from the venom of the mammal, *Ornithorhynchus anatinus*, the Australian platypus. FEBS Lett 524:172–176

Yeaman MR, Yount NY (2003) Mechanisms of antimicrobial peptide action and resistance. Pharmacol Rev 55:27–55

Zasloff M (2002) Antimicrobial peptides of multicellular organisms. Nature 415:389–395

Zhao H, Kinnunen PK (2002) Binding of the antimicrobial peptide temporin L to liposomes assessed by Trp fluorescence. J Biol Chem 277:25170–25177

Research Article

Journal of PeptideScience

Received: 20 October 2010 Accepted: 12 December 2010 Published online in Wiley Online Library: 18 February 2011

(wileyonlinelibrary.com) DOI 10.1002/psc.1350

Alanine scanning analysis and structure–function relationships of the frog-skin antimicrobial peptide temporin-1Ta‡

Paolo Grieco,[a] Vincenzo Luca,[b] Luigia Auriemma,[a] Alfonso Carotenuto,[a] Maria Rosaria Saviello,[a] Pietro Campiglia,[c] Donatella Barra,[b] Ettore Novellino[a] and Maria Luisa Mangoni[b]*

The increasing resistance of bacteria and fungi to the available antibiotic/antimycotic drugs urges for a search for new anti-infective compounds with new modes of action. In line of this, natural CAMPs represent promising and attractive candidates. Special attention has been devoted to frog-skin temporins, because of their short size (10–14 residues long) and their unique features. In particular, temporin-1Ta has the following properties: (i) it is mainly active on Gram-positive bacteria; (ii) it can synergize, when combined with temporin-1Tl, in inhibiting both gram-negative bacterial growth and the toxic effect of LPS; (iii) it preserves biological activity in the presence of serum; and (iv) it is practically not hemolytic. Rational design of CAMPs represents a straightforward approach to obtain a peptide with a better therapeutic index. Here, we used alanine scanning analogs to elucidate the contribution of the side chains of each amino acid residue to the peptide's antimicrobial and hemolytic activity. Beside providing insight into the biophysical attributes and the critical positions within the peptide sequence, which govern the antimicrobial/hemolytic activity of this temporin isoform, our studies assist in optimizing the design of temporin-based lead structures for the production of new anti-infective agents. Copyright © 2011 European Peptide Society and John Wiley & Sons, Ltd.

Keywords: temporin; alanine scanning; antimicrobial peptides; frog skin

Introduction

Because of the increasing frequency of bacterial and fungal strains resistant to existing drugs, the identification of alternative antibiotics with a new mode of action to slow down the alarming trend of resistance is vital. Primitive innate defence mechanisms in the form of gene-encoded CAMPs [1–3], originally discovered in insects [4,5], are now considered well-suitable candidates for the design and development of new therapeutics [6–9]. These relatively low-molecular weight peptides were later found to be present in all living organisms, sometimes in large quantities freely circulating or sequestered in compartments throughout the organism [10,11]. However, beside being crucial components of the host innate immunity, CAMPs also mediate the adaptive immune response, by causing mast-cell degranulation, by acting as chemo-attractants [1,12] or by blocking the LPS-induced cytokine production and subsequent septic shock syndrome [13–15]. In contrast to conventional antibiotics, most of which work by interfering with a specific biochemical reaction within the cell, numerous CAMPs are believed to perturb the microbial membrane in a non-receptor-mediated fashion. Despite substantial variation in their chain length and structural conformation, most CAMPs do possess: (i) a size ranging from 11 to 50 amino acids; (ii) a net positive charge at neutral pH; and (iii) an amphiphatic structure upon contact with the membrane of the target cell [16–18]. The search for novel CAMPs as lead structures of natural origin has led to the discovery of interesting peptides from the skin glands of amphibian anura. Among them, a marked attention has been devoted to the short and mildly cationic temporins. Initially isolated from the skin of the European red frog *Rana temporaria*

* *Correspondence to: Maria Luisa Mangoni, Dipartimento di Scienze Biochimiche, Università La Sapienza, Piazzale Aldo Moro, 5-00185-Rome, Italy. E-mail: marialuisa.mangoni@uniroma1.it*

a *Department of Pharmaceutical and Toxicological Chemistry, University of Naples 'Federico II', I-80131 Naples, Italy*

b *Istituto Pasteur-Fondazione Cenci Bolognetti, Istituto di Biologia e Patologia Molecolari del CNR, Dipartimento di Scienze Biochimiche, Università "La Sapienza", 00185 Roma, Italy*

c *Department of Pharmaceutical Science, University of Salerno, I-84084 Fisciano, Salerno, Italy*

‡ *Special issue devoted to contributions presented at the 12th Naples Worshop on Bioactive Peptides and 2nd Italy-Korea Symposium on Antimicrobial Peptides, 4-7 June 2010, Naples, Italy.*

Abbreviations used: *CAMP, cationic antimicrobial peptide; CFU, colony-forming units; CH_3CN, acetonitrile; DIEA, N,N-diisopropylethyl-amine; DPC, dodecylphosphocholine; Et_3SiH, triethylsilane; HBTU, 2-(1 H-benzotriazole-1-yl)-1,1,3,3-tetramethyluronium hexafluoro-phosphate; LC-MS, liquid-mass spectroscopy; LPS, lipopolysaccharide; MHB, Mueller-Hinton broth; RP-HPLC, reversed-phase high performance liquid chromatography.*

[19], new members were then identified in skin secretions of other ranid frogs of both American and Eurasian origin, enlarging the temporin family to more than 100 different isoforms [20]. Temporins are among the smallest CAMPs (10–14 residues long, except for temporin-SHf and temporin-LTa bearing 8 and 17 amino acids, respectively [21,22]), and with a net charge ranging from +2 to +3. Indeed, with the exclusion of temporin-1Ja, carrying an aspartic acid (net charge 0), and a few isoforms devoid of basic or acidic amino acids (net charge +1, due to the free N-terminal amino group), all the remaining members have only a single or a double positively charged residue in their sequence [20]. This low cationic character is unique and is an exception compared to known CAMPs from other sources [23,24]. In addition, unlike the majority of Ranidae CAMPs, such as brevinins, ranalexins, ranatuerins, and esculentins [25,26], temporins lack the C-terminal heptapeptide ring stabilized by a disulfide bridge and are amidated at their carboxyl end as a result of a post-translational enzymatic reaction [27]. Generally, temporins are active particularly against Gram-positive bacteria, Candida species, and fungi, including antibiotic-resistant strains [28,29]. A large number of studies has revealed that their bacterial killing process is rapid and concomitant with the perturbation of the microbial membrane [20,30]. Furthermore, recent papers have shown the existence of a synergistic effect in two pairs of temporins (temporin-1Ta + temporin-1Tl and temporin-1Tb + temporin-1Tl) in inhibiting both the Gram-negative bacterial growth and the toxic effect of the outer membrane component LPS [31,32]. Interestingly, LPS was found to be the key molecule underlying the molecular mechanism of both types of synergism [33], and this finding represents the first case reported so far in the literature. While temporin-1Tl is highly active on a wide range of microorganisms, but with a lytic effect on red blood cells, temporin-1Ta is mainly active on Gram-positive bacteria and is not hemolytic. This might be linked to the lower α-helical content of temporin-1Ta than Tl, and, as a result, to its inability to deeply insert into the hydrophobic core of zwitterionic membranes, such as those of eukaryotic cells [34]. Importantly, rational design of CAMPs represents an attractive approach to the improvement of their antimicrobial properties.

Here, to address the influence of each amino acid residue of temporin-1Ta on the selective activity of this peptide, an Ala-scanning analysis was carried out. Besides getting insight into the structure–function relationships of this temporin isoform, the results of our studies provide important information for the optimization of temporin-based anti-infective agents and the design of temporin analogs to be employed in biophysical studies for a better understanding of their membrane-active properties.

Materials and Methods

Peptide Synthesis

N^{α}-Fmoc-protected amino acids, HBTU, HOBt, and Rink amide resin were purchased from GL Biochem Ltd (Shanghai, China). Peptide synthesis solvents, reagents, as well as CH_3CN for HPLC were reagent grade and were acquired from commercial sources and used without further purification unless otherwise noted. The syntheses of temporin-1Ta analogs were performed in a stepwise manner via the solid-phase method [35]. For example, for the synthesis of Ta, N^{α}-Fmoc-Leu-OH was coupled to Rink amide resin (0.5 g, 0.7 mmol NH_2/g). The following protected amino acids were then added stepwise: N^{α}-Fmoc-Ile-OH, N^{α}-Fmoc-Gly-OH, N^{α}-Fmoc-Ser-OH, N^{α}-Fmoc-Leu-OH, N^{α}-Fmoc-Val-OH, N^{α}-Fmoc-Arg(Pbf)-OH, N^{α}-Fmoc-Gly-OH, N^{α}-Fmoc-Ile-OH, N^{α}-Fmoc-Leu-OH, N^{α}-Fmoc-Pro-OH, N^{α}-Fmoc-Leu-OH, and N^{α}-Fmoc-Phe-OH. Each coupling reaction was accomplished using a threefold excess of amino acid with HBTU and HOBt in the presence of DIEA. The N^{α}-Fmoc protecting groups were removed by treating the protected peptide resin with a 25% solution of piperidine in DMF (1 × 5 min and 1 × 20 min). The peptide resin was washed three times with DMF and the next coupling step was initiated in a stepwise manner. All reactions were performed under an Ar atmosphere. The peptide resin was washed with DCM (3×), DMF (3×) and DCM (4×), and the deprotection protocol was repeated after each coupling step. The N-terminal Fmoc group was removed as described above and the peptide was released from the resin with TFA/Et_3SiH/H_2O (90 : 5:5) for 3 h. The resin was removed by filtration and the crude peptide was recovered by precipitation with cold anhydrous ethyl ether to give a white powder which was purified by RP-HPLC on a semi-preparative C18-bonded silica column (Vydac 218TP1010, 1.0 × 25 cm) using a gradient of CH_3CN in 0.1% aqueous TFA (from 10 to 90% in 30 min) at a flow rate of 1.0 ml/min. The product was obtained by lyophilization of the appropriate fractions after removal of the CH_3CN by rotary evaporation. Analytical RP-HPLC indicated a purity >98% and molecular weights were confirmed by LC-MS (6110 Quadrupole, Agilent Technologies) (Table 1).

Table 1. Analytical data for temporin-1Ta and its analogs

Peptide	HPLC[a] k'	MS (M+H) Found[b]	MS (M+H) Calculated
1Ta	6.86	1397.13	1396.79
Ta A1	7.87	1321.90	1320.69
Ta A2	8.40	1355.70	1354.71
Ta A3	8.09	1370.51	1370.75
Ta A4	7.98	1355.54	1354.71
Ta A5	8.00	1355.81	1354.71
Ta A6	7.55	1411.10	1410.82
Ta A7	10.37	1312.62	1311.68
Ta A8	9.23	1368.69	1368.74
Ta A9	8.13	1355.18	1354.71
Ta A10	8.85	1381.80	1380.79
Ta A11	7.41	1411.30	1410.82
Ta A12	8.21	1354.62	1354.71
Ta A13	7.66	1354.36	1354.71

[a] k' [(peptide retention time – solvent retention time)/solvent retention time].
[b] Molecular masses were determined by LC-MS.

Microorganisms

The strains used for the antimicrobial assays were the following: the Gram-negative bacteria *Escherichia coli* ATCC 25922, *Yersinia pseudotuberculosis* YPIII; the Gram-positive bacteria *Bacillus megaterium* Bm11, *Staphylococcus aureus* Cowan I, *Staphylococcus capitis* 1, and the yeast *Candida albicans* ATCC 10231.

Antimicrobial Assay

Susceptibility testing was performed by adapting the microbroth dilution method outlined by the Clinical and Laboratory Standards Institute using sterile 96-well plates (Falcon, NJ, USA). Aliquots

(50 µl) of bacteria in mid-log phase at a concentration of 2×10^6 CFU/ml in culture medium (MHB) were added to 50 µl of MHB broth containing the peptide in serial twofold dilutions in 20% ethanol. The ranges of peptide dilutions used were 1.25–40 µM. The same procedure was followed with yeast strains, but using Winge medium [36]. Inhibition of microbial growth was determined by measuring the absorbance at 600 nm, after an incubation of 18–20 h at 37 °C (30 °C for yeasts), with a 450-Bio-Rad Microplate Reader. Antimicrobial activities were expressed as the MIC, the concentration of peptide at which 100% inhibition of microbial growth is observed after 18–20 h of incubation.

Hemolytic Assay

The hemolytic activity of the peptides was determined using fresh human erythrocytes from healthy donors. Blood was centrifuged and the erythrocytes were washed three times with 0.9% NaCl. Peptides dissolved in 20% ethanol were added to the erythrocyte suspension (5%, v : v), at a final concentration ranging from 1.25 to 40 µM in a final volume of 100 µl. Samples were incubated with agitation at 37 °C for 40 min. The release of hemoglobin was monitored by measuring the absorbance (Abs) of the supernatant at 540 nm. Control for zero hemolysis (blank) consisted of erythrocytes suspended in the presence of peptide solvent (20% ethanol at a final concentration of 0.6%). Hypotonically lysed erythrocytes were used as a standard for 100% hemolysis. The percentage of hemolysis was calculated using the following equation: $\%\ \text{hemolysis} = [(\text{Abs}_{\text{sample}} - \text{Abs}_{\text{blank}})/(\text{Abs}_{\text{total lysis}} - \text{Abs}_{\text{blank}})] \times 100$.

Circolar Dicroism

All CD spectra were recorded using a JASCO J710 spectropolarimeter at 25 °C with a cell of 1 mm path length. The CD spectra were acquired by the range from 260 nm to 190 nm 1 nm bandwidth, four accumulations, and 100 nm/min scanning speed. The CD spectra of the peptides at a concentration of 100 µM were performed in water (pH = 7.4), in SDS (20 mM) and in DPC (20 mM) micellar solutions.

Results

Antibacterial Activity

In order to assess the role of each individual amino acid in the antimicrobial activity of temporin-1Ta, we performed an Ala scan study by systematically replacing single residues with the neutral amino acid Ala. The antimicrobial activity of these analogs was analyzed by the microbroth dilution method against two Gram-negative bacteria (*E. coli* ATCC 25922 and *Y. pseudotuberculosis* YPIII), three Gram-positive bacteria (*S. aureus* Cowan I, *B. megaterium* Bm11 and *S. capitis* 1), and the yeast *C. albicans* ATCC 10231. The results are shown in Table 2. The data pointed out that the following substitutions had marked impact on the antimicrobial activity of the natural peptide, exhibiting multiple MIC values (2-4-8-fold higher) than those of temporin-1Ta, against all microorganisms. These were: (i) the replacement of the N-terminal Phe (Ta A1); (ii) the substitution of the hydrophobic Leu in positions 2, 4, 9, and 13 (Ta A2, Ta A4, Ta A9, and Ta A13); (iii) the change of Ile in positions 5 and 12 (Ta A5 and Ta A12); (iv) the change of the positively charged Arg^7 (Ta A7), as well as (v) the replacement of the hydrophobic Val^8 (Ta A8). In contrast, substitution of Pro^3, Gly^6, Ser^{10} or Gly^{11} with Ala (Ta A3, Ta A6, Ta A10, Ta A11) preserved the antibacterial activity of the parent peptide on *Y. pseudotuberculosis, B. megaterium*, and *S. capitis*, and increased its activity against both the Gram-positive bacterium *S. aureus* and the yeast *C. albicans,* giving two to fourfold lower MICs (Table 2).

Hemolysis

Hemolytic activity was determined against human erythrocytes, as described in the Experimental section. The data highlighted a correlation between the antibacterial and the hemolytic activities. Indeed, the most active antimicrobial analogs (Ta A3, Ta A6, Ta A10, and Ta A11) also displayed the highest hemolytic activity at a peptide concentration range from 20 to 40 µM, while a comparable hemolysis caused by the parent peptide 1Ta was observed at the lower concentrations (Table 3). An exception was given by Ta A3 and Ta A11, whose lytic effect was found to be two to threefold more potent than that of 1Ta, also at 10 µM. Interestingly, a considerable enhancement of hemolytic activity was induced by the presence of Ala at the N-terminus of the natural temporin (Ta A1), as well as by the replacement of the single basic residue Arg^7 (Ta A7) (Table 3). Conversely, all the other analogs with Ala substitution in positions 2, 4, 5, 8, 9, 12, and 13 appeared to be almost devoid of toxic effect on human erythrocytes (Table 3).

Conformational Studies

The secondary structure of the analogs Ta A1-A13 was investigated using CD spectroscopy in water, SDS/water, and DPC/water solutions. CD spectra in water (pH 7.4) demonstrated the presence of disordered conformers for all compounds, with a minimum close to 198 nm (data not shown). In contrast, in SDS and DPC micelles solution, which were used to mimic the negatively charged (microbial) and the zwitterionic (eukaryotic) cell membranes, respectively, the shape of the CD spectra indicated that peptides adopted a defined secondary structure. In particular, the CD spectra displayed two minima around 209 and 222 nm, characteristic of α-helix structures (Figure 1). Helical contents were predicted from the CD spectra using the SOMCD method [38] (Table 2). Generally, helical contents observed in SDS and DPC micelle solutions were similar, with a certain reduction in SDS (about 5–10%) compared to DPC. The highest helical content was noted in Ta A3, Ta A6, and in Ta A11 (about 70% and 60% in DPC and SDS, respectively). In these peptides, the replacement of a proline (Ta A3) or a glycine residue (Ta A6 and Ta A11) clearly increased the helical content compared to that of the native peptide 1Ta (55% and 50% in DPC and SDS, respectively). An increase of the α-helical content with respect to 1Ta was also observed in Ta A7. In contrast, replacement of the aliphatic residues $Leu^{2,4,9}$, Ile^5, and Val^8 reduced the helical percentage. In particular, Ta A5 and Ta A9 showed the lowest helicity (about 50% and 46% in DPC and SDS, respectively) probably due to the central position of the replaced amino acids along the peptide sequence. Note that earlier studies had evidenced that in both SDS and DPC micelles, temporin-1Ta adopted an amphiphatic α-helix when considering the central residues 6–9 [34]. Finally, no variation in the α-helical content was detected when Ile^{12} and the C-terminal Leu^{13} were replaced, whereas substitution of Phe^1 or Ser^{10} (Ta A1 or Ta A10) increased the helical content of the native peptide in DPC (60 or 56%, respectively), but not in SDS solution.

Table 2. Temporin-1Ta Ala-scan comparison with respect to charge, H, μ_H, % helicity, and MIC on different microbial strains

					% Helix		MIC (μM)					
							Gram-negatives		Gram-positives			Yeasts
Peptides	Amino acid sequences	Charge	H	μ_H	DPC	SDS	*E. coli*	*Y. pseudo-tuberculosis*	*S. aureus*	*B. megaterium*	*S. capitis*	*C. albicans*
1Ta	FLPLIGRVLSGIL-NH_2	+2	0.22	0.35	55	50	>40	20	5	2.5	5	5
Ta A1	ALPLIGRVLSGIL-NH_2	+2	0.2	0.33	60	50	>40	>40	>40	20	>40	>40
Ta A2	FAPLIGRVLSGIL-NH_2	+2	0.2	0.34	54	49	>40	40	20	5	20	10
Ta A3	FLALIGRVLSGIL-NH_2	+2	0.25	0.33	69	57	>40	20	2.5	2.5	2.5	1.25
Ta A4	FLPAIGRVLSGIL-NH_2	+2	0.2	0.36	53	49	>40	40	40	5	20	10
Ta A5	FLPLAGRVLSGIL-NH_2	+2	0.19	0.31	50	46	>40	>40	40	20	40	20
Ta A6	FLPLIARVLSGIL-NH_2	+2	0.23	0.35	71	65	>40	20	2.5	2.5	5	2.5
Ta A7	FLPLIGAVLSGIL-NH_2	+1	0.38	0.21	63	52	>40	>40	>40	>40	>40	>40
Ta A8	FLPLIGRALSGIL-NH_2	+2	0.2	0.34	54	51	>40	40	20	5	20	10
Ta A9	FLPLIGRVASGIL-NH_2	+2	0.2	0.34	51	46	>40	>40	>40	>40	>40	>40
Ta A10	FLPLIGRVLAGIL-NH_2	+2	0.26	0.32	56	50	>40	20	2.5	2.5	5	2.5
Ta A11	FLPLIGRVLSAIL-NH_2	+2	0.23	0.35	71	61	>40	20	2.5	2.5	5	2.5
Ta A12	FLPLIGRVLSGAL-NH_2	+2	0.19	0.32	55	49	>40	>40	40	20	>40	20
Ta A13	FLPLIGRVLSGIA-NH_2	+2	0.2	0.35	55	50	>40	>40	>40	20	>40	40

Mean residue hydrophobicity and hydrophobic moment were calculated using the Eisenberg scale of hydrophobicity [37].

J. Pept. Sci. 2011; 17: 358–365 wileyonlinelibrary.com/journal/jpepsci

Mean Hydrophobicity *H* and Mean Hydrophobic Moment μ_H

Eisenberg consensus scale was used to calculate both the mean hydrophobicity *H* and the mean hydrophobic moment μ_H [37]. The mean hydrophobicity is a measure of the amino acid residue relative affinities for hydrophobic phases. The hydrophobic moment is a measure of the amphiphilicity or asymmetry of hydrophobicity of a polypeptide chain's segment. The helical wheel presentation of temporin-1Ta is given in Figure 2. We noted that temporin-1Ta analogs with *H* ranging from 0.23 to 0.26 (Table 2) and with a mean hydrophobic moment μ_H calculated to range between 0.32 and 0.36, had the same or a two to fourfold lower MIC than that of the natural temporin ($H = 0.22$ and $\mu_H = 0.35$), against all the tested microorganims, but with an increased hemolytic activity (Tables 2 and 3). A different behavior was manifested by the analog lacking the single basic residue, Ta A7. Indeed, despite its high hydrophobicity ($H = 0.38$) and hemolytic activity, ranging from 15 to 52% at a peptide concentration between 2.5 and 20 μM (Table 3), Ta A7 was the least active peptide against both bacteria and fungi, together with Ta A9 ($H = 0.2$) (Table 2). Otherwise, peptide analogs whose hydrophobicity was lower than that of temporin-1Ta were almost devoid of antimicrobial and hemolytic activities, except for Ta A1, where the loss of the N-terminal Phe increased the lytic effect on red blood cells (Table 3). Importantly, the hydrophobic moment was not found to influence the biological activity of the peptide.

Discussion

All living organisms are constantly exposed to multiple harmful microbes and the capacity to overcome infections is essential for their survival. Therefore, several host defence mechanisms have been engendered during evolution, including the generation of fast acting weapons, such as the CAMPs [39–41]. Among the several sources for natural CAMPs, amphibian skin is the major one [42], especially that of frogs of the genus *Rana,* which has a worldwide distribution with approximately 250 species [26]. Their synthesis is transcriptionally regulated by the NF-κB/Iκ Bα machinery [43] and modulated by exposure to microorganisms [44]. In these animals, CAMPs are stored in granules of holocrine-type dermal glands and released into the skin secretion, as a reaction to stress or injury [25]. Remarkably, temporins represent the largest family and are among the shortest α-helical CAMPs found in nature to date. In addition, they have unique properties: (i) they contain only one or two basic amino acids; (ii) most of them are not toxic toward mammalian cells; (iii) they have a fast killing activity; (iv) some of them synergize in both the antimicrobial and anti-endotoxin activities; (v) they partially preserve antimicrobial activity in serum [45]; and (vi) they are endowed with chemotactic activity towards human phagocytes [46], which represents an important link between the innate and adaptive immune system, recruiting immune cells to the sites of infection. Note that the first stage of a CAMP in selecting the target microorganism includes its electrostatic attraction to the cell surface, which contains anionic molecules such as LPS in Gram-negative bacteria [47], and teichoic acids in Gram-positive bacteria. Following electrostatic binding, the CAMP reaches the cell membrane, composed predominantly of phosphatidylethanolamine and the negatively charged phosphatidylglycerol, and alters its permeability by making transmembrane pores or destroying the membrane's structure in a detergent-like manner [17]. Importantly, several studies have pointed out that temporins are membrane-active CAMPs. However, the range of the crucial peptide parameters required for their molecular mechanism is still not yet completely known.

We have presented a structure-activity study of the frog-skin peptide temporin-1Ta by replacing each individual amino acid with Ala. This standard Ala-positional scanning has identified four analogs (Ta A3, Ta A6, Ta A10, and Ta A11) with a higher hydrophobicity and a higher percentage of α-helix compared to the natural peptide, in both DPC and SDS. All of them display not only the same or a better antimicrobial activity than temporin-1Ta but also a higher lytic effect on human erythrocytes. It is worthwhile noting that all these substitutions reside at the hydrophilic face of the peptide (Figure 2). However, substitution of Arg with Ala (Ta A7), also located at the polar face of the peptide, suppresses its antimicrobial effect against all microorganisms (Table 2). This is in agreement with reports of other authors [48] and is probably due to the loss of the single positively charged residue (Arg) in the sequence, causing a weaker electrostatic interaction with the microbial membrane. In comparison, when amino acid substitutions with the neutral and inert Ala take place at the hydrophobic side of the molecule (Ta A1, Ta A2, Ta A4, Ta A5, Ta A8, Ta A9, Ta A12, and Ta A13), (Figure 2) a clear decrease or almost abolishment of the antimicrobial activity occurs, along with a significant decrease in the hemolytic activity. Ta A1 is an exception, because it exhibits two to threefold higher hemolytic activity compared to the parent peptide (Table 3).

Overall, our data have indicated that hydrophobicity and cationicity, more than helicity, are the main critical biophysical properties that determine the antimicrobial potency of temporin-1Ta, whereas the mean peptide hydrophobicity and helicity represent the main parameters that govern the peptide's toxicity towards eukaryotic cells. In fact, a direct correlation between the helical content in DPC and the hemolytic activity could be detected (Tables 2 and 3). The most hemolytic peptides of the series are those (Ta A1, Ta A3, Ta A6, Ta A7, and Ta A11) adopting the highest helical content in DPC, while the less hemolytic ones have the lowest helical percentage (Ta A5 and Ta A9). However, an exception is given by Ta A12 and Ta A13: indeed, despite their negligible hemolytic activity, their helical content is similar to that of 1Ta. Probably, highly hydrophobic residues at the C-terminus, such as Ile^{12} and Leu^{13}, are needed for the peptide interactions with zwitterionic membranes. Noteworthy, because the cationicity is a fundamental requisite for the 'carpet-like' mechanism of action of CAMPs and both helicity and hydrophobicity play a crucial role in the membrane interaction of CAMPs that act via the 'barrel-stave' mechanism [17], our findings seem to fit well with the 'carpet-like' and the 'barrel-stave' models that explain the antimicrobial and hemolytic activities of temporins, respectively [34,49]. Nevertheless, in regard to the latter model, which includes the formation of a transmembrane pore, it should be recalled that temporins are not long enough to span a phospholipid bilayer as α-helices, a property requiring a length of 20 amino acids for a 30 Å thick phospholipid bilayer [50]. Therefore, these peptides tend to form holes in a more elaborated way, perhaps due to their end-to-end dimerization [51].

The finding that enhancement of hydrophobicity increases the hemolytic and antibacterial activities of temporin-1Ta is consistent with what has already been found in magainin-2 [52]; on the contrary, no correlation between hydrophobicity and hemolytic/antimicrobial activity could be detected in other members of the temporin family, such as temporin-1Tl analogs, the percentage of helicity being the principal parameter controlling

Table 3. Hemolytic activity of temporin-1Ta Ala-scan on human erythrocytes, at different peptide concentrations

Peptide concentration (μM)	% Hemolysis													
	Peptide													
	1Ta	Ta A1	Ta A2	Ta A3	Ta A4	Ta A5	Ta A6	Ta A7	Ta A8	Ta A9	Ta A10	Ta A11	Ta A12	Ta A13
40	27.5	62.5	15	100	11.5	3.5	97	39	10.5	3.5	70	100	1	3.5
20	12.5	39	5.5	89.5	10	2.5	27.5	52.5	10	4	14	92.5	0.5	3.5
10	9.5	11.5	2.5	23.5	8	1.5	10.5	39	12	1.5	5.5	32.5	0	3
5	3.5	8	1.5	4.5	6.5	0.5	3.5	27.5	8.5	1	5.5	13	0	0
2.5	0.5	5.5	0.5	2	2	0.5	3.5	15	6.5	1	1	5.5	0	0
1.25	0.5	2	0	0	2	0	1	6	1.5	0	0	3.5	0	0

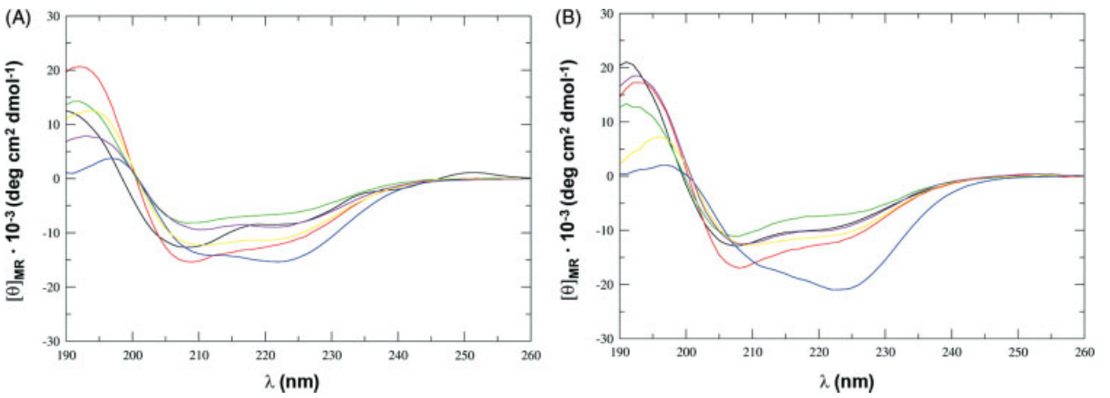

Figure 1. CD spectra of 1Ta analogs in (A) DPC, (B) SDS (1Ta, purple line; Ta A1, black line; Ta A3, red line; Ta A5, green line; Ta A6, blue line; Ta A7, yellow line). For the sake of clarity, Ta A2, Ta A4, Ta A8, Ta A10, Ta A12, and Ta A13 spectra were not reported since they were almost superposable with those of 1Ta. Similarly, Ta A9 and Ta A11 spectra were not shown because very similar to those of Ta A5 and Ta A3, respectively. $[Q]_{MR}$: mean residue molar ellipticity.

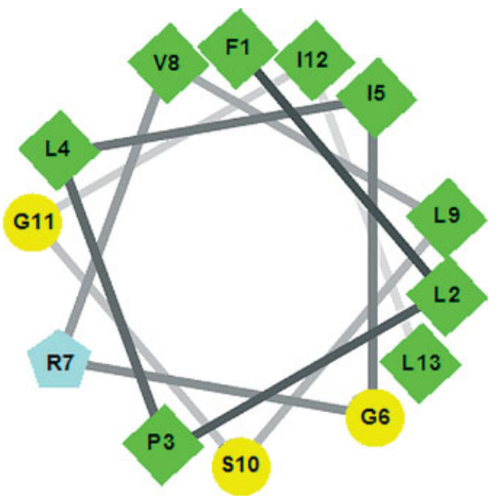

Figure 2. Helical wheel projection of temporin-1Ta. Green squares, yellow circles, and blue pentagons refer to non polar, polar uncharged, and basic residues, respectively.

the peptide's hemolytic effect (Mangoni ML *et al*., unpublished results). Obviously, a large number of factors (peptide's charge distribution, hydrophobicity, helicity, oligomeric state, amphiphilicity, and composition of the target cell membrane) cooperate in modulating the ability of a CAMP to disturb the organization of microbial membranes, and the target cell selectivity and potency of a CAMP cannot be easily predicted.

In conclusion, we can state that despite other structure–function relationship studies that have been performed with some analogs of temporin-1Ta [48,50,53], this work is the first report demonstrating the contribution of each amino acid residue to the antimicrobial/hemolytic activity of temporin-1Ta, by the standard alanine-positional scanning. The correlation found between the net charge, helicity, hydrophobicity, and hydrophobic moment due to a single substitution has increased our knowledge on the physicochemical attributes and structural properties underlying the biological activity of temporin-1Ta, and should assist in optimizing the design and manufacturing of temporin-based lead structures for the development of new anti-infective agents with expanding properties.

Acknowledgement

This work was supported by grants from Sapienza Università di Roma, Italian Ministero dell'Istruzione, Università e Ricerca (PRIN 2008).

References

1 Yang D, Chertov O, Oppenheim JJ. The role of mammalian antimicrobial peptides and proteins in awakening of innate host defenses and adaptive immunity. *Cell. Mol. Life Sci.* 2001; **58**: 978–989.

2 Zasloff M. Antimicrobial peptides of multicellular organisms. *Nature* 2002; **415**: 389–395.
3 Nicolas P, Mor A. Peptides as weapons against microorganisms in the chemical defense system of vertebrates. *Annu. Rev. Microbiol.* 1995; **49**: 277–304.
4 Yeaman MR, Yount NY. Mechanisms of antimicrobial peptide action and resistance. *Pharmacol. Rev.* 2003; **55**: 27–55.
5 Bulet P, Hetru C, Dimarcq JL, Hoffmann D. Antimicrobial peptides in insects; structure and function. *Dev. Comp. Immunol.* 1999; **23**: 329–344.
6 Hancock REW, Patrzykat A. Clinical development of cationic antimicrobial peptides: from natural to novel antibiotics. *Curr. Drug. Targets Infect. Disord.* 2002; **2**: 79–83.
7 Easton DM, Nijnik A, Mayer ML, Hancock RE. Potential of immunomodulatory host defense peptides as novel anti-infectives. *Trends Biotechnol.* 2009; **27**: 582–590.
8 Hadley EB, Hancock RE. Strategies for the discovery and advancement of novel cationic antimicrobial peptides. *Curr. Top. Med. Chem.* 2010; **8**: 1872–1881.
9 Mookherjee N, Hancock RE. Cationic host defence peptides: innate immune regulatory peptides as a novel approach for treating infections. *Cell. Mol. Life Sci.* 2007; **64**: 922–933.
10 Lehrer RI, Ganz T. Cathelicidins: a family of endogenous antimicrobial peptides. *Curr. Opin. Hematol.* 2002; **9**: 18–22.
11 Ganz T. Defensins and other antimicrobial peptides: a historical perspective and an update. *Comb. Chem. High Throughput Screen.* 2005; **8**: 209–217.
12 Niyonsaba F, Iwabuchi K, Someya A, Hirata M, Matsuda H, Ogawa H, Nagaoka I. A cathelicidin family of human antibacterial peptide LL-37 induces mast cell chemotaxis. *Immunology* 2002; **106**: 20–26.
13 Cohen J. The immunopathogenesis of sepsis. *Nature* 2002; **420**: 885–891.
14 Scott MG, Vreugdenhil AC, Buurman WA, Hancock RE, Gold MR. Cutting edge: cationic antimicrobial peptides block the binding of lipopolysaccharide (LPS) to LPS binding protein. *J. Immunol.* 2000; **164**: 549–553.
15 Ding L, Yang L, Weiss TM, Waring AJ, Lehrer RI, Huang HW. Interaction of antimicrobial peptides with lipopolysaccharides. *Biochemistry* 2003; **42**: 12251–12259.
16 Shai Y. Mechanism of the binding, insertion and destabilization of phospholipid bilayer membranes by alpha-helical antimicrobial and cell non-selective membrane-lytic peptides. *Biochim. Biophys. Acta* 1999; **1462**: 55–70.
17 Shai Y. Mode of action of membrane active antimicrobial peptides. *Biopolymers* 2002; **66**: 236–248.
18 Park Y, Hahm KS. Antimicrobial peptides (AMPs): peptide structure and mode of action. *J. Biochem. Mol. Biol.* 2005; **38**: 507–516.
19 Simmaco M, Mignogna G, Canofeni S, Miele R, Mangoni ML, Barra D. Temporins, antimicrobial peptides from the European red frog *Rana temporaria*. *Eur. J. Biochem.* 1996; **242**: 788–792.
20 Mangoni ML. Temporins, anti-infective peptides with expanding properties. *Cell. Mol. Life Sci.* 2006; **63**: 1060–1069.
21 Abbassi F, Lequin O, Piesse C, Goasdoue N, Foulon T, Nicolas P, Ladram A. Temporin-SHf, a new type of phe-rich and hydrophobic ultrashort antimicrobial peptide. *J. Biol. Chem.* 2010; **285**: 16880–16892.
22 Wang H, Lu Y, Zhang X, Hu Y, Yu H, Liu J, Sun J. The novel antimicrobial peptides from skin of Chinese broad-folded frog, *Hylarana latouchii* (Anura : Ranidae). *Peptides* 2009; **30**: 273–282.
23 Ouellette AJ. Paneth cell alpha-defensins: peptide mediators of innate immunity in the small intestine. *Springer Semin. Immunopathol.* 2005; **27**: 133–146.
24 Zanetti M. Cathelicidins, multifunctional peptides of the innate immunity. *J. Leukoc. Biol.* 2004; **75**: 39–48.
25 Simmaco M, Mignogna G, Barra D. Antimicrobial peptides from amphibian skin: what do they tell us? *Biopolymers* 1998; **47**: 435–450.
26 Conlon JM, Kolodziejek J, Nowotny N. Antimicrobial peptides from ranid frogs: taxonomic and phylogenetic markers and a potential source of new therapeutic agents. *Biochim. Biophys. Acta* 2004; **1696**: 1–14.
27 Bradbury AF, Smyth DG. Peptide amidation. *Trends Biochem. Sci.* 1991; **16**: 112–115.
28 Mangoni ML, Maisetta G, Di Luca M, Gaddi LM, Esin S, Florio W, Brancatisano FL, Barra D, Campa M, Batoni G. Comparative analysis of the bactericidal activities of amphibian peptide analogues against multidrug-resistant Nosocomial Bacterial Strains. *Antimicrob. Agents Chemother.* 2008; **52**: 85–91.
29 Mangoni ML, Rinaldi AC, Di Giulio A, Mignogna G, Bozzi A, Barra D, Simmaco M. Structure–function relationships of temporins, small antimicrobial peptides from amphibian skin. *Eur. J. Biochem.* 2000; **267**: 1447–1454.
30 Mangoni ML, Marcellini HG, Simmaco M. Biological characterization and modes of action of temporins and bombinins H, multiple forms of short and mildly cationic anti-microbial peptides from amphibian skin. *J. Pept. Sci.* 2007; **13**: 603–613.
31 Rosenfeld Y, Barra D, Simmaco M, Shai Y, Mangoni ML. A synergism between temporins toward gram-negative bacteria overcomes resistance imposed by the lipopolysaccharide protective layer. *J. Biol. Chem.* 2006; **281**: 28565–28574.
32 Mangoni ML, Epand RF, Rosenfeld Y, Peleg A, Barra D, Epand RM, Shai Y. Lipopolysaccharide, a key molecule involved in the synergism between temporinsin inhibiting bacterial growth and in endotoxin neutralization. *J. Biol. Chem.* 2008; **283**: 22907–229017.
33 Mangoni ML, Shai Y. Temporins and their synergism against Gram-negative bacteria and in lipopolysaccharide detoxification. *Biochim. Biophys. Acta* 2009; **1788**: 1610–1619.
34 Carotenuto A, Malfi S, Saviello MR, Campiglia P, Gomez-Monterrey I, Mangoni ML, Gaddi LM, Novellino E, Grieco P. A different molecular mechanism underlying antimicrobial and hemolytic actions of temporins A and L. *J. Med. Chem.* 2008; **51**: 2354–2362.
35 Atherton E, Sheppard RC. *Solid-phase Peptide Synthesis: A Practical Approach*. IRL: Oxford; 1989.
36 Valenti P, Visca P, Antonini G, Orsi N. Antifungal activity of ovotransferrin towards genus Candida. *Mycopathologia* 1985; **89**: 169–175.
37 Eisenberg D. Three-dimensional structure of membrane and surface proteins. *Annu. Rev. Biochem.* 1984; **53**: 595–623.
38 Unneberg P, Merelo JJ, Chacon P, Moran F. SOMCD: method for evaluating protein secondary structure from UV circular dichroism spectra. *Proteins* 2001; **42**: 460–470.
39 Mygind PH, Fischer RL, Schnorr KM, Hansen MT, Sonksen CP, Ludvigsen S, Raventos D, Buskov S, Christensen B, De Maria L, Taboureau O, Yaver D, Elvig-Jorgensen SG, Sorensen MV, Christensen BE, Kjaerulff S, Frimodt-Moller N, Lehrer RI, Zasloff M, Kristensen HH. Plectasin is a peptide antibiotic with therapeutic potential from a saprophytic fungus. *Nature* 2005; **437**: 975–980.
40 Glaser R, Harder J, Lange H, Bartels J, Christophers E, Schroder JM. Antimicrobial psoriasin (S100A7) protects human skin from *Escherichia coli* infection. *Nat. Immunol.* 2005; **6**: 57–64.
41 Holmberg SD, Solomon SL, Blake PA. Health and economic impacts of antimicrobial resistance. *Rev. Infect. Dis.* 1987; **9**: 1065–1078.
42 Rinaldi AC. Antimicrobial peptides from amphibian skin: an expanding scenario. *Curr. Opin. Chem. Biol.* 2002; **6**: 799–804.
43 Miele R, Ponti D, Boman HG, Barra D, Simmaco M. Molecular cloning of a bombinin gene from *Bombina orientalis*: detection of NF-kappaB and NF-IL6 binding sites in its promoter. *FEBS Lett.* 1998; **431**: 23–28.
44 Mangoni ML, Miele R, Renda TG, Barra D, Simmaco M. The synthesis of antimicrobial peptides in the skin of *Rana esculenta* is stimulated by microorganisms. *FASEB J.* 2001; **15**: 1431–1432.
45 Mangoni ML, Saugar JM, Dellisanti M, Barra D, Simmaco M, Rivas L. Temporins, small antimicrobial peptides with leishmanicidal activity. *J. Biol. Chem.* 2005; **280**: 984–990.
46 Chen Q, Wade D, Kurosaka K, Wang ZY, Oppenheim JJ, Yang D. Temporin A and related frog antimicrobial peptides use formyl peptide receptor-like 1 as a receptor to chemoattract phagocytes. *J. Immunol.* 2004; **173**: 2652–2659.
47 Aurell CA, Wistrom AO. Critical aggregation concentrations of gram-negative bacterial lipopolysaccharides (LPS). *Biochem. Biophys. Res. Commun.* 1998; **253**: 119–123.
48 Kamysz W, Mickiewicz B, Greber K, Rodziewicz-Motowidlo S. Conformational solution studies of the anti-microbial temporin A retro-analogues by using NMR spectroscopy. *J. Pept. Sci.* 2007; **13**: 327–333.
49 Saviello MR, Malfi S, Campiglia P, Cavalli A, Grieco P, Novellino E, Carotenuto A. New insight into the mechanism of action of the temporin antimicrobial peptides. *Biochemistry* 2010; **49**: 1477–1485.
50 Wade D, Silberring J, Soliymani R, Heikkinen S, Kilpelainen I, Lankinen H, Kuusela P. Antibacterial activities of temporin A analogs. *FEBS Lett.* 2000; **479**: 6–9.
51 Rinaldi AC, Di Giulio A, Liberi M, Gualtieri G, Oratore A, Bozzi A, Schinina ME, Simmaco M. Effects of temporins on molecular

Journal of PeptideScience

dynamics and membrane permeabilization in lipid vesicles. *J. Pept. Res.* 2001; **58**: 213–220.

52 Wieprecht T, Dathe M, Beyermann M, Krause E, Maloy WL, MacDonald DL, Bienert M. Peptide hydrophobicity controls the activity and selectivity of magainin 2 amide in interaction with membranes. *Biochemistry* 1997; **36**: 6124–6132.

53 Wade D, Flock JI, Edlund C, Lofving-Arvholm I, Sallberg M, Bergman T, Silveira A, Unson C, Rollins-Smith L, Silberring J, Richardson M, Kuusela P, Lankinen H. Antibiotic properties of novel synthetic temporin A analogs and a cecropin A-temporin A hybrid peptide. *Protein Pept. Lett.* 2002; **9**: 533–543.

Biochimica et Biophysica Acta 1828 (2013) 652–660

Contents lists available at SciVerse ScienceDirect

Biochimica et Biophysica Acta

journal homepage: www.elsevier.com/locate/bbamem

The effect of D-amino acid substitution on the selectivity of temporin L towards target cells: Identification of a potent anti-*Candida* peptide☆,☆☆

Paolo Grieco [a,1], Alfonso Carotenuto [a,1], Luigia Auriemma [a], Maria Rosaria Saviello [a], Pietro Campiglia [b], Isabel M. Gomez-Monterrey [a], Ludovica Marcellini [c], Vincenzo Luca [c], Donatella Barra [c], Ettore Novellino [a], Maria Luisa Mangoni [c,*]

[a] *Department of Pharmaceutical and Toxicological Chemistry, University of Naples 'Federico II', I-80131 Naples, Italy*
[b] *Department of Pharmaceutical and Biomedical Sciences, University of Salerno, I-84084, Fisciano, Salerno, Italy*
[c] *Istituto Pasteur-Fondazione Cenci Bolognetti, Istituto di Biologia e Patologia Molecolari del CNR, Department of Biochemical Sciences, La Sapienza University, 00185 Rome, Italy*

ARTICLE INFO

Article history:
Received 3 June 2012
Received in revised form 27 August 2012
Accepted 30 August 2012
Available online 10 September 2012

Keywords:
Antimicrobial peptide
Temporin L
D-Amino acid
Peptide–membrane interaction
Drug-resistance
NMR spectroscopy

ABSTRACT

The frog skin peptide temporin L (TL, 13-residues long) has a wide and potent spectrum of antimicrobial activity, but it is also toxic on mammalian cells at its microbicidal concentrations. Previous studies have indicated that its analogue [Pro^3]TL has a slightly reduced hemolytic activity and a stable helical conformation along residues 6–13. Here, to expand our knowledge on the relationship between the extent/position of α-helix in TL and its biological activities, we systematically replaced single amino acids within the α-helical domain of [Pro^3]TL with the corresponding D isomers, known as helix breakers. Structure–activity relationship studies of these analogues, by means of CD and NMR spectroscopy analyses as well as antimicrobial and hemolytic assays were performed. Besides increasing our understanding on the structural elements that are responsible for cell selectivity of TL, this study revealed that a single L to D amino acid substitution can preserve strong anti-*Candida* activity of [Pro^3]TL, without giving a toxic effect towards human cells.

1. Introduction

Extensive clinical usage of classical antibiotics/antimycotics has led to the growing emergence of many medically relevant resistant microbes making the discovery of alternative drugs remarkably critical [1,2]. Antimicrobial peptides (AMPs) existing in virtually all species of life have been shown to exert direct killing activity on a large number of invading microorganisms. They represent the most ancient and fast-acting elements of the host's innate defence system against microbial pathogens [3,4]. At present, these AMPs are considered as promising candidates for the generation of a new class of anti-infective agents [5–8]. They have been thoroughly investigated particularly in those animals (e.g. insects) lacking an adaptive immune system [9]. However, a large part of the current knowledge on the peptide-mediated innate immunity comes from studies performed with mammalian AMPs and with AMPs from amphibian skin secretions that are known to be a rich storehouse of various bioactive peptides [10,11]. Although the exact mode of action of AMPs has not been established yet, all of them interact with microbial membranes. They accumulate within the membranes and increase their permeability causing the loss of barrier function and death of the microbe [12,13]. Note that recent high resolution structural studies have provided important mechanistic insights into the conformation of AMPs required for their translocation across the lipopolysaccharide (LPS or endotoxin) outer membrane of Gram-negative bacteria [14,15], as well as for their ability to permeate phospholipid bilayers mimicking various membranes, via the barrel-stave or carpet-like mechanism (as e.g. in the case of pardaxin [16,17], LL-37 [18], and MSI-594, a synthetic hybrid of MSI-78 and melittin [19,20]). Alternatively, peptides can enter the cell and inhibit vital

Abbreviations: 1D, and 2D, one and two-dimensional; CD, circular dichroism; Cho, cholesterol; CL, cardiolipin; DCM, dichloromethane; DMEM, Dulbecco's modified Eagle's medium; DIEA, diisopropyl ethylamine; DMF, *N*,*N*-dimethylformamide; DPC, dodecylphosphocholine; DQF-COSY, double quantum filtered correlated spectroscopy; EDTA, ethylenediaminetetraacetic acid; Et_3SiH, triethylsilane; Fmoc, 9-fluorenylmethoxycarbonyl; HBTU, 2-(1H-benzotriazole-1-yl)-1,1,3,3-tetramethyluronium hexafluoro-phosphate; HOBt, *N*-hydroxy-benzotriazole; LUV, large unilamellar vesicles; MTT, 3-(4,5-dimethylthiazol-2-yl)-2,5-diphenyltetrazolium bromide; NMR, nuclear magnetic resonance; NOE, nuclear Overhauser effect; NOESY, nuclear Overhauser enhancement spectroscopy; Pbf, 2,2,4,6,7-pentamethyldihydrobenzo-furan-5-sulfonyl; POPC, 1-palmitoyl-2-oleoyl-sn-glycero-3-phosphocholine; POPE, 1-palmitoyl-2-oleoyl-sn-glycero-3-phosphoethanolamine; POPG, 1-palmitoyl-2-oleoyl-sn-glycero-3-phosphoglycerol; RP-HPLC, reversed-phase high performance liquid chromatography; SAR, structure activity relationship; SDS, sodium dodecylsulphate; TL, temporin TL; TOCSY, total correlation spectroscopy

☆ This paper is dedicated to Professors Donatella Barra and Francesco Bossa on the occasion of their 70th birthday.

☆☆ Abbreviations used for amino acids and designation of peptides follow the rules of the IUPAC-IUB Commission of Biochemical Nomenclature in *J. Biol. Chem.* 1972, *247*, 977–983. Amino acid symbols denote L-configuration unless indicated otherwise.

* Corresponding author at: Department of Biochemical Sciences, La Sapienza University, Via degli Apuli, 9-00185 Rome, Italy. Tel.: +39 06 49917693; fax: +39 06 49917566
E-mail address: marialuisa.mangoni@uniroma1.it (M.L. Mangoni).

[1] Share equal first authorship.

0005-2736/$ – see front matter © 2012 Elsevier B.V. All rights reserved.
http://dx.doi.org/10.1016/j.bbamem.2012.08.027

processes, e.g. DNA duplication, protein/cell wall synthesis [21–25]. This multiple targeting and physical disruption of fundamental physiological cell structures (i.e. the cytoplasmic membrane) makes bacteria and fungi less likely to become resistant to AMPs, compared to conventional antimicrobials that usually act via a receptor-mediated mechanism [26,27].

The skin of several frog species, such as those belonging to the *Rana* genus, has proved to be an inexhaustible source of AMPs with a wide spectrum of activity [28,29]. For example, the amphibian temporins represent one of the largest families (more than 100 members) and are among the smallest-sized AMPs (10–14 amino acids) found in nature to date. They are mildly cationic peptides, due to the presence of only 1 or 2 basic residues in their sequence; they are amidated at the C-terminus and adopt an amphipathic α-helical preferential conformation in a hydrophobic environment [30]. Generally speaking, temporins are known to be active particularly against Gram-positive bacteria, with minimal inhibitory concentrations ranging from 2.5 μM to 20 μM. The only exception is given by the isoform temporin TL (TL, H-Phe^1-Val^2-Gln^3-Trp^4-Phe^5-Ser^6-Lys^7-Phe^8-Leu^9-Gly^{10}-Arg^{11}-Ile^{12}-Leu^{13}-NH_2), as it is strongly active also against Gram-negative bacteria and yeast strains [31]. The bacterial killing kinetics of temporins overlaps that of membrane perturbation [32]. As found for other AMPs, some temporins have shown immunomodulatory properties (e.g. chemotactic to human phagocytes [33]) and can neutralize the toxic effect of LPS [34]. In this context, important NMR studies of different native or de-novo designed host-defence peptides have recently been carried out to know the specific conformation of AMPs in their LPS-bound state [14,20,35].

Furthermore, temporins synergize when combined with other temporin-isoforms (i.e. the couples TA + TL and TB + TL) in both the antimicrobial and anti-endotoxin activities [36,37]. Most of them are practically non-hemolytic, but the highly potent temporin L kills human erythrocytes at microbicidal concentrations [31] and was revealed to be toxic in vivo, when tested on *Caenorhabditis elegans* worms [38]. Therefore, to be developed as a future broad spectrum antibiotic, it is necessary to increase its therapeutic index which is defined as the ratio between the concentration of its hemolytic activity and antimicrobial activity [39]. Recent studies on the structure/activity relationships of both native TL and its synthetic analogues have clearly indicated the existence of a direct correlation between the hemolytic activity of the peptide and its α-helical content [40]. In contrast, no such connection was found with the antimicrobial activity. Indeed, disrupting the peptide's α-helix at its N-terminus by replacing Gln^3 with a proline ([Pro^3]TL) did not significantly affect the antibacterial activity, while the hemolytic activity was reduced by more than half, up to 12 μM, a concentration causing about 90% hemolysis for the native TL [41]. Interestingly, the effects of proline substitution on the biological activity of other amphibian skin AMPs, such as maculatin peptide from the Australian tree frog species *Litoria genimaculata*, have been previously evaluated [42]. Similar to our findings with TL analogues, removal of proline in maculatin 1.1 increased the peptide's interaction with neutral phospholipid bilayers, together with enhanced hemolytic activity. However, in contrast with what has been found with TL analogues, this was accompanied by a strong reduction in the antibiotic activity and lytic effect of maculatin on anionic membranes [42,43].

Nevertheless, the disruption of the α-helix of TL at its N and C-terminal ends, by replacing Gln^3 and Gly^{10} with Pro ([Pro^3, Pro^{10}]TL), induced a drastic decrease in both the hemolytic and antibacterial activities [40]. Previous NMR studies with [Pro^3]TL in sodium dodecylsulphate (SDS) and dodecylphosphocholine (DPC) micelles, mimicking the anionic and zwitterionic character of bacterial and erythrocyte membrane, respectively [41], revealed a stable helical conformation along residues 6–13 [44]. Here, to get a deeper insight into the relationship between the extent/position of the α-helix along the sequence of TL and the biological activity of this peptide, six derivatives of [Pro^3]TL were synthesized and analyzed by means of antimicrobial and hemolytic assays combined with CD and NMR spectroscopy. More specifically, such derivatives were obtained by a systematic replacement of single residues within the α-helix domain (Lys^7 to Leu^{13}) of [Pro^3]TL with D enantiomers, known as helical breakers. The results provide a better understanding on the structural elements that are responsible for the cell selectivity of TL. Most importantly, we have identified an analogue endowed with high anti-*Candida* activity, a slightly reduced antibacterial potency than the native TL, but practically devoid of any lytic effect on mammalian cells. This novel TL derivative represents a fascinating template for the development of novel temporin-based anti-infective drugs with increased therapeutic index.

2. Materials and methods

2.1. Materials

N^{α}-Fmoc-protected amino acids, 2-(1H-benzotriazole-1-yl)-1,1,3,3-tetramethyluronium hexafluoro-phosphate (HBTU), *N*-hydroxybenzotriazole (HOBt) and Rink amide resin were purchased from GL Biochem Ltd (Shanghai, China). Peptide synthesis solvents, reagents, as well as CH_3CN for HPLC were reagent grade and were acquired from commercial sources and used without further purification unless otherwise noted. See Supplementary material for more details on peptide synthesis and analytical data (Supplementary Table S1).

The following lipids: 1-palmitoyl-2-oleoyl-sn-glycero-3-phosphoethanolamine (POPE); 1-palmitoyl-2-oleoyl-sn-glycero-3-phosphoglycerol (POPG); cardiolipin (CL); 1-palmitoyl-2-oleoyl-sn-glycero-3-phosphocholine (POPC) and cholesterol (Cho) were purchased from Avanti Polar Lipids (Alabaster, AL, USA). SDS-d25 and DPC-d38 were obtained from Cambridge Isotope Laboratories, Inc. (Andover, MA); calcein, from Sigma (St Louis, MO, USA). All other chemicals used were of reagent grade.

2.2. Microorganisms

The strains used for the antimicrobial assays were the following: the Gram-negative bacteria *Acinetobacter baumannii* ATCC 19606, *Acinetobacter junii* RT-4, *Escherichia coli* ATCC 25922, *E. coli* D21, *Pseudomonas aeruginosa* ATCC 15692, *P. aeruginosa* ATCC 27853, *Pseudomonas syringae* pv tabaci 1918NCPPB, and *Yersinia pseudotuberculosis* YPIII; the Gram-positive bacteria *Bacillus megaterium* Bm11, *Staphylococcus aureus* ATCC 25923, *S. aureus* Cowan I, *Staphylococcus capitis* 1, *Staphylococcus epidermidis* ATCC 12228, and *Streptococcus pyogenes* ATCC 21547 and the yeasts *Candida albicans* ATCC 10231, *C. albicans* clinical isolates (strains n. 1, 2, 3 and 4), *Saccharomyces cerevisiae*, and *Saccharomyces pombe*.

2.3. Antimicrobial assay

Susceptibility testing was performed by adapting the microbroth dilution method outlined by the Clinical and Laboratory Standards Institute, using sterile 96-well plates (Falcon NJ, USA). The growth of the bacterial and yeast cells was aseptically measured by absorbance at 590 nm with a spectrophotometer (UV-1700 Pharma Spec Shimadzu, Tokyo, Japan). Afterwards, aliquots (50 μL) of bacteria in mid-log phase at a concentration of 2×10^6 colony-forming units (CFU)/mL in culture medium (Mueller-Hinton, MH) were added to 50 μL of MH broth containing the peptide in serial 2-fold dilutions ranging from 0.75 to 48 μM. The same procedure was followed with yeasts in Winge medium [45] (a final cell concentration of approximately 3.5×10^4 CFU/mL and 3×10^5 CFU/mL for *Candida* and *Saccharomyces* strains, respectively). Inhibition of microbial growth was determined by measuring the absorbance at 590 nm, after an incubation of 18 h at 37 °C (30 °C for yeasts), with a microplate reader (Infinite M200; Tecan,

Salzburg, Austria). Antimicrobial activities were expressed as the minimal inhibitory concentration (MIC), the concentration of peptide at which 100% inhibition of microbial growth is observed after 18 h of incubation.

2.4. Hemolytic assay

The hemolytic activity was measured on human red blood cells as reported previously [40]. Freshly collected human blood with EDTA was centrifuged for 10 min at 1000×*g* and the erythrocytes obtained were washed three times with 0.9% (w/v) NaCl, centrifuged as above, and resuspended in 0.9% NaCl to approximately 1.5×10^8 cells/mL. Then, 95 μL aliquots of the erythrocyte suspension were incubated with 5 μL of serial two-fold dilutions of the peptide for 40 min at 37 °C with gentle mixing. The samples were then centrifuged and the absorbance of the supernatant was measured at 415 nm. Complete lysis was measured by suspending erythrocytes in distilled water [46].

2.5. Cytotoxic activity

The cytotoxic effect of the peptides was determined by the inhibition of 3-(4,5-dimethylthiazol-2-yl)-2,5-diphenyltetrazolium bromide (MTT) reduction to insoluble formazan, by mitochondrial reductases, on the immortalized human keratinocyte (HaCaT) cells. Cells were cultured in Dulbecco's modified Eagle's medium (DMEM; Sigma) supplemented with 10% heat-inactivated fetal bovine serum, glutamine (4 mM) and antibiotics (penicillin and streptomycin) and then plated in triplicate wells at 1×10^4 cells/well (96-well plates were used). After 2 h at 37 °C in a 5% CO_2 atmosphere, the medium was replaced with 100 μL fresh DMEM supplemented with the peptide at different concentrations. The plate was then incubated for 90 min at 37 °C in a 5% CO_2 atmosphere. Afterwards, the medium was removed and replaced with fresh DMEM containing 0.5 mg/mL MTT. After 4-h incubation, the formazan crystals were dissolved by adding 100 μL of acidified isopropanol and viability was determined by absorbance measurements at 595 nm. Cell viability was calculated with respect to control cells (cells not treated with peptide).

2.6. Calcein-loaded large unilamellar vesicles (LUV) and leakage assay

Lipid films of POPE/POPG (7:3, w/w), POPG/CL (6:4, w/w), and POPC/Cho (9:1, w/w) were prepared by dissolving dry lipids (2 mg of each lipid mixture) in chloroform/methanol (2:1, v/v) and evaporating the solvents under a nitrogen stream. The lipid film was then hydrated with 10 mM Tris and 150 mM NaCl (pH 7.4) containing 60 mM calcein solution. The liposome suspension was extruded 10 times through a polycarbonate filter (pore size, 0.1 μm), and free calcein was removed by gel filtration, using a Sephadex G-25 column (1.5×10 cm; Pharmacia Biotech AB Uppsala, Sweden) at room temperature. Calcein in the vesicles is highly concentrated, and the fluorescence is self-quenched. Calcein release induced by the peptide was monitored at 37 °C by the fluorescence increase (λexcitation = 485 nm; λemission = 535 nm). Complete dye release was obtained using 0.1% Triton X-100, which causes total destruction of lipid vesicles [47].

2.7. Circular dichroism (CD)

All CD spectra were recorded using a JASCO J710 spectropolarimeter at 25 °C with a cell of 1 mm path length. The CD spectra were acquired in the range of 260–190 nm, 1 nm bandwidth, 4 accumulations, and 100 nm/min scanning speed. The CD spectra of TL and TL derivates, at a concentration of 100 μM, were performed in phosphate buffer (pH = 7.4), SDS (20 mM), DPC (20 mM), or DPC/SDS 18/2 mM micellar solutions.

2.8. Nuclear magnetic resonance (NMR) spectroscopy

The samples for NMR spectroscopy were prepared by dissolving the appropriate amount of [Pro^3, DLeu^9]TL in 0.55 mL of ^1H_2O, 0.05 mL of ^2H_2O to obtain a concentration of 1–2 mM peptide and 200 mM SDS-d_{25} or DPC-d_{38}. The NMR experiments were performed at pH 5.0. NH exchange studies were performed by dissolving peptide in 0.60 mL of ^2H_2O and 200 mM SDS-d_{25} or DPC-d_{38}. NMR spectra were recorded on a Varian Unity INOVA 700 MHz spectrometer equipped with a z-gradient 5 mm triple-resonance probe head. All the spectra were recorded at a temperature of 25 °C. The spectra were calibrated relative to 3-(trimethylsilanyl)propionic acid (0.00 ppm) as internal standard. One-dimensional (1D) NMR spectra were recorded in the Fourier mode with quadrature detection. 2D DQF-COSY [48,49], TOCSY [50], and NOESY[51] spectra were recorded in the phase-sensitive mode using the method from States [52]. Data block sizes were 2048 addresses in t_2 and 512 equidistant t_1 values. A mixing time of 70 ms was used for the TOCSY experiments. NOESY experiments were run with mixing times in the range of 150–300 ms. The water signal was suppressed by gradient echo [53]. The 2D NMR spectra were processed using the NMRPipe package [54]. Before Fourier transformation, the time domain data matrices were multiplied by shifted $\sin^2$ functions in both dimensions, and the free induction decay size was doubled in F1 and F2 by zero filling. The qualitative and quantitative analyses of DQF-COSY, TOCSY and NOESY spectra were obtained using the interactive program package XEASY [55]. $^3J_{HN\text{-}H\alpha}$ couplings were difficult to measure probably because of a combination of small coupling constants and broad lines. The temperature coefficients of the amide proton chemical shifts were calculated from 1D ^{1}H NMR and 2D TOCSY experiments performed at different temperatures in the range of 298–320 K by means of linear regression.

2.9. Structural determinations

The NOE-based distance restraints were obtained from NOESY spectra collected with a mixing time of 200 ms. Peak volumes were translated into upper distance bounds with the CALIBA routine from the DYANA software package [56]. The requisite pseudoatom corrections were applied for non-stereospecifically assigned protons at prochiral centers and for the methyl group. After discarding redundant and duplicated constraints, the final list of constraints was used to generate an ensemble of 200 structures by the standard DYANA protocol of simulated annealing in torsion angle space. No dihedral angle restraints and no hydrogen bond restraints were applied. An error tolerant target function (tf type 3) was used to account for the peptide intrinsic flexibility. Then, 20/200 structures were chosen, whose interproton distances best fitted NOE derived distances, and refined through successive steps of restrained and unrestrained energy minimization calculations using the Discover algorithm (Accelrys, San Diego, CA) and the consistent valence force field [57]. No residue was found in the disallowed region of the Ramachandran plot. The final structures were analyzed using the InsightII program (Accelrys, San Diego, CA). Graphical representations were carried out with the InsightII program. The root-mean-squared-deviation analysis between energy-minimized structures was carried out with the program MOLMOL [58]. The PROMOTIF program was used to extract details on the location and types of structural secondary motifs [59].

3. Results

3.1. Biological activity

The antibacterial, anti-yeast and hemolytic activities of the synthesized [Pro^3]TL analogues (Table 1) were compared with those of TL and [Pro^3]TL. The data highlighted the following: (i) Replacement of Lys^7 with its DLys enantiomer considerably reduced the

Table 1
Sequences of TL analogues.

Compound	Sequences[a]
TL[b]	H-Phe^1-Val^2-Gln^3-Trp^4-Phe^5-Ser^6-Lys^7-Phe^8-Leu^9-Gly^{10}-Arg^{11}-Ile^{12}-Leu^{13}-NH_2
[Pro^3]TL[b]	H-Phe^1-Val^2-**Pro^3**-Trp^4-Phe^5-Ser^6-Lys^7-Phe^8-Leu^9-Gly^{10}-Arg^{11}-Ile^{12}-Leu^{13}-NH_2
[Pro^3, DLys^7]TL	H-Phe^1-Val^2-**Pro^3**-Trp^4-Phe^5-Ser^6-**DLys^7**-Phe^8-Leu^9-Gly^{10}-Arg^{11}-Ile^{12}-Leu^{13}-NH_2
[Pro^3, DPhe^8]TL	H-Phe^1-Val^2-**Pro^3**-Trp^4-Phe^5-Ser^6-Lys^7-**DPhe^8**-Leu^9-Gly^{10}-Arg^{11}-Ile^{12}-Leu^{13}-NH_2
[Pro^3, DLeu^9]TL	H-Phe^1-Val^2-**Pro^3**-Trp^4-Phe^5-Ser^6-Lys^7-Phe^8-**DLeu^9**-Gly^{10}-Arg^{11}-Ile^{12}-Leu^{13}-NH_2
[Pro^3, DArg^{11}]TL	H-Phe^1-Val^2-**Pro^3**-Trp^4-Phe^5-Ser^6-Lys^7-Phe^8-Leu^9-Gly^{10}-**DArg^{11}**-Ile^{12}-Leu^{13}-NH_2
[Pro^3, DIle^{12}]TL	H-Phe^1-Val^2-**Pro^3**-Trp^4-Phe^5-Ser^6-Lys^7-Phe^8-Leu^9-Gly^{10}-Arg^{11}-**DIle^{12}**-Leu^{13}-NH_2
[Pro^3, DLeu^{13}]TL	H-Phe^1-Val^2-**Pro^3**-Trp^4-Phe^5-Ser^6-Lys^7-Phe^8-Leu^9-Gly^{10}-Arg^{11}-Ile^{12}-**DLeu^{13}**-NH_2

[a] Residue variations compared to TL are highlighted in bold.
[b] Already described in references [40,41].

antimicrobial activity of the peptide on Gram-positive and Gram-negative bacteria. Indeed, its MIC value was 2 to 8-fold higher than that of TL and [Pro^3]TL (Table 2). More specifically, [Pro^3, DLys^7]TL almost lost activity against the Gram-negative *P. aeruginosa* and *E. coli* strains. Furthermore, a 2-fold higher MIC was found against *C. albicans* and *S. pombe*. However, the lytic effect on human red blood cells was dramatically reduced compared to [Pro^3]TL (8% hemolysis versus 92% at 24 μM) (Table 3). (ii) Replacing the flanking Phe^8 with DPhe ([Pro^3, DPhe^8]TL), reduced 2–4 fold the antibacterial/anti-yeast activity, whereas the hemolytic activity became lower than that observed with [Pro^3]TL but higher compared to [Pro^3, DLys^7]TL (Table 3). (iii) Interestingly, when Leu^9 was replaced with DLeu ([Pro^3, DLeu^9]TL), the antibacterial activity was equal or two-fold lower than that of TL (a 4-fold reduction against two strains out of 14), with an identical efficacy against *Candida* and *Saccharomyces* strains. Furthermore, the lytic activity on erythrocytes was almost completely abolished, causing only 9% hemolysis at a concentration of 48 μM (Table 3). (iv) Replacing the Arg residue in position 11 with its D enantiomer also resulted in a lower activity (2 to 4-fold higher MIC for the analogue compared with the wild type TL) against both Gram-positive and Gram-negative bacteria (8-fold higher MIC only in the case of *S. capitis*). However, the anti-yeast activity was weakly affected (Table 2). The percentage of hemolysis caused by this peptide was much lower than that of TL (16% lysis at 24 μM and 22% lysis at 48 μM); nevertheless, it was higher than that shown by the aforementioned [Pro^3, DLys^7]TL and [Pro^3, DLeu^9]TL analogues (Table 3). (v) When the chirality of the penultimate Ile residue changed to the D configuration, a 4-fold lower activity than TL was displayed against Gram-positive strains. The activity on Gram-negative bacteria also decreased, but to a lesser extent. The toxic effect on human erythrocytes was comparable to that of [Pro^3, DArg^{11}]TL. (vi) Finally, when the last residue Leu^{13} was replaced by its D enantiomer, the antibacterial/anti-yeast/hemolytic activities were generally found to overlap those of [Pro^3, DIle^{12}]TL.

3.2. Peptides' activity on C. albicans clinical isolates

To further expand our knowledge on the anti-*Candida* activity of the best analogue ([Pro^3, DLeu^9]TL), several clinical isolates of *C. albicans* were analyzed for their susceptibility to this analogue and to the native TL. An antimycotic resistant strain was also included for comparison. As indicated in Table 4, the same MICs were obtained for the two peptides on all the microorganisms tested.

3.3. Cytotoxicity towards human keratinocytes

The finding of a TL derivative ([Pro^3, DLeu^9]TL) with a highly reduced hemolytic activity and with a similar or identical antimicrobial potency on bacteria or *Candida* cells, prompted us to determine its toxicity against another important type of eukaryotic cells, i.e. the mammalian keratinocytes, which are present in several tissues colonized by *Candida* cells such as the skin, the oral mucosa as well as the corneal, conjunctival and genital epithelia. Remarkably, as reported in Table 5, viability of human keratinocytes after treatment with the native peptide ranged from 39% to 23%, at a concentration range from 6 to 48 μM; in

Table 2
Antimicrobial activity of the synthesized compounds.

	MIC[a] (μM)							
Strains	TL	[Pro^3] TL	[Pro^3, DLys^7] TL	[Pro^3, DPhe^8] TL	[Pro^3, DLeu^9] TL	[Pro^3, DArg^{11}] TL	[Pro^3, DIle^{12}] TL	[Pro^3, DLeu^{13}] TL
Gram-negative bacteria								
Acinetobacter baumannii ATCC 19606	6	6	24	12	12	12	24	12
Acinetobacter junii RT-4	3	6	6	12	3	6	3	3
Escherichia coli ATCC 25922	12	24	>48	12	12	24	24	24
Escherichia coli D21	12	12	48	24	12	24	12	12
Pseudomonas syringae pv tabaci	6	6	>48	12	24	12	12	12
Pseudomonas aeruginosa ATCC 15692	24	24	>48	>48	>48	>48	48	48
Pseudomonas aeruginosa ATCC 27853	>48	>48	>48	>48	>48	>48	48	>48
Yersinia pseudotuberculosis YPIII	3	3	12	6	6	12	12	6
Gram-positive bacteria								
Bacillus megaterium Bm11	1.5	1.5	3	3	1.5	3	3	3
Staphylococcus aureus ATCC 25923	3	3	24	6	6	12	12	12
Staphylococcus aureus Cowan I	3	1.5	12	6	6	6	12	6
Staphylococcus capitis 1	1.5	1.5	12	6	6	12	12	12
Staphylococcus epidermidis ATCC 12228	3	1.5	6	6	6	6	12	12
Streptococcus pyogenes ATCC 21547	6	6	12	6	6	12	12	12
Yeasts								
Candida albicans ATCC 10231	3	3	6	6	3	6	6	6
Saccharomyces pombe	6	3	12	6	6	6	6	6
Saccharomyces cerevisiae	6	6	6	12	6	6	6	6

[a] The reported MIC values are those obtained from at least three readings out of four independent measurements.

Table 3
Hemolytic activity of TL-analogues on human erythrocytes.

	Hemolysis (%)[a]							
[Peptide] (μM)	TL[b]	[Pro^3] TL[b]	[Pro^3, DLys^7] TL	[Pro^3, DPhe^8] TL	[Pro^3, DLeu^9] TL	[Pro^3, DArg^{11}] TL	[Pro^3, DIle^{12}] TL	[Pro^3, DLeu^{13}] TL
48	100	100	18	94	9	22	17	15
24	94	92	8	19	8	16	14	17
12	92	42	5	19	7	8	10	17
6	48	10	7	17	3	6	5	8
3	13	6	4	5	2	4	4	6
1.5	3	4.5	2	4	2	2	2	3

[a] Values are the mean of three independent experiments with SD not exceeding 1.5%.
[b] Values already reported in references [31,32].

contrast, only a slightly toxic effect was recorded by [Pro^3, DLeu^9]TL at the highest peptide concentration used (48 μM).

3.4. Structural studies

3.4.1. CD analysis

To explore the conformational changes of TL analogues, we performed CD spectroscopy studies in phosphate buffer (pH 7.4), DPC, SDS, and DPC/SDS micelle solutions. These micelles were used as rough mimetics of mammalian, bacterial and yeast membranes, respectively. CD spectra in phosphate buffer revealed the presence of disordered conformers for all compounds with a minimum close to 198 nm (data not shown). In contrast, in DPC (Fig. 1a), SDS (Fig. 1b), and DPC/SDS (Fig. 1c) micelle solutions, the shape of the CD spectra displaying two minima around 209 and 222 nm supports the contribution of an α-helix. CD spectra of [Pro^3, DLeu^9]TL in the three environments are shown in Fig. 1d. Helical content was predicted from CD spectra using the SOMCD method [60] (Table 6). Since CD spectra for short peptides are more affected by the termini than for long proteins, the error bars for helical content would be of order 10%. The helical content of [Pro^3]TL is included for comparison. All the D analogues showed a reduction in the percentage of helicity compared to [Pro^3]TL, in agreement with the design strategy. Furthermore, helical content observed in both SDS and DPC/SDS was about 20% reduced compared to DPC. Indeed, as illustrated in Table 6, helical content of all peptides ranged from 24% to 10% in DPC, from 18% to 7% in SDS and from 20% to 8% in DPC/SDS.

3.4.2. NMR analysis

[Pro^3, DLeu^9]TL was also investigated by NMR spectroscopy. Due to the very similar behavior of this peptide in the presence of SDS and DPC/SDS micelles, as manifested by CD analysis (Fig. 1d and Table 6), NMR spectroscopy was performed only in SDS and DPC micellar solutions. Complete ^{1}H NMR chemical shift assignments were effectively achieved for the peptide according to the Wüthrich procedure [61] (Supplementary Tables S2–S3).

3.4.2.1. [Pro^3, DLeu^9]TL in SDS solution. Diagnostic NMR parameters observed for [Pro^3, DLeu^9]TL in SDS solution indicated some conformational propensity toward helical or turn structures. Hα atoms from residue 2 to residue 13 experienced an upfield shift of the NMR signals compared to those found for the same amino acids in the random coil state [62,63] (Supplementary Fig. S1). Only amide protons of residues Phe^5, Lys^7, and Ile^{12} showed exchange rates and temperature coefficients indicating that they were shielded from the solvent (Supplementary Table S2). The presence of a number of $d_{\alpha N}(i,i+2)$ NOE contacts indicated the presence of helical and turn structures along the peptide, in line with CD results. Structure calculation gave an ensemble of 20 structures satisfying the NMR-derived constraints (structural statistics are reported in Table 7). Many structures (17 of 20) of [Pro^3, DLeu^9]TL showed a β-turn centered on Pro^3 and Trp^4 followed by an α-helix along residues 5–8 (Fig. 2a). Also, a β-turn centered on Arg^{11} and Ile^{12} could be observed in several structures (15 of 20).

3.4.2.2. [Pro^3, DLeu^9]TL in DPC solution. [Pro^3, DLeu^9]TL in DPC solution exhibited NMR spectral features (Supplementary Fig. S1 and Table S3) resembling those of the parent [Pro^3]TL in the same solution [44]. Upfield shift of the Hα NMR signals, low values of the exchange rates and temperature coefficients of the amide protons, and diagnostic NOEs (Supplementary Table S3) indicated that central residues are in a helical conformation. Structure calculation gave an ensemble of 20 structures satisfying the NMR-derived constraints (violations smaller than 0.50 Å). As found for [Pro^3]TL, a β-turn centered on Pro^3 and Trp^4 was detected in the structure of [Pro^3, DLeu^9]TL in DPC micelles. It was followed by a 3–10 helix along residues 5–7, and a bulged helical structure along residues 5–10 (18 of 20 structures). The bulged helix was stabilized by a H-bond between the NH group of Gly^{10} and the C═O group of Phe^5 (Fig. 2b). An α-helical conformation along residues 10–13 was noted in 5 of 20 structures.

3.5. Permeabilization of large unilamellar vesicles (LUV) by the peptides

To know whether the highly reduced hemolytic activity of [Pro^3, DLeu^9]TL was due to its inability to permeate the erythrocyte membrane, we used calcein LUV made of POPC/Cho (9:1,w:w) which mimic the lipid composition of the outer leaflet of mammalian erythrocyte membrane. In addition, liposomes made of POPE/POPG (7:3, w:w) were also included to mimic the lipid composition of the

Table 4
Peptides' activity on clinical isolates of *C. albicans*.

Microorganisms	MIC[a] (μM)	
	TL	[Pro^3, DLeu^9]TL
Candida albicans strain n. 1	6	6
Candida albicans strain n. 2	3	3
Candida albicans strain n. 3	6	6
Candida albicans strain n. 4[b]	3	3

[a] The reported MIC values are those obtained from at least three readings out of four independent measurements.
[b] Resistance phenotype: fluconazol, amphotericin B.

Table 5
Peptides' cytotoxicity on HaCat cells.

Peptide concentration (μM)	Cell viability[a] (%)	
	TL	[Pro^3, DLeu^9]TL
48	23	85
24	26	100
12	29	100
6	39	100
3	77	100

[a] Cell viability is expressed as percentage with respect to the control (cells not treated with the peptide). Values are the mean of three independent experiments with SD not exceeding 2%.

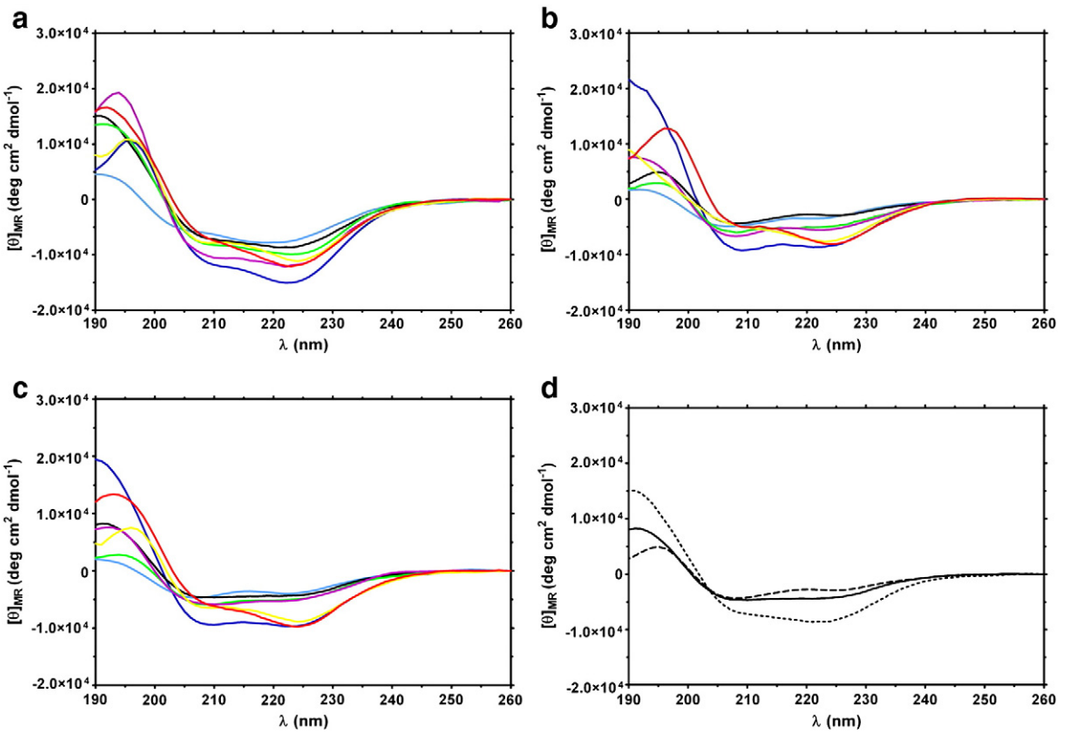

Fig. 1. CD spectra of [Pro^3]TL and its analogues in a) DPC, b) SDS, c) DPC/SDS. ([Pro^3]TL, blue line; [Pro^3, DLys^7]TL, heavenly line; [Pro^3, DPhe^8]TL, violet line; [Pro^3, DLeu^9]TL, black line; [Pro^3, DArg^{11}]TL, green line; [Pro^3, DIle^{12}]TL, yellow line; [Pro^3, DLeu^{13}]TL, red line). d) CD spectra of [Pro^3, DLeu^9]TL in DPC (dotted line), SDS (dashed line), and DPC/SDS (solid line).

cytoplasmic membrane of a representative Gram-negative bacterium (e.g. *E. coli*). The membrane of a representative Gram-positive bacterium (e.g. *S. aureus*) was, instead, mimicked by POPG/CL (6:4, w/w) LUV.

Different concentrations of the peptide were added to the LUV suspension and membrane permeability was measured by following fluorescence recovery due to calcein release from the vesicles (Fig. 3). Interestingly, the effect induced by [Pro^3, DLeu^9]TL (empty symbols) on the permeation of both POPE/POPG (blue triangles) and POPG/CL (red squares) LUV was similar to that of TL (filled symbols) at a peptide/lipid molar ratio of 0.002 and 0.004. Differently, at the highest peptide/lipid molar ratio used (0.08), the extent of calcein release caused by TL was about 2-fold higher than that of [Pro^3, DLeu^9]TL. The overall low calcein leakage from these lipid vesicles could be related to a different peptide's conformation/oligomeric state with respect to that adopted upon contact with bacterial cell wall components which are absent in model membranes. Furthermore, the preference of both TL and [Pro^3, DLeu^9]TL for Gram-positive over Gram-negative model membrane systems correlated with the higher antimicrobial activity of these peptides towards Gram-positive bacterial strains compared to Gram-negatives (see the corresponding MIC values in Table 2).

Table 6
α-Helix percentage of TL-analogues.

Peptides	[Pro^3] TL	[Pro^3, DLys^7] TL	[Pro^3, DPhe^8] TL	[Pro^3, DLeu^9] TL	[Pro^3, DArg^{11}] TL	[Pro^3, DIle^{12}] TL	[Pro^3, DLeu^{13}] TL
DPC	25[a]	10	24	15	18	20	22
SDS	22[a]	7	14	10	12	15	18
DPC–SDS	23	8	14	11	12	17	20

[a] See reference [44].

In contrast, when the zwitterionic POPC/Cho LUV (black circles) were employed, the effect of [Pro^3, DLeu^9]TL was drastically less pronounced (3 to 8-fold lower) than that of TL at all concentrations used, suggesting that the loss in hemolytic activity of [Pro^3, DLeu^9]TL is mainly related to its incapability to damage the erythrocyte membrane.

4. Discussion

Therapeutic peptide antibiotics should have advantages over conventional drugs, due to their diverse potential applications, ranging from antimicrobial to immunomodulatory and/or endotoxin-neutralizing activities. They can be used either alone or in combination to synergize one with each other [64]. Although the efficacy of these AMPs is in general less than certain traditional antibiotics, one of their attractive properties is the ability to kill sensitive and multi-drug resistant strains at similar concentrations [32]. Moreover, compared to classical antibiotics, AMPs act extremely rapidly and can attack multiple bacterial cellular targets [22]. Among AMPs from frog skin, temporins represent promising potential molecules to be developed for clinics.

Table 7
Structural statistics for the final 20 structures of [Pro^3, DLeu^9]TL in SDS and in DPC micelles.

Parameter	[Pro^3, DLeu^9]TL in SDS	[Pro^3, DLeu^9]TL in DPC
NOE distance restraints		
Total	109	135
Intra	51	55
Short	48	57
Medium	10	23
Backbone RMSD (Å)	0.79	0.48
Overall RMSD (Å)	1.45	0.99
Max restraint violation (Å)	0.68	0.50

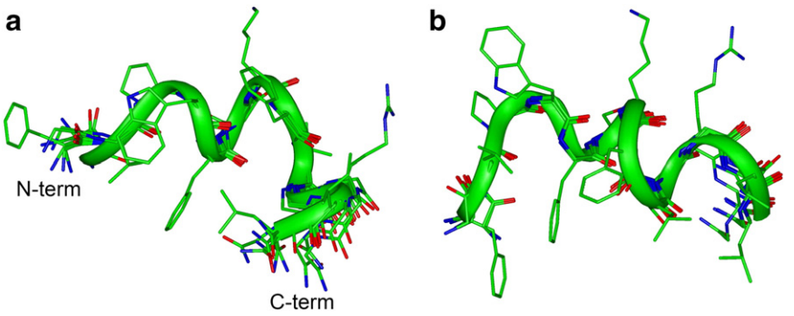

Fig. 2. Superposition of the 10 lowest energy conformers of [Pro^3, DLeu^9]TL in SDS (a), and DPC (b). Structures were superimposed using the backbone heavy atoms. Heavy atoms are shown with different colors (carbon, green; nitrogen, blue; oxygen, red). Hydrogen atoms are not shown for clarity. Only side chains of the lowest energy conformer are displayed for clarity. Backbone atoms of the lowest energy conformer were evidenced as a ribbon.

Previously, we studied the effect of the replacement of cationic and hydrophobic residues of the native TL on its antimicrobial and hemolytic activities. Furthermore, the effects of such substitutions on the helicity, hydrophobicity and hydrophobic moment of the peptide were analyzed. We demonstrated that the nature of cationic residues can differently modify the antimicrobial/hemolytic activity of TL, without changing its helical content. In contrast, a direct correlation was revealed between the percentage of peptide's helicity in zwitterionic micelles and its toxicity on human red blood cells. In addition, we observed that replacement of Gly^{10} with a leucine residue almost abrogated the antimicrobial efficacy of TL causing a dramatic enhancement of hemolysis, probably due to oligomerization of the peptide.

Here, we performed SAR studies using six different analogues of TL, each containing a single D amino acid starting from position 7 (Table 1). Biological data have proved that interruption of the helical content of [Pro^3]TL by replacement of D versus L amino acids diminishes the peptide's antibacterial activity (Table 3). Interestingly, anti-yeast activity is slightly decreased for all D analogues, but it is preserved for [Pro^3, DLeu^9]TL (Table 2). Hemolytic activity drops below 8% at 6 μM for all analogues but [Pro^3, DPhe^8]TL (Table 3). However, the most promising outcome is that the anti-*Candida* activity of [Pro^3, DLeu^9]TL analogue is preserved also against an antimycotic resistant strain (Table 4), while the peptide is practically non-toxic towards human erythrocytes and keratinocytes (Tables 3 and 5). Considering the conformational behavior, the incorporation of D amino acids reduces the α-helical structure of [Pro^3]TL to different degrees, depending on their position and composition of the lipid environment (Table 6). These substitutions can also differently influence the peptide's biological activity (Table 2). Reduction of the helicity is higher when the central Lys^7 residue is replaced by DLys compared to the effects caused by D substitution at other positions. In the case of [Pro^3, DLeu^9]TL, NMR analysis indicated that the helical structure in DPC micelles is partially conserved by an unusual i to $i+5$ hydrogen bond between Phe^5 and Gly^{10} residues (Fig. 2b). The parent peptides TL and [Pro^3]TL showed a classical α-helical structure along these residues [44]. Changing of the backbone conformation also affects the distribution of the side chains of the peptide. As the main difference, Phe^8 and DLeu^9 side chains are closer to the polar side of the helix (defined by the side chains of Lys^7 and Arg^{11}) in [Pro^3, DLeu^9]TL compared to TL and [Pro^3]TL (Supplementary Fig. S2), thus decreasing the amphipathicity of the first peptide. Note that detergent micelles represent a reliable membrane mimetic model and have been used extensively for solution NMR spectroscopy of AMPs and membrane proteins [19]. However, to verify whether the peptide's conformation is preserved in more complex lipid environments that better mimic a biological membrane, solid-state NMR studies in phospholipid bilayers will be next performed.

In agreement with our previous results [40], the hemolytic activity of the D amino acid containing analogues correlates well with their increased helical content in DPC (see Tables 3 and 6). Thus, [Pro^3, DLys^7]TL and [Pro^3, DLeu^9]TL are the less toxic peptides; [Pro^3, DPhe^8]TL, with the highest percentage of α-helix, the most hemolytic one. Furthermore, in line with our recent findings [40], breaking of the helical structure at the C-terminal half reduces the antibacterial activity of [Pro^3]TL. In contrast, the anti-yeast efficacy is not directly dependent on the helicity of the peptide. Indeed, among the six analogues, [Pro^3, DLeu^9]TL is endowed with the highest anti-yeast activity, despite having a very low content of helix in DPC/SDS micelle solutions (11% vs 23% of [Pro^3]TL). Therefore, we can conclude that interruption of the α-helix of [Pro^3]TL at position 9 does not compromise anti-*Candida* and anti-*Saccharomyces* activities of this peptide and practically abolishes its toxicity towards mammalian cells. This is presumably due to its inability to disrupt the membrane of these cells, as revealed by the LUV leakage experiments (Fig. 3).

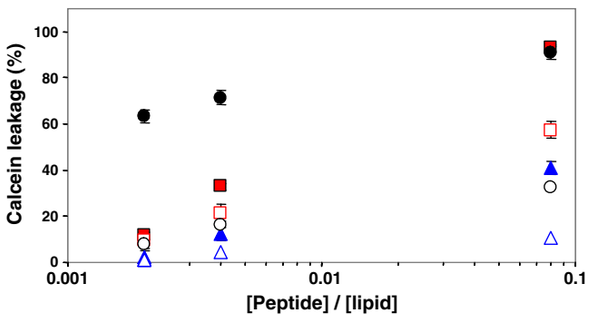

Fig. 3. Calcein leakage from POPE/POPG (blue triangles), POPG/CL (red squares) and POPC/Cho (black circles) LUV after addition of TL (filled symbols) or [Pro^3, DLeu^9]TL (empty symbols) at different concentrations. Fluorescence recovery was measured for 10 min after the peptides were mixed with the vesicles, and its maxima were reported. Leakage was calculated as indicated in the Materials and methods. Values are means of three independent measurements with ±SD.

Although usually harbored as a harmless commensal microbe of healthy humans, *C. albicans* can cause a variety of superficial and deep-seated mycoses, particularly in immunocompromised and neutropenic hosts [65]. Such *Candida* can either circulate in the blood (e.g. the erythrocytes) or be located at many infection sites (e.g. the skin, the oral, ocular and genital epithelia). In these cases, candidosis is becoming a life-threatening disease in patients undergoing aggressive chemotherapy or having T-cell leukemia virus-associated immunodeficiencies. Relatively few antifungal agents are available, particularly for deep-seated *Candida* mycoses. Amphotericin B and the azole drugs such as itraconazole and ketoconazole are currently used. More recently, fluconazole has been employed, but its use is quite restricted due to the

limited spectrum of activity and to the emerging appearance of *Candida* strains resistant to it. Therefore, the discovery of new compounds to treat *Candida*-associated infections, without being toxic to mammalian cells, is urgently needed.

5. Conclusion

Importantly, the results of the present study have lead to the identification of a TL analogue ([Pro^3, DLeu^9]TL) practically devoid of cytolytic effects in vitro and which preserves the effectiveness of the native peptide against *C. albicans*. Overall, our studies have shown that substitution of Gln^3 with a proline residue and replacement of Leu^9 with its D enantiomer play a key role in breaking the helicity of TL as well as in distinguishing between eukaryotic and prokaryotic membranes. Indeed, while such changes retain the peptide's antimicrobial activity, presumably by preserving its ability to lead to microbial membrane injury, they cause a drastic reduction in peptide's ability to damage mammalian cell membranes, thus abolishing the toxic effects of the peptide on human cells such as erythrocytes and keratinocytes. In addition, incorporation of a D amino acid within the peptide sequence should increase its biostability to proteolytic enzymes, a fundamental requirement for potential use in clinics. Overall, these findings should assist in the future development of selective and economically feasible anti-*Candida* agents, starting from the short-sized TL template.

Acknowledgements

This work was supported by grants from Sapienza Università di Roma, Italian Ministero dell'Istruzione, Università e Ricerca (PRIN 2008) and CNR, Istituto di Biologia e Patologia Molecolari.

Appendix A. Supplementary data

Supplementary data to this article can be found online at http://dx.doi.org/10.1016/j.bbamem.2012.08.027.

References

[1] R. Maviglia, R. Nestorini, M. Pennisi, Role of old antibiotics in multidrug resistant bacterial infections, Curr. Drug Targets 10 (2009) 895–905.
[2] M.T. Osterholm, Emerging infectious diseases. A real public health crisis? Postgrad. Med. 100 (1996) 15–16.
[3] H.G. Boman, Antibacterial peptides: basic facts and emerging concepts, J. Intern. Med. 254 (2003) 197–215.
[4] L. Steinstraesser, U. Kraneburg, F. Jacobsen, S. Al-Benna, Host defense peptides and their antimicrobial–immunomodulatory duality, Immunobiology 216 (2011) 322–333.
[5] A.T. Yeung, S.L. Gellatly, R.E. Hancock, Multifunctional cationic host defence peptides and their clinical applications, Cell. Mol. Life Sci. 68 (2011) 2161–2176.
[6] N. Mookherjee, R.E. Hancock, Cationic host defence peptides: innate immune regulatory peptides as a novel approach for treating infections, Cell. Mol. Life Sci. 64 (2007) 922–933.
[7] R.E. Hancock, Cationic peptides: effectors in innate immunity and novel antimicrobials, Lancet Infect. Dis. 1 (2001) 156–164.
[8] L.M. Gottler, A. Ramamoorthy, Structure, membrane orientation, mechanism, and function of pexiganan — a highly potent antimicrobial peptide designed from magainin, Biochim. Biophys. Acta 1788 (2009) 1680–1686.
[9] J.L. Imler, P. Bulet, Antimicrobial peptides in *Drosophila*: structures, activities and gene regulation, Chem. Immunol. Allergy 86 (2005) 1–21.
[10] M. Simmaco, G. Mignogna, D. Barra, Antimicrobial peptides from amphibian skin: what do they tell us? Biopolymers 47 (1998) 435–450.
[11] V. Erspamer, Bioactive secretions of the amphibian integument, in: H. Heatwole (Ed.), Amphibian Biology, 1, Surray Beatty and Sons, Chipping Norton, 1994, pp. 395–414.
[12] R.E. Hancock, R. Lehrer, Cationic peptides: a new source of antibiotics, Trends Biotechnol. 16 (1998) 82–88.
[13] H. Jenssen, P. Hamill, R.E. Hancock, Peptide antimicrobial agents, Clin. Microbiol. Rev. 19 (2006) 491–511.
[14] P.N. Domadia, A. Bhunia, A. Ramamoorthy, S. Bhattacharjya, Structure, interactions, and antibacterial activities of MSI-594 derived mutant peptide MSI-594F5A in lipopolysaccharide micelles: role of the helical hairpin conformation in outer-membrane permeabilization, J. Am. Chem. Soc. 132 (2010) 18417–18428.
[15] A. Bhunia, A. Ramamoorthy, S. Bhattacharjya, Helical hairpin structure of a potent antimicrobial peptide MSI-594 in lipopolysaccharide micelles by NMR spectroscopy, Chemistry 15 (2009) 2036–2040.
[16] F. Porcelli, B. Buck, D.K. Lee, K.J. Hallock, A. Ramamoorthy, G. Veglia, Structure and orientation of pardaxin determined by NMR experiments in model membranes, J. Biol. Chem. 279 (2004) 45815–45823.
[17] A. Ramamoorthy, D.K. Lee, T. Narasimhaswamy, R.P. Nanga, Cholesterol reduces pardaxin's dynamics — a barrel-stave mechanism of membrane disruption investigated by solid-state NMR, Biochim. Biophys. Acta 1798 (2010) 223–227.
[18] F. Porcelli, R. Verardi, L. Shi, K.A. Henzler-Wildman, A. Ramamoorthy, G. Veglia, NMR structure of the cathelicidin-derived human antimicrobial peptide LL-37 in dodecylphosphocholine micelles, Biochemistry 47 (2008) 5565–5572.
[19] F. Porcelli, B.A. Buck-Koehntop, S. Thennarasu, A. Ramamoorthy, G. Veglia, Structures of the dimeric and monomeric variants of magainin antimicrobial peptides (MSI-78 and MSI-594) in micelles and bilayers, determined by NMR spectroscopy, Biochemistry 45 (2006) 5793–5799.
[20] S. Bhattacharjya, A. Ramamoorthy, Multifunctional host defense peptides: functional and mechanistic insights from NMR structures of potent antimicrobial peptides, FEBS J. 276 (2009) 6465–6473.
[21] H.G. Boman, B. Agerberth, A. Boman, Mechanisms of action on *Escherichia coli* of cecropin P1 and PR-39, two antibacterial peptides from pig intestine, Infect. Immun. 61 (1993) 2978–2984.
[22] K.A. Brogden, Antimicrobial peptides: pore formers or metabolic inhibitors in bacteria? Nat. Rev. Microbiol. 3 (2005) 238–250.
[23] A. Patrzykat, C.L. Friedrich, L. Zhang, V. Mendoza, R.E. Hancock, Sublethal concentrations of pleurocidin-derived antimicrobial peptides inhibit macromolecular synthesis in *Escherichia coli*, Antimicrob. Agents Chemother. 46 (2002) 605–614.
[24] G. Kragol, S. Lovas, G. Varadi, B.A. Condie, R. Hoffmann, L. Otvos Jr., The antibacterial peptide pyrrhocoricin inhibits the ATPase actions of DnaK and prevents chaperone-assisted protein folding, Biochemistry 40 (2001) 3016–3026.
[25] E. Podda, M. Benincasa, S. Pacor, F. Micali, M. Mattiuzzo, R. Gennaro, M. Scocchi, Dual mode of action of Bac7, a proline-rich antibacterial peptide, Biochim. Biophys. Acta 1760 (2006) 1732–1740.
[26] M.R. Yeaman, N.Y. Yount, Mechanisms of antimicrobial peptide action and resistance, Pharmacol. Rev. 55 (2003) 27–55.
[27] T. Koprivnjak, A. Peschel, Bacterial resistance mechanisms against host defense peptides, Cell. Mol. Life Sci. 68 (2011) 2243–2254.
[28] J.M. Conlon, Structural diversity and species distribution of host-defense peptides in frog skin secretions, Cell. Mol. Life Sci. 68 (2011) 2303–2315.
[29] M.L. Mangoni, Temporins, anti-infective peptides with expanding properties, Cell. Mol. Life Sci. 63 (2006) 1060–1069.
[30] M.L. Mangoni, Y. Shai, Temporins and their synergism against Gram-negative bacteria and in lipopolysaccharide detoxification, Biochim. Biophys. Acta 1788 (2009) 1610–1619.
[31] A.C. Rinaldi, M.L. Mangoni, A. Rufo, C. Luzi, D. Barra, H. Zhao, P.K. Kinnunen, A. Bozzi, A. Di Giulio, M. Simmaco, Temporin L: antimicrobial, haemolytic and cytotoxic activities, and effects on membrane permeabilization in lipid vesicles, Biochem. J. 368 (2002) 91–100.
[32] M.L. Mangoni, Y. Shai, Short native antimicrobial peptides and engineered ultrashort lipopeptides: similarities and differences in cell specificities and modes of action, Cell. Mol. Life Sci. 68 (2011) 2267–2280.
[33] Q. Chen, D. Wade, K. Kurosaka, Z.Y. Wang, J.J. Oppenheim, D. Yang, Temporin A and related frog antimicrobial peptides use formyl peptide receptor-like 1 as a receptor to chemoattract phagocytes, J. Immunol. 173 (2004) 2652–2659.
[34] A. Giacometti, O. Cirioni, R. Ghiselli, F. Mocchegiani, F. Orlando, C. Silvestri, A. Bozzi, A. Di Giulio, C. Luzi, M.L. Mangoni, D. Barra, V. Saba, G. Scalise, A.C. Rinaldi, Interaction of antimicrobial peptide temporin L with lipopolysaccharide in vitro and in experimental rat models of septic shock caused by gram-negative bacteria, Antimicrob. Agents Chemother. 50 (2006) 2478–2486.
[35] A. Bhunia, P.N. Domadia, J. Torres, K.J. Hallock, A. Ramamoorthy, S. Bhattacharjya, NMR structure of pardaxin, a pore-forming antimicrobial peptide, in lipopolysaccharide micelles: mechanism of outer membrane permeabilization, J. Biol. Chem. 285 (2010) 3883–3895.
[36] Y. Rosenfeld, N. Papo, Y. Shai, Endotoxin (lipopolysaccharide) neutralization by innate immunity host-defense peptides. Peptide properties and plausible modes of action, J. Biol. Chem. 281 (2006) 1636–1643.
[37] M.L. Mangoni, R.F. Epand, Y. Rosenfeld, A. Peleg, D. Barra, R.M. Epand, Y. Shai, Lipopolysaccharide, a key molecule involved in the synergism between temporinsin inhibiting bacterial growth and in endotoxin neutralization, J. Biol. Chem. (2008) 22907–22917.
[38] D. Uccelletti, E. Zanni, L. Marcellini, C. Palleschi, D. Barra, M.L. Mangoni, Anti-*Pseudomonas* activity of frog skin antimicrobial peptides in a *Caenorhabditis elegans* infection model: a plausible mode of action in vitro and in vivo, Antimicrob. Agents Chemother. 54 (2010) 3853–3860.
[39] Y. Chen, C.T. Mant, S.W. Farmer, R.E. Hancock, M.L. Vasil, R.S. Hodges, Rational design of alpha-helical antimicrobial peptides with enhanced activities and specificity/therapeutic index, J. Biol. Chem. 280 (2005) 12316–12329.
[40] M.L. Mangoni, A. Carotenuto, L. Auriemma, M.R. Saviello, P. Campiglia, I. Gomez-Monterrey, S. Malfi, L. Marcellini, D. Barra, E. Novellino, P. Grieco, Structure–activity relationship, conformational and biological studies of temporin L analogues, J. Med. Chem. 54 (2011) 1298–1307.
[41] A. Carotenuto, S. Malfi, M.R. Saviello, P. Campiglia, I. Gomez-Monterrey, M.L. Mangoni, L.M. Gaddi, E. Novellino, P. Grieco, A different molecular mechanism underlying antimicrobial and hemolytic actions of temporins A and L, J. Med. Chem. 51 (2008) 2354–2362.

[42] D.I. Fernandez, M.-A. Sani, F. Separovic, Interactions of the antimicrobial peptide maculatin 1.1 and analogues with phospholipid bilayers, Aust. J. Chem. 64 (2011) 798–805.
[43] E.E. Ambroggio, F. Separovic, J.H. Bowie, G.D. Fidelio, L.A. Bagatolli, Direct visualization of membrane leakage induced by the antibiotic peptides: maculatin, citropin, and aurein, Biophys. J. 89 (2005) 1874–1881.
[44] M.R. Saviello, S. Malfi, P. Campiglia, A. Cavalli, P. Grieco, E. Novellino, A. Carotenuto, New insight into the mechanism of action of the temporin antimicrobial peptides, Biochemistry 49 (2010) 1477–1485.
[45] P. Valenti, P. Visca, G. Antonini, N. Orsi, Antifungal activity of ovotransferrin towards genus *Candida*, Mycopathologia 89 (1985) 169–175.
[46] M.L. Mangoni, A.C. Rinaldi, A. Di Giulio, G. Mignogna, A. Bozzi, D. Barra, M. Simmaco, Structure–function relationships of temporins, small antimicrobial peptides from amphibian skin, Eur. J. Biochem. 267 (2000) 1447–1454.
[47] A. Makovitzki, D. Avrahami, Y. Shai, Ultrashort antibacterial and antifungal lipopeptides, Proc. Natl. Acad. Sci. U. S. A. 103 (2006) 15997–16002.
[48] U. Piantini, O.W. Sorensen, R.R. Ernst, Multiple quantum filters for elucidating NMR coupling networks, J. Am. Chem. Soc. 104 (1982) 6800–6801.
[49] D. Marion, K. Wuthrich, Application of phase sensitive two-dimensional correlated spectroscopy (COSY) for measurements of 1H–1H spin–spin coupling constants in proteins, Biochem. Biophys. Res. Commun. 113 (1983) 967–974.
[50] L. Braunschweiler, R.R. Ernst, Coherence transfer by isotropic mixing: application to proton correlation spectroscopy, J. Magn. Reson. 53 (1983) 521–528.
[51] J. Jeener, B.H. Meier, P. Bachman, R.R. Ernst, Investigation of exchange processes by two-dimensional NMR spectroscopy, J. Chem. Phys. 71 (1979) 4546–4553.
[52] D.J. States, RA Haberkorn, D.J. Ruben, A two-dimensional nuclear Overhauser experiment with pure absorption phase in four quadrants, J. Magn. Reson. 48 (1982) 286–292.
[53] T.L. Hwang, A.J. Shaka, Water suppression that works. Excitation sculpting using arbitrary wave-forms and pulsed-field gradients, J. Magn. Reson. 112 (1995) 275–279.
[54] F. Delaglio, S. Grzesiek, G.W. Vuister, G. Zhu, J. Pfeifer, A. Bax, NMRPipe: a multidimensional spectral processing system based on UNIX pipes, J. Biomol. NMR 6 (1995) 277–293.
[55] R. Glaser, J. Harder, H. Lange, J. Bartels, E. Christophers, J.M. Schroder, Antimicrobial psoriasin (S100A7) protects human skin from *Escherichia coli* infection, Nat. Immunol. 6 (2005) 57–64.
[56] P. Guntert, C. Mumenthaler, K. Wuthrich, Torsion angle dynamics for NMR structure calculation with the new program DYANA, J. Mol. Biol. 273 (1997) 283–298.
[57] J.R. Maple, U. Dinur, A.T. Hagler, Derivation of force fields for molecular mechanics and dynamics from ab initio energy surfaces, Proc. Natl. Acad. Sci. U. S. A. 85 (1988) 5350–5354.
[58] R. Koradi, M. Billeter, K. Wuthrich, MOLMOL: a program for display and analysis of macromolecular structures, J. Mol. Graph. 14 (1996) 51–55.
[59] E.G. Hutchinson, J.M. Thornton, PROMOTIF — a program to identify and analyze structural motifs in proteins, Protein Sci. 5 (1996) 212–220.
[60] P. Unneberg, J.J. Merelo, P. Chacon, F. Moran, SOMCD: method for evaluating protein secondary structure from UV circular dichroism spectra, Proteins 42 (2001) 460–470.
[61] K. Wuthrich, in: NMR of Proteins and Nucleic Acids, John Wiley & Sons, Inc., New York, 1986.
[62] D.S. Wishart, B.D. Sykes, F.M. Richards, The Chemical Shift Index: a fast method for the assignment of protein secondary structure through NMR spectroscopy, Biochemistry 31 (1992) 1647–1651.
[63] N.H. Andersen, Z. Liu, K.S. Prickett, Efforts toward deriving the CD spectrum of a 3(10) helix in aqueous medium, FEBS Lett. 399 (1996) 47–52.
[64] M. Zasloff, Antimicrobial peptides of multicellular organisms, Nature 415 (2002) 389–395.
[65] D. Pittet, R.P. Wenzel, Nosocomial bloodstream infections. Secular trends in rates, mortality, and contribution to total hospital deaths, Arch. Intern. Med. 155 (1995) 1177–1184.

OPEN ACCESS Freely available online

PLOS ONE

Isomerization of an Antimicrobial Peptide Broadens Antimicrobial Spectrum to Gram-Positive Bacterial Pathogens

Chiara Falciani[1☯], Luisa Lozzi[1☯], Simona Pollini[1], Vincenzo Luca[2], Veronica Carnicelli[3], Jlenia Brunetti[4], Barbara Lelli[1], Stefano Bindi[1,5], Silvia Scali[1], Antonio Di Giulio[3], Gian Maria Rossolini[1,5], Maria Luisa Mangoni[2], Luisa Bracci[1,5], Alessandro Pini[1,5]*

1 Dipartimento di Biotecnologie Mediche, Università degli Studi di Siena, Siena, Italy, **2** Dipartimento di Scienze Biochimiche A. Fanelli, Università di Roma, La Sapienza, Roma, Italy, **3** Dipartimento di Scienze e Tecnologie Biomediche, Università di L'Aquila, L'Aquila, Italy, **4** SetLance srl, Siena, Italy, **5** Azienda Ospedaliera Universitaria Senese, Policlinico Le Scotte, Siena, Italy

Abstract

The branched M33 antimicrobial peptide was previously shown to be very active against Gram-negative bacterial pathogens, including multidrug-resistant strains. In an attempt to produce back-up molecules, we synthesized an M33 peptide isomer consisting of D-aminoacids (M33-D). This isomeric version showed 4 to 16-fold higher activity against Gram-positive pathogens, including *Staphylococcus aureus* and *Staphylococcus epidermidis,* than the original peptide, while retaining strong activity against Gram-negative bacteria. The antimicrobial activity of both peptides was influenced by their differential sensitivity to bacterial proteases. The better activity shown by M33-D against *S. aureus* compared to M33-L was confirmed in biofilm eradication experiments where M33-L showed 12% activity with respect to M33-D, and *in vivo* models where Balb-c mice infected with *S. aureus* showed 100% and 0% survival when treated with M33-D and M33-L, respectively. M33-D appears to be an interesting candidate for the development of novel broad-spectrum antimicrobials active against bacterial pathogens of clinical importance.

Citation: Falciani C, Lozzi L, Pollini S, Luca V, Carnicelli V, et al. (2012) Isomerization of an Antimicrobial Peptide Broadens Antimicrobial Spectrum to Gram-Positive Bacterial Pathogens. PLoS ONE 7(10): e46259. doi:10.1371/journal.pone.0046259

Editor: Stefan Bereswill, Charité-University Medicine Berlin, Germany

Received July 25, 2012; **Accepted** August 31, 2012; **Published** October 2, 2012

Funding: This research was financed by the Italian Foundation for Cystic Fibrosis (project FFC#24/2011 adopted by FFC delegations from Legnago, Varese, Reggio Emilia and Assistgroup), the Tuscan Regional Administration (Project SPAC: POR CReO FESR 2007–2013) and PROGETTO PRIN (2008KCLR7M_004). The funders had no role in study design, data collection and analysis, decision to publish, or preparation of the manuscript.

Competing Interests: The authors have the following interests: The peptide M33 and molecules it derived from are covered by the following three patents: 1. WO2006006195 B1 "Antibacterial peptides and analogues thereof" (patent issued); 2. WO2010038220 A1 "Peptide sequences, their branched form and use thereof for antimicrobial applications" (pending); 3. WO2012010266 A1 "Antimicrobial peptide, branched forms and uses thereof for the cure of bacterial infections" (pending). The patents WO2006006195 B1 and WO2010038220 A1 were filed by University of Siena and then licensed to the company SetLance srl (www.setlance.com). The patent WO2012010266 A1 was directly filed by SetLance srl. Jlenia Brunetti is employed by SetLance srl. There are no further patents, products in development or marketed products to declare. This does not alter the authors' adherence to all the PLOS ONE policies on sharing data and materials, as detailed online in the guide for authors.

* E-mail: alessandro.pini@unisi.it

☯ These authors contributed equally to this work.

Introduction

Antimicrobial resistance (AMR) is not a recent phenomenon, but it is a critical health issue today. Over several decades, to varying degrees, bacteria causing common infections have developed resistance to each new antibiotic, and AMR has evolved to become a worldwide health threat. With a dearth of new antibiotics coming to market, the need for action to avert a developing global crisis in health care is increasingly urgent [1]. Antimicrobial peptides (AMPs) are seen with great interest for the development of new agents against bacterial infections, because most of them show strong bactericidal activity against multidrug-resistant (MDR) bacterial pathogens, and may also contribute to innate immunity by modulating dendritic cell differentiation and maturation, angiogenesis and chemokine production [2]. These features are particularly attractive and many natural host defense peptides (HDPs) or artificial AMPs are currently under experimentation for drug development [3]. Unfortunately, certain drawbacks have limited the development of AMPs as drugs for bacterial infections: i) toxicity to eukaryotic cells, that may lead to nephrotoxicity, neurotoxicity and neuromuscular blockade [4,5]; ii) selection of resistant strains that may be cross-resistant to human-neutrophil-defensin-1, a key component of the innate immune response to infection [6]; iii) the fact that natural AMPs are generally very short peptides easily attacked by circulating proteolytic enzymes, making their half-life too short to be active against bacteria *in vivo*. Researchers and industry have been seeking new AMPs of natural and non-natural origin, with low toxicity and the longer half-life necessary for drug development.

A few years ago, we observed that short peptides synthesized in oligodendrimeric form [7] showed high resistance to proteolytic degradation, making them suitable for use *in vivo* [8–10]. The synthetic peptide M33 was obtained by random selection from

a home-made phage-display peptide library panned against *E. coli* cells and a successive optimization phase for biological activity, synthesis and purification procedures [11–14]. The M33 sequence (KKIRVRLSA) is amphipathic and cationic, which is typical for AMPs, but did not show any sequence homology with known AMPs of natural or non-natural origin. M33 was synthesized in tetra-branched form, proving resistant to proteolytic degradation and very active *in vitro* against clinical isolates of several Gram-negative pathogens, including MDR strains of *Pseudomonas aeruginosa*, *Acinetobacter baumannii*, *Klebsiella pneumoniae* and *Escherichia coli*, while being less active against the Gram-positive pathogen *Staphylococcus aureus*. The peptide also protected mice lethally infected with multi-resistant clinical isolates of *P. aeruginosa* and is currently under preclinical characterization for the development of a new drug for bloodstream and lower respiratory tract infections.

In previous reports [11–14] the peptide was always synthesized and used with L aminoacids (M33-L). Recently, we used the same sequence synthesized in the tetra-branched form using D aminoacids (M33-D). Here we report that compared to M33-L, M33-D has stronger activity against *S. aureus* and coagulase-negative staphylococci, including methicillin-resistant strains, with MIC values comparable to those of many antimicrobial agents used in clinical practice. We also report a study of the mechanism of action of M33-D compared to M33-L. Since M33-D retains strong activity against Gram-negative pathogens, it appears to be an interesting candidate for the development of novel broad-spectrum AMPs.

Results and Discussion

MIC Determination

MICs of M33-L and M33-D were determined against strains of different bacterial species, including major Gram-negative and Gram-positive pathogens (Table 1). Compared to M33-L, M33-D exhibited the same activity against *P. aeruginosa* and the same or a slightly lower (2–4 fold) activity against Enterobacteriaceae. On the other hand, M33-D showed higher antimicrobial activity than M33-L against the Gram-positive bacteria *S. aureus* and *S. epidermidis*, including methicillin-resistant and vancomycin-intermediate strains, with MICs 4 to 16-fold lower than those of M33-L. As previously observed with M33-L [13], M33-D exhibited antimicrobial activity (MIC values) against antibiotic-susceptible reference bacterial strains and MDR strains of clinical origin expressing several different mechanisms of antibiotic resistance.

Binding of M33-L and M33-D to Lipopolysaccharide (LPS) and Lipoteichoic Acid (LTA)

In a previous report [13] we hypothesized that LPS was the first bacterial structure to interact with M33-L. In order to evaluate possible differential binding of M33-L and M33-D to Gram-negative LPS and to Gram-positive LTA, we therefore analyzed the interactions of both peptides with LPS and LTA by surface plasmon resonance. LTA from *S. aureus* and *Streptococcus faecalis*, and LPS from *E. coli*, *P. aeruginosa* and *K. pneumoniae* were injected at a concentration of 10 μg/ml over immobilized M33-L or M33-D peptides. No significant difference in binding or kinetic rates that could explain such dissimilar antimicrobial activity of the two peptides was observed (Fig. 1).

Interaction of M33 with Liposomes Mimicking Bacterial Cells

To investigate interaction of peptides M33-D and M33-L with the bacterial membrane, including possible perturbation, we used vesicles with two lipid compositions to mimic the membrane of *S. aureus* (CL/PG, 4:6 mol/mol) and *E. coli* (PE/PG, 7:3 mol/mol) [15]. Both liposome preparations were treated with increasing peptide concentrations from 0,5 to 15 μM and the membrane permeability was revealed by measuring the fluorescence increase due to the calcein leakage from the vesicles. The dose-response curves obtained from CL/PG or PE/PG liposomes are reported in Fig. 2a. The peptide-induced effect was dose-dependent in both vesicle lipid compositions. However, effectiveness on the two lipid compositions was significantly different, since maximum calcein release from CL/PG liposomes was obtained at peptide concentrations greater than 10 μM, whereas in PE/PG liposomes total leakage occurred at peptide concentration of 5 μM. No significant differences in the effects induced by M33-D and M33-L were evident, although the D peptide seemed slightly more efficient towards CL/PG liposomes at doses above 8 μM. Fig. 2b shows the time-course of probe release when the vesicles were treated with M33-D or M33-L at 1 or 5 μM final concentrations. In all cases, the peptide-induced increase in fluorescence showed a typical biphasic kinetic profile, in which a fast phase due to the initial membrane-peptide interaction was followed by a slow steady-state. The greater perturbing effect of both forms of M33 on PE/PG vesicles, compared to vesicles containing cardiolipin, was evident.

These tests, along with the Biacore analysis described above, revealed that M33-D and M33-L have substantially similar behavior in terms of binding to LPS and LTA and of perturbation of membranes of different phospholipid composition. We deduced that the mechanism used by M33-L and M33-D for interacting with bacterial surfaces and disruption of bacterial membranes was basically the same.

Stability to Bacterial Proteases

Peptide stability to bacterial proteases was analyzed with purified aureolysin and elastase enzymes derived from *S. aureus* and *P. aeruginosa*, respectively. These proteins play a key role in bacterial virulence by breaking down natural HDPs produced by the infected individuals [16–18]. *S. aureus* aureolysin and *P. aeruginosa* elastase are members of the family of M4 metallopeptidases (thermolysin family) [19–21] and have similar specificity, hydrolyzing peptide bonds preferentially on the amino-terminal side of hydrophobic residues. To determine whether these proteases affect the performance of M33 peptides, M33-L and M33-D were incubated with aureolysin and elastase, respectively, and after appropriate time intervals the crude solutions were analyzed by HPLC and mass spectroscopy. Unlike M33 incubated without enzymes (Figs. 3a, 3b, 3c and 3d), M33-L was degraded within 1h by staphylococcal aureolysin (Fig. 3e), through hydrolysis at R6-L7 and S8-A9 peptide bonds (Fig. 3f). Conversely, M33-D was completely stable to proteolysis by this metalloprotease, remaining unaltered after 24 h of incubation (Figs. 3g and 3h). Incubation of M33-L with *P. aeruginosa* elastase showed moderate peptide stability after 5 h (a peak corresponding to a retention time of 23 min is still present in Fig. 3i), and again the cleavage sites were R6-L7 and S8-A9 peptide bonds (Fig. 3j). In contrast, the M33-D peptide resisted degradation by elastase for 24 h (Figs. 3k and 3l). The cleavage sites of both peptides are illustrated in Fig. 3m and the MS peaks are assigned to the fragments.

Altogether, these results suggest that the increased stability of M33-D to staphylococcal aureolysin could be at least partly responsible for the increased activity exhibited by this isomer against *S. aureus*. The same phenomenon could also explain the

Table 1. MICs of M33-L and M33-D for different bacteria species and strains.

Species and strains	Relevant features[a]	M33-L (μM)	M33-D (μM)
P.aeruginosa ATCC 27853	Reference strain, wild type	1.5	1.5
P.aeruginosa AV 65	FQ^r AG^r ESC^r NEM^r (MBL/IMP-13)	3	3
K.pneumoniae ATCC 13833	Reference strain, wild type	1.5	3
K.pneumoniae 7086042	FQ^r AG^r ESC^r NEM^r (MBL/VIM-1)	3	6
E.coli ATCC 25922	Reference strain, wild type	3	3
E.coli W03BG0025	FQ^r AG^r ESC^r (ESBL/CTX-M-15)	0.7	3
S.aureus ATCC 29213	Reference strain, wild type	6	1.5
S.aureus USA 300	MR	6	1.5
S.aureus 3851	MR VAN^i	12	0.7
S.epidermidis ATCC 14990	Reference strain, wild type	1.5	0.4
S.epidermidis 6154	MR	3	0.7

[a]M33 antimicrobial activity was evaluated on reference strains and clinical isolates (mostly with an MDR phenotype). Relevant resistance phenotypes and resistance determinants are indicated. Resistance phenotypes: FQ^r, resistant to fluoroquinolones; AG^r, resistant to aminoglycosides (gentamycin, amikacin, and/or tobramycin); ESC^r, resistant to expanded-spectrum cephalosporins; NEM^r, resistant to carbapenems (imipenem and/or meropenem); MR^r, methicillin-resistant; VAN^i, vancomycin-intermediate. Resistance determinants: ESBL, extended spectrum β-lactamase; MBL, metallo-β-lactamase.
doi:10.1371/journal.pone.0046259.t001

increased activity of M33-D against *S. epidermidis* (Table 1), which produces an ortholog of aureolysin (the metallo-protease SepA, with 71% aminoacid identity [22–23]).

Assessment of Anti-biofilm Activity

In biofilms, bacteria grow as multicellular aggregates within an extracellular matrix that protects the cells from host defences. Biofilms are also more resistant to antimicrobial agents due to the physiological state of bacterial cells and, in some cases, reduced antibiotic penetration [24]. Bacterial biofilms form in natural, medical and industrial settings, and play a major role in several human infections, including infections of prosthetic devices and intravascular catheters, bone and joint infections, chronic rhinosinusitis and otitis media [25,26]. The search for new antimicrobials that eradicate microbial biofilms has therefore become extremely pressing.

M33-L and M33-D were tested for their anti-biofilm activity against the Gram-negative strains *E. coli* ATCC 25922 and *P. aeruginosa* ATCC 27853, as well as the Gram-positive strain *S. aureus* ATCC 25923. As reported in Table 2, the minimum biofilm eradication concentrations (MBECs) of the two peptides observed with Gram-negatives were on the whole similar. On the other hand, M33-D exhibited higher anti-biofilm activity against *S. aureus* than M33-L (MBEC, 1.5 μM vs. 12 μM), which is consistent with the difference in MIC of the two isomers for this strain (Table 1). The minimum bactericidal concentration on biofilm (MBCb), i.e. the concentration that kills 99.9% of biofilm cells, was also investigated. The two isomers showed an MBCb of

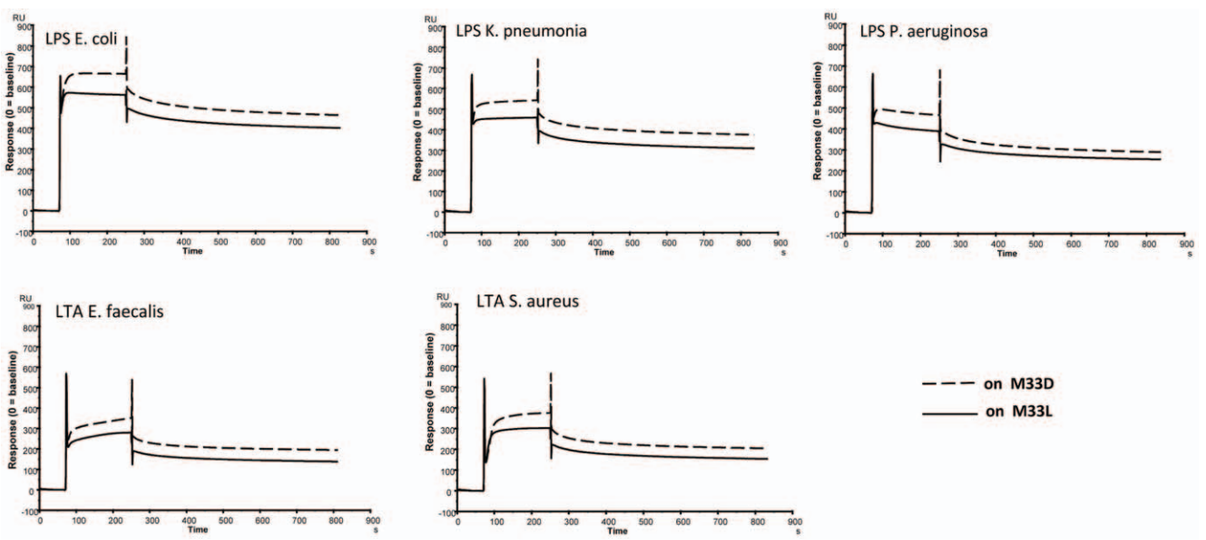

Figure 1. Binding of LTA and LPS on M33-L or M33-D measured by surface plasmon resonance. LPS from *P. aeruginosa*, *K. pneumoniae*, *E. coli* and LTA from S. *faecalis* and *S. aureus*, diluted to 10 μg/ml were injected over M33-L and M33-D immobilized peptides.
doi:10.1371/journal.pone.0046259.g001

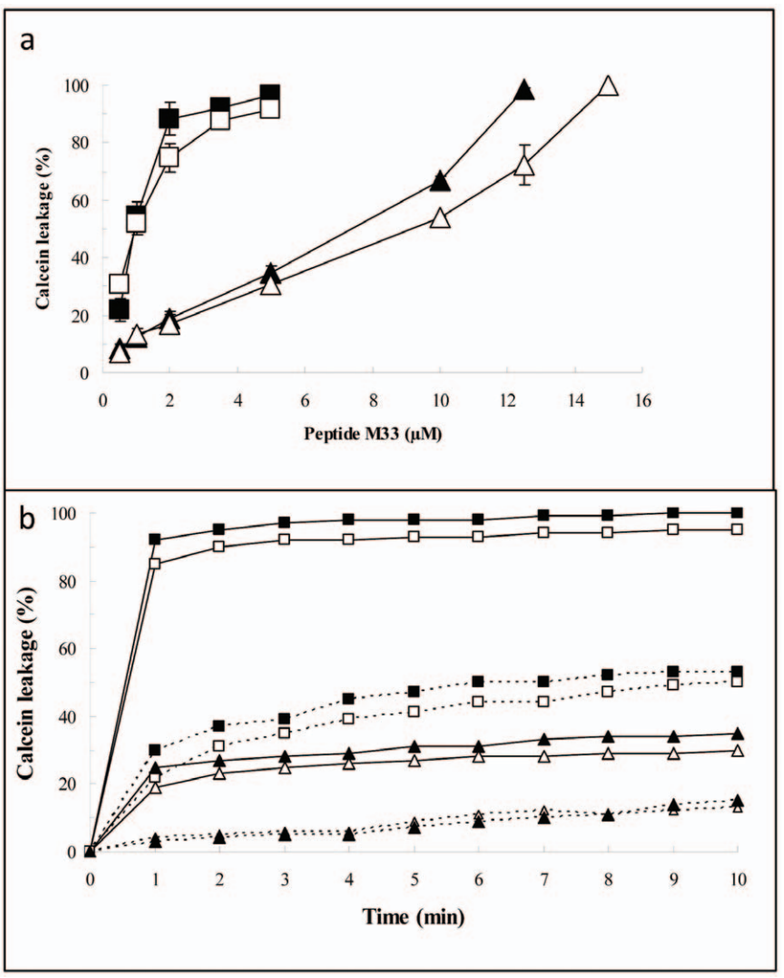

Figure 2. Release of calcein from bacterial-surface-mimicking liposomes. a, dose-response of M33-induced calcein release**.** The vesicles were incubated with different concentration of M33 peptide for 10 min at 20°C (for details see Methods section). CL/PG liposomes (triangles); PE/PG liposomes (squares); M33-D: full symbols; M33-L: empty symbols. Values are means ± SE of three independent experiments. **b**, time course of calcein release from: CL/PG liposomes (triangles) and from PE/PG liposomes (squares); M33-D: full symbols; M33-L: empty symbols. continuous line 5 μM, dotted line 1 μM.
doi:10.1371/journal.pone.0046259.g002

6 μM against the Gram-negatives *E. coli* and *P. aeruginosa* (Table 2), whereas the MBCbs of M33-L and M33-D for the Gram-positive *S. aureus* matched the respective MBECs, being 12 and 1.5 μM, respectively.

In vivo Anti-MRSA Activity of M33-D *vs.* M33-L

Given the good *in vitro* activity shown by M33-D against methicillin-resistant *S. aureus* (MRSA), we compared the *in vivo* activity of this peptide and the original M33-L in an animal model of infection caused by the highly virulent MRSA strain USA 300, a lineage that has become a dominant cause of community-associated MRSA infections in North America [27,28].

The smallest number of bacteria causing 100% lethal infection (LD100) after intra-peritoneal (i.p.) injection was 1×10^6 in the presence of 7% mucin. An LD100 killed mice within 20 hours. Mice were infected with the LD100 of bacteria and treated i.p. with the peptides 30 minutes later. 100% survival after 7 days was obtained with mice treated with M33-D, while mice treated with M33-L showed a mortality overlapping that of controls (Fig. 4), confirming the potent anti-MRSA activity of M33-D.

Conclusions

The M33 peptide, previously reported as active against a broad spectrum of Gram-negative bacteria [13], is also strongly active against staphylococci when synthesized with D-aminoacids. We hypothesized that the increased stability of M33-D to staphylococcal proteases could at least partly explain this different activity. It was known that branched peptides, like those used in this study, are particularly resistant to circulating proteases produced by higher animals [8–10,29–31]. It was also known that peptides with D-aminoacids show increased stability to circulating proteases [32]. Stability of D-peptides to bacterial proteases has also been reported [33,34]. In our case the concomitant improvement of stability of M33-D to infected individual proteases and to infectious agent proteases dramatically increased the overall performance of the peptide. This is particularly evident in

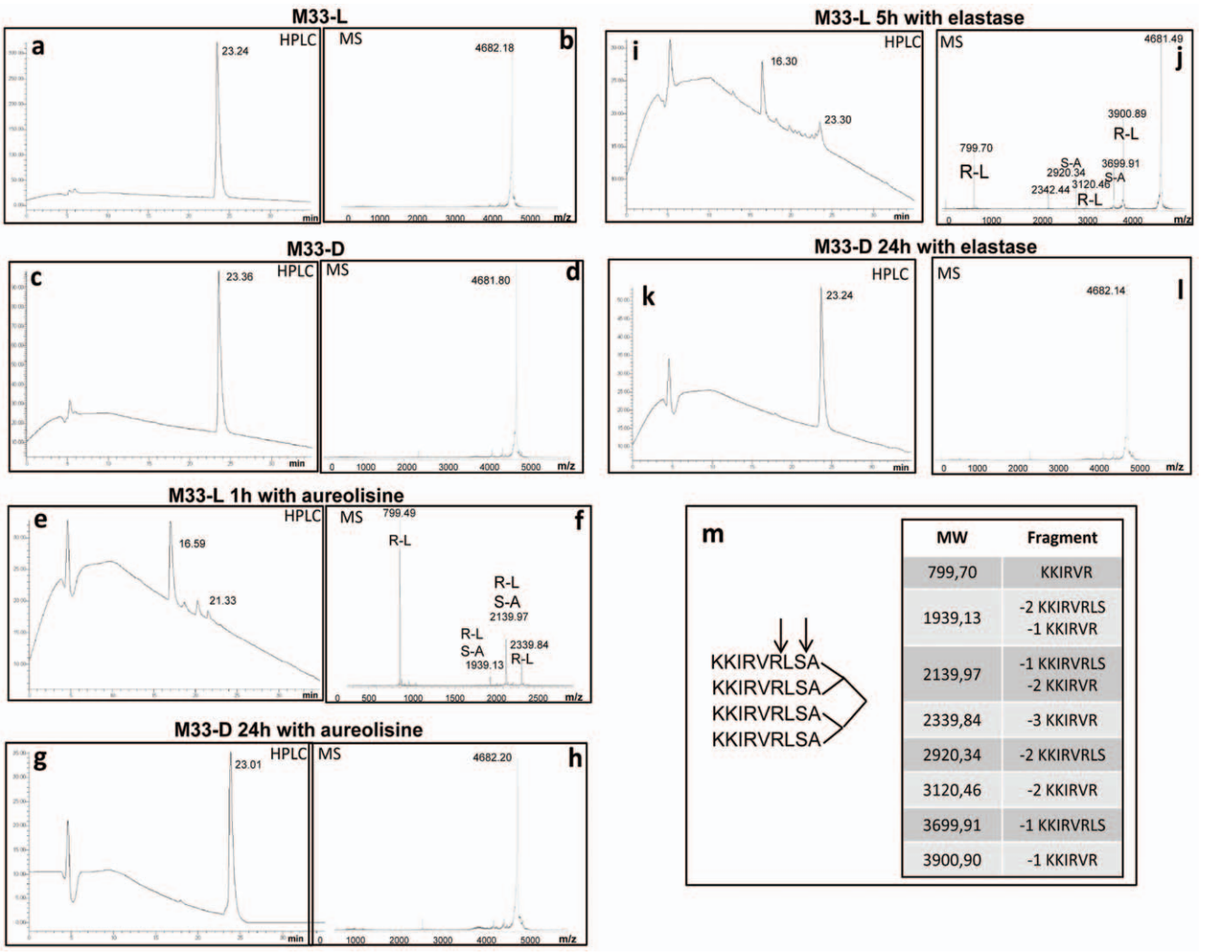

Figure 3. Proteolytic activity of aureolysin and elastase on peptides M33-L and M33-D. a and **b**, HPLC and MS profiles, respectively, of M33-L before incubation with enzymes. **c** and **d**, HPLC and MS profiles, respectively, of M33-D before incubation with enzymes. In HPLC the retention time of M33-L and M33-D was 23 minutes. The calculated MW of M33 was 4682. **e** and **f**, HPLC and MS, respectively, of M33-L incubated for 1 hour with aureolysin. **f** shows the peaks indicating the proteolytic site (RL or SA). **g** and **h**, HPLC and MS, respectively, of M33-D incubated for 24 hours with aureolysin. **i** and **j**, HPLC and MS, respectively, of M33-L incubated for 5 hours with elastase. **j** shows the peaks indicating the proteolytic site (RL or SA). **k** and **l**, HPLC and MS, respectively, of M33-D incubated for 24 hours with elastase. **m**, proteolytic sites of the two enzymes on the tetrabranched M33 are indicated by arrows. The table assigns MS peaks to the cleavage fragments.
doi:10.1371/journal.pone.0046259.g003

Table 2. Anti-biofilm activity of M33-L and M33-D towards different bacterial species.

Bacterial species	Minimum biofilm eradication concentration (MBEC, μM)[a]		Minimum bactericidal concentration on biofilm (MBCb, μM)[b]	
	M33-L	M33-D	M33-L	M33-D
Gram-negatives				
E. coli ATCC 25922	3	3	6	6
P. aeruginosa ATCC 27853	1.5	3	6	6
Gram-positive				
S. aureus ATCC 25923	12	1.5	12	1.5

[a]MBEC is the minimum peptide concentration preventing regrowth of bacteria from the treated biofilm within 4 hours.
[b]MBCb is the minimum peptide concentration required to reduce the number of viable biofilm cells by $\geq$3 $\log_{10}$ (99.9% killing) after 2 h.
doi:10.1371/journal.pone.0046259.t002

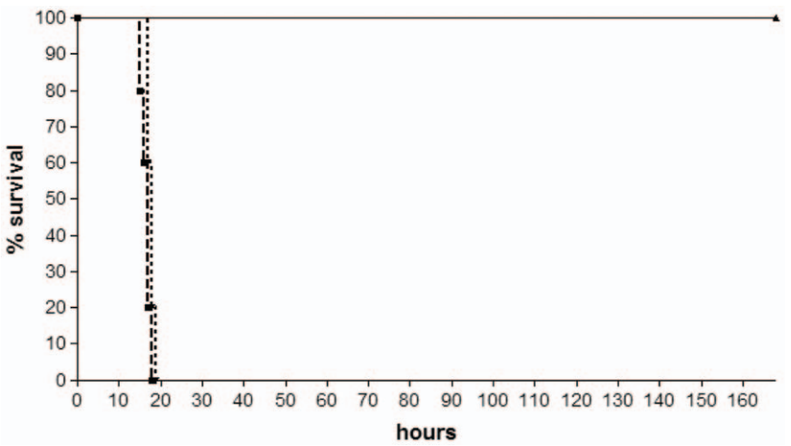

Figure 4. *In vivo* antibacterial activity of tetrabranched M33-L and M33-D peptides. Balb-c mice (20 g) were injected i.p. with a lethal amount of *S. aureus* USA300 cells. Dashed line (Ctr), injection with bacteria and no peptides; dotted line, injection with bacteria and a single injection of M33-L peptide (25 mg/kg) 30 min later; continuous line, injection with bacteria and a single injection of M33-D peptide (25 mg/kg) 30 min later.
doi:10.1371/journal.pone.0046259.g004

experiments *in vivo* where M33-D neutralized signs of sepsis due to *S. aureus* USA300, while M33-L, stable to mouse [13] but not to bacterial proteases, was not active at all.

M33-D was highly stable to the proteases aureolysin, from *S. aureus*, and elastase, from *P. aeruginosa*. M33-L was not at all stable to aureolysin and poorly stable to elastase, as confirmed by its activity *in vivo* against *P. aeruginosa* [13]. For M33-D we propose the following mechanism of action. M33-D binds LTA and persists on the bacterial surface for some time by virtue of its resistance to bacterial proteases, causing membrane perturbation that kills the bacteria.

Concluding, we identified a new form of the peptide M33, which is strongly active against *S. aureus* and retains its antimicrobial activity irrespective of strain-resistance phenotypes and mechanisms. MRSA and *S. aureus* strains with altered susceptibility to glycopeptides pose a serious clinical threat and major therapeutic challenge. In this context, development of a new broad-spectrum therapeutic agent with no cross-resistance to available drugs would be a major achievement.

Materials and Methods

Peptide Synthesis

Solid-phase synthesis was carried out by standard Fmoc chemistry on Fmoc4-Lys2-Lys-β-Ala Wang resin with a Syro multiple peptide synthesizer (MultiSynTech, Witten, Germany). Side chain protecting groups were 2,2,4,6,7-pentamethyldihydrobenzofuran-5-sulfonyl for R, t-butoxycarbonyl for K and t-butyl for S. M33-L was synthesized using Fmoc-L-aminoacids, and M33-D with Fmoc-D-aminoacids with the exception of the three lysins of the branched core which were Fmoc-L-Lys(Fmoc)-OH (M33-D is consequently a diastereomer). The final products were cleaved from the solid support, deprotected by treatment with TFA containing triisopropylsilane and water (95/2.5/2.5), and precipitated with diethyl ether. Crude peptides were purified by reversed-phase chromatography on a Phenomenex Jupiter C18 column (300 Å, 10 μm, 250×10 mm) in linear gradient form for 30 min, using 0.1% TFA/water as eluent A and methanol as eluent B. Purified peptides were obtained as trifluoroacetate salts (TFacetate). The exchange from TFacetate to acetate form was carried out using a quaternary ammonium resin in acetate form (AG1-X8, 100–200 mesh, 1.2 meq/ml capacity, Bio-Rad). The resin-to-peptide ratio was 2000:1, resin and peptide were stirred for 1 h, the resin was filtered off, washed extensively and the peptide recovered and freeze-dried. Final peptide purity and identity were confirmed by reversed phase chromatography on a Phenomenex Jupiter C18 analytical column (300 Å, 5 μm, 250×4.6 mm) and by mass spectrometry with a Bruker Daltonics ultraflex MALDI TOF/TOF.

MIC Testing

MICs were determined using a standard microdilution assay as recommended by the Clinical and Laboratory Standards Institute. Assays were performed in triplicate using cation-supplemented Mueller-Hinton (MH) broth (Becton Dickinson, Franklin Lakes, NJ, USA) and a bacterial inoculum of $5x10^4$ CFU/well, in a final volume of 100 μl. The tested concentrations ranged from 0.1 μM to 24 μM for both peptides. Results were recorded after 18–20 h of incubation at 37°C.

Surface Plasmon Resonance

Biotinylated peptides were immobilized on SA coated flow cells. M33-L and M33-D peptides, diluted to 10 μg/ml in HBS-EP+ buffer (10 mM Hepes, 150 mM NaCl, 3.4 mM EDTA, 0.05% polysorbate 20 pH 7.4), were injected for 90 sec at a flow rate of 10 μl/min, obtaining 550 RU and 580 RU for M33-L and M33-D respectively.

LTA and LPS molecules from different species (LPS from *E. coli*, *K. pneumonia*, *P. aeruginosa* and LTA from *S. aureus* and *S. faecalis*, were obtained from Sigma-Aldrich: L-3012, L-4268, L9143, L2515 and L4015, respectively) were diluted in HBS-EP+ buffer at the concentration of 10 μg/ml and injected for 180 sec with a flow rate of 30 μl/min over immobilized peptides. An empty flow cell was used as reference. Regeneration was achieved with a short pulse of SDS 0.05%.

Preparation of Calcein-liposomes and Leakage Measurement

L-α-phosphatidylethanolamine (PE), L-α-phosphatidyl-DL-glycerol (PG), cardiolipin (CL), calcein, ammonium thiocyanate and

iron (III) chloride hexahydrate and all other chemical (reagent grade) were obtained from Sigma.

Calcein-loaded liposomes of two different composition (PE/PG, 7:3 mol/mol and CL/PG, 4:6 mol/mol) were prepared as follows. The lipids were dissolved in chloroform (1 ml) and sonicated together with 60 mM calcein solution (1 ml in phosphate buffer, pH 7.0); the liposomes were obtained by the reverse phase evaporation method [35]. The calcein excess was removed by gel filtration (Sephadex G-50) followed by centrifuging at 22000 *g* for 30 min. For vesicle size homogeneity, the pellet was passed several times through 200 μm polycarbonate membranes in a Mini-extruder apparatus (Avanti Polar Lipids Inc., Alabaster AL) [36]. Lipid concentration of vesicles was measured by the method of Stewart [37] and the final concentration used for all measurements was 50 μM. Calcein fluorescence in the vesicles is self-quenched and leakage was measured by relief of quenching; the measurements were carried out at 517 nm, exciting at 490 nm, with a Perkin-Elmer LS 50B spectrofluorimeter. The maximum value of leakage was obtained by addition of 10 μl of Triton X-100 (10%, v/v in water) to the liposome suspension, which caused total disruption of vesicles. Leakage was calculated by the equation:

$$\text{Leakage } (\%) = 100 \times (F - F_0)/(F_t - F_0),$$

where F and F_t are fluorescence before and after addition of detergent and F_0 the fluorescence of intact vesicles [38].

Protease Sensitivity Assay

Tetrabranched M33-L or M33-D peptides (300 μg) were incubated at 37°C with *Staphylococcus aureus* aureolysin (3 μg, BioCol GmbH) or *Pseudomonas aeruginosa* elastase (3 μg, Calbiochem) in 300 μl 20 mM Tris-HCl, 1 mM $CaCl_2$ pH 7.8. At indicated time intervals, 50 μl aliquots were removed, diluted with 950 μl of 0.1% trifluoroacetic acid (TFA)/water and analyzed by HPLC and mass spectrometry. Liquid chromatography was performed on Phenomenex Jupiter C18 analytical column (300 Å, 5 μm, 250×4.6 mm) in a 30 min gradient, using TFA 0.1%/water as solvent A and methanol as solvent B. Mass spectrometry analysis was performed on withdrawn samples and repeated on HPLC-eluted peaks with a Bruker Daltonic ultraflex MALDI TOF/TOF mass spectrometer.

Anti-biofilm Activity

Biofilm formation was performed by adapting the procedure described in [39] using the Calgary Biofilm Device (Innovotech, Innovotech Inc. Edmonton, Canada). Briefly, 96-well plates containing the bacterial inoculum were sealed with lids bearing 96 pegs on which the biofilm could build up. The plates were placed in an orbital incubator at 35°C (for *P. aeruginosa* and *E. coli*) or 37°C (for *S. aureus*) for 20 h under agitation at 125 rpm. Once biofilms formed, the lids were removed from the plates and the pegs were rinsed twice with phosphate buffered saline (PBS) to remove planktonic cells. The peg-lid was then transferred to a 96-well challenge microtiter plate, each well containing 200 μl of a twofold serial dilution of each peptide in LB medium. The challenge plate was incubated at 37°C for 2 hours. Peptide activity on pre-formed biofilm was evaluated by two independent methods: (i) visual observation of bacterial growth and (ii) counting of living bacterial cells after peptide treatment. In the first case, the peg-lid was removed from the challenge plate, rinsed with PBS and used to cover a 96-well recovery microtiter plate, each well containing 200 μl LB medium. The recovery plate was sealed, incubated at 37°C for 4 hours and then observed for any visible growth of bacteria detached from the peptide-treated biofilm. Growth of bacteria in a particular well indicated regrowth of planktonic cells from surviving biofilm. Minimum biofilm eradication concentration (MBEC) was defined as the minimum peptide concentration preventing regrowth of bacteria from the treated biofilm within 4 hours.

In the second case, to determine viable cell counts of biofilms after peptide treatment, pegs from the challenge microtiter plate were removed and transferred to Eppendorf tubes containing 500 μl PBS. After sonication at room temperature for 15 min to break up the biofilm and remove bacterial cells from the peg, aliquots of bacterial suspension were plated on LB-agar plates for counting. Colony forming units (CFU) were expressed as percentage with respect to control (peptide-untreated biofilms). Minimum bactericidal concentration (MBCb) was defined as the lowest peptide concentration required to reduce the number of viable biofilm cells by ≥ 3 $\log_{10}$ (99.9% killing) [40].

In vivo Experiments

Animal procedures were approved by the Ethical Committee of the Azienda Ospedaliera Universitaria Senese on November 18, 2010. Balb-c mice (20 g) were infected i.p. with lethal amounts of bacteria (see results) mixed in 500 μl PBS +7% mucin (mucin from porcine stomach, type II, Sigma-Aldrich). Bacteria were cultured overnight, centrifuged, mixed in sterile PBS, and measured by spectrophotometer. Possible further dilutions in PBS were sometimes necessary to obtain the right amount of bacteria. Groups consisted of 5 animals. Moribund animals were killed humanely to avoid unnecessary distress. Surviving mice were monitored for 7 days. Thirty minutes after bacterial administration, peptides were inoculated i.p. with 0.5 ml PBS solution containing the indicated amount of peptide (see Results). Control animals received only PBS. P values were calculated using GraphPad Prism software.

Author Contributions

Conceived and designed the experiments: CF LL LB GMR AP. Performed the experiments: SP VL VC JB BL SB SS LL. Analyzed the data: AP GMR LB MLM ADG CF. Contributed reagents/materials/analysis tools: SP VL VC JB BL SB SS LL MLM. Wrote the paper: AP CF GMR LB.

References

1. World Health Organization (2012) The evolving threat of antimicrobial resistance. Options for action. Geneva: WHO Library Cataloguing-in-Publication Data. 119 p.
2. Hancock RE, Sahl HG (2006) Antimicrobial and host-defense peptides as new anti-infective therapeutic strategies. Nat Biotechnol 24: 1551–1557.
3. Yeung ATY, Gellatly SL, Hancock RE (2011) Multifunctional cationic host defence peptides and their clinical applications. Cell Mol Life Sci 68: 2161–2176.
4. Arnold TM, Forrest GN, Messmer KJ (2007) Polymyxin antibiotics for gram-negative infections. Am J Health Syst Pharm 64: 819–826.
5. Michalopoulos A, Falagas ME (2008) Colistin and polymyxin B in critical care. Crit Care Clin 24: 377–391.
6. Habets MG, Brockhurst MA (2012) Therapeutic antimicrobial peptides may compromise natural immunity. Biol Lett 8: 416–418.
7. Tam JP (1988) Synthetic peptide vaccine design: synthesis and properties of a high density multiple antigenic peptide system. Proc Natl Acad Sci USA 85: 5409–5413.
8. Bracci L, Falciani C, Lelli B, Lozzi L, Runci Y, et al. (2003) Synthetic peptides in the form of dendrimers become resistant to protease activity. J Biol Chem 278: 46590–46595.
9. Falciani C, Lozzi L, Pini A, Corti F, Fabbrini M, et al. (2007) Molecular basis of branched peptide resistance to enzyme proteolysis. Chem Biol Drug Des 69: 216–221.

10. Pini A, Falciani C, Bracci L (2008) Branched peptides as therapeutics. Curr Protein Pept Sci 9: 468–477.
11. Pini A, Giuliani A, Falciani C, Runci Y, Ricci C, et al. (2005) Antimicrobial activity of novel dendrimeric peptides obtained by phage display selection and rational modification. Antimicrob Agents Chemother 49: 2665–2672.
12. Pini A, Giuliani A, Falciani C, Fabbrini M, Pileri S, al. (2007) Characterization of the branched antimicrobial peptide M6 by analyzing its mechanism of action and *in vivo* toxicity. J Pept Sci 13: 393–399.
13. Pini A, Falciani C, Mantengoli E, Bindi S, Brunetti J, et al. (2010) A novel tetrabranched antimicrobial peptide that neutralizes bacterial lipopolysaccharide and prevents septic shock *in vivo*. FASEB J. 24: 1015–1022.
14. Pini A, Lozzi L, Bernini A, Brunetti J, Falciani C, et al. (2012) Efficacy and toxicity of the antimicrobial peptide M33 produced with different counter-ions. Amino Acids 43: 467–473.
15. Coccia C, Rinaldi AC, Luca V, Barra D, Bozzi A, et al. (2011) Membrane interaction and antibacterial properties of two mildly cationic peptide diastereomers, bombinins H2 and H4, isolated from Bombina skin. Eur Biophys J 40: 577–588.
16. Schmidtchen A, Frick IM, Andersson E, Tapper H, Björck L (2002) Proteinases of common pathogenic bacteria degrade and inactivate the antibacterial peptide LL-37. Mol Microbiol 46: 157–168.
17. Sieprawska-Lupa M, Mydel P, Krawczyk K, Wójcik K, Puklo M, et al. (2004) Degradation of human antimicrobial peptide LL-37 by Staphylococcus aureus-derived proteinases. Antimicrob Agents Chemother 48: 4673–4679.
18. Hornef M W, Normark S, Henriques-Normark B, Rhen M (2005) Bacterial evasion of innate defense at epithelial linings. Chem Immunol Allergy 86: 72–98.
19. Banbula A, Potempa J, Travis J, Fernandez-Catalán C, Mann K, et al. (1998) Amino-acid sequence and three-dimensional structure of the Staphylococcus aureus metalloproteinase at 1.72 A resolution. Structure 6: 1185–1193.
20. Morihara K (1964) Production of elastase and proteinase by Pseudomonas aeruginosa. J Bacteriol 88: 745–757.
21. de Kreij A, Venema G, van den Burg B (2000) Substrate specificity in the highly heterogeneous M4 peptidase family is determined by a small subset of amino acids. J Biol Chem 275: 31115–31120.
22. Teufel P, Götz F (1993) Characterization of an extracellular metalloprotease with elastase activity from Staphylococcus epidermidis. J Bacteriol 175: 4218–4224.
23. Lai Y, Villaruz AE, Li M, Cha DJ, Sturdevant DE, et al. (2007) The human anionic antimicrobial peptide dermicidin induces proteolytic defence mechanisms in staphylococci. Mol Microbiol 63: 497–506.
24. Høiby N, Bjarnsholt T, Givskov M, Molin S, Ciofu O (2010) Antibiotic resistance of bacterial biofilms. Int J Antimicrob Agents 35: 322–332.
25. Boles BR, Horswill AR (2011) Staphylococcal biofilm disassembly. Trends Microbiol 19: 449–455.
26. Peters BM, Jabra-Rizk MA, O'May GA, Costerton JW, Shirtliff ME (2012) Polymicrobial interactions: impact on pathogenesis and human disease. Clin Microbiol Rev 25: 193–213.
27. Thurlow LR, Joshi GS, Richardson AR (2012) Virulence strategies of the dominant USA300 lineage of community-associated methicillin-resistant Staphylococcus aureus (CA-MRSA). FEMS Immunol Med Microbiol 65: 5–22.
28. Jarvis WR, Jarvis AA, Chinn RY (2012) National prevalence of methicillin-resistant Staphylococcus aureus in patients at United States health care facilities, 2010. Am J Infect Control 40: 194–200.
29. Pini A, Runci Y, Falciani C, Lelli B, Brunetti J, et al. (2006) Stable peptide inhibitors prevent binding of lethal and oedema factors to protective antigen and neutralize anthrax toxin *in vivo*. Biochem J 395: 157–163.
30. Falciani C, Fabbrini M, Pini A, Lozzi L, Lelli B, et al. (2007) Synthesis and biological activity of stable branched neurotensin peptides for tumor targeting. Mol Cancer Ther 6: 2441–2448.
31. Falciani C, Lelli B, Brunetti J, Pileri S, Cappelli A, et al. (2010) Modular branched neurotensin peptides for tumor target tracing and receptor-mediated therapy: a proof-of-concept. Curr Cancer Drug Targets 10: 695–704.
32. Hamamoto K, Kida Y, Zhang Y, Shimizu T, Kuwano K (2002) Antimicrobial activity and stability to proteolysis of small linear cationic peptides with D-amino acid substitutions. Microbiol Immunol 46: 741–749.
33. Strömstedt AA, Pasupuleti M, Schmidtchen A, Malmsten M (2009) Evaluation of strategies for improving proteolytic resistance of antimicrobial peptides by using variants of EFK17, an internal segment of LL-37. Antimicrob Agents Chemother 53: 593–602.
34. Bachrach G, Altman H, Kolenbrander PE, Chalmers NI, Gabai-Gutner M, et al. (2008) Resistance of Porphyromonas gingivalis ATCC 33277 to Direct Killing by Antimicrobial Peptides Is Protease Independent. Antimicrob Agents Chemother 52: 638–642.
35. Szoka F Jr, Papahadjopoulos D (1978) Procedure for preparation of liposomes with large internal aqueous space and high capture by reverse-phase evaporation. Proc Natl Acad Sci USA 4194–4198.
36. Epand RM, Epand RF (2003) Liposomes as models for antimicrobial peptides. Meth Enzymol 372: 124–133.
37. Stewart JC (1980) Colorimetric determination of phospholipids with ammonium ferrothiocyanate. Anal Biochem 104: 10–14.
38. Matsuzaki K, Sugishita K, Miyajima K (1999) Interactions of an antimicrobial peptide, magainin 2, with lipopolysaccharide-containing liposomes as a model for outer membranes of gram-negative bacteria. FEBS Lett 449: 221–224.
39. Ceri H, Olson M, Morck D, Storey D, Read R, et al. (2001) The MBEC Assay System: multiple equivalent biofilms for antibiotic and biocide susceptibility testing. Meth Enzymol 337: 377–385.
40. Harrison JJ, Stremick CA, Turner RJ, Allan ND, Olson ME, et al. (2010) Microtiter susceptibility testing of microbes growing on peg lids: a miniaturized biofilm model for high-throughput screening. Nat Protoc 5: 1236–1254.

Cell. Mol. Life Sci. (2013) 70:2773–2786
DOI 10.1007/s00018-013-1291-7

Cellular and Molecular Life Sciences

RESEARCH ARTICLE

Esculentin(1-21), an amphibian skin membrane-active peptide with potent activity on both planktonic and biofilm cells of the bacterial pathogen *Pseudomonas aeruginosa*

Vincenzo Luca · Annarita Stringaro · Marisa Colone · Alessandro Pini · Maria Luisa Mangoni

Received: 23 November 2012 / Revised: 26 January 2013 / Accepted: 5 February 2013 / Published online: 16 March 2013

Abstract *Pseudomonas aeruginosa* is an opportunistic bacterial pathogen that forms sessile communities, named biofilms. The non-motile forms are very difficult to eradicate and are often associated with the establishment of persistent infections, especially in patients with cystic fibrosis. The resistance of *P. aeruginosa* to conventional antibiotics has become a growing health concern worldwide and has prompted the search for new anti-infective agents with new modes of action. Naturally occurring antimicrobial peptides (AMPs) represent promising future template candidates. Here we report on the potent activity and membrane-perturbing effects of the amphibian AMP esculentin(1-21), on both the free-living and sessile forms of *P. aeruginosa*, as a possible mechanism for biofilm disruption. Furthermore, the findings that esculentin(1-21) is able to prolong survival of animals in models of sepsis and pulmonary infection indicate that this peptide can be a promising template for the generation of new antibiotic formulations to advance care of infections caused by *P. aeruginosa*.

V. Luca · M. L. Mangoni (✉)
Dipartimento di Scienze Biochimiche "A. Rossi Fanelli", Istituto Pasteur-Fondazione Cenci Bolognetti, Sapienza Università di Roma, Rome, Italy
e-mail: marialuisa.mangoni@uniroma1.it

A. Stringaro · M. Colone
Dipartimento di Tecnologie e Salute, Istituto Superiore di Sanità, Rome, Italy

A. Pini
Dipartimento di Biotecnologie Mediche, Università degli Studi di Siena, Siena, Italy

M. L. Mangoni
Department of Biochemical Sciences, La Sapienza University, Via degli Apuli 9, 00185 Rome, Italy

Keywords Antimicrobial peptide · Anti-biofilm activity · Cystic fibrosis · Membrane-permeation · Anti-*Pseudomonas* activity · Scanning electron microscopy

Abbreviations

CF	Cystic fibrosis
CFU	Colony-forming unit
CV	Crystal violet
EDTA	Ethylenediaminetetraacetic acid
Esc(1-21)	Esculentin(1-21)
LB	Luria-Bertani broth
MBCb	Minimum bactericidal concentration on biofilm cells
MBEC	Minimum biofilm eradication concentration
MDR	Multi-drug resistance
MH	Mueller-Hinton
MIC	Minimal inhibitory concentration
MTT	3-(4,5-dimethylthiazol-2-yl)-2,5-diphenyltetrazolium bromide
ONPG	2-nitrophenyl β-D-galactoside
PBS	Phosphate buffered saline
SDS	Sodium dodecyl sulphate

Introduction

The emergence of microbial strains resistant to conventional antibiotics has become a serious threat for human health, particularly in hospitals, where immunocompromised patients can easily be affected by bacterial infections mainly those caused by *Pseudomonas aeruginosa* [1, 2]. This bacterium is quite difficult to eradicate because of its ability to form sessile communities named biofilms [3–5]. Bacterial biofilms are a structured consortium of embedded cells into a self-promoted polymeric matrix consisting

of polysaccharides, proteins, and extracellular DNA. These confer protection on the bacterial population from antibiotics, chemicals, as well as opsonization and phagocytosis by host immune cells [3, 6–9]. Importantly, biofilm formation is often associated with the establishment of persistent infections, like those found in the lungs of most cystic fibrosis (CF) sufferers [10, 11], where the gradual pulmonary deterioration, thick airway mucus and high salt concentration hamper clearance of bacteria, leading to lethality. Despite the prominent role of biofilms in the infection, limited studies have been reported on the identification of compounds active on both free-living and sessile forms of *P. aeruginosa* [12]. Recently, natural antimicrobial peptides (AMPs) have attracted the interest of many researchers as fascinating templates for the development of alternative therapeutics with a new mode of action [13–15]. AMPs are produced by almost all unicellular and multicellular organisms and act as the first line of defense against noxious microorganisms [16–18]. However, there is increasing evidence, mainly in vertebrate species, that these peptides display crucial functions also in the regulation of the host's immune system [19–24]. The majority of AMPs have a net positive charge at neutral pH and a substantial proportion of hydrophobic residues, both favoring AMPs' binding and insertion into the negatively charged microbial membranes [21, 25–29]. Among natural sources for AMPs, amphibian skin of *Rana* genus is one of the richest storehouses [15, 30], and esculentin-1 represents the family of frog skin AMPs with the longest chain (46 amino acids) [31, 32]. Interestingly, studies with esculentin-1b, originated from the green edible frog *Pelophylax lessonae/ridibundus* (formerly *R. esculenta* [33]), showed that its N-terminal 1-18 region [Esc(1-18)] retained the wide spectrum of antimicrobial activity of the full-length peptide [34]. Lately, we demonstrated that esculentin(1-21) [Esc(1-21)], bearing the first 20 residues of the native esculentin-1a (see Table 1) had a higher activity than Esc(1-18) in inhibiting the growth of Gram-negative bacteria, such as *Escherichia coli* and *P. aeruginosa* [35]. On the basis of such findings, we decided to investigate the in vitro and in vivo anti-*Pseudomonas* activity of the N-terminal region of esculentin-1 peptides by choosing the Esc(1-21) fragment. Specifically, we have analyzed the activity and underlying molecular mechanism of Esc(1-21) on both the planktonic and biofilm growing cells of *P. aeruginosa*, together with its in vivo efficacy in fighting infections caused by this pathogen at different anatomical regions. Importantly, we show that this frog skin AMP is a membrane-active peptide highly effective on *P. aeruginosa* strains, including those isolated from CF patients. It also has the ability to prolong survival of animals in models of peritoneal or pulmonary *P. aeruginosa* infection, using a systemic or topical peptide administration, respectively.

Materials and methods

Materials

Synthetic Esc(1-21) was purchased from Selleck Chemicals (Houston, TX, USA). Briefly, Esc(1-21) was assembled by step-wise solid-phase synthesis using a standard F-moc strategy and purified by RP-HPLC on a semipreparative C18-bonded silica column (Kromasyl, 5 μm, 100 Å, 25 cm × 4.6 mm) using a gradient of acetonitrile in 0.1 % aqueous trifluoroacetic acid (from 25 to 100 % in 30 min) at a flow rate of 1.0 ml/min. The product was obtained by lyophilization of the appropriate fraction. Analytical RP-HPLC indicated a purity >98 %. The molecular mass was verified by using MALDI-TOF Voyager DE (Applied Biosystems, Carlsbad, CA, USA) as previously described [34]. Sytox Green was from Molecular Probes (Invitrogen, Carlsbad, CA, USA). Crystal violet (CV), 3-(4,5-dimethylthiazol-2-yl)-2,5-diphenyltetrazolium bromide (MTT) and 2-nitrophenyl β-D-galactoside (ONPG) were all purchased from Sigma (St. Louis, MO, USA). All other chemicals were reagent grade.

Microorganisms

The strains of *P. aeruginosa* used for the antimicrobial assays were: the standard non-mucoid ATCC 27853 [36] and PAO1, the clinical multidrug resistant (MDR)

Table 1 Amino acid sequences of esculentin peptides

Peptide designation	*Sequence*[a]
Esculentin-1a(1-21)	GIFSKLAGKK**I**KNLLISGLKG-NH_2
Esculentin-1a[b]	GIFSKLAGKK**I**KNLLISGLKNVGKEVGMDVVRTGIDIAGCKIKGEC

[a] Amino acid differences are boldfaced. Basic and acidic residues are indicated by red and blue letters, respectively

[b] Peptide sequence taken from [31]

isolates MDR1, MDR2, and MDR3 and the following strains from CF patients: the mucoid AA11 and non-mucoid TR1 isolated at the onset of chronic lung colonization; both mucoid AA43 and TR67 isolated after years of chronic colonization, according to what was reported in [37, 38]. These CF strains were chosen from the strains collection of the CF clinic Medizinische Hochschule of Hannover, Germany [37]. Mode of action studies and β-galactosidase activity measurements were carried out with *P. aeruginosa* PAO1 carrying plasmid pP*rsaL*190 [39], kindly provided by Prof. Livia Leoni (Roma Tre University, Rome, Italy).

Antibacterial activity on free-living bacteria

Susceptibility testing was performed by adapting the microbroth dilution method outlined by the Clinical and Laboratory Standards Institute using sterile 96-well plates ("BD Falcon", BD Biosciences, Franklin Lakes, NJ, USA). Aliquots (50 μl) of bacteria in mid-log phase at a concentration of 2×10^6 colony-forming units (CFU)/ml in culture medium (Müller-Hinton agar) were added to 50 μl of MH broth containing the peptide in serial twofold dilutions. The ranges of peptide concentrations used were 0.125–32 μM. Inhibition of microbial growth was determined by measuring the absorbance at 590 nm, after an incubation of 16–18 h at 37 °C with a microplate reader (Infinite M200; Tecan, Salzburg, Austria). Antimicrobial activities were expressed as the minimal inhibitory concentration (MIC), the concentration of peptide at which 100 % inhibition of microbial growth is observed.

Anti-biofilm activity

Biofilm formation was performed by adapting the procedure described in [40, 41] using the Calgary Biofilm Device (Innovotech, Innovotech Inc. Edmonton, Canada). Briefly, 96-well plates (each well containing 150 μl of the bacterial inoculum (1×10^7 cells/ml) in Luria-Bertani (LB) medium) were sealed with 96 pegs-lids on which biofilm cells can build up. Afterwards, the plates were placed in a humidified orbital incubator at 35 °C for 20 h under agitation at 125 rpm. Once the biofilms were allowed to form, the pegs were rinsed twice with phosphate buffered saline (PBS) to remove planktonic cells. Each peg-lid was then transferred to a "challenge 96-well microtiter plate", each well containing 200 μl of a twofold serial dilution of Esc(1-21) in PBS. The "challenge plate" was incubated at 37 °C for 2 h. Peptide activity on preformed biofilm was evaluated by three independent methods: (i) visual observation of bacterial growth; (ii) numbering of living bacterial cells after peptide treatment, and (iii) evaluation of biomass. In the first case, the peg-lid was removed from the "challenge plate", rinsed with PBS, and used to cover a 96-well "recovery microtiter plate", each well containing 200 μl LB. The "recovery plate" was sealed, incubated at 37 °C for 4 h, and then observed for detection of any visible growth of bacteria detached from the peptide-treated biofilm. Growth of bacteria in a particular well indicates re-growth of planktonic cells from surviving biofilm. Minimum biofilm eradication concentration (MBEC) was defined as the minimum peptide concentration preventing re-growth of bacteria from the treated biofilm, within 4 h.

In the second case, to determine viable cell counts after peptide treatment, pegs were broken from the lid and each peg was transferred into an Eppendorf tube containing 500 μl of PBS. After sonication to remove bacterial cells from the peg, aliquots of bacterial suspension were plated on LB-agar plates for counting. Colony-forming units (CFU) were expressed as a percentage with respect to the control (peptide-untreated biofilms). The minimum bactericidal concentration (MBCb) was defined as the lowest peptide concentration required to reduce the number of viable biofilm cells of ≥ 3 $\log_{10}$ (99.9 % killing) after 2 h [42]. Viable biofilm cells were also determined by the reduction of MTT to its insoluble formazan. Briefly, after peptide treatment, the peg lid was washed with PBS and used to close another 96-well microtiter plate, each well containing 200 μl of 0.5 mg/ml MTT in PBS. The plate was incubated at 37 °C for 4 h. Afterwards, 50 μl of 25 % sodium dodecyl sulphate (SDS) were added to each well to dissolve formazan crystals. Bacterial viability was determined by absorbance measurements at 595 nm [43] and calculated with respect to control cells (bacteria not treated with the peptide).

In the third case, to determine the biofilm biomass, peptide-treated pegs were washed in PBS, fixed in 99 % methanol for 15 min at room temperature, and air-dried. Then, by using a 96-well microtiter plate, pegs were stained with 200 μl of a CV solution (0.05 % in water). After 20 min, the excess CV was removed by washing the pegs with water. Finally, bound CV was released from pegs by adding 200 μl of 33 % acetic acid. The absorbance was measured at 600 nm.

Time-killing curves

About 1×10^5 CFU in 100 μl PBS were incubated at 37 °C with Esc(1-21) at 0.5 or 1 μM. Aliquots of 10 μl were withdrawn at different intervals, diluted in MH, and spread onto LB-agar plates. After overnight incubation at 37 °C, the number of CFU was counted. Controls were run without peptide and in the presence of peptide solvent (water). Bactericidal activity was defined as the peptide concentration necessary to cause a reduction in the number of viable bacteria of ≥ 3 $\log_{10}$ CFU/ml.

Permeation of the cytoplasmic membrane

Sytox Green assay

To assess the ability of Esc(1-21) to alter the bacterial membrane permeability of planktonic cells of *Pseudomonas*, 1×10^6 cells in 100 µl of PBS were mixed with 1 µM Sytox Green for 5 min in the dark. After adding the peptide, the increase in fluorescence, owing to the binding of the dye to intracellular DNA, was measured at 37 °C in the microplate reader (excitation and emission wavelengths were 485 and 535 nm, respectively). The peptide concentrations ranged from 0.125 to 32 µM. Controls were cells without a peptide, whereas the maximal membrane perturbation was obtained after treating bacteria with the highest peptide concentration used (32 µM) followed by the addition of 1 mM ethylenediaminetetraacetic acid (EDTA) + 0. 5 % Triton X-100 (final concentration) to completely destabilize the lipopolysaccharide-outer membrane and solubilize the phospholipid bilayer of the cytoplasmic membrane [44]. Note that the addition of EDTA + Triton X-100 to the bacteria with the highest peptide concentration did not induce any change in the fluorescence intensity, thus excluding any possible interference between the peptide and the detergent used.

In the case of 20 h preformed biofilm, after 2-h peptide treatment in the "challenge microtiter plate" [each well containing 200 µl of a twofold serial dilution of Esc(1-21) in PBS supplemented with 1 µM Sytox Green], pegs were broken from the lid and each peg was transferred into an Eppendorf tube together with the corresponding 200 µl from the "challenge well". After sonication to detach bacterial cells from the peg, the cell suspension of each sample (200 µl volume) was transferred into wells of another microtiter plate for measurement (excitation and emission wavelengths were 485 and 535 nm, respectively). Also in this case, controls were given by cells without peptide, whereas the maximal membrane perturbation was obtained after treating biofilm cells with the highest peptide concentration (48 µM), followed by the addition of 1 mM EDTA + 0.5 % Triton X-100 to dissolve the extracellular matrix [45] and make the bacterial membranes fully permeable [44].

β-galactosidase assay

The ability of Esc(1-21) to cause more pronounced damage to the cytoplasmic membrane of *Pseudomonas* was determined by measuring the extracellular release of β-galactosidase, using ONPG as a substrate [46]. For the planktonic form, *P. aeruginosa* PAO1 was grown at 37 °C in LB to an $OD_{590\ nm}$ of approximately 0.8, washed twice, centrifuged for 10 min (1.4 × *g*) and resuspended in PBS at the same OD. About 1×10^6 cells (in 100 µl PBS) were incubated with different concentrations of Esc(1-21) for 30 min at 37 °C. Controls were bacteria without peptide, whereas the maximal membrane perturbation was obtained as described for the Sytox Green assay on planktonic cells. At the end of the incubation time, 2-µl aliquots were withdrawn, diluted 1:100 in LB, and spread on LB plates for counting. Afterwards, 450 µl of PBS was added to the remaining bacterial suspension, which was passed through a 0.2-µm filter. The hydrolysis of 2 mM ONPG, added to the culture filtrate, was recorded at 420 nm using a spectrophotometer (UV-1700 Pharma Spec Shimadzu).

In the case of preformed biofilm, pegs were broken from the lid of the "challenge plate", transferred into Eppendorf tubes together with the corresponding 200 µl from the wells of the "challenge plate", and then sonicated. Then, 2-µl aliquots of the cell suspension were withdrawn and diluted as described above, for counting. One ml of PBS was added to the sonicated cell suspension, which was filtered; hydrolysis of 2 mM ONPG was followed as described above. Controls and maximal membrane perturbation were obtained as for the Sytox Green assay on biofilm cells.

Scanning electron microscopy

Approximately 1×10^6 bacterial cells in PBS were treated with the peptide at different concentrations for 30 min at 37 °C and then fixed with 2.5 % glutaraldehyde in 0.2 M cacodylate buffer (pH 7.2). The samples were deposited on glass coverslips of 12-mm diameter. Afterwards, they were washed three times in cacodylate buffer, post-fixed with 1 % (w/v) osmium tetroxide for 1 h, and dehydrated using a graded ethanol series (70; 85; 95 %). After the passage in 100 % ethanol, the samples were air-dried (overnight) and gold coated by sputtering (SCD 040 Balzers device, Bal-Tec). The samples were examined with a scanning electron microscope (FEI Quanta Inspect FEG, USA)

To visualize biofilm-colonized pegs, after 20 h of biofilm formation by *P. aeruginosa* ATCC 27853 or *P. aeruginosa* PAO1 on Calgary microtiter plates, pegs were broken from the lid, washed with PBS, and fixed with 2.5 % glutaraldehyde in 0.2 M cacodylate buffer. Pegs were placed in this solution at 4 °C for 16 h. Following this fixing step, the pegs were washed in 0.2 M cacodylate buffer for approximately 10 min. Then, they were post-fixed, dehydrated, and gold coated as described above. The pegs were examined under the same scanning electron microscope and those portions containing bacterial cells were photographed.

Hemolytic and cytotoxic activity

The hemolytic activity of Esc(1-21) was determined using fresh human erythrocytes. The blood was centrifuged and the erythrocytes were washed three times with 0.9 % NaCl. Peptide solutions were incubated with the erythrocyte

suspension (1×10^7 cells/ml) at 37 °C for a short (1 h) and a long (24 h) time. Then, the extent of hemolysis was measured on the supernatant, from the optical density at 540 nm of the supernatant. Hypotonically lysed erythrocytes were used as a standard for 100 % hemolysis.

The cytotoxic effect of Esc(1-21) was determined by the inhibition of MTT reduction to insoluble formazan, by mitochondrial reductases. We used the murine Raw 264.7 macrophage cell line and the human lung adenocarcinoma epithelial cell line A549 from the American Type Culture Collection (ATCC, Manassas, VA). Cells were cultured in Dulbecco's modified Eagle's medium (DMEM; Sigma) supplemented with 10 % heat inactivated fetal bovine serum, glutamine (4 mM), and antibiotics (penicillin and streptomycin). Afterwards, cells were plated in triplicate wells of a microtiter plate at 1×10^5 cells/well in DMEM supplemented with 2 % serum without antibiotics. After overnight incubation at 37 °C in a 5 % CO_2 atmosphere, the medium was replaced with 100 μl fresh DMEM supplemented with Esc(1-21) at different concentrations. The plate was incubated for a short (1 h) and a long (24 h) time at 37 °C in a 5 % CO_2 atmosphere. Afterwards, the medium was removed and replaced with Hank's medium (136 mM NaCl; 4.2 mM Na2HPO4; 4.4 mM KH2PO4; 5.4 mM KCl; 4.1 mM NaHCO3, pH 7.2, supplemented with 20 mM D-glucose) containing 0.5 mg/ml MTT. After 4 h incubation, the formazan crystals were dissolved by adding 100 μl of acidified isopropanol and viability was determined by absorbance measurements at 570 nm. Cell viability was calculated with respect to control cells (cells not treated with peptide).

In vivo experiments

Animal procedures were approved by the Ethics Committee of the Azienda Ospedaliera Universitaria Senese on November 18, 2010. For both mice models of sepsis and lung infections, Balb-c mice (20 g) were rendered neutropenic by cyclophosphamide (Sigma-Aldrich C7397) given intraperitoneally (i.p.) 150 mg/kg (300 μl of a solution 10 mg/ml) 4 days and 1 day before the infection.

Regarding the sepsis model [47], animals were infected i.p. with a lethal amount of *P. aeruginosa* PAO1 (1.5×10^3 CFU/mouse) mixed in 500 μl PBS. Groups consisted of five animals. Moribund animals were killed humanely to avoid unnecessary distress. After 24 and 72 h from the bacterial administration, the peptide was inoculated intravenously (i.v.) with 0.2 ml PBS solution containing 5 mg/kg of Esc(1-21). Control animals received only PBS. Surviving mice were monitored for 12 days.

In the pneumonia model, the infection was initiated through intra-tracheal (i.t.) instillation of *P. aeruginosa* PAO1 ($1–3 \times 10^3$ CFU/mouse). Animals were first anesthetized with Avertin (Sigma-Aldrich 2,2,2-Tribromoethanol T48402) (600 μl i.p. of a solution 10 mg/ml) and, after 10 min from anesthesia, bacteria were administered i.t. through a small incision at the trachea level where a 22-G catheter connected to a syringe was inserted (volume injected 60 μl). Approximately 2–3 min later, using the same catheter inserted in the trachea, 60 μl of PBS solution containing the peptide (5 or 2.5 or 1.25 mg/kg) were injected in the lungs with a different syringe. Afterwards, the wound was closed by a small clip. Animals were generally awake after 30 min. Groups consisted of 16 animals. Moribund animals were killed humanely as above. All *p* values were calculated using GraphPad Prism 5.0 software.

Table 2 Resistance phenotype of MDR-clinical isolates of *P. aeruginosa*

MDR strain	Resistance phenotype
1	AMP–CAZ–CIP–CTX–CXM–FEP–GEN–MEM–PIP–SXT–TOB
2	AMP–CFZ–CIP–CTX–CXM–GEN–LVX–IPM–MEM–SXT–TET
3	AMP–CFZ–CTX–CIP–GEN–IPM–LVX–SXT–TET–TOB

AMP ampicillin; *CAZ* ceftazidime; *CFZ* cefazolin; *CIP* ciprofloxacin; *CTX* cefotaxime; *CXM* cefuroxime; *FEP* cefepime; *GEN* gentamicin; *IPM* imipenem; *LVX* levofloxacin; *MEM* meropenem; *PIP* piperacillin; *SXT* trimethoprim/sulfamethoxazole; *TET* tetracyclin; *TOB* tobramicin

Results

Antimicrobial activity on planktonic and biofilm cells of *P. aeruginosa*

The antimicrobial activity of Esc(1-21) was tested by the microdilution broth assay on reference strains (ATCC 27853 and PAO1) and MDR-clinical isolates of *P. aeruginosa* (i.e., MDR1, MDR2, and MDR3) whose resistance phenotype is illustrated in Table 2. In addition, *P. aeruginosa* strains from CF patients were included for comparison. Esc(1-21) was equally active on both reference and MDR-strains, with a MIC value of 4 μM except for MDR2 (8 μM) (Table 3). Furthermore, it displayed the same efficacy also against CF strains either with a mucoid or non-mucoid phenotype. To verify whether the anti-*Pseudomonas* activity of Esc(1-21) was preserved against the sessile form of this microorganism, the peptide's activity on 20-h pre-formed biofilm of *P. aeruginosa* ATCC 27853 (a well-known biofilm-forming strain) was studied by three independent methods, as described in the Experimental procedure section, using microtiter plates endowed with a 96-peg lid: (i) visual observation of bacterial growth; (ii) evaluation of living bacterial cells after peptide treatment, and (iii) estimation

Table 3 Anti-*Pseudomonas* activity of Esc(1-21)[a]

MIC (μM)[b]									
Pseudomonas aeruginosa strains									
	Reference strains		MDR clinical isolates[d]			CF clinical isolates			
						Early		Late	
Peptide	ATCC 27853[c]	PAO1[c]	MDR1	MDR2	MDR3	AA11[e]	TR1[c]	AA43[e]	TR67[e]
Esc(1-21)	4	4	4	8	4	4	4	4	4
Anti-biofilm activity on *P. aeruginosa* ATCC 27853									
Minimum biofilm eradication concentration (MBEC, μM)[f]						Minimum bactericidal concentration (MBCb, μM)[g]			
6						12			

[a] Values are those obtained from at least three readings out of four independent measurements

[b] The minimum growth inhibitory concentration (MIC) is reported against the planktonic form of *P. aeruginosa* strains

[c] Non-mucoid strains

[d] The mucoid phenotype was not investigated

[e] Mucoid phenotype

[f] MBEC is defined as the minimum peptide concentration preventing re-growth of bacteria from the treated biofilm, within 4 h

[g] MBCb is defined as the minimum peptide concentration required to reduce the number of viable biofilm cells of ≥ 3 $\log_{10}$ (99.9 % killing) after 2 h

Table 4 Anti-biofilm activity of Esc(1-21) at different concentrations[a]

Peptide concentration (μM)	Viable biofilm cells (%)[b]		Biofilm biomass (%)[c]
	Colony counts	MTT reduction	
48	0	0	15
24	0.08	0	17
12	0.1	0	32
6	32	28	53
3	50	47	65
1.5	75	71	100
0.75	100	100	100

[a] The activity was evaluated as enumeration of viable cells and biofilm biomass. The results are the mean of three independent experiments with SD not exceeding 0.6 %

[b] The percentage of viable cells was determined either by colony counts of pegs after sonication or by MTT reduction to its insoluble formazan with respect to control samples (bacterial biofilm not treated with the peptide)

[c] The percentage of biofilm biomass was determined by CV staining. See "Materials and methods" for further experimental details

of the peptide's effect on the bacterial biomass. As shown in Table 3, the minimum peptide concentration able to inhibit re-growth of bacteria from peptide-treated biofilm (MBEC) was found to be equal to 6 μM. Most importantly, the same peptide caused a 3-$\log_{10}$ reduction in the number of viable biofilm *Pseudomonas* cells (i.e., MBCb in Table 3) at a concentration twofold higher the MBEC. Note that the percentage of living cells in biofilm-colonized pegs upon treatment with different concentrations of Esc(1-21) was determined either by colony counts or by MTT reduction (Table 4). Using the latter procedure, a slightly lower percentage of viable bacteria was recorded, whereas, by CV staining, from 15 to 32 % biofilm biomass was detected at those concentrations giving rise to almost total microbial death (from 48 to 12 μM, respectively) (Table 4).

Mode-of-action studies on planktonic cells

Killing kinetics

Esculentin(1-21) was first analyzed for its killing kinetic on reference (Fig. 1a) and some representative CF strains of *Pseudomonas* (Fig. 1b) in physiologic solution. Interestingly, in all cases, bactericidal effects (99.9 % killing) were apparent with 1 μM peptide within 15 min, which excludes inhibition of intracellular processes (e.g., DNA, protein or cell wall synthesis) as the major mechanism(s) for the bactericidal activity of Esc(1-21) against *Pseudomonas.*

Membrane perturbation

The ability of Esc(1-21) to injure the cytoplasmic membrane of planktonic cells of *P. aeruginosa* PAO1 was evaluated within the first 50 min after addition of the peptide at concentrations ranging from 0.125 to 32 μM, by means of the Sytox Green assay (Fig. 2). Sytox Green (MW 900 Da) is an impermeant probe, which is excluded from intact cells, but not from those having lesions whose size is enough to allow its entrance. As found for the killing kinetic assay (Fig. 1), the bacterial membrane perturbation occurred

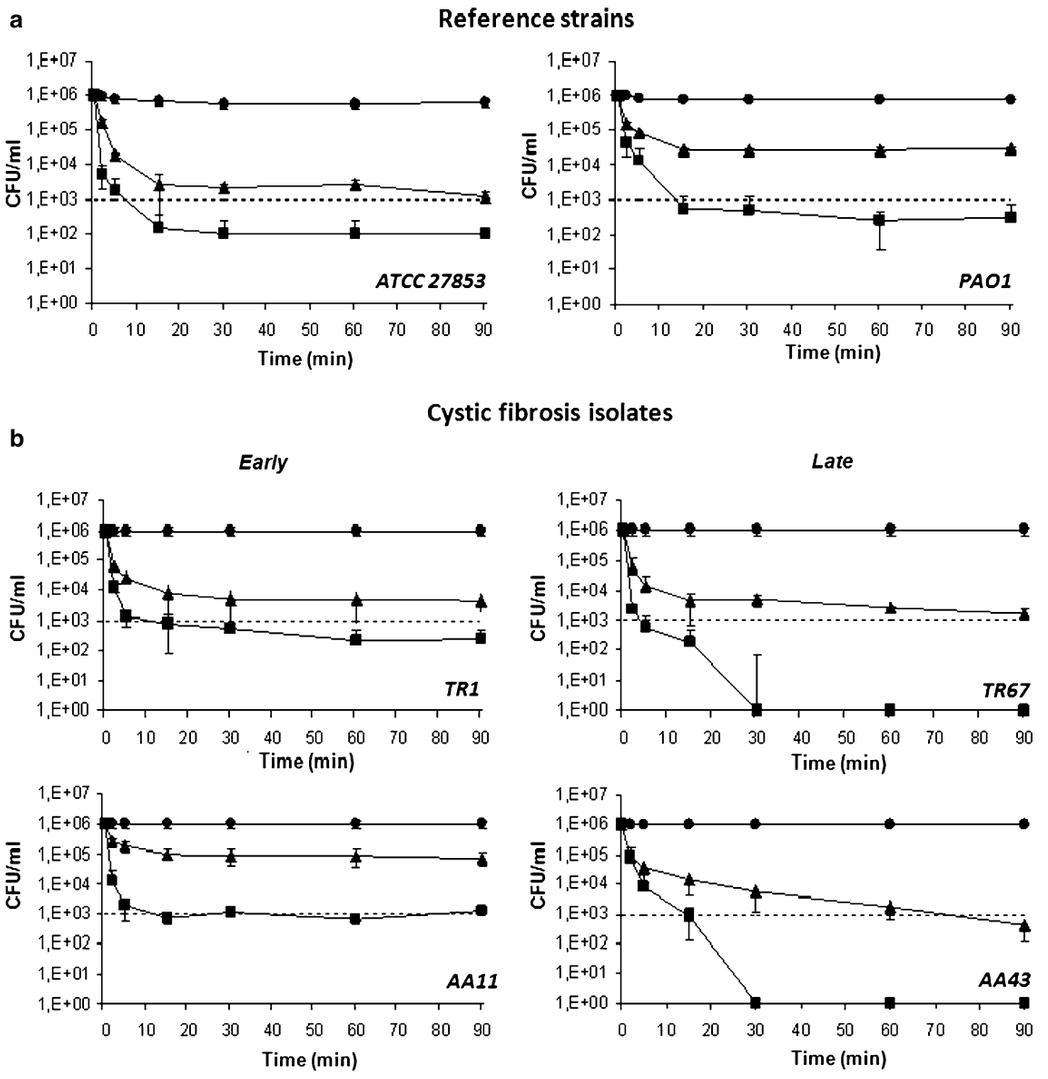

Fig. 1 Killing kinetic of Esc(1-21) on *P. aeruginosa* strains. Bacteria (1×10^6 CFU/ml) were incubated with 0.5 μM (*triangle*) or 1 μM (*square*) of Esc(1-21) in PBS at 37 °C. The number of surviving cells at different incubation time is indicated as CFU/ml. The control (*circle*) is given by bacteria without peptide. Data points represent the mean of triplicate samples ± SD from a single experiment, representative of three independent experiments. The *dotted lines* indicate 99.9 % bacterial killing

within the first 15 min from peptide addition and in a dose-dependent manner (Fig. 2). Similar results were obtained with *P. aeruginosa* ATCC 27853 (data not shown). Note that an optimal detection of membrane perturbation by the Sytox Green assay required a higher number of bacterial cells (1×10^7 CFU/ml) compared to the regular amount (1×10^6 CFU/ml) used for MIC (Table 3) and killing kinetics assays (Fig. 1). However, the relationship between the peptide's effect on the viability of PAO1 cells and the perturbation of their membrane under the same conditions (e.g. number of cells and incubation time) is reported in Fig. 3a, where the results of bactericidal and membrane perturbation assays performed with 1×10^7 CFU/ml after 30 min of peptide treatment are compared. This higher number of bacterial cells explains the differences in viable counts previously shown in Fig. 1 at 0.5 and 1 μM peptide concentrations. The maximal membrane perturbation was reached at 8 μM; however, a membrane disturbing activity was observed already at peptide concentrations of 0.25–0.5 μM, which did not significantly affect the survival of bacteria (Fig. 3a). To further expand our knowledge on the extent of peptide-induced membrane disruption, the leakage of large cytosolic

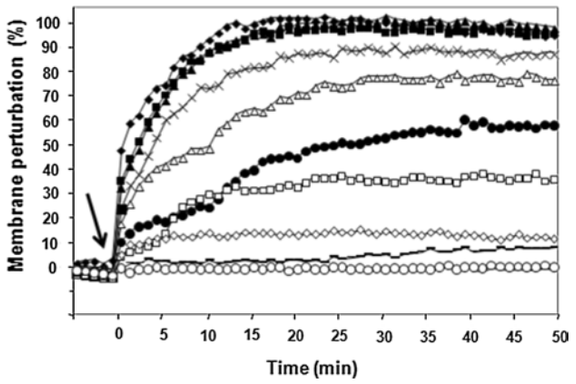

Fig. 2 Kinetics of cytoplasmic membrane permeabilization of the planktonic form of *P. aeruginosa* PAO1. Cells (1×10^7 CFU/ml) were incubated with 1 μM Sytox Green in PBS. Once basal fluorescence reached a constant value, the peptide was added (*arrow*, $t = 0$) and changes in fluorescence ($\lambda_{exc} = 485$ nm, $\lambda_{ems} = 535$ nm) were monitored for 50 min and plotted as the percentage of membrane perturbation relative to that obtained after treating bacteria with the highest peptide concentration (32 μM) and the addition of 1 mM EDTA + 0.5 % Triton-X100. Data points represent the average values of three independent experiments, with SD not exceeding 2.5 %. Peptide concentrations used were the following: 0.125 μM (*hyphen*); 0.25 μM (*diamond*); 0.5 μM (*square*); 1 μM (*filled circle*); 2 μM (*triangle*); 4 μM (*cross*); 8 μM (*filled triangle*); 16 μM (*filled square*); 32 μM (*filled diamond*). Control (*circle*) is given by bacteria without peptide

components, such as the enzyme β-galactosidase, from peptide-treated cells was investigated. As reported in the "Materials and methods" section, the *P. aeruginosa* PAO1 recombinant strain, used in our experiments, constitutively expresses the β-galactosidase. As shown in Fig. 3a, Esc(1-21) provoked from ~50–60 % enzyme release at those concentrations (from 8 to 32 μM) causing the complete microbial death and making the membrane fully permeable to Sytox Green. Hereafter, to shed light onto the direct effect of the peptide on the morphology of bacterial cells, we used scanning electron microscopy. Untreated bacteria appeared as rods with a bright surface (Fig. 4). In contrast, Esc(1-21) elicited a remarkable modification of the cell shape with the formation of blebs (pustules) and cell debris arising from the bacteria (Fig. 4).

Mode-of-action studies on bacterial biofilm

The ability of Esc(1-21) to harm the membrane of *Pseudomonas* PAO1 cells in their sessile form was also studied by measuring both the intracellular influx of Sytox Green and the extracellular release of β-galactosidase, 2 h after peptide treatment at different concentrations (Fig. 3b). Surprisingly, similar results to those achieved with the motile form of this microorganism were found, although a weaker

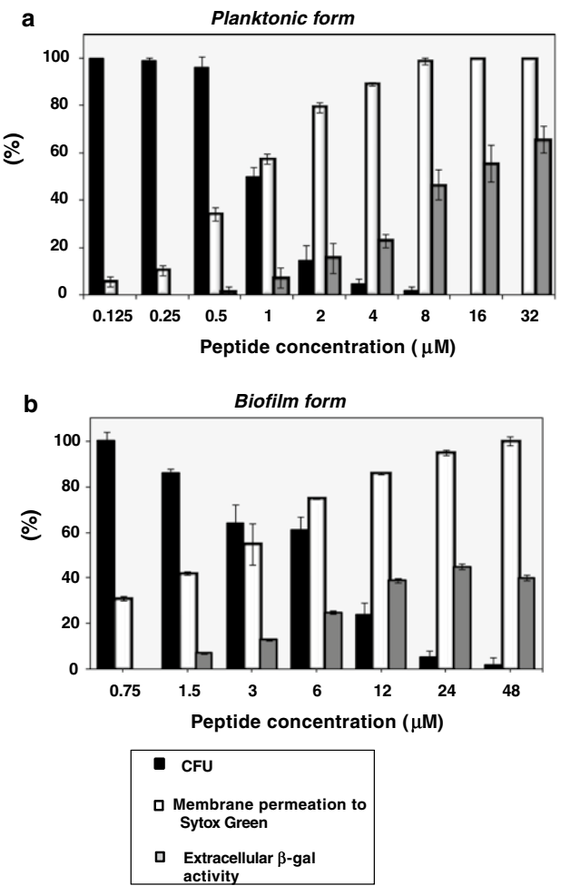

Fig. 3 Effect of Esc(1-21) on the viability and membrane perturbation of the planktonic (**a**) and biofilm (**b**) forms of *P. aeruginosa* PAO1. Planktonic cells (1×10^7 CFU/ml in PBS) were incubated with the peptide at different concentrations for 30 min at 37 °C. The number of CFU is given as percentage with respect to the control (bacteria not treated with the peptide). Membrane perturbation was evaluated by the Sytox Green and β-galactosidase assay. In the first case, bacteria (1×10^7 CFU/ml) were incubated with 1 μM Sytox Green in PBS. Once basal fluorescence reached a constant value, the peptide was added and changes in fluorescence ($\lambda_{exc} = 485$ nm, $\lambda_{ems} = 535$ nm) were monitored. The fluorescent signal obtained after 30 min was plotted as the percentage of membrane perturbation as described in the legend to Fig. 2. All readings were normalized by subtracting fluorescence values of control (bacteria without peptide). In the second case, β-galactosidase activity was measured in the culture filtrate following the hydrolysis of 2 mM ONPG at 420 nm. Enzymatic activity detected in the control (bacteria without peptide) was subtracted from all values, which are expressed as percentage with respect to that found after treating bacteria with the highest peptide concentration and 1 mM EDTA + 0.5 % Triton X-100 (see "Materials and methods" section for more details). Bacterial biofilms grown on pegs were treated with the peptide diluted in PBS at different concentrations for 2 h at 37 °C. The percentage of surviving biofilm cells and membrane perturbation (measured by both the Sytox Green and β-galactosidase assays) were expressed as described for the planktonic cells. All data points represent the means of three independent measurements ± SD

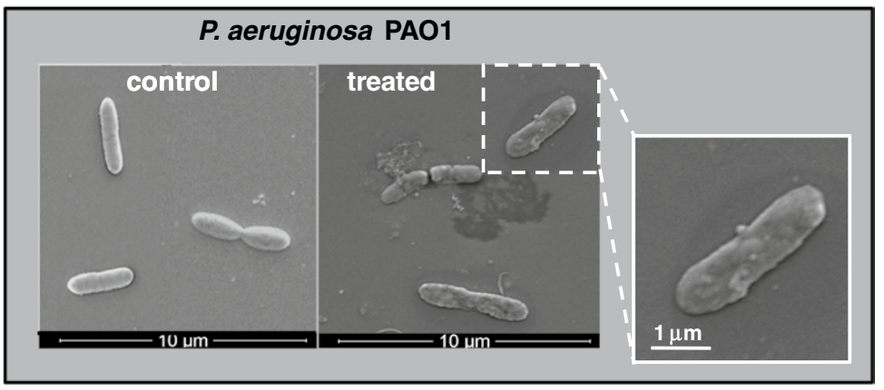

Fig. 4 Scanning electron microscopy of *Pseudomonas* PAO1 cells in their planktonic form after 30 min peptide treatment at 8 μM (causing ~100 % killing, as shown in Fig. 3). Controls are cells not treated with the peptide. See Results section for other experimental details and descriptions of the images. *Inset* is a magnification of a portion indicated by the *white dotted frame*

damage to the membrane was recorded, as demonstrated by the minor leakage of β-galactosidase at those peptide concentrations causing ~100 % microbial killing. Overall, these findings are indicative of membrane perturbation as a plausible mechanism subtending the anti-biofilm activity of Esc(1-21) towards *Pseudomonas*. As evidenced from electron microscopy analysis (Fig. 5), cells embedded in an unordered extracellular matrix were observed after 20 h of biofilm formation (Fig. 5a). Remarkably, clear protrusions from the surface of bacteria were detected at a peptide concentration bringing about 95 % killing of biofilm (24 μM) with an evident disintegration of the extracellular matrix, becoming less packed and thinner (Fig. 5c). In contrast, no appreciable morphological changes were discerned at a sublethal peptide dosage (e.g., 0.75 μM, Fig. 5b). Note that *P. aeruginosa* PAO1 formed a more consistent biofilm with respect to *P. aeruginosa* ATCC 27853 (1×10^7 CFU/peg after 20-h biofilm growth versus 1×10^6 of *P. aeruginosa* ATCC 27853 in agreement with the supplementary Table of ref [42]), thus explaining the lower anti-biofilm potency of Esc(1-21) towards the former strain (see cell viability in Fig. 3b; Table 4).

Besides, when the peptide's effect on the morphology of *P. aeruginosa* ATCC 27853 biofilm cells was visualized, we found that Esc(1-21) led to a dose-dependent shrinking shape of bacterial cells, even if trapped into the extracellular polymeric substances (Fig. 5e–f). Such an outcome was noticed at a peptide concentration causing approximately 50 % biofilm eradication (3 μM, Fig. 5e), and it became more pronounced at 24 μM Esc(1-21), when almost all biofilm cells were killed (Table 4; Fig. 5f).

In vitro cytotoxic activity

The potential toxic effect of the peptide toward mammalian cells was investigated on human erythrocytes, lung epithelial cells, and murine macrophages, at a short (1-h) and long (24 h) incubation time, at its MIC (4 μM). Esc(1-21) was devoid of lethal effect on these cell types even after 24 h of treatment. Interestingly, no appreciable cytotoxic activity was detected when macrophages and lung epithelial cells were incubated for 24 h with a peptide concentration up to eightfold the MIC (data not shown).

In vivo anti-*Pseudomonas* activity

The promising results of the in vitro experiments prompted us to seek insight into the in vivo activity of Esc(1-21) against two different types of *P. aeruginosa* infection by employing mice models of sepsis or lung infection. In the sepsis model, the peptide was injected i.v. (5 mg/kg) at 24 and 72 h post-infection and the animals were monitored for their survival. As illustrated in Fig. 6a, the peptide was able to protect 40 % of animals from death after 12 days from the start of the infection, whereas the control mice (infected but not treated with the peptide) died within the first 72 h. In the lung infection model, the peptide was i.t. administered in a single dose at the concentrations of 5, 2.5, or 1.25 mg/kg. Esc(1-21) allowed 50 and 33 % survival at 5 and 2.5 mg/kg, respectively, after 40 h from the infection, and 31 and 13 % survival at 5 and 2.5 mg/kg, respectively, at 50 h post-infection (Fig. 6b). However, after 60 h, only the dosage of 5 mg/kg gave an appreciable animal survival (25 %). Control animals died within the first 40 h. The good percentage of animal survival after many hours from the infection, along with the dose-dependent response, confirmed the in vivo efficacy of Esc(1-21), also when applied into the lungs.

Discussion

Pseudomonas aeruginosa infections and their persistence to aggressive antibiotic therapy has been the subject of many investigations during the past decades [48–50]. *P. aeruginosa* is an opportunistic Gram-negative bacterium infecting burns, wounds, colonizing medical devices (e.g., catheters

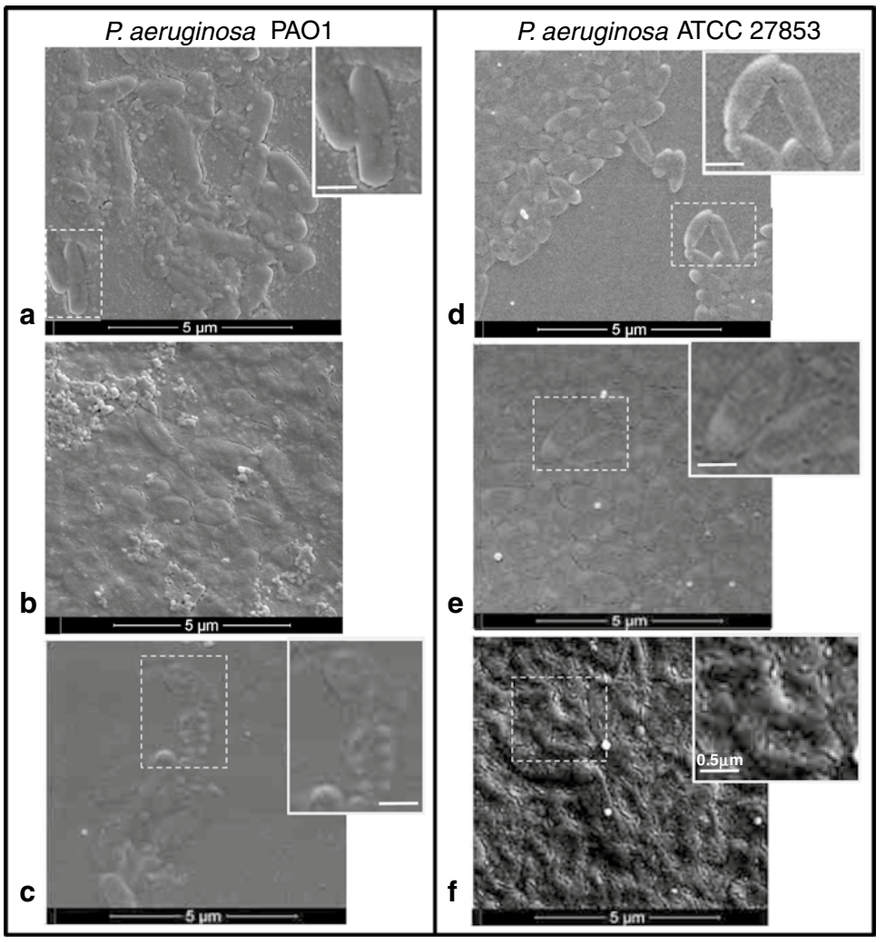

Fig. 5 Scanning electron microscopy of biofilm cells of *Pseudomonas* after 2-h incubation at 37 °C at different concentrations of Esc(1-21): 0.75 µM (**b**); 3 µM (**e**) and 24 µM (**c**, **f**). Controls (**a**, **d**) are given by biofilm cells not treated with the peptide. *Left panels P. aeruginosa* PAO1; *right panels P. aeruginosa* ATCC 27853. See Results section for other experimental details and description of the images. *Insets* are magnifications of a portion indicated by the *white dotted frame*

and implants) and different types of human tissues, such as the pulmonary epithelium, especially in patients with CF, the most common eventually fatal recessive genetic disease in Caucasian populations [51, 52]. Colonization of lungs by *Pseudomonas* usually starts with the tissue adhesion of non-mucoid strains followed by secretion of anionic polysaccharides, mainly alginate, to create a protective layer around the cells [53, 54]. Subsequently, motility is repressed and bacteria frequently evolve a mucoid phenotype forming thicker biofilms, which are more resistant to antibiotic therapy [55]. Importantly, to date, only a few studies on the activity of naturally occurring AMPs on preformed *P. aeruginosa* biofilm have been reported [2, 56]. However, they do not deal with the mechanism(s) underlying the killing of biofilm cells. In addition, some peptides have recently been found to inhibit biofilm formation, but without being active on the planktonic form of this microorganism [57].

Overall, our study provides information regarding five important properties that make frog skin AMPs promising candidates for anti-*Pseudomonas* therapeutics.

Activity on free-living *P. aeruginosa* strains

Esculentin(1-21) displays the same efficacy against reference and CF clinical isolates of *P. aeruginosa* with a rapid bactericidal activity (15 min), regardless of their resistance or mucoid phenotype, as revealed by the similar MIC values (Table 2) and killing kinetics (Fig. 1). This is in contrast with currently available drugs for the treatment of lung infection by this bacterium, such as the aminoglycoside tobramycin, whose effectiveness is highly reduced towards *P. aeruginosa* mucoid strains [58].

Activity on *P. aeruginosa* biofilm and the corresponding assays

Esculentin(1-21) is able to inhibit re-growth of cells from *Pseudomonas*-treated biofilm and to eliminate biofilm cells within 2 h (Table 3). Note that the MBCb, 12 µM, is three-fold higher than the MIC, whereas some medically used antibiotics such as aminoglycosides, fluoroquinolones, and

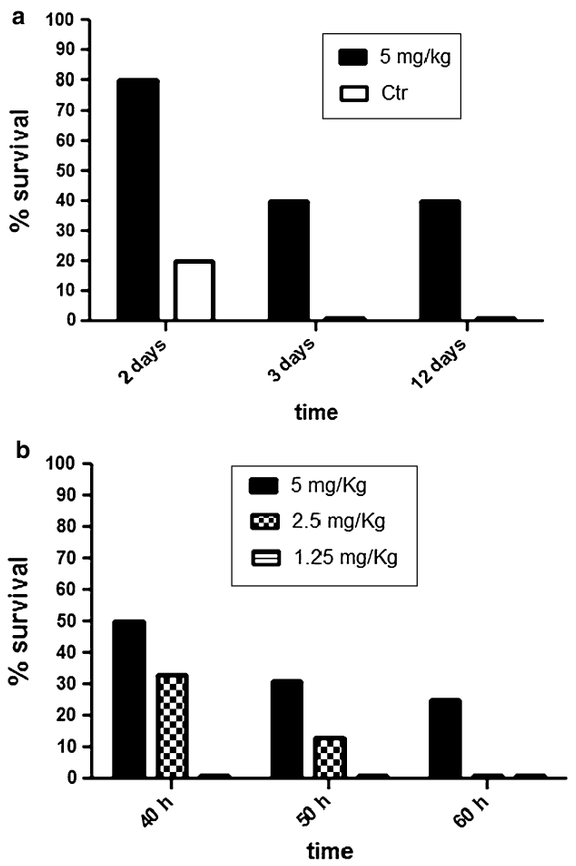

Fig. 6 In vivo antibacterial activity of Esc(1-21). **a** Neutropenic Balb-c mice were injected i.p. with a lethal amount of *P. aeruginosa* PAO1 cells. The percentage of animal survival is indicated at 2, 3, and 12 days post-infection for both controls (Ctr, *white bars*) and animals treated with Esc(1-21) at 5 mg/kg after 24 and 72 h from the infection (*black bars*). **b** Neutropenic Balb-c mice were injected i.t. with a lethal amount of *P. aeruginosa* PAO1 cells. The percentage of animal survival after treatment with Esc(1-21) (a single dose at 5, 2.5, and 1.25 mg/kg) is indicated at *40*, *50*, and *60 h* post-infection. Animals not treated with the peptide (0 % survival at 40 h) are not indicated. The experiments derived by repeated tests in animals where different preparations of bacteria were used. $p < 0.05$

tetracycline require a concentration that is 100-fold higher the MIC, in order to kill sessile bacteria [3, 59]. Moreover, it has been demonstrated that some conventional drugs can even act as intercellular signaling molecules stimulating bacterial biofilm formation at sub-inhibitory concentrations [60, 61].

Regarding biofilm quantitation methods, it is worthwhile noting that although CV staining has been used for several years as a common and cheap assay to explore the antibiofilm activity of antimicrobial compounds [62, 63], it cannot provide any information on the efficacy of such compounds in killing biofilm cells: this is due to the ability of CV to bind both living and dead bacteria, as well as the extracellular polymeric substances of biofilm communities. Indeed, in our hands, from 15 to 32 % biomass was obtained after treating *Pseudomonas* biofilm with peptide concentrations inducing almost its complete killing, suggesting that such a percentage was only related to the presence of lifeless biological material. The reduction of MTT to its insoluble formazan may also give inaccurate results on the quantity of viable biofilm cells. As reported in Table 4, a slightly lower amount of viable cells was found by this method with respect to the results of colony counts. This may be due to an impaired enzymatic activity in peptide-treated cells, despite being still alive. In addition, the minimal number of bacterial cells necessary to get detectable signals in this assay (i.e., absorbance measurement of reduced MTT) is much higher (approximately 3×10^5 cells) compared to that needed for CFU counting on plates that we believe to be a more accurate and appropriate viability method [64].

The peptide is active at high salt concentration and is devoid of cytotoxic effects

Esculentin(1-21) is endowed with antimicrobial activity at high salt concentration against both reference and CF strains. This is a considerable advantage taking into account that elevated salt concentrations in airways mucus of CF patients [51, 52] hinder endogenous bactericidal peptides, i.e., LL-37 and hBD-2 found in mammalian mucosal surfaces, including airways epithelia [65]. Furthermore, according to our previous studies [35], Esc(1-21) was found to be devoid of toxic effect on mammalian cells (e.g., erythrocytes, macrophages, and lung epithelial cells), when tested at its microbicidal concentrations at short (1 h) and long (24 h) incubation time.

The peptide acts via membrane permeation

Esculentin(1-21) perturbs the membrane of planktonic and sessile *Pseudomonas* cells in a dose-dependent fashion. In both cases, this effect is manifested also at concentrations below those decreasing bacterial survival. The degree of membrane injury enhances in parallel with the peptide dosage, presumably enlarging the size of membrane breakages that lead to an increasing loss of bulky intracellular compounds, such as the β-galactosidase (Stokes radius 69 Å [66]). As highlighted by SEM images, the peptide elicits similar changes on the morphology of *Pseudomonas* PAO1 cells either in their motile or non-motile forms. However, a different outcome could be appreciated between biofilms of the two strains: the appearance of surface corrugation with distinct blisters in case of PAO1, and a collapse of the cellular structure with a ghost-like appearance for *P. aeruginosa* ATCC 27853. Importantly, such alterations represent

an obvious sign of serious deformation of the bacterial wall, according to the peptide-induced membrane perturbation, as proved by the results of the Sytox Green and β-galactosidase assays (Figs. 2, 3). On the basis of our data, we may speculate that Esc(1-21) has the same mode of action on the static and dynamic forms of *Pseudomonas*, with a different upshot on the target cell's shape, depending on the peptide concentration or bacterial strain used.

In vivo activity

Esculentin(1-21) has the capability to significantly prolong survival of mice with *P. aeruginosa* sepsis or lung infection. We chose these types of mouse models to mimic some of the most common human infections by this pathogen, such as those provoked by abdominal trauma (e.g., organ perforation) or highly diffused in CF patients. The percentage of animal survival obtained upon i.v. or i.t. administration of Esc(1-21), although not very high, is very promising, considering that Esc(1-21) is a short-sized linear peptide deriving from the N-terminal region of a native AMP to which only the addition of a glycinamide at the C-terminus was introduced. Note that the amidation of the C-terminal residue represents a common post-translational enzymatic modification for the majority of linear AMPs from amphibian skin [67, 68]. Overall, we think that the protective effects of Esc(1-21) in these animal models is mainly due to a direct antibacterial activity of the peptide rather than to the immune system of the mouse. This is because the animals are made neutropenic before infection, producing an impairment of native and adaptive immune response. However, we cannot exclude the possibility that an immunomodulatory activity of Esc(1-21) is involved in promoting the animal's survival, by enhancing the elimination of bacteria from the body.

Conclusions

To our knowledge, this study represents the first demonstration of the potent and rapid activity of an amphibian AMP on both planktonic and biofilm cells of *Pseudomonas* along with the underlying molecular mechanism. In addition, to the best of our knowledge, this is the first report showing the effect(s) of AMPs on the membrane permeability of sessile bacterial communities, as a plausible mechanism for biofilm eradication. This should reduce the development of biofilm resistance. Furthermore, considering: (i) the ability of Esc(1-21) to preserve activity at high salt concentrations and against mucoid strains of *Pseudomonas*; and (ii) the results of its in vivo efficacy in mouse models, this peptide may serve as a promising template for the generation of new drugs to be applied either systemically or topically (e.g., in a nebulized form by inhalation) for the treatment of *P. aeruginosa* infection, mainly in CF sufferers.

Acknowledgments The authors thank Professor Burkhard Tummler (Klinische Forschergruppe, OE 6710, Medizinische Hochschule Hannover, Hannover, Germany) for the *P. aeruginosa* clinical isolates; Prof. Livia Leoni (Roma Tre University, Rome, Italy) for providing *P. aeruginosa* PAO1 strain; Stefano Bindi (Siena University, Italy) for the help in animal experiments and Prof. Donatella Barra (La Sapienza University, Rome) for her critical reading of the manuscript. This work was supported by grants from Sapienza Università di Roma and the Italian Foundation for Cystic Fibrosis (Project FFC#14/2011).

References

1. Manfredi R, Nanetti A, Ferri M, Chiodo F (2000) *Pseudomonas* spp. complications in patients with HIV disease: an eight-year clinical and microbiological survey. Eur J Epidemiol 16:111–118
2. Overhage J, Campisano A, Bains M, Torfs EC, Rehm BH, Hancock RE (2008) Human host defense peptide LL-37 prevents bacterial biofilm formation. Infect Immun 76:4176–4182
3. Hoiby N, Ciofu O, Johansen HK, Song ZJ, Moser C, Jensen PO, Molin S, Givskov M, Tolker-Nielsen T, Bjarnsholt T (2011) The clinical impact of bacterial biofilms. Int J Oral Sci 3:55–65
4. Costerton JW, Stewart PS, Greenberg EP (1999) Bacterial biofilms: a common cause of persistent infections. Science 284:1318–1322
5. Fux CA, Costerton JW, Stewart PS, Stoodley P (2005) Survival strategies of infectious biofilms. Trends Microbiol 13:34–40
6. Stephens C (2002) Microbiology: breaking down biofilms. Curr Biol 12:132–134
7. Kuchma SL, O'Toole GA (2000) Surface-induced and biofilm-induced changes in gene expression. Curr Opin Biotechnol 11:429–433
8. Mah TF, Pitts B, Pellock B, Walker GC, Stewart PS, O'Toole GA (2003) A genetic basis for *Pseudomonas aeruginosa* biofilm antibiotic resistance. Nature 426:306–310
9. Drenkard E, Ausubel FM (2002) *Pseudomonas* biofilm formation and antibiotic resistance are linked to phenotypic variation. Nature 416:740–743
10. Brugha RE, Davies JC (2011) *Pseudomonas aeruginosa* in cystic fibrosis: pathogenesis and new treatments. Br J Hosp Med 72:614–619
11. Bjarnsholt T, Jensen PO, Fiandaca MJ, Pedersen J, Hansen CR, Andersen CB, Pressler T, Givskov M, Hoiby N (2009) *Pseudomonas aeruginosa* biofilms in the respiratory tract of cystic fibrosis patients. Pediatr Pulmonol 44:547–558
12. Tre-Hardy M, Vanderbist F, Traore H, Devleeschouwer MJ (2008) In vitro activity of antibiotic combinations against *Pseudomonas aeruginosa* biofilm and planktonic cultures. Int J Antimicrob Agents 31:329–336
13. Afacan NJ, Yeung AT, Pena OM, Hancock RE (2012) Therapeutic potential of host defense peptides in antibiotic-resistant infections. Curr Pharm Des 18:807–819
14. Fjell CD, Hiss JA, Hancock RE, Schneider G (2011) Designing antimicrobial peptides: form follows function. Nat Rev Drug Discov 11:37–51
15. Mangoni ML (2006) Temporins, anti-infective peptides with expanding properties. Cell Mol Life Sci 63:1060–1069
16. Boman HG (1995) Peptide antibiotics and their role in innate immunity. Annu Rev Immunol 13:61–92
17. Boman HG (2003) Antibacterial peptides: basic facts and emerging concepts. J Intern Med 254:197–215
18. Brown KL, Hancock RE (2006) Cationic host defense (antimicrobial) peptides. Curr Opin Immunol 18:24–30

19. Yeung AT, Gellatly SL, Hancock RE (2011) Multifunctional cationic host defence peptides and their clinical applications. Cell Mol Life Sci 68:2161–2176
20. Gough M, Hancock RE, Kelly NM (1996) Antiendotoxin activity of cationic peptide antimicrobial agents. Infect Immun 64:4922–4927
21. Periti P, Mazzei T (1999) New criteria for selecting the proper antimicrobial chemotherapy for severe sepsis and septic shock. Int J Antimicrob Agents 12:97–105
22. Yang D, Biragyn A, Kwak LW, Oppenheim JJ (2002) Mammalian defensins in immunity: more than just microbicidal. Trends Immunol 23:291–296
23. Bals R, Wilson JM (2003) Cathelicidins–a family of multifunctional antimicrobial peptides. Cell Mol Life Sci 60:711–720
24. Bowdish DM, Davidson DJ, Lau YE, Lee K, Scott MG, Hancock RE (2005) Impact of LL-37 on anti-infective immunity. J Leukoc Biol 77:451–459
25. Hancock RE, Rozek A (2002) Role of membranes in the activities of antimicrobial cationic peptides. FEMS Microbiol Lett 206:143–149
26. Shai Y (1999) Mechanism of the binding, insertion and destabilization of phospholipid bilayer membranes by alpha-helical antimicrobial and cell non-selective membrane-lytic peptides. Biochim Biophys Acta 1462:55–70
27. Shai Y (2002) Mode of action of membrane active antimicrobial peptides. Biopolymers 66:236–248
28. Shai Y (2002) From innate immunity to de novo designed antimicrobial peptides. Curr Pharm Des 8:715–725
29. Powers JP, Hancock RE (2003) The relationship between peptide structure and antibacterial activity. Peptides 24:1681–1691
30. Mangoni ML, Papo N, Mignogna G, Andreu D, Shai Y, Barra D, Simmaco M (2003) Ranacyclins, a new family of short cyclic antimicrobial peptides: biological function, mode of action, and parameters involved in target specificity. Biochemistry 42:14023–14035
31. Simmaco M, Mignogna G, Barra D, Bossa F (1994) Antimicrobial peptides from skin secretions of *Rana esculenta.* Molecular cloning of cDNAs encoding esculentin and brevinins and isolation of new active peptides. J Biol Chem 269:11956–11961
32. Ponti D, Mignogna G, Mangoni ML, De Biase D, Simmaco M, Barra D (1999) Expression and activity of cyclic and linear analogues of esculentin-1, an anti-microbial peptide from amphibian skin. Eur J Biochem 263:921–927
33. Conlon JM (2008) Reflections on a systematic nomenclature for antimicrobial peptides from the skins of frogs of the family Ranidae. Peptides 29:1815–1819
34. Mangoni ML, Fiocco D, Mignogna G, Barra D, Simmaco M (2003) Functional characterisation of the 1–18 fragment of esculentin-1b, an antimicrobial peptide from *Rana esculenta*. Peptides 24:1771–1777
35. Islas-Rodriguez AE, Marcellini L, Orioni B, Barra D, Stella L, Mangoni ML (2009) Esculentin 1-21: a linear antimicrobial peptide from frog skin with inhibitory effect on bovine mastitis-causing bacteria. J Pept Sci 15:607–614
36. Li J, Turnidge J, Milne R, Nation RL, Coulthard K (2001) In vitro pharmacodynamic properties of colistin and colistin methanesulfonate against *Pseudomonas aeruginosa* isolates from patients with cystic fibrosis. Antimicrob Agents Chemother 45:781–785
37. Bragonzi A, Paroni M, Nonis A, Cramer N, Montanari S, Rejman J, Di Serio C, Doring G, Tummler B (2009) *Pseudomonas aeruginosa* microevolution during cystic fibrosis lung infection establishes clones with adapted virulence. Am J Respir Crit Care Med 180:138–145
38. Bragonzi A, Worlitzsch D, Pier GB, Timpert P, Ulrich M, Hentzer M, Andersen JB, Givskov M, Conese M, Doring G (2005) Nonmucoid *Pseudomonas aeruginosa* expresses alginate in the lungs of patients with cystic fibrosis and in a mouse model. J Infect Dis 192:410–419
39. Rampioni G, Schuster M, Greenberg EP, Bertani I, Grasso M, Venturi V, Zennaro E, Leoni L (2007) RsaL provides quorum sensing homeostasis and functions as a global regulator of gene expression in *Pseudomonas aeruginosa*. Mol Microbiol 66:1557–1565
40. Ceri H, Olson M, Morck D, Storey D, Read R, Buret A, Olson B (2001) The MBEC Assay System: multiple equivalent biofilms for antibiotic and biocide susceptibility testing. Methods Enzymol 337:377–385
41. Falciani C, Lozzi L, Pollini S, Luca V, Carnicelli V, Brunetti J, Lelli B, Bindi S, Scali S, Di Giulio A, Rossolini GM, Mangoni ML, Bracci L, Pini A (2012) Isomerization of an antimicrobial peptide broadens antimicrobial spectrum to Gram-positive bacterial pathogens. PLoS ONE 7:e46259
42. Harrison JJ, Stremick CA, Turner RJ, Allan ND, Olson ME, Ceri H (2010) Microtiter susceptibility testing of microbes growing on peg lids: a miniaturized biofilm model for high-throughput screening. Nat Protoc 5:1236–1254
43. Mangoni ML, Saugar JM, Dellisanti M, Barra D, Simmaco M, Rivas L (2005) Temporins, small antimicrobial peptides with leishmanicidal activity. J Biol Chem 280:984–990
44. Uccelletti D, Zanni E, Marcellini L, Palleschi C, Barra D, Mangoni ML (2010) Anti-*Pseudomonas* activity of frog skin antimicrobial peptides in a *Caenorhabditis elegans* infection model: a plausible mode of action in vitro and in vivo. Antimicrob Agents Chemother 54:3853–3860
45. Baillie GS, Douglas LJ (2000) Matrix polymers of Candida biofilms and their possible role in biofilm resistance to antifungal agents. J Antimicrob Chemother 46:397–403
46. Marcellini L, Borro M, Gentile G, Rinaldi AC, Stella L, Aimola P, Barra D, Mangoni ML (2009) Esculentin-1b(1–18)–a membrane-active antimicrobial peptide that synergizes with antibiotics and modifies the expression level of a limited number of proteins in *Escherichia coli*. The FEBS journal 276:5647–5664
47. Pini A, Falciani C, Mantengoli E, Bindi S, Brunetti J, Iozzi S, Rossolini GM, Bracci L (2010) A novel tetrabranched antimicrobial peptide that neutralizes bacterial lipopolysaccharide and prevents septic shock in vivo. FASEB J 24:1015–1022
48. Hancock RE, Speert DP (2000) Antibiotic resistance in *Pseudomonas aeruginosa*: mechanisms and impact on treatment. Drug Resist Updat 3:247–255
49. Stover CK, Pham XQ, Erwin AL, Mizoguchi SD, Warrener P, Hickey MJ, Brinkman FS, Hufnagle WO, Kowalik DJ, Lagrou M, Garber RL, Goltry L, Tolentino E, Westbrock-Wadman S, Yuan Y, Brody LL, Coulter SN, Folger KR, Kas A, Larbig K, Lim R, Smith K, Spencer D, Wong GK, Wu Z, Paulsen IT, Reizer J, Saier MH, Hancock RE, Lory S, Olson MV (2000) Complete genome sequence of *Pseudomonas aeruginosa* PAO1, an opportunistic pathogen. Nature 406:959–964
50. Breidenstein EB, de la Fuente-Nunez C, Hancock RE (2011) *Pseudomonas aeruginosa*: all roads lead to resistance. Trends Microbiol 19:419–426
51. Goldberg JB, Pier GB (2000) The role of the CFTR in susceptibility to *Pseudomonas aeruginosa* infections in cystic fibrosis. Trends Microbiol 8:514–520
52. Doring G, Gulbins E (2009) Cystic fibrosis and innate immunity: how chloride channel mutations provoke lung disease. Cell Microbiol 11:208–216
53. Flemming HC, Wingender J (2010) The biofilm matrix. Nat Rev Microbiol 8:623–633
54. Moreau-Marquis S, Stanton BA, O'Toole GA (2008) *Pseudomonas aeruginosa* biofilm formation in the cystic fibrosis airway. Pulm Pharmacol Ther 21:595–599
55. Boucher JC, Yu H, Mudd MH, Deretic V (1997) Mucoid *Pseudomonas aeruginosa* in cystic fibrosis: characterization of muc

mutations in clinical isolates and analysis of clearance in a mouse model of respiratory infection. Infect Immun 65:3838–3846
56. Pompilio A, Crocetta V, Scocchi M, Pomponio S, Di Vincenzo V, Mardirossian M, Gherardi G, Fiscarelli E, Dicuonzo G, Gennaro R, Di Bonaventura G (2012) Potential novel therapeutic strategies in cystic fibrosis: antimicrobial and anti-biofilm activity of natural and designed alpha-helical peptides against *Staphylococcus aureus*, *Pseudomonas aeruginosa*, and *Stenotrophomonas maltophilia*. BMC Microbiol 12:145
57. de la Fuente-Nunez C, Korolik V, Bains M, Nguyen U, Breidenstein EB, Horsman S, Lewenza S, Burrows L, Hancock RE (2012) Inhibition of bacterial biofilm formation and swarming motility by a small synthetic cationic peptide. Antimicrob Agents Chemother 56:2696–2704
58. Whiteley M, Bangera MG, Bumgarner RE, Parsek MR, Teitzel GM, Lory S, Greenberg EP (2001) Gene expression in *Pseudomonas aeruginosa* biofilms. Nature 413:860–864
59. Olson ME, Ceri H, Morck DW, Buret AG, Read RR (2002) Biofilm bacteria: formation and comparative susceptibility to antibiotics. Can J Vet Res 66:86–92
60. Hoffman LR, D'Argenio DA, MacCoss MJ, Zhang Z, Jones RA, Miller SI (2005) Aminoglycoside antibiotics induce bacterial biofilm formation. Nature 436:1171–1175
61. Linares JF, Gustafsson I, Baquero F, Martinez JL (2006) Antibiotics as intermicrobial signaling agents instead of weapons. Proc Natl Acad Sci 103:19484–19489
62. Stepanovic S, Vukovic D, Dakic I, Savic B, Svabic-Vlahovic M (2000) A modified microtiter-plate test for quantification of staphylococcal biofilm formation. J Microbiol Methods 40:175–179
63. O'Toole GA, Kolter R (1998) Flagellar and twitching motility are necessary for *Pseudomonas aeruginosa* biofilm development. Mol Microbiol 30:295–304
64. Peeters E, Nelis HJ, Coenye T (2008) Comparison of multiple methods for quantification of microbial biofilms grown in microtiter plates. J Microbiol Methods 72:157–165
65. Bals R, Wang X, Zasloff M, Wilson JM (1998) The peptide antibiotic LL-37/hCAP-18 is expressed in epithelia of the human lung where it has broad antimicrobial activity at the airway surface. Proc Natl Acad Sci 95:9541–9546
66. Johansson E, Majka J, Burgers PM (2001) Structure of DNA polymerase delta from *Saccharomyces cerevisiae*. J Biol Chem 276:43824–43828
67. Mangoni ML, Shai Y (2009) Temporins and their synergism against Gram-negative bacteria and in lipopolysaccharide detoxification. Biochim Biophys Acta 1788:1610–1619
68. Mangoni ML, Shai Y (2011) Short native antimicrobial peptides and engineered ultrashort lipopeptides: similarities and differences in cell specificities and modes of action. Cell Mol Life Sci 68:2267–2280

OPEN ACCESS Freely available online

PLOS ONE

Novel α-MSH Peptide Analogues with Broad Spectrum Antimicrobial Activity

Paolo Grieco[1☯], Alfonso Carotenuto[1☯], Luigia Auriemma[1], Antonio Limatola[1], Salvatore Di Maro[1], Francesco Merlino[1], Maria Luisa Mangoni[2], Vincenzo Luca[2], Antonio Di Grazia[2], Stefano Gatti[3], Pietro Campiglia[4], Isabel Gomez-Monterrey[1], Ettore Novellino[1], Anna Catania[3]*

1 Department of Pharmacy, University of Naples Federico II, Naples, Italy, **2** Istituto Pasteur-Fondazione Cenci Bolognetti, Department of Biochemical Science, 'A. Rossi Fanelli', University of Rome 'La Sapienza', Rome, Italy, **3** Center for Preclinical Investigation, Fondazione IRCCS Ca'Granda - Ospedale Maggiore Policlinico, Milano, Italy, **4** Department of Pharmaceutical Science, University of Salerno, Fisciano, Salerno, Italy

Abstract

Previous investigations indicate that α-melanocyte-stimulating hormone (α-MSH) and certain synthetic analogues of it exert antimicrobial effects against bacteria and yeasts. However, these molecules have weak activity in standard microbiology conditions and this hampers a realistic clinical use. The aim in the present study was to identify novel peptides with broad-spectrum antimicrobial activity in growth medium. To this purpose, the Gly10 residue in the [*D*Nal(2′)-7, Phe-12]-MSH(6–13) sequence was replaced with conventional and unconventional amino acids with different degrees of conformational rigidity. Two derivatives in which Gly10 was replaced by the residues Aic and Cha, respectively, had substantial activity against Candida strains, including *C. albicans*, *C. glabrata*, and *C. krusei* and against gram-positive and gram-negative bacteria. Conformational analysis indicated that the helical structure along residues 8–13 is a key factor in antimicrobial activity. Synthetic analogues of α-MSH can be valuable agents to treat infections in humans. The structural preferences associated with antimicrobial activity identified in this research can help further development of synthetic melanocortins with enhanced biological activity.

Citation: Grieco P, Carotenuto A, Auriemma L, Limatola A, Di Maro S, et al. (2013) Novel α-MSH Peptide Analogues with Broad Spectrum Antimicrobial Activity. PLoS ONE 8(4): e61614. doi:10.1371/journal.pone.0061614

Editor: Gunnar F. Kaufmann, The Scripps Research Institute and Sorrento Therapeutics, Inc., United States of America

Received November 20, 2012; **Accepted** March 12, 2013; **Published** April 23, 2013

Funding: This work was supported by Italian Ministry of Education, University and Research (PRIN 2008, 2010MCLBCZ_002) and by Fondazione Fiera Milano, Italy. The funders had no role in study design, data collection and analysis, decision to publish, or preparation of the manuscript.

Competing Interests: The authors have declared that no competing interests exist.

* E-mail: anna.catania@guest.unimi.it

☯ These authors contributed equally to this work.

Introduction

α-Melanocyte stimulating hormone (α-MSH), a pro-opiomelanocortin (POMC) derivative, is an ancient tridecapeptide that exerts pleiotropic influences on the host physiology [1]. A major contribution of α-MSH to tissue protection resides in its capacity to prevent cell injury induced by harmful stimuli including endotoxin, reperfusion injury, blood loss, and oxidative stress [1,2]. Of interest, α-MSH involvement in host defense includes antimicrobial activity [3,4]. Indeed, the peptide and its C-terminal sequence Lys-Pro-Val were found to inhibit growth of both the yeast *Candida albicans* and the gram-positive bacterium *Staphylococcus aureus* [4]; further, the N-terminal sequence His-Phe-Arg-Trp showed antimicrobial activity against *Cryptococcus neoformans* [5].

Although the natural α-MSH peptide has a very short half-life that makes it unsuitable for clinical use, synthetic analogues of it could form the basis for novel antimicrobial agents. However, key issues need to be solved before a therapeutic use is realistic. A crucial question concerns potency of the antimicrobial activity. Indeed, α-MSH and the synthetic derivatives described to date were found to exert their activity against infectious agents that were suspended in physiologic solution or in water but not in culture media that allow microorganisms to grow [4,6,7,8,9,10]. Therefore, although data indicate a potential for melanocortin derivatives to combat infections, none of the known molecules is active against microorganisms in growth medium. Because this is a major obstacle to a realistic clinical use, the aim in this research was to design novel melanocortin analogues that could overwhelm this weakness. The lead sequence selected was [*D*Nal(2′)-7, Phe-12]–MSH(6–13) (*D.Nal*), a promising antimicrobial compound that contains the invariant '*core*' sequence His-Phe-Arg-Trp (6–9) common to all melanocortins [7]. Indeed, although *D.Nal* did not kill Candida in growth medium, it did kill 100% organisms incubated in distilled water [7]. Conformational analysis of *D.Nal* indicated the presence of two β-turns along residues 7–10 and 10–13 (type I, and distorted type III, respectively) [11]; these two turns, which likely form the pharmacophoric moieties, are linked by a highly flexible glycine residue that can orient them differently [11]. Therefore, in the present research we produced novel antimicrobial peptides based on replacement of Gly10 in the *D.Nal* sequence with natural and unnatural amino acids with different degrees of conformational rigidity (Table 1). Activity against various pathogenic agents including gram-positive and gram-negative bacteria and yeasts was assessed using standard culture tests. We report results of a conformational study on the most effective peptides.

Table 1. Lead sequence *DNal* and Gly10 substituted peptides.

Peptide	Sequence
DNal	H-His-*D*(2′)Nal-Arg-Trp-**Gly**-Lys-Phe-Val-NH_2
1	H-His-*D*(2′)Nal-Arg-Trp-**Aib**-Lys-Phe-Val-NH_2
2	H-His-*D*(2′)Nal-Arg-Trp-**Deg**-Lys-Phe-Val-NH_2
3	H-His-*D*(2′)Nal-Arg-Trp-**tBuGly**-Lys-Phe-Val-NH_2
4	H-His-*D*(2′)Nal-Arg-Trp-**Ac3c**-Lys-Phe-Val-NH_2
5	H-His-*D*(2′)Nal-Arg-Trp-**Ac4c** -Lys-Phe-Val-NH_2
6	H-His-*D*(2′)Nal-Arg-Trp-**Ac5c**-Lys-Phe-Val-NH_2
7	H-His-*D*(2′)Nal-Arg-Trp-**Ac6c** -Lys-Phe-Val-NH_2
8	H-His-*D*(2′)Nal-Arg-Trp-**Aic**-Lys-Phe-Val-NH_2
9	H-His-*D*(2′)Nal-Arg-Trp-**Phe**-Lys-Phe-Val-NH_2
10	H-His-*D*(2′)Nal-Arg-Trp-**Cha**-Lys-Phe-Val-NH_2
11	H-His-*D*(2′)Nal-Arg-Trp-**βAla**-Lys-Phe-Val-NH_2
12	H-His-*D*(2′)Nal-Arg-Trp-**Acpc**-Lys-Phe-Val-NH_2
13	H-His-*D*(2′)Nal-Arg-Trp-**Gly-Gly**-Lys-Phe-Val-NH_2

doi:10.1371/journal.pone.0061614.t001

Materials and Methods

Materials

*N*9-fluorenylmethoxycarbonyl (Fmoc)-protected natural amino acids were purchased from GLS Biochem (Shangai-China), *N*Fmoc-protected special amino acids from NeoMPS (Stasbourg-France) and Chem-Impex International, Inc. (Wood Dale-Illinois), 2-(1*H*-benzotriazole-1-yl)-1,1,3,3-tetramethyluroniumhexafluorophosphate (HBTU) and *N*-hydroxybenzotriazole (HOBt) from Iris Biotech GmbH (Marktredwitz-Germany) and Rink amide resin from Advanced Chemtech (Lousville-KY). For the *N*–Fmoc-protected amino acids, the following side chain protecting groups were used: Arg(N^Y-2,2,4,6,7-pentamethyl-dihydrobenzofuran-5-sulfonyl (Pbf)), His(N^{im}- triphenylmethyl(trityl) (Trt)), Trp(N^{in}- *tert*-butyloxycarbonyl (Boc)), Lys(Boc). Peptide synthesis solvents, reagents, as well as CH_3CN for HPLC were reagent grade and were acquired from commercial sources and used without further purification unless otherwise noted. ESI-MS analyses were performed by API 2000. The purity of the finished peptides was checked by analytical reversed-phase high performance liquid chromatography (RP-HPLC) using a Shimadzu mod. CL-10ADVP system with a built-in diode array detector. In all cases, the purity of the finished peptides was greater than 95% as determined by these methods.

General Method for Peptide Synthesis and Purification

All peptides were synthesized using the solid-phase method of peptide synthesis and purified by RP-HPLC. Each peptide was synthesized on 0.250 g of Rink amide resin (substitution 0.75 mmol/g) by manual method using *N*-Fmoc chemistry and an orthogonal side chain protection strategy. The resin was first swollen in dichloromethane (DCM)/(*N*,*N*-dimethylformamide) DMF (1:1) for 2 h and the following amino acids were then added to the growing peptide chain by stepwise addition of *N*-Fmoc-Val-OH, *N*-Fmoc-Phe-OH, *N*-Fmoc-Lys(Boc)-OH, *N*-Fmoc-(L)-AA-OH (AA: Gly-Gly dipeptide, β-alanine, β-cyclohexylalanine, 1-amino-cyclopentane carboxylic acid, 1-amino-cyclopropane carboxylic acid, α-t-butylglycine, 2-aminoindane-2-carboxylic acid, 1-amino-cyclobutane carboxylic acid, (1R,2R)-2-aminocyclopentane-1-carboxylic acid, diethylglycine, 1-amino-cyclohexanecarboxylic acid, phenylalanine; Figure S1), *N*-Fmoc-Trp(Boc)-OH, *N*-Fmoc-Arg(N^Y-Pbf)-OH, *N*-Fmoc-(D)-2-Nal-OH, and *N*-Fmoc-His(N^{im}-Trt)-OH, using standard solid phase methods. Each coupling reaction was achieved using a 3-fold excess of each amino acid, HBTU, and HOBt in presence of a 6-fold excess of (*N*,*N*-diisopropylethylamine) DIPEA for 1 h. Deprotection of the *N*-Fmoc group was carried out by treating the protected peptide resin with 25% piperidine solution in DMF (1×4 mL, 20 min). After each coupling and deprotection, the peptide resin was washed with DMF (3×4 mL), DCM (3×50 mL) and again with DMF. The peptide sequences were thereafter assembled by alternate cycles of coupling and deprotection. After coupling of the *N*-terminal amino acid, the *N*-terminal Fmoc group was deblocked as described above and the peptide-resin was thoroughly washed with DCM (4×25 mL) and dried under argon to yield dried peptide-resin.

The peptide-resin was then cleaved by treatment with 5 mL of a solution of triethylsilane (Et_3SiH) (5%), water (5%), in trifluoroacetic (TFA) with shaking at room temperature for 3 h. The resin was then removed from the solution by filtration and the crude peptide was recovered by precipitation with cold anhydrous ethyl ether. Centrifugation at 1500 *g* for 3 min followed by decantation of the supernatant ether and air-drying of the residue yielded the crude peptide as a white to pale beige-colored amorphous solid.

Final peptide purification was achieved using a preparative RP-HPLC Phenomenex Jupiter Proteo, 10 m 90 Å. The peptide samples were injected onto the column at a concentration of 20 mg/mL in 20% aqueous CH_3CN and were eluted with a CH_3CN gradient (10 to 90%) over 40 min at a flow rate of 15.0 mL/min, with a constant concentration of TFA (0.1% v/v). The separations were monitored at 230 and 254 nm and integrated with a Shimadzu diode array detector mod. SPD-M10AVP dual wavelength absorbance detector model UV-D. Fractions corresponding to the major peak were collected, pooled, and lyophilized to yield the final peptides as pure (>95%) white solids. The final yields of the peptides ranged between 42 and 57%. The analytical data and the amino acid analysis for each compound are reported in Tables S1, S2 and Figure S2.

Candida spp

Two *Candida albicans* isolates were purchased from the ATCC (No. 24433 and 76615). The other yeast isolates were obtained from the collection of Fondazione Ca' Granda- Ospedale Maggiore Policlinico, Milano. The collection included *C. albicans* (7 isolates), *C. glabrata* (3 isolates), and *C. krusei* (3 isolates).

Bacteria

The strains used for the antimicrobial assays were the Gram-negative bacteria *Acinetobacter baumani* ATCC 19606, *Escherichia coli* D21, *Pseudomonas aeruginosa* ATCC 27853, and *Pseudomonas syringae* pv tabaci 1918NCPPB and the Gram-positive bacteria *Bacillus megaterium* Bm11, *Staphylococcus aureus* ATCC 25923, and *Staphylococcus epidermidis* ATCC 12228.

Anti-Candida assay

Antifungal susceptibility testing was performed using the broth microdilution method according to the NCCLS M27-A guidelines (National Committee for Clinical Laboratory Standards. 1997, Reference method for broth dilution antifungal susceptibility testing of yeasts and approved standard NCCLS document M27-A. National Committee for Clinical Laboratory Standards, Wayne, Pa.). The organisms were removed from frozen glycerol stock (10% sterile glycerol suspensions stored at −70°C),

subcultured onto Sabouraud's dextrose plates, and incubated at 35°C. After 48 h of incubation, the plates were inspected for purity. A colony was taken from the agar plate and transferred into 5 mL Sabouraud-dextrose broth and incubated for 48 h at 35°C. Cells were centrifuged at 1,000× g for 10 min and the pellet was washed twice with distilled water. Cells were counted and suspended in RPMI 1640 medium buffered to pH 7.0 with 0.165 mol l^{-1} morpholinepropanesulphonic acid (MOPS) buffer (Sigma) to obtain the two times test inoculum (1×10^3 to 5×10^3 CFU/mL). Each well of 96 U-shaped well-plates received 100 µl of each antifungal peptide in concentrations from 10^{-4} to 7.8×10^{-7} M.

The plates were incubated at 35 C and were observed for growth at 48 h. The MIC90, i.e. the minimum inhibitory concentrations endpoint were determined as 90% reduction in turbidity measured using a spectrophotometer (Titertek multiscan at 690 nm wave length).

Antibacterial assay

Susceptibility testing was performed by adapting the microbroth dilution method outlined by the Clinical and Laboratory Standards Institute, using sterile 96-well plates (Falcon NJ, USA). The bacterial growth was aseptically measured by absorbance at 590 nm with a spectrophotometer (UV-1700 Pharma Spec Shimadzu, Tokyo, Japan). Afterwards, aliquots (50 µl) of bacteria in mid-log phase at a concentration of 2×10^6 colony-forming units (CFU)/mL in culture medium (Mueller-Hinton, MH) were added to 50 µl of MH broth containing the peptide in serial 2-fold dilutions ranging from 1.56 to 100 µM. Inhibition of microbial growth was determined by measuring the absorbance at 590 nm, after an incubation of 18 h at 37°C with a microplate reader (Infinite M200; Tecan, Salzburg, Austria). Antibacterial activity was expressed as the minimal inhibitory concentration (MIC), the concentration of peptide at which 100% inhibition of microbial growth is observed after 18 h of incubation.

Hemolytic assay

The hemolytic activity was measured on human red blood cells as reported previously [12]. Briefly, aliquots of a human erythrocyte suspension in 0.9% (w/v) NaCl were incubated with serial two-fold dilutions of peptide (dissolved in 20% ethanol prior to use) for 40 min at 37°C with gentle mixing. The samples were then centrifuged for 5 min at 900 g and the absorbance of the supernatant was measured at 415 nm. Complete lysis was measured by suspending erythrocytes in distilled water [13].

Cytotoxic activity

Effects on viability was tested in the immortalised keratinocyte cell line HaCaT using the [3(4,5-dimethylthiazol-2yl)2,5-diphenyltetrazolium bromide] (MTT) colorimetric method in which the intensity of the dye is proportional to the number of viable cells. MTT is a tetrazolium salt which is reduced to a colored formazan product by mitochondrial reductases present only in metabolically active cells. Cells were cultured in Dulbecco's modified Eagle's medium (DMEM; Sigma) supplemented with 10% heat inactivated fetal bovine serum, glutamine (4 mM) and gentamicin. Afterwards, cells were plated in triplicate wells of a microtiter plate, at 4×10^4 cells/well in DMEM supplemented with 2% serum without antibiotic. After overnight incubation at 37°C in a 5% CO_2 atmosphere, the medium was replaced with 100 l fresh DMEM supplemented with the peptides at different concentrations. The plate was incubated for 24 h at 37°C in a 5% CO_2 atmosphere. Then, DMEM was removed and replaced with Hank's medium (136 mM NaCl; 4.2 mM Na_2HPO_4; 4.4 mM KH_2PO_4; 5.4 mM KCl; 4.1 mM $NaHCO_3$, pH 7.2, supplemented with 20 mM D-glucose) containing 0.5 mg/ml MTT. After 4 h incubation, the formazan crystals were dissolved by adding 100 l of acidified isopropanol and absorption of each well was measured using a microplate reader (Infinite M200; Tecan, Salzburg, Austria) at 570 nm. Cell viability was e expressed as percentage of viability in control cells (cells not treated with peptide).

Nuclear Magnetic Resonance (NMR) spectroscopy

The samples for NMR spectroscopy were prepared by dissolving the appropriate amount of peptide in 0.55 mL of ^1H_2O, 0.05 mL of ^2H_2O and 160/40 mM dodecylphosphocholine (DPC) -d_{38}/sodium dodecylsulphate (SDS)-d_{25} micelles solution to obtain a concentration of 1–2 mM peptide. The NMR experiments were performed at pH 5.0. NH exchange studies were made by dissolving peptide in 0.60 mL of ^2H_2O and 200 mM 160/40 mM DPC-d_{38}/SDS-d_{25}. NMR spectra were recorded on a Varian Unity INOVA 700 MHz spectrometer equipped with a z-gradient 5 mm triple-resonance probe head. All the spectra were recorded at a temperature of 25°C. The spectra were calibrated relative to 3-(trimethylsilanyl)propionic acid (0.00 ppm) as internal standard. One-dimensional (1D) NMR spectra were recorded in the Fourier mode with quadrature detection. 2D double quantum filtered correlated spectroscopy (DQF-COSY) [14], total correlation spectroscopy (TOCSY) [15], and nuclear Overhauser enhancement spectroscopy (NOESY) [16] spectra were recorded in the phase-sensitive mode using the method from States [17]. Data block sizes were 2048 addresses in t_2 and 512 equidistant t_1 values. A mixing time of 70 ms was used for the TOCSY experiments. NOESY experiments were run with mixing times in the range of 150–300 ms. The water signal was suppressed by gradient echo [18]. The 2D NMR spectra were processed using the NMRPipe package [19]. Before Fourier transformation, the time domain data matrices were multiplied by shifted sin^2 functions in both dimensions, and the free induction decay size was doubled in F1 and F2 by zero filling. The qualitative and quantitative analysis of DQF-COSY, TOCSY and NOESY spectra were obtained using the interactive program package XEASY [20]. $\mathcal{J}_{HN\text{-}H\alpha}$ couplings were difficult to measure probably because of a combination of small coupling constants and broad lines. The temperature coefficients of the amide proton chemical shifts were calculated from 1D ^1H NMR and 2D TOCSY experiments performed at different temperatures in the range 298–320 K by means of linear regression.

Structural determinations

The NOE-based distance restraints were obtained from NOESY spectra collected with a mixing time of 200 ms. Peak volumes were translated into upper distance bounds with the CALIBA routine from the DYANA software package [21]. The requisite pseudoatom corrections were applied for non-stereospecifically assigned protons at prochiral centers and for the methyl group. After discarding redundant and duplicated constraints, the final list of constraints was used to generate an ensemble of 200 structures by the standard DYANA protocol of simulated annealing in torsion angle space. No dihedral angle restraints and no hydrogen bond restraints were applied. An error tolerant target function (tf type 3) was used to account for the peptide intrinsic flexibility. Then, 20/200 structures were chosen, whose interproton distances best fitted NOE derived distances, and refined through successive steps of restrained and unrestrained energy minimization calculations using the Discover algorithm (Accelrys, San Diego, CA) and the consistent valence force field [22]. No residue was found in the disallowed region of the Ramachandran plot. The final structures were analyzed using the

InsightII program (Accelrys, San Diego, CA). Graphical representations were carried out with the InsightII program. The root-mean-squared-deviation analysis between energy-minimized structures was carried out with the program Molmol [23].

Results and Discussion

In preliminary tests, the antimicrobial activity of the lead compound *DNal* was tested using the present standard culture conditions. As expected, the peptide did not have substantial antimicrobial activity in broth culture medium (Tables 2 and 3). However, despite these negative results, *DNal* was a valuable basis for development of novel analogues.

The Gly10 residue was replaced with several conventional and unconventional amino acids characterized by different degrees of conformational rigidity (Table 1 and Figure S1). Such changes were expected to significantly influence the folding preference of the peptide and, consequently, the antimicrobial activity. The Gly10-substituted peptides were tested against several pathogenic strains of *C. albicans*, *C. glabrata*, and *C. krusei* (Table 2) and against a panel of gram-positive and gram-negative bacteria (Table 3).

The peptides **1** and **2** are Cα,α-disubstituted. Cα-alkylation, and in particular Cα-methylation, by means, for example, of 2-aminoisobutyric acid (Aib), has been widely used to explore the conformational requirements for bioactivity [24]. A further rationale for introduction of Cα,α- disubstituted glycine residues was that the isovaline (α-methyl-α-ethylglycine) residue is present in antifungal peptides such as alamethicin, zervamicin, and antiamboebin [25]. Among Cα,α-disubstituted glycine, Aib-^{L}Xxx segments are the preferred option to populate local type-I/III conformations [24]. In addition, the conformational behavior of the cycloaliphatic sub-family of the Cα.α-symmetrically disubstituted Gly residues, generally denoted as Ac_nc, is closely correlated to that of Aib [26]. Conversely, diethylglycine (Deg) containing peptides have a greater tendency to form extended backbone conformations in strongly interacting solvents such as water [26]. Similarly, the *tert*-butyl glycine (tButGly) also called *tert*-leucine residue, inserted in peptide **3**, prefers extended (β sheet-like) or semiextended [$(Pro)_n$-like] conformations [27]. Peptides **1** and **2** containing an Aib and a Deg residue in position 10, respectively, did not show antimicrobial activity. The L-α-t-butylglycine (tButGly) substituted peptide **3** was likewise inactive.

Subsequently, we designed derivatives containing the cyclic achiral dialkylglycine residues 1-amino-cyclopropane carboxylic acid (Ac3c), 1-amino-cyclobutane carboxylic acid (Ac4c), 1-amino-

Table 3. Antibacterial activity of selected peptides expressed as MIC 100 (μM) at 18 h.

Peptide						
Bacterial strain	***DNal***	**3**	**4**	**8**	**9**	**10**
Gram-negative bacteria						
Acinetobacter b. ATCC 19606	>100	100	50	12.5	25	12.5
Escherichia coli D21	>100	50	100	12.5	50	6.25
Pseudomonas a. ATCC 27853	100	50	50	50	25	25
Pseudomonas syringae pv tobaci	>100	>100	>100	25	100	25
Gram-positive bacteria						
Bacillus megaterium Bm 11	6	6.25	6.25	1.56	3.125	3.125
Staphylococcus a. ATCC 25923	>100	>100	100	12.5	50	12.5
Staphylococcus e. ATCC 12228	50	50	25	6.25	12.5	6.25

Each MIC value is the average of at least three independent experiments.
doi:10.1371/journal.pone.0061614.t003

Table 2. Anti-Candida activity of *DNal* and Gly10 substituted peptides expressed as MIC 90 (μM) at 48 h.

	Peptide													
Candida strain	***DNal***	**1**	**2**	**3**	**4**	**5**	**6**	**7**	**8**	**9**	**10**	**11**	**12**	**13**
C.albicans														
ATCC 76615	>100	>100	>100	>100	>100	>100	>100	51	25	>100	52	>100	>100	>100
ATCC 24433	>100	>100	>100	>100	>100	>100	51	51	25	>100	26	>100	>100	>100
995439	>100	>100	>100	>100	>100	99	51	51	25	>100	26	>100	>100	>100
995147	>100	>100	>100	>100	>100	>100	>100	51	25	>100	26	>100	>100	>100
000954	>100	>100	>100	>100	>100	>100	>100	51	25	>100	52	>100	>100	>100
991185	>100	>100	>100	>100	>100	99	51	51	25	51	52	>100	>100	>100
994199	>100	>100	>100	>100	>100	99	51	51	25	51	26	>100	>100	>100
983201- R1	>100	>100	>100	>100	>100	>100	>100	51	50	>100	52	>100	>100	>100
011587	>100	97	>100	>100	>100	99	>100	51	50	>100	26	>100	>100	>100
C.glabrata														
18012	>100	>100	>100	>100	>100	>100	>100	>100	100	>100	>100	>100	>100	>100
995667	>100	>100	>100	>100	>100	>100	>100	>100	100	>100	>100	>100	>100	>100
995651	>100	>100	>100	>100	>100	>100	>100	>100	100	>100	>100	>100	>100	>100
C.krusei														
995668	>100	97	>100	>100	>100	99	>100	>100	50	>100	52	>100	>100	>100
991388	>100	97	>100	>100	>100	99	>100	>100	50	>100	26	>100	>100	>100
004490	>100	97	>100	>100	>100	99	>100	51	25	>100	26	>100	>100	>100

Each MIC value is the average of at least three independent experiments.
doi:10.1371/journal.pone.0061614.t002

Table 4. Hemolytic activity[a] (%) of selected peptides.

Peptide conc. (μM)	1.5	3	6.25	12.5	25	50	100
DNal	0±0.2	0±0.9	1±0.6	1±0.5	2±1.06	5±1.5	7±2.1
3	5±1.9	5.6±3	6±1.6	7±0.4	15±3.1	16±1	23±0.1
4	0±0	2±0.5	4±0.4	10±1	20±2.1	22±0.5	30±0.2
8	0.5±1	2±1.7	2±1.1	3±1.7	9±1.9	13±1.8	24±0.4
9	4±0.1	6±0.4	9±1.9	14±1.4	24±0.1	33±1.3	49±4.1
10	1±0.7	2±1.3	5±0.1	5±0.4	10±1.5	10±0.2	34±1

Values are the mean of three independent experiments ± SD.
doi:10.1371/journal.pone.0061614.t004

cyclopentane carboxylic acid (Ac5c), and 1-amino-cyclohexane carboxylic acid (Ac6c) (Figure S1) in the same position 10. Compound **4**, in which Gly10 was replaced by Ac3c containing a cyclopropane moiety, was inactive. Conversely, the peptides **5**, **6**, and **7**, in which the size of cycloalkyl moiety of the residues Ac4c, Ac5c, and Ac6c progressively increases, showed a parallel increase in their antimicrobial activity. Indeed, whereas compound **5** showed only weak activity, compounds **6** and **7**, containing the Ac5c and Ac6c residues, respectively, possessed substantial activity.

Based on these results, we designed the compound **8** containing the 2-aminoindane-2-carboxylic acid (Aic) residue that, from a structural point of view, can be considered an aromatic analogue of the Ac5c. Considering the conformational preferences, Aic torsional angles are limited to values around $\varphi = -50^\circ$, $\psi = -50^\circ$, and $\varphi = +50^\circ$, $\psi = +50^\circ$ [28]. Compound **8** showed a quite good anti-Candida activity. In addition to the anti-Candida activity, compound **8** effectively inhibited the bacterial strains examined. Therefore, this compound represents a promising agent, marked by both antifungal and antibacterial activity. Because compound **8** can also be considered as a phenylalanine with a constrained side chain, we synthesized an analogue bearing a Phe residue in position 10. However, the resulting compound, peptide **9**, had decreased activity in all biological assays. Therefore, it appears that the conformational constraints imposed by the Aic residue are essential for activity.

Activity was preserved when a L-cyclohexylalanine (Cha) residue was inserted in position 10 (peptide **10**). Cha can be considered an aliphatic analogue of phenylalanine with high tendency to helical formation [29]. This compound exerted both anti-Candida and antibacterial activity with a potency similar to that of peptide **8**.

A comprehensive toxicological investigation was not an aim in this paper. Indeed, the objective was definition of structure/activity relationship that could help design of melanocortin-based novel antimicrobials. However, as a preliminary assessment of potential toxicity, peptides *DNal*, **3, 4, 8, 9**, and **10** were tested for their hemolytic activity (Table 4). No significant hemolysis was noted for the peptides *DNal*, **3**, **8**, and **10** up to a concentration of 12.5 μM. A weak activity (<10% hemolysis) was associated with the parent peptide *DNal* up to 100 μM whereascompounds **3**, **8**, and **10** caused moderate lysis of human red blood cells (from 10% to 24–34%) at concentrations from 25 to 100 μM, with a slightly greater effect for compound **10**. Peptides **4** and **9** exerted the greatest hemolytic effect, causing from ~20% to 30 or 49% cell lysis at concentrations ranging from 25 μM to 100 μM. The potential cytotoxic activity of these compounds was also investigated in nucleated mammalian cells, such as human keratinocytes. As reported in Figure 1, peptide **10** was completely devoid of toxic activity up to a concentration of 12.5 μM, but it exerted toxic effects at 50–100 μM concentrations. Conversely, a moderate toxic effect (less than 20% mortality), was found for the other compounds up to 25 M. At the highest peptide concentration used (100 μM) peptides **3**, **4** and **9** produced less than 30% cell death, whereas a more pronounced toxicity was found for the peptides *DNal* and **8**, that caused approximately 50–100% killing.

In further investigations on structure-activity relationships, Gly10 was replaced with -amino acids. The α-amino acids exist as part of certain natural occurring peptides isolated from prokaryotes and marine organisms. Because of their extra methylene group, β-amino acids are not recognized by mammal proteases and are intrinsically resistant to enzymatic degradation [30]. Further, they show precise conformational preferences. In particular, the conformationally flexible noncoding β-alanine (β-Ala) residue shows two energetically preferred conformations: a folded conformation (μ~±65±10°) and an extended conformation (μ~±165±10°) that are easily accommodated in both acyclic and cyclic peptides where they determine the overall molecular structures [31]. The cyclic (1R,2R)-2-aminocyclopentane carbox-

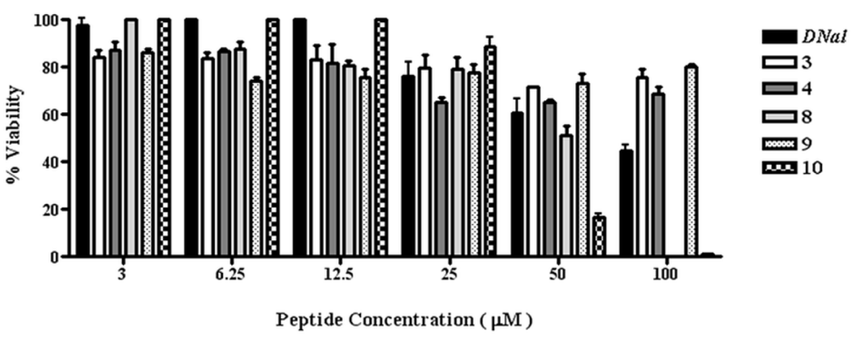

Figure 1. Effects of the synthetic melanocortins on viability of HaCat cells. Cells were plated in wells of a microtiter plate, at 4×10^4 cells/well in DMEM supplemented with 2% serum without antibiotic. After overnight incubation at 37°C in a 5% CO_2 atmosphere, the medium was replaced with 100 μl fresh DMEM supplemented with the peptides at different concentrations. After 24 h of peptide treatment, cell viability was determined by the inhibition of MTT reduction to insoluble formazan (see Materials and Methods for additional information). Cell viability is expressed as percentage of viability in control cells (cells not treated with the peptide).
doi:10.1371/journal.pone.0061614.g001

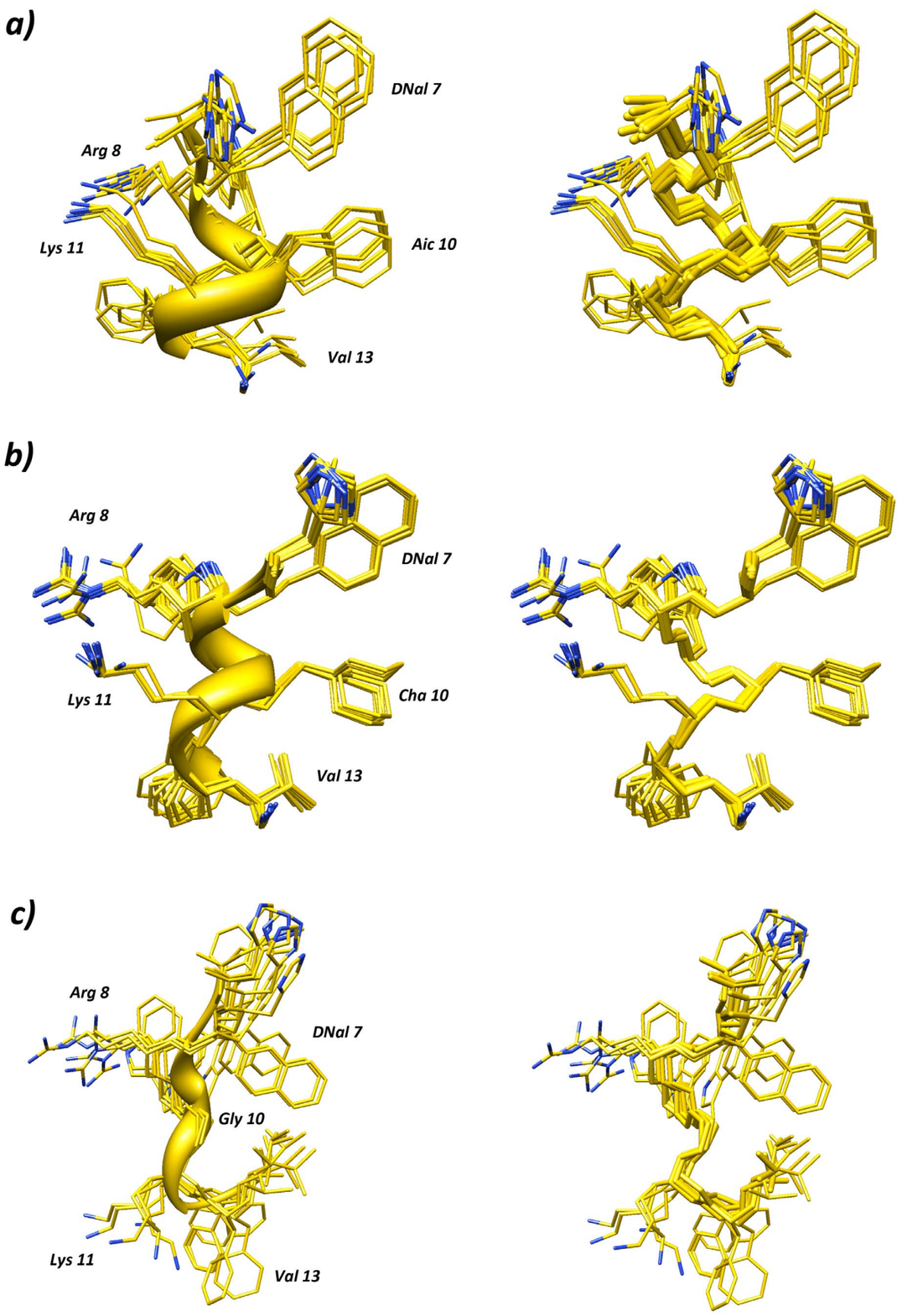
a)
DNal 7
Arg 8
Lys 11
Aic 10
Val 13
b)
Arg 8
DNal 7
Lys 11
Cha 10
Val 13
c)
Arg 8
DNal 7
Gly 10
Lys 11
Val 13

Figure 2. Stereoview of the superimposition of the 10 lowest energy conformers of peptide 8 (a), 10 (b), and *DNal* (c) in SDS/DPC 8:2 solution. Structures were superimposed using the backbone heavy atoms. Heavy atoms are shown in yellow (except for nitrogen, in blue). To improve clarity, hydrogen atoms are not shown. Backbone atoms of the lowest energy conformer are denoted as a ribbon.
doi:10.1371/journal.pone.0061614.g002

ylic acid (Acpc) is a more constrained -amino acid that determines a so called "12-helix" (a 12-membered ring hydrogen bonds) when inserted into a peptide sequence [32]. Compounds **11** and **12**, containing β-Ala and Acpc in position 10, respectively, were synthesized and examined; both showed no anti-Candida activity.

Finally, we synthesized an analogue of *DNal* in which an additional Gly residue was inserted between the Trp9 and the Lys11 residues (peptide **13**). The aim was to evaluate the effect of increased peptide flexibility on antimicrobial activity; compound **13** showed no activity.

Subsequently, we performed a conformational study using solution NMR on compounds **8** and **10**; the parent peptide *DNal* was investigated for comparison. NMR spectroscopy studies were performed in DPC/SDS 8:2 micelles solution. These micelles were used as rough mimetics of yeast membranes [33]. Complete ^{1}H NMR chemical shift assignments were effectively achieved for the peptides according to the Wüthrich procedure [34]. (Tables S3, S4, S5). For both compounds **8** and **10**, upfield shift of the Hα NMR signals, low values of the temperature coefficients of the amide protons, and diagnostic NOEs (Tables S6 and S7) indicated that residues 8–13 are in a helical conformation. Few medium range NOEs between the hydrophobic side chains of residues 7 and 10 were observed in the NOESY spectrum of **10** but not in that of **8** (Tables S6 and S7), suggesting higher conformational stability for the former peptide. Conversely, NMR parameters, including for example lower number of medium range diagnostic NOEs (Table S8), indicate that *DNal* has greater conformational flexibility relative to peptides **8** and **10**.

NMR-derived constraints for peptides **8**, **10**, and *DNal* were used as input data for a simulated annealing structure calculation according to the standard protocol of DYANA program [21]. Figures 2a and 2b show the superposition of the best 10 NMR structures of the peptides **8** and **10**, respectively, overlapped at the level of backbone atoms. The bundle reveals a high structural similarity (backbone RMSD≤0.40 Å for peptide **8**, and ≤0.20 Å for peptide **10**), suggesting that NMR structures are defined with high precision.

Analysis of these NMR structures using Molmol [23] identified the prevalence of regular α-helices in the Arg8-Val13 segment of both peptides. Interestingly, the helical structure showed amphipathic distribution of the side chains, with Arg8 and Lys11 side chains on one side of the helix and *D*Nal(2′)7, Aic10 (Cha10), Phe12 and Val13 on the other side (Figure 2a, b).

The *DNal* structure was much more flexible (backbone RMSD = 0.84 Å) and only turn motifs could be detected along its structure. In particular, two β-turns along residues 7–10 and 10–13 (Figure 2c) are consistent with our earlier results [11]. The *DNal* structure is better described as a nascent helix i.e. a helix in equilibrium with disordered structures [35].

Conformational differences could account for the enhanced antimicrobial activity observed in peptides **8** and **10** relative to the parent sequence *DNal*. The amphipathic helical structure along residues 8–13 is likely responsible for the superior antimicrobial activity of the substituted peptides whereas the partial lack of helicity in *DNal* probably contributes to its reduced activity. Indeed, the residues Deg [26], tButGly [27], Ac3c [36], β-Ala [31], and Acpc [32], which do not stabilize regular right handed helices, did not promote activity in the corresponding peptides.Therefore, consistent with previous observations, the amphipathic helical content proved to be a key factor in the activity of antimicrobial peptides [37,38].

Conclusions

The present research discovered novel synthetic melanocortins that exert broad-spectrum antimicrobial activity. The main advance of these molecules, relative to the known α-MSH-related compounds, consists of their capacity of killing growing organisms in standard culture conditions. Indeed, previous investigations on antimicrobial melanocortins were not performed in culture media that allow microorganisms to grow. Although, those studies were very helpful to promote discovery of synthetic antimicrobial melanocortins, standard microbiology testing is required for a realistic use in clinical settings. This prerequisite was clearly met by the peptides **8** and **10**, in which Gly10 of *DNal* was replaced by the residues Aic and Cha, respectively. Although these peptides also reduced viability of human cells, these detrimental influences occurred at greater concentrations relative to effective antibacterial concentrations. Overall, the structural preferences associated with antimicrobial activity identified in this research can help further development of synthetic melanocortins with enhanced therapeutic index.

Supporting Information

Figure S1 Chemical structure of amino acids replacing Gly10 of α-MSH.
(DOC)

Figure S2 Analytical HPLC data of synthesized peptides.
(DOC)

Table S1 Physico-chemical properties of the peptides.
(DOC)

Table S2 Amino acid analysis of the peptides.
(DOC)

Table S3 NMR Resonance Assignments of Peptide **8** in DPC/SDS Solution at 25°C.
(DOC)

Table S4 NMR Resonance Assignments of Peptide **10** in DPC/SDS Solution at 25°C.
(DOC)

Table S5 NMR Resonance Assignments of Peptide *DNal* in DPC/SDS Solution at 25°C.
(DOC)

Table S6 NOE Derived Upper Limit Constraints of Peptide **8** in DPC/SDS Solution at 25°C.
(DOC)

Table S7 NOE Derived Upper Limit Constraints of Peptide **10** in DPC/SDS Solution at 25°C.
(DOC)

Table S8 NOE Derived Upper Limit Constraints of Peptide *DNal* in DPC/SDS Solution at 25°C.
(DOC)

Author Contributions

Conceived and designed the experiments: A. Catania PG A. Carotenuto. Performed the experiments: LA SDM AL FM VL ADG SG IGM PC. Analyzed the data: A. Catania PG MLM A. Carotenuto EN SG. Contributed reagents/materials/analysis tools: PG A. Catania MLM. Wrote the paper: A. Catania PG MLM A. Carotenuto.

References

1. Catania A, Gatti S, Colombo G, Lipton JM (2004) Targeting melanocortin receptors as a novel strategy to control inflammation. Pharmacol Rev 56: 1–29.
2. Catania A (2007) The melanocortin system in leukocyte biology. J Leukoc Biol 81: 383–392.
3. Catania A, Colombo G, Rossi C, Carlin A, Sordi A, et al. (2006) Antimicrobial properties of alpha-MSH and related synthetic melanocortins. ScientificWorld-Journal 6: 1241–1246.
4. Cutuli M, Cristiani S, Lipton JM, Catania A (2000) Antimicrobial effects of alpha-MSH peptides. J Leukoc Biol 67: 233–239.
5. Masman MF, Rodriguez AM, Svetaz L, Zacchino SA, Somlai C, et al. (2006) Synthesis and conformational analysis of His-Phe-Arg-Trp-NH2 and analogues with antifungal properties. Bioorg Med Chem 14: 7604–7614.
6. Grieco P, Rossi C, Colombo G, Gatti S, Novellino E, et al. (2003) Novel alpha-melanocyte stimulating hormone peptide analogues with high candidacidal activity. J Med Chem 46: 850–855.
7. Grieco P, Rossi C, Gatti S, Colombo G, Carlin A, et al. (2005) Design and synthesis of melanocortin peptides with candidacidal and anti-TNF-alpha properties. J Med Chem 48: 1384–1388.
8. Madhuri, Shireen T, Venugopal SK, Ghosh D, Gadepalli R, et al. (2009) In vitro antimicrobial activity of alpha-melanocyte stimulating hormone against major human pathogen Staphylococcus aureus. Peptides 30: 1627–1635.
9. Shireen T, Singh M, Dhawan B, Mukhopadhyay K (2012) Characterization of cell membrane parameters of clinical isolates of Staphylococcus aureus with varied susceptibility to alpha-melanocyte stimulating hormone. Peptides 37: 334–339.
10. Singh M, Mukhopadhyay K (2011) C-terminal amino acids of alpha-melanocyte-stimulating hormone are requisite for its antibacterial activity against Staphylococcus aureus. Antimicrob Agents Chemother 55: 1920–1929.
11. Carotenuto A, Saviello MR, Auriemma L, Campiglia P, Catania A, et al. (2007) Structure-function relationships and conformational properties of alpha-MSH(6–13) analogues with candidacidal activity. Chem Biol Drug Des 69: 68–74.
12. Rinaldi AC, Mangoni ML, Rufo A, Luzi C, Barra D, et al. (2002) Temporin L: antimicrobial, haemolytic and cytotoxic activities, and effects on membrane permeabilization in lipid vesicles. Biochem J 368: 91–100.
13. Mangoni ML, Rinaldi AC, Di Giulio A, Mignogna G, Bozzi A, et al. (2000) Structure-function relationships of temporins, small antimicrobial peptides from amphibian skin. Eur J Biochem 267: 1447–1454.
14. Piantini U, Sorensen O, Ernst RR (1982) Multiple quantum filters for elucidating NMR coupling networks. J Am Chem Soc 104 6800–6801.
15. Braunschweiler, L. Ernst RR (1983) Coherence transfer by isotropic mixing: application to proton correlation spectroscopy. J Magn Reson 53: 521–528.
16. Jeener J, Meier BH, Bachman P, Ernst RR (1979) Investigation of exchange processes by two-dimensional NMR spectroscopy. J Chem Phys 71: 4546–4553.
17. States DJ, Haberkorn RA, Ruben DJ (1982) A two-dimensional nuclear Overhauser experiment with pure absorption phase in four quadrants. J Magn Reson 48: 286–292.
18. Hwang TL, Shaka A (1995) Water suppression that works. Excitation sculpting using arbitrary wave-forms and pulsed-field gradients. J Magn Reson 112: 275–279.
19. Delaglio F, Grzesiek S, Vuister GW, Zhu G, Pfeifer J, et al. (1995) NMRPipe: a multidimensional spectral processing system based on UNIX pipes. J Biomol NMR 6: 277–293.
20. Bartels C, Xia TH, Billeter M, Guntert P, Wuthrich K (1995) The program XEASY for computer-supported NMR spectral analysis of biological macromolecules. J Biomol NMR 6: 1–10.
21. Guntert P, Mumenthaler C, Wuthrich K (1997) Torsion angle dynamics for NMR structure calculation with the new program DYANA. J Mol Biol 273: 283–298.
22. Maple JR, Dinur U, Hagler AT (1988) Derivation of force fields for molecular mechanics and dynamics from ab initio energy surfaces. Proc Natl Acad Sci U S A 85: 5350–5354.
23. Koradi R, Billeter M, Wuthrich K (1996) MOLMOL: a program for display and analysis of macromolecular structures. J Mol Graph 14: 51–55, 29–32.
24. Venkatraman J, Shankaramma SC, Balaram P (2001) Design of folded peptides. Chem Rev 101: 3131–3152.
25. Degenkolb T, Bruckner H (2008) Peptaibiomics: towards a myriad of bioactive peptides containing C(alpha)-dialkylamino acids? Chem Biodivers 5: 1817–1843.
26. Vijayalakshmi S, Rao RB, Karle IL, Balaram P (2000) Comparison of helix-stabilizing effects of alpha,alpha-dialkyl glycines with linear and cycloalkyl side chains. Biopolymers 53: 84–98.
27. Formaggio F, Baldini C, Moretto V, Crisma M, Kaptein B, et al. (2005) Preferred conformations of peptides containing tert-leucine, a sterically demanding, lipophilic alpha-amino acid with a quaternary side-chain Cbeta atom. Chemistry 11: 2395–2404.
28. Schiller PW, Weltrowska G, Nguyen TM, Lemieux C, Chung NN, et al. (1991) Conformational restriction of the phenylalanine residue in a cyclic opioid peptide analogue: effects on receptor selectivity and stereospecificity. J Med Chem 34: 3125–3132.
29. Schnarr NA, Kennan AJ (2001) Coiled-coil formation governed by unnatural hydrophobic core side chains. J Am Chem Soc 123: 11081–11082.
30. Frackenpohl J, Arvidsson PI, Schreiber JV, Seebach D (2001) The outstanding biological stability of beta- and gamma-peptides toward proteolytic enzymes: an in vitro investigation with fifteen peptidases. Chembiochem 2: 445–455.
31. Thakur AK, Kishore R (2001) Influence of hydrophobic interactions on the conformational adaptability of the beta-Ala residue. J Pept Res 57: 455–461.
32. Appella DH, Christianson LA, Klein DA, Powell DR, Huang X, et al. (1997) Residue-based control of helix shape in beta-peptide oligomers. Nature 387: 381–384.
33. Grieco P, Carotenuto A, Auriemma L, Saviello MR, Campiglia P, et al. (2013) The effect of d-amino acid substitution on the selectivity of temporin L towards target cells: Identification of a potent anti-Candida peptide. Biochim Biophys Acta 1828: 652–660.
34. Wüthrich K (1986) NMR of Proteins and Nucleic Acids. New York: John Wiley & Sons, Inc.
35. Dyson HJ, Rance M, Houghten RA, Wright PE, Lerner RA (1988) Folding of immunogenic peptide fragments of proteins in water solution. II. The nascent helix. J Mol Biol 201: 201–217.
36. Benedetti E, Di Blasio B, Pavone V, Pedone C, Santini A, et al. (1989) Structural versatility of peptides containing Cα,α-dialkylated glycines. An X-ray diffraction study of six 1-aminocyclopropane-1-carboxylic acid rich peptides. Int J Biol Macromol, 11: 353–360.
37. Giangaspero A, Sandri L, Tossi A (2001) Amphipathic alpha helical antimicrobial peptides. Eur J Biochem 268: 5589–5600.
38. Carotenuto A, Malfi S, Saviello MR, Campiglia P, Gomez-Monterrey I, et al. (2004) A different molecular mechanism underlying antimicrobial and hemolytic actions of temporins A and L. J Med Chem, 51: 2354–2362.

Cell. Mol. Life Sci.
DOI 10.1007/s00018-013-1500-4

Cellular and Molecular Life Sciences

RESEARCH ARTICLE

Anti-*Candida* activity of 1–18 fragment of the frog skin peptide esculentin-1b: in vitro and in vivo studies in a *Caenorhabditis elegans* infection model

Vincenzo Luca · Massimiliano Olivi · Antonio Di Grazia · Claudio Palleschi · Daniela Uccelletti · Maria Luisa Mangoni

Received: 22 August 2013 / Revised: 10 October 2013 / Accepted: 14 October 2013

Abstract *Candida albicans* represents one of the most prevalent species causing life-threatening fungal infections. Current treatments to defeat *Candida albicans* have become quite difficult, due to their toxic side effects and the emergence of resistant strains. Antimicrobial peptides (AMPs) are fascinating molecules with a potential role as novel anti-infective agents. However, only a few studies have been performed on their efficacy towards the most virulent hyphal phenotype of this pathogen. The purpose of this work is to evaluate the anti-*Candida* activity of the N-terminal 1–18 fragment of the frog skin AMP esculentin-1b, Esc(1–18), under both in vitro and in vivo conditions using *Caenorhabditis elegans* as a simple host model for microbial infections. Our results demonstrate that Esc(1–18) caused a rapid reduction in the number of viable yeast cells and killing of the hyphal population. Esc(1–18) revealed a membrane perturbing effect which is likely the basis of its mode of action. To the best of our knowledge, this is the first report showing the ability of a frog skin AMP-derived peptide (1) to kill both growing stages of *Candida*; (2) to promote survival of *Candida*-infected living organisms and (3) to inhibit transition of these fungal cells from the roundish yeast shape to the more dangerous hyphal form at sub-inhibitory concentrations.

Keywords Antimicrobial peptide · Anti-*Candida* activity · Membrane permeabilization · *Caenorhabditis elegans* · Simple infection model

Abbreviations

AMP	Antimicrobial peptide
CFU	Colony-forming units
Esc(1–18)	Esculentin-1b(1–18)
HP	Hyphal growth-promoting medium
MH	Mueller-Hinton
MFC	Minimal fungicidal concentration
MIC	Minimal inhibitory concentration
MTT	3-(4,5-Dimethylthiazol-2-yl)-2,5-diphenyltetrazolium bromide
NaPB	Sodium phosphate buffer, pH 7.4
NGM	Nematode growth medium
rho-Esc(1–18)	Rhodamine-labelled Esc(1–18)

Introduction

Candida species are normally harmless commensals of the gastrointestinal and urinary tracts of human beings. However, under some circumstances, e.g., when the immune system is weakened or competing bacterial flora is eliminated following a broad-spectrum antibiotic treatment, *Candida* cells can invade host tissues and cause life-threatening infections. Invasive candidiasis is particularly common in intensive care units where mortality rates reach 45–49 % [1–4]. In North America, it is the fourth most common cause of

V. Luca and M. Olivi equally contributed to the work.

Part of this work will be submitted in partial fulfillment of the requirements of a Ph.D degree at Sapienza University of Rome (by V.L.).

V. Luca · A. Di Grazia · M. L. Mangoni (✉)
Dipartimento di Scienze Biochimiche "A. Rossi Fanelli", Istituto Pasteur-Fondazione Cenci Bolognetti, Sapienza Università di Roma, Piazzale Aldo Moro, 5, 00185 Rome, Italy
e-mail: marialuisa.mangoni@uniroma1.it

M. Olivi · C. Palleschi · D. Uccelletti
Dipartimento di Biologia e Biotecnologie "Charles Darwin", Sapienza Università di Roma, Piazzale Aldo Moro, 5, 00185 Rome, Italy

Published online: 10 November 2013

hospital-acquired infections [5–7], with *Candida albicans* being the most prevalent species either in mucosal or systemic diseases [8, 9]. A striking feature of *C. albicans* biology is its ability to grow in different morphological forms that range from unicellular budding yeast, more suited for dissemination in the bloodstream [10–12], to the filamentous form (pseudo and true-hyphae) responsible for promoting tissue penetration and colonization [13–15]. The hyphal stage has often been considered essential for adhesion to mucosal surfaces and initiation of clinical infectious diseases [14, 16, 17]. Treatment of these infections with conventional antifungals, e.g., fluconazole and amphotericin B [18–21], is frequently ineffective. In addition, amphotericin B is toxic to the kidneys and hematopoietic and nervous systems [22, 23]. Therefore, the search for new anti-*Candida* compounds is critical [24], and naturally occurring antimicrobial peptides (AMPs) represent attractive candidates for the generation of new anti-mycotics. AMPs are produced by almost all unicellular and multicellular organisms and act as the first line of defense against noxious microorganisms [25–31]. The majority of these peptides are positively charged at neutral pH and with an amphiphatic character in a membrane-mimicking environment. These characteristics enhance selective binding and insertion of AMPs into microbial membranes, which are much richer in anionic phospholipids than mammalian cells [32, 33].

In view of the potential role of *Candida* dimorphism, the evaluation and understanding of the activity of new antifungal agents on the two morphological phenotypes of this pathogen can help in the development of better anti-*Candida* agents. To this aim, we performed an in-depth study on the activity and related molecular mechanism of the 1–18 fragment of the frog skin AMP esculentin-1b [Esc(1–18): GIFSKLAGKKLKNLLISG-NH_2] [34], on the two forms of growth of *C. albicans*. Previous studies reported on the anti-*Candida* activity of the full 46-residue peptide esculentin-1 when tested in solid medium against the yeast form, and showed that it was only slightly higher than that of Esc(1–18) [35, 36]. Note that the 19–46 C-terminal tail of esculentin-1 has five basic residues that are neutralized by the four negatively charged amino acids located in this region. According to what was stated by Avrahami and Shai [37], this could assist in peptide assembly and partitioning into the fungal membrane. By contrast, no acidic residues are present in Esc(1–18), and its four positively charged amino acids are spread along the entire peptide sequence, presumably hampering the formation of peptide oligomers and their partition from the cell wall into the membrane. However, it is worth noting that the difference in the anti-*Candida* activity between Esc(1–18) and the full-length parental esculentin-1 is not very large [34, 35]. Furthermore, recent studies revealed a microbial membrane-perturbing activity of Esc(1–18) as one of the major mechanisms underlying its killing activity [38]. This should limit the induction of resistance to it, thus making the shorter-sized Esc(1–18) a more attractive candidate for further antifungal studies.

Importantly, experiments described in this work were carried out under both in vitro and in vivo conditions, using a simple model system, the nematode *Caenorhabditis elegans*. Historically, *C. elegans* has been of great value in many fields of biological research [39]. It is a differentiated multicellular organism with a nervous system, reproductive organs and digestive apparatus. Furthermore, it has a simple structure, a short life-cycle (< 3 days) and can be infected by different human pathogens (including *Candida* species) that can replace the regular *Escherichia coli* food source. Indeed, they can pass through the mouth, ultimately reaching the nematode's gut [40]. Once the microbes start to proliferate, an infection process is initiated, which leads to the animal's death. We have recently demonstrated that Esc(1–18) peptide is highly effective in promoting survival of *C. elegans* worms following infection by a multi-drug resistant strain of *Pseudomonas aeruginosa* [39]. Importantly, this peptide shows no toxicity towards mammalian cells, such as erythrocytes, lymphocytes [34, 38], macrophages and keratinocytes at microbicidal concentrations (Mangoni et al. unpublished data).

Results of the present study suggest that Esc(1–18) is an attractive membrane-perturbing anti-*Candida* AMP with the ability to block hyphal development, also in vivo.

Materials and methods

Materials

Synthetic all-L and all-D Esc(1–18) as well as the rhodamine-labelled form of the all-L peptide [rho-Esc(1–18)] were purchased from Selleck Chemicals (Houston, TX, USA). The purity of the peptides, their sequences and concentrations were determined as previously described [34]. Sytox Green was from molecular probes (Invitrogen, Carlsbad, CA, U.S.A.); 3-(4,5-dimethylthiazol-2-yl)-2,5-diphenyltetrazolium bromide (MTT), and poly-L-lysine (150,000–300,000 mol wt) were purchased from Sigma (St. Louis, MO, USA). All other chemicals were reagent-grade.

Microorganisms and nematode strains

The following *C. albicans* strains were used: the reference ATCC 10231, ATCC 90028 and the clinical isolates *C. albicans* n. 1s and *C. albicans* n.1r. The wild-type *C. elegans* strain N2 was used in all experiments and propagated on nematode grow medium (NGM) plates containing *E. coli* OP50 as a food source [41]. *C. albicans* ATCC 10231 was used for all the experiments with *C. elegans.*

Anti-yeast activity

Susceptibility testing was performed by the microbroth dilution method, according to the procedures outlined by the National Committee for Clinical Laboratory Standards (2001) using sterile 96-well plates according to [42]. Minimal inhibitory concentration (MIC) was determined as the lowest peptide concentration at which 100 % inhibition of growth was observed after 18 h at 37 °C.

Peptide's effect on the viability of yeast cells and hyphae

The peptide's effect on the viability of both yeast and hyphal forms of *C. albicans* ATCC 10231 was determined by the MTT colorimetric method. In the first case, 100 µl of yeast cells suspension in 10 mM sodium phosphate buffer (NaPB), pH 7.4 (about 1×10^7 CFU/ml) were incubated at 37 °C with Esc(1–18) at different concentrations for 10, 20, 30 and 60 min. After incubation time with the peptide, samples were centrifuged and resuspended in 100 µl RPMI 1640 medium (Sigma) supplemented with 0.5 mg/ml MTT. After 2 h incubation at 37 °C, MTT formazan crystals were solubilized by adding 100 µl of 10 % sodium dodecyl sulphate. The absorbance at 590 nm of triplicate samples was measured spectrophotometrically with a microplate reader (Infinite M200; Tecan, Salzburg, Austria). Cell viability was expressed as percentage of survival with respect to the control (yeast cells not treated with the peptide) at the corresponding time intervals.

In the second case, RPMI supplemented with 2 mM L-glutamine and 0.165 M morpholinepropanesulfonic acid (pH 7.0) was used as the hyphal growth-promoting (HP) medium [43, 44]. About 3×10^4 or 1×10^4 yeast-form cells in HP medium were transferred into wells of a 96-well flat-bottom poly-L-lysine-coated microplate and incubated for 3 h or a longer time (12 and 18 h) respectively, at 37 °C, as indicated in the Results section. The medium was then discarded and the adhesive *Candida* hyphae were treated with different concentrations of Esc(1–18) dissolved in NaPB, at 37 °C for different times. The peptide was then removed, 100 µl of MTT solution (0.5 mg/ml in HP medium) were added to each well and the plate was incubated at 37 °C for 4 h. Afterwards, formazan crystals were solubilized and their absorbance was measured as described above. The minimal fungicidal concentrations (MFC_{50} and MFC_{90}) were defined as the minimal peptide concentrations causing a reduction in hyphae viability by 50 and 90 %, respectively, within 60 min, compared with the control.

Inhibition of hyphal development

Briefly, 100 µl of yeast suspension (1×10^6 CFU/ml) in Winge broth [45] were transferred into poly-L-lysine-coated wells of a 96-well plate and incubated at 37 °C for 3 h in the presence of different concentrations of Esc(1–18). The inhibition of hyphal development was visualized microscopically under an inverted microscope (Olympus CKX41) at ×40 magnification and photographed with a Color View II digital camera.

Membrane permeabilization

The ability of Esc(1–18) to alter the membrane permeability of fungal cells was assessed by the Sytox Green assay in microtiter plates, according to [46]. Briefly, 1×10^6 yeast cells or 3 h-grown hyphae obtained as described above were incubated in 95 µl of NaPB supplemented with 1 µM Sytox Green. After 20 min in the dark, 5 µl of peptide were added. The increase in fluorescence, owing to the binding of the dye to intracellular DNA, was measured at different times at 37 °C in the microplate reader (excitation and emission wavelengths were 485 and 535 nm, respectively).

Staining protocols: fluorescent probes for assessment of peptide's distribution and fungal membrane integrity

To visualize, in a single preparation, the distribution of Esc(1–18) and to detect, at the same time, the membrane permeabilization induced by the peptide on yeast or hyphal forms of *Candida*, we used rho-Esc(1–18) and the two following fluorochromes: (1) the double-stranded DNA-binding dye DAPI, to stain the nuclei of all cells, and (2) the green fluorescent probe Sytox Green, to stain membrane perturbation. After exposure of yeast cells (1×10^7 CFU/ml in NaPB) to 16 µM rho-Esc(1–18) (100 µl as a final volume) for 30 min at 37 °C, the microbial suspension was centrifuged, washed with NaPB and incubated with 100 µl of 1 µM Sytox Green (in NaPB) for 15 min at room temperature. The sample was washed again and treated with 100 µl of DAPI solution (10 µg/ml in NaPB) for 15 min at room temperature [47]. Afterwards, yeast cells were resuspended in a drop of NaPB, poured onto a glass slide and examined by phase-contrast and fluorescence microscopy. Both phase-contrast and fluorescence images were recorded using the Olympus optical microscope equipped with an oil-immersion objective (×100).

In the case of hyphae, 96-well glass bottom microplates (MGB096-1-2-LG-L, Matrical Bioscience Spokane WA, USA) were used and coated with poly-L-lysine. About 3×10^4 yeast cells in HP medium were added to each single well and the plate was incubated at 37 °C for 3 h to permit hyphal development. Afterwards, treatment with rho-Esc(1–18) and staining with Sytox Green and DAPI solutions were performed as described above. Finally, 50 µl of NaPB were added to each well prior microscope observation. In all cases, controls were run in the absence of peptide.

C. elegans infection

Freshly grown *Candida* cells were inoculated into 2 ml of yeast extract-peptone-dextrose (YPD) broth and grown overnight with agitation at 28 °C. Fungal lawns used for *C. elegans* infection assays were prepared by spreading 100 µl of the overnight culture (diluted 1:100 in distilled water) on brain heart infusion (BHI) agar plates. The plates were then incubated for approximately 20 h at 28 °C before being seeded with adult hermaphrodite nematodes from a synchronized culture grown at 16 °C [41]. About 100–200 worms were washed with M9 buffer [41] and placed in the middle of *C. albicans* lawns. The infection was performed at 25 °C for 20 min.

Worm survival assay

The infected worms were washed with M9 buffer to remove *C. albicans* cells from their surface. Twenty worms were then transferred into plates (3-cm diameter) containing 2 ml of liquid medium (79 % M9, 20 % BHI, 10 µg/ml cholesterol and 90 µg/ml kanamycin) according to [48]. The peptide was either added to the plates, or omitted as indicated. The plates were incubated at 25 °C and examined for worm survival after 24 h. Worms were considered to be dead if they did not respond to being touched by a platinum wire pick. Living nematodes maintain a sinusoidal shape, whereas dead nematodes appear as straight, rigid rods as the corpses become filled with fungal cells [49].

Peptide's effect on the number of yeast cells and their switch to the hyphal form, within the nematode intestine

Twenty infected nematodes in triplicate were treated (or not treated in case of controls) with the peptide at 25 °C for 24 h. Afterwards, for each replicate, worms were broken with 50 µl of M9 buffer-1 % TritonX-100. Appropriate dilutions of whole-worm lysates were plated on YPD agar plates for colony counts. In parallel, to evaluate the effect of Esc(1–18) on the morphology of fungal cells, peptide-treated and untreated infected worms were mounted onto pads of 3 % agarose in M9 buffer supplemented with 20 mM sodium azide to paralyze them. Animals were then observed under a Zeiss AXIOVERT25 microscope and photographed with a Zeiss AxioCam camera using Axiovision 4.6 (Zeiss) software.

In another set of experiments, infected nematodes were treated with 25 µM rho-Esc(1–18) for 3 h and observed by fluorescence microscopy as reported above.

Statistical analysis

Data are presented as mean ± SD, and the Student's test (GraphPad Prism 4.0 software) was used to determine the statistical significance between experimental groups. The difference was considered significant if the p value was < 0.05.

Results

In vitro studies

MIC determination

The activity of Esc(1–18) in inhibiting the growth of *C. albicans* yeast cells was evaluated using a standard inoculum of 3.5×10^4 CFU/ml. Note that the MIC was 4 µM against all the strains tested with the exception of *C. albicans* n.1r (Table 1), and that the same MIC value was obtained when samples were incubated at 28 °C instead of 37 °C (data not shown). The conventional antifungal amphotericin B was also included for comparison (Table 1). In our experiments *C. albicans* ATCC 10231 was selected as a representative strain to perform further additional studies, since it is a well-characterized standard strain with the ability to grow under both yeast and hyphal forms under the experimental conditions [50]. As most of the experiments described below required a higher number of yeast cells, i.e., 1×10^6 and 1×10^7 CFU/ml, such cell densities were also used as an inoculum to determine the MICs against the ATCC 10231 strain. They were found to be directly related to cell number: 16 and 64 µM, respectively.

Time kill on both yeast and hyphal forms

In order to confirm a fungicidal activity of Esc(1–18), a killing kinetics study with different peptide concentrations was first carried out on the yeast cells. A dose-dependent candidacidal activity was observed, with approximately 80 % reduction in cell survival within the first 20 min at 16 µM (Fig. 1a).

As found for the yeast cells, Esc(1–18) provoked about 80 % killing of 3 h-grown hyphae at 16 µM after 20 min

Table 1 Antimicrobial activity of Esc(1–18) and amphotericin B on different *C. albicans* strains

MIC[a] (µM)				
Compound	*C. albicans* ATCC 10231	*C. albicans* ATCC 90028	*C. albicans* n.1s	*C. albicans* n.1r
Esc(1–18)	4	4	4	2
Amphotericin B	0.5	0.5	2	2

[a] The reported MIC values are those obtained from at least three readings out of four independent measurements

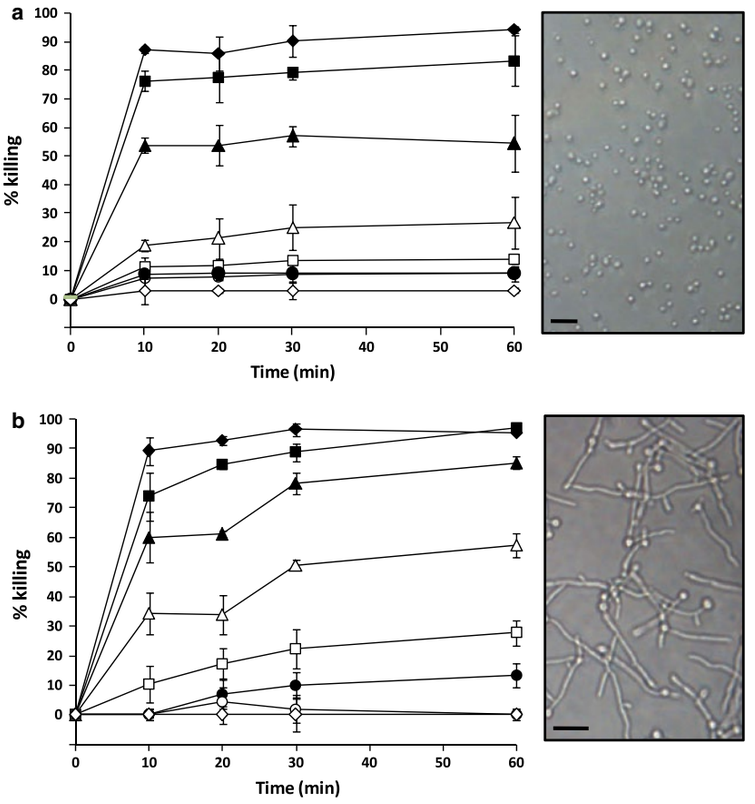

Fig. 1 Killing kinetic of Esc(1–18) on *C. albicans* ATCC 10231 yeast (*panel* **a**) and hyphal (*panel* **b**) cells in NaPB. Either yeast cells or 3 h-grown hyphae, were incubated at 37 °C with different peptide concentrations: 0.25 μM (*unfilled diamond*); 0.5 μM (*unfilled circle*); 1 μM (*filled circle*); 2 μM (*unfilled square*); 4 μM (*unfilled triangle*); 8 μM (*filled triangle*); 16 μM (*filled square*); 32 μM (*filled diamond*). Data points represent the mean of triplicate samples ± SD from a single experiment, representative of three independent experiments. The killing activity was determined with respect to the control at each time interval. *Right insets* show phase-contrast images of yeast and hyphal forms of *Candida* used for the experiments. *Scale bars* are 10 μm long

from peptide addition (Fig. 1b), whereas approximately 90 % killing of hyphal population was recorded after a longer incubation time (60 min) at the same concentration of 16 μM (MFC_{90}). Importantly, when hyphae were grown for 12 or 18 h instead of 3 h, a well-organized cellular community, named biofilm, was formed (Fig. 2 upper panels). Indeed, an inner layer containing microcolonies of yeast cells and an outer layer rich in pseudohyphae and hyphae were observed, according to the typical phenotype of *Candida* biofilm [51, 52]. Remarkably, the peptide's efficacy was found to be only fourfold or eightfold lower, as indicated by the corresponding MFC_{50} and MFC_{90} on 12 or 18 h-grown biofilm, respectively, after 60 min of peptide treatment (Table 2). Phase-contrast images of *Candida* biofilm treated or not treated with the peptide at its MFC_{90}, after MTT colorimetric assay, are reported in Fig. 2 (lower panels).

Effect on membrane perturbation

The ability of Esc(1–18) to alter the membrane permeability of *Candida* cells was monitored by the intracellular influx of Sytox Green upon addition of the peptide to the cells. Esc(1–18) caused dose-dependent membrane damage, as supported by increased fluorescence signal at increasing peptide concentrations (Fig. 3a), with kinetics overlapping that of yeasts killing (Fig. 1a). Note that only a modest increase in fluorescence intensity was generated within the first 20 min after the addition of amphotericin B, even when used at a concentration up to 64-fold the MIC (data not shown). However, it gradually increased with time, reaching its maximum value, which was found to be identical to that obtained with 16 μM Esc(1–18), within 3 h. This finding is in agreement with the slower fungicidal activity (higher than 2–3 h, depending on the strain [53]) of this membrane-perturbing antifungal drug [54, 55] with respect to that of Esc(1–18). In line with what was obtained for the unicellular budding cells, Esc(1–18) disturbed the structural organization of the membrane of the filamentous form of *Candida* in a concentration-dependent manner (Fig. 3b) that directly correlates with its killing activity (Fig. 1b).

Furthermore, to find out whether the peptide-induced membrane-perturbation was mediated by interaction with chiral components of the lipid membrane and/or recognition of specific targets, we also investigated the influx of Sytox Green into yeast and hyphal cells, upon their treatment with the all-D enantiomer of Esc(1–18), which was found to display the same MIC (4 μM) of the all-L isoform.

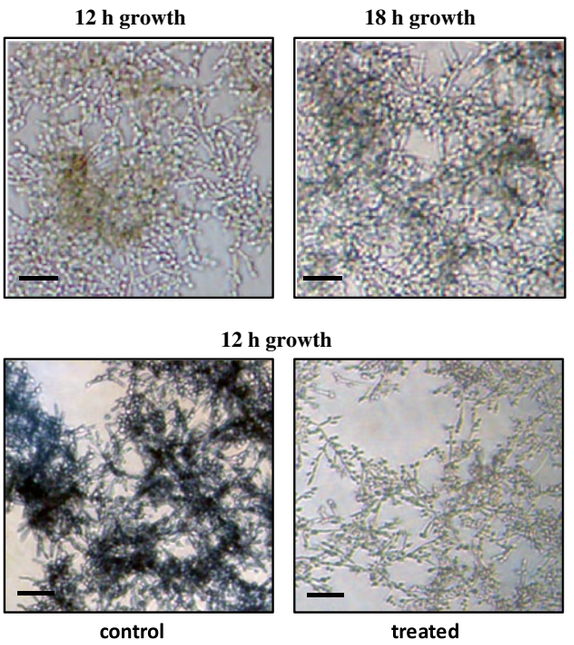

Fig. 2 Phase-contrast images of *Candida* biofilm obtained after 12 and 18 h growth of yeast cells at 37 °C (*upper panels*). The peptide's effect on the viability of 12 h-grown biofilm is shown after the MTT colorimetric assay (*lower panels*). The *black color* in the peptide-untreated (control) sample indicates viable cells, whereas the transparency in the peptide-treated sample indicates the presence of dead yeast and hyphal cells. *Scale bar* is 20 μm long

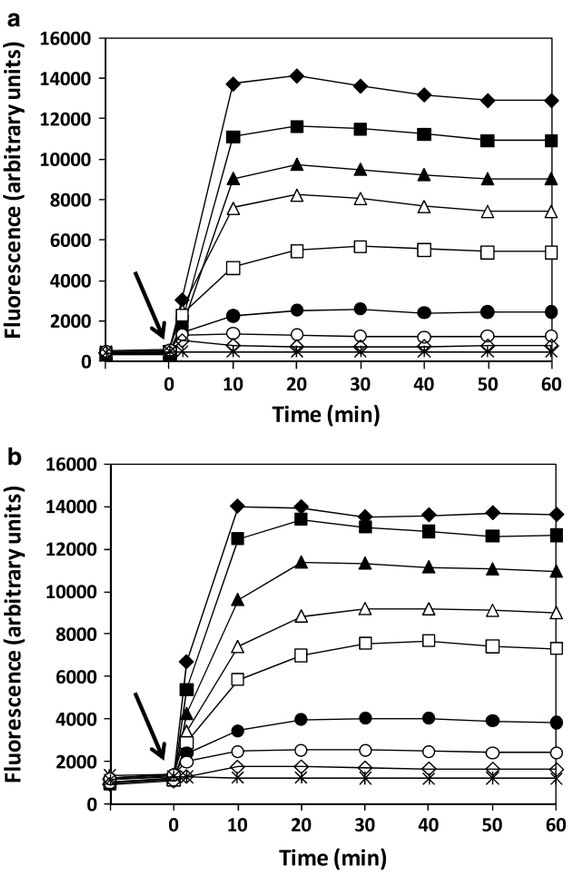

Fig. 3 Peptide-induced membrane permeabilization of yeast cells (*panel* **a**) and 3 h-grown hyphae (*panel* **b**). Samples were incubated with 1 μM Sytox Green in NaPB. Once basal fluorescence reached a constant value, the peptide was added (*arrow*, $t = 0$) and changes in fluorescence were monitored. Peptide concentrations used are the following: 0.25 μM (*unfilled diamond*); 0.5 μM (*unfilled circle*); 1 μM (*filled circle*); 2 μM (*unfilled square*); 4 μM (*unfilled triangle*); 8 μM (*filled triangle*); 16 μM (*filled square*); 32 μM (*filled diamond*). Control (*asterisk*) is given by bacteria without peptide. Data points represent the mean of triplicate samples from a single experiment, representative of three independent experiments

Table 2 Fungicidal activity of Esc(1–18) on the biofilm form of *C. albicans* ATCC 10231

Minimal fungicidal concentration (MFC, μM)[a] on *C. albicans* hyphae		
	12 h growth	18 h growth
MFC_{50}	16	32
MFC_{90}	64	> 64

[a] The reported MFC values are those obtained from at least three readings out of four independent measurements. MFC_{50} and MFC_{90} are defined as the minimal peptide concentrations causing 50 and 90 % fungal killing, respectively, within 60 min. Note that MFC_{50} and MFC_{90} on 3 h-grown hyphae are equal to 4 and 16 μM, respectively (see Fig. 1b)

Interestingly, the all-D peptide showed similar ability to kill yeast and hyphal forms and to permeabilize their cell membrane as the L form (data not shown).

Fluorescence studies

To visualize the distribution of Esc(1–18) and its induced alteration of the cell membrane integrity, either yeast or hyphal forms were treated with 16 μM of rho-Esc(1–18), followed by DAPI and Sytox Green staining. We noted that rhodamine did not affect the anti-*Candida* activity of Esc(1–18), since the MIC value of rho-Esc(1–18) was equal to that of the unlabelled peptide (data not shown). As reported in Fig. 4, rho-Esc(1–18) appeared to be distributed evenly over the yeast cells and hyphae, and the membrane perturbation (as detected by the green fluorescence of Sytox Green) occurred in a similar manner along the entire cell structure.

Inhibition of hyphae formation

It is largely known that the ability of a drug to prevent the morphological change of fungal cells from their budding

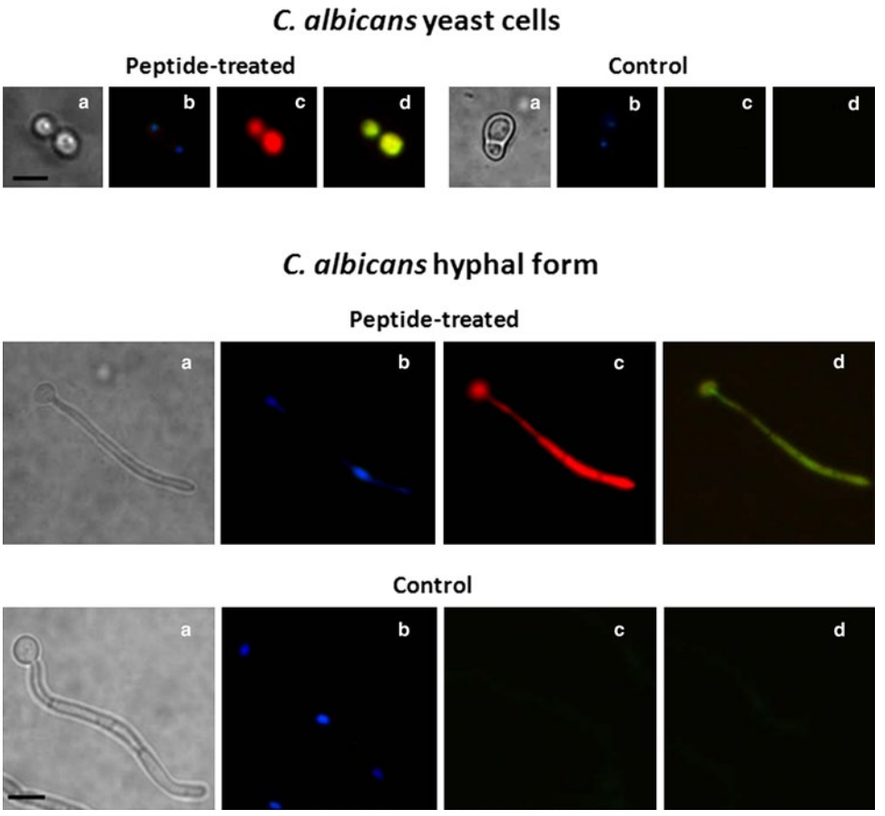

Fig. 4 Detection of peptide distribution and membrane perturbation in both yeast cells (*upper panels*) and hyphae (*lower panels*). Samples were treated with 16 μM of rho-Esc(1–18) and then stained with DAPI and Sytox Green. Afterwards, they were examined by light (**a**) and fluorescence microscopy (**b**–**d**). *Blue* (**b**); *red* (**c**) and *green* (**d**) fluorescence indicate the distribution of DAPI, the labelled-Esc(1–18) and Sytox-Green, respectively. *Scale bars* are 5 μm long and apply to all images

shape into the filamentous form would be extremely advantageous. We therefore studied the capability of Esc(1–18) to block hyphal formation and found out that this effect was more pronounced when 1×10^6 CFU/ml were used. Indeed, a clear inhibition of germ tubes was detected after a 3 h treatment of yeast cells with sub-inhibitory concentrations of Esc(1–18) (Fig. 5). More precisely, the minimal peptide concentration causing such inhibition was found to be 4 μM, corresponding to 1/4 the MIC (16 μM with 1×10^6 CFU/ml). Importantly, this effect was maintained up to 24 h, despite the achieved high cell density, due to cell proliferation (data not shown).

In vivo studies

When infected wild-type nematodes were transferred to liquid medium (see experimental section), yeast cells underwent hyphal development, likely induced by environmental factors of the animal's intestine. This usually results in a very aggressive infection leading to worm lethality in about 40 h. Indeed, hyphae penetrate and destroy the cuticle to finally pierce through the body. In our case, Esc(1–18) was added to the worms, at 50 μM, after 20 min of their exposure to *Candida*. Interestingly, the peptide increased *C. elegans* survival by more than 50 % within 24 h (Fig. 6a), causing approximately 40 % reduction in the number of CFU within the nematode's intestine (Fig. 6b). In addition, in line with our in vitro results, Esc(1–18) dramatically hampered hyphae formation within the worm's gut in 3 h (Fig. 7). In order to accurately assess the in vivo distribution of the peptide, the rho-Esc(1–18) analog was used. As illustrated in Fig. 8, the peptide was homogeneously confined to the worm's intestinal lumen and uniformly associated with the cell perimeter of *Candida* cells.

Discussion

C. albicans is a versatile microorganism that can become an important pathogen in superficial (e.g., oral and vaginitis) and systemic fungal infections [56]. Currently available antifungals are limited in both number and level of effectiveness, mainly due to their undesirable side effects and to the emergence of resistant strains [2, 57, 58]. For these reasons, novel anti-infective agents are of great interest to the medical community [59]. In this context, we have studied the anti-*Candida* properties of Esc(1–18) along with the underlying molecular mechanism.

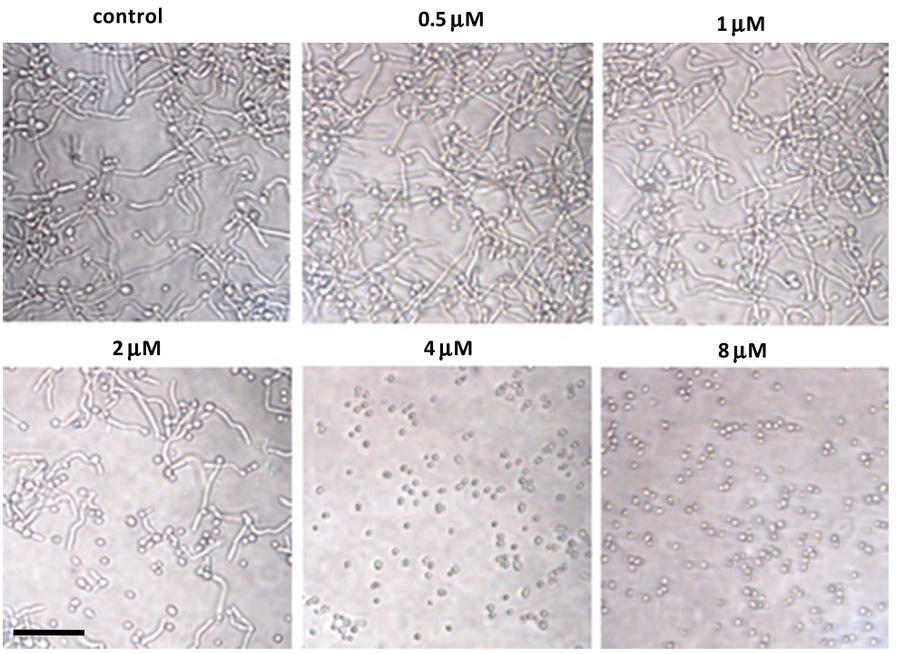

Fig. 5 Effect of Esc(1–18) on the development of the hyphal form of *C. albicans* after 3 h from peptide addition at different sub-MIC concentrations to yeast cells. *Scale bar* is 20 µm long and applies to all images

Although a considerable amount of effort has been devoted to the study of the effect(s) of native and de novo designed AMPs on *C. albicans* (e.g. the human cathelicidins [60], piscidin [61], lactoferrin, istatins [62], lipopeptides [63], Leu/Lys-rich peptides [64], plant defensins [65, 66] temporins [42], pleurocidin [67] and synthetic dodecapeptides [68]), very little is known regarding their efficacy against the hyphal and biofilm forms of this microorganism [69], as well as the subtending mechanism of action. Remarkably, *Candida* biofilms are highly resistant to the action of conventional antifungal agents and very difficult to eradicate either from biological surfaces or implant devices [70]. Here, we have shown that Esc(1–18) displays a fast fungicidal activity (within 20 min), causing approximately 80 % reduction in the number of viable yeast/hyphal cells at 16 µM. Furthermore, a quite good fungicidal activity is exerted by the peptide on an intermediate developmental phase of *C. albicans* biofilm, produced after 12 and 18 h of cell growth. In addition, according to the results of the Sytox Green assay (Fig. 3), this peptide has a membrane-perturbing activity against both stages of *Candida*, despite their different membrane lipid composition [71, 72]. Overall, we can conclude that a direct peptide interaction with membrane lipids followed by membrane permeabilization is likely the primary cause of antifungal activity of Esc(1–18) and one that is probable to limit the emergence of fungal resistance. This conclusion is supported by the following findings: (1) a fast membrane perturbation process that is concomitant with the killing activity on the two morphological phenotypes; (2) a direct correlation between the extent of membrane damage and the percentage of microbial death; (3) the ability to cause release of fluorescent dyes entrapped in artificial phospholipid vesicles [38], which does not occur for those antifungal AMPs, e.g., plant defensins, provoking membrane perturbation in *Candida* as a final result of a mechanism of specific peptide-induced intracellular signaling pathways (e.g., involving the generation of reactive oxygen species, ROS) [65, 66, 73]; and (4) a non-significant production of ROS from Esc(1–18)-treated yeast and hyphal forms (data not shown), in contrast with plant defensins and what has recently been found for de novo designed low molecular weight cationic peptides [68]. Importantly, we can also exclude that the membrane perturbation is the consequence of a binding-site mediated insertion of Esc(1–18) into the fungal membrane, as in the case of the plant defensin RsAFP2 [74]. Indeed, such a stereospecific mechanism would likely not allow the all-L and all-D enantiomers of Esc(1–18) to achieve the same results, in terms of MIC, fungicidal activity and membrane perturbation.

As evidenced by fluorescence microscopy (Fig. 4), the membrane alteration appears to be distributed over the cell structure, ruling out a local peptide-induced membrane disruption. Moreover, the even distribution of the

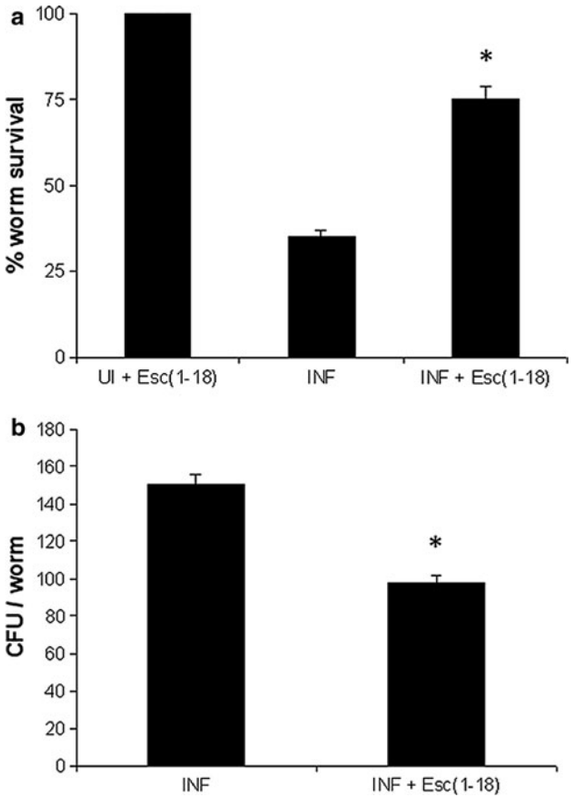

Fig. 6 Effect of Esc(1–18) on both the survival (*panel* **a**) and the number of live *Candida* cells within the gut (*panel* **b**) of infected nematodes after 24 h of peptide treatment [INF + Esc(1–18)] in comparison with untreated infected nematodes (INF). Control uninfected worms treated with the peptide [UI + Esc(1–18)] exhibited 100 % viability. Values represent the means of at least three independent experiments; the error bars indicate SD. *Indicates $p < 0.05$ compared to values from INF

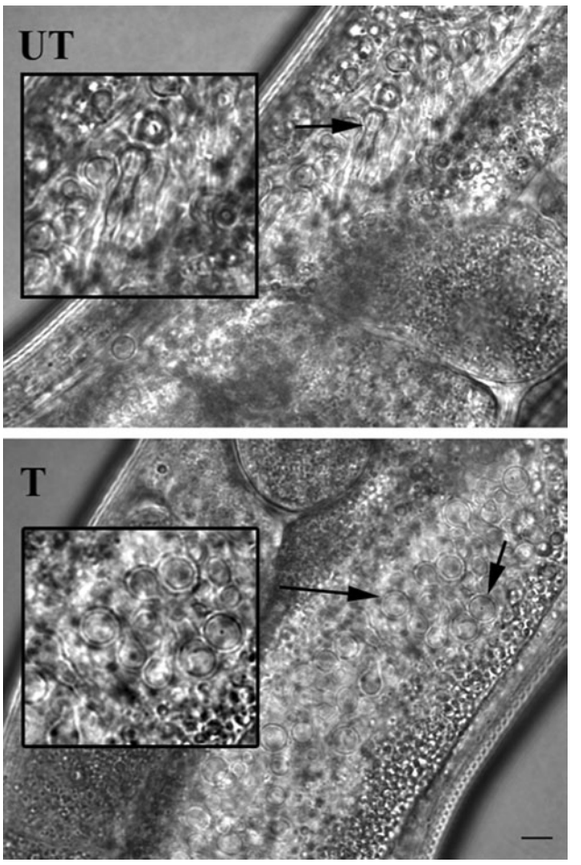

Fig. 7 Morphology of *Candida* cells within the gut of a representative infected animal, after 3 h of peptide treatment (T). A representative infected nematode not treated with the peptide (UT) is included for comparison. *Arrows* and corresponding insets at higher magnification indicate germ tube formation or yeast budding cells in the untreated or peptide-treated sample, respectively. *Scale bar* is 8 μm long

rho-Esc(1–18) along the hyphae excludes intracellular organelles (i.e., the nucleus and mitochondria) as its potential targets. Such an outcome is in contrast with what is manifested by other membrane-active AMPs, e.g., the fragment LL13–37 of the human cathelicidin LL-37, which was found to affect the membrane permeability of only some of the hyphae [75]. Interestingly, when tested on infected *C. elegans*, the frog skin Esc(1–18) is able to prolong worm survival by twofold within 24 h and to hinder hyphal development from the yeast form. Presumably, these findings are due to a direct effect of Esc(1–18) on *Candida* cells, reducing their number (Fig. 6b) and avoiding their shift to the more virulent and toxic phenotype (Fig. 7). This is consistent with the results obtained with the labelled peptide, showing: (1) the presence of Esc(1–18) exclusively along the worm's gut, without diffusing to other tissues; and (2) its adhesion around the fungal cells, which mainly appear in their yeast budding form (Figs. 7b and 8). However, further experiments are required to better elucidate the in vivo mode(s) of action of Esc(1–18). In fact, we cannot leave out the possibility that additional processes, mediated by an enhanced host's immune reaction, can contribute to increase survival of *Candida*-infected worms after peptide treatment. Crucial pathways controlling immune responses have been highly conserved throughout evolution, from nematodes to mammals [76], and the genome of *C. elegans* has been fully sequenced and annotated. Even if this mini-host model cannot substitute for mammalian models, it offers a number of advantages over vertebrates, including the study of strain collections without the ethical considerations associated with studies in mammals [40]. Note that *Candida* infection in *C. elegans* occurs through the gastrointestinal tract upon cell ingestion by the nematode [77],

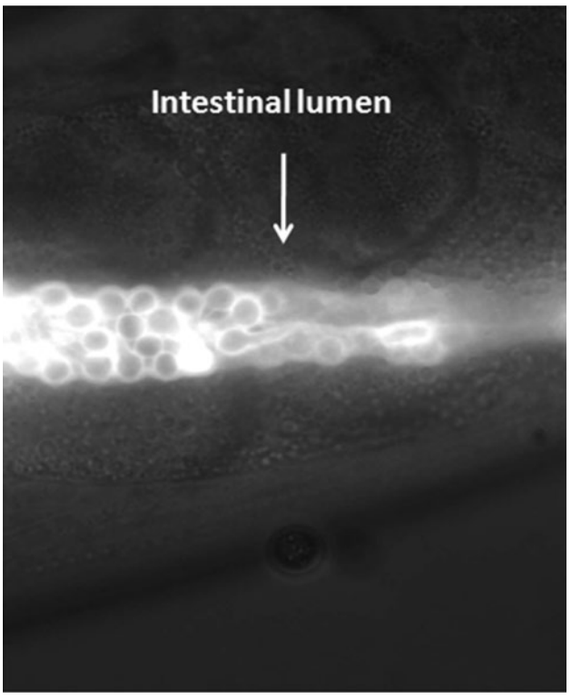

Fig. 8 Fluorescence photomicrograph of a representative infected worm, 3 h after the addition of rho-Esc(1–18) at 25 °C. The *red* fluorescence (*white* in the *photo*) indicates the in vivo distribution of the labelled peptide

which is an accurate representation of what physiologically takes place in susceptible human hosts, where fungal cells in the intestinal mucosa can disseminate to other organs [78]. Conversely, in other simple invertebrate animal models, such as *Drosophila*, infection by *Candida* requires the injection of the yeast into the thorax. Another important benefit in using *C. elegans* is linked to the transparency of its body. Indeed, this makes it possible for researchers to directly examine and visualize in real time, under a dissecting microscope, yeast cell distribution within the host together with their change into hyphae, at all stages of infection. Overall, *C. elegans* can certainly provide an advanced step for a rapid and cost-effective high-throughput screening of in vivo anti-infective agents [79], as well as for identifying their location and their effect(s) on the outcome of the infection (e.g., amount of microbial cells and their form of growth). To the best of our knowledge, this report is the first to demonstrate: (1) the fungicidal activity and plausible mode of action of a frog skin AMP on the two cell shapes of *C. albicans;* (2) its ability to prolong survival of *Candida*-infected living multicellular organisms; and (3) its capability to inhibit transition from the roundish yeast cell to the more dangerous hyphal form at sub-MIC dosages, which is a very important finding for a rational design of new antifungal agents with more favorable properties. It is worthwhile underlining that transition of yeast cells to their filamentous form is a pivotal biological process required for biofilm formation in *C. albicans*. Finally, this paper highlights *C. elegans* as a convenient infection model to select anti-*Candida* compounds to be further investigated in more complex animal models for a future application in the treatment of candidiasis.

Acknowledgments This work was supported by grants from Sapienza Università di Roma. The authors thank Prof. Donatella Barra (University of Rome La Sapienza) and Dr. John P. Mayer (Indiana University, USA) for critical reading of the manuscript.

References

1. Leleu G, Aegerter P, Guidet B (2002) Systemic candidiasis in intensive care units: a multicenter, matched-cohort study. J Crit Care 17:168–175
2. Leroy O, Gangneux JP, Montravers P, Mira JP, Gouin F, Sollet JP, Carlet J, Reynes J, Rosenheim M, Regnier B, Lortholary O (2009) Epidemiology, management, and risk factors for death of invasive *Candida* infections in critical care: a multicenter, prospective, observational study in France (2005–2006). Crit Care Med 37:1612–1618
3. Alangaden GJ (2011) Nosocomial fungal infections: epidemiology, infection control, and prevention. Infect Dis Clin North Am 25:201–225
4. Bajwa S, Kulshrestha A (2013) Fungal infections in intensive care unit: challenges in diagnosis and management. Ann Med Health Sci Res 3:238–244
5. Kao AS, Brandt ME, Pruitt WR, Conn LA, Perkins BA, Stephens DS, Baughman WS, Reingold AL, Rothrock GA, Pfaller MA, Pinner RW, Hajjeh RA (1999) The epidemiology of candidemia in two United States cities: results of a population-based active surveillance. Clin Infect Dis 29:1164–1170
6. Klotz SA, Chasin BS, Powell B, Gaur NK, Lipke PN (2007) Polymicrobial bloodstream infections involving *Candida* species: analysis of patients and review of the literature. Diagn Microbiol Infect Dis 59:401–406
7. Lockhart SR, Iqbal N, Cleveland AA, Farley MM, Harrison LH, Bolden CB, Baughman W, Stein B, Hollick R, Park BJ, Chiller T (2012) Species identification and antifungal susceptibility testing of *Candida* bloodstream isolates from population-based surveillance studies in two US cities from 2008 to 2011. J Clin Microbiol 50:3435–3442
8. Sudbery P, Gow N, Berman J (2004) The distinct morphogenic states of *Candida albicans*. Trends Microbiol 12:317–324
9. Maganti H, Yamamura D, Xu J (2011) Prevalent nosocomial clusters among causative agents for candidemia in Hamilton, Canada. Med Mycol 49:530–538
10. Gow NA, Brown AJ, Odds FC (2002) Fungal morphogenesis and host invasion. Curr Opin Microbiol 5:366–371
11. Saville SP, Lazzell AL, Monteagudo C, Lopez-Ribot JL (2003) Engineered control of cell morphology in vivo reveals distinct roles for yeast and filamentous forms of *Candida albicans* during infection. Eukaryot Cell 2:1053–1060
12. Huang G (2012) Regulation of phenotypic transitions in the fungal pathogen *Candida albicans*. Virulence 3:251–261
13. Kumamoto CA, Vinces MD (2005) Contributions of hyphae and hypha-co-regulated genes to *Candida albicans* virulence. Cell Microbiol 7:1546–1554

14. Berman J (2006) Morphogenesis and cell cycle progression in *Candida albicans*. Curr Opin Microbiol 9:595–601
15. Sudbery PE (2011) Growth of *Candida albicans* hyphae. Nat Rev Microbiol 9:737–748
16. Odds FC (1987) *Candida* infections: an overview. Crit Rev Microbiol 15:1–5
17. Berman J, Sudbery PE (2002) *Candida albicans:* a molecular revolution built on lessons from budding yeast. Nat Rev Genet 3:918–930
18. White TC, Marr KA, Bowden RA (1998) Clinical, cellular, and molecular factors that contribute to antifungal drug resistance. Clin Microbiol Rev 11:382–402
19. Prasad R, Kapoor K (2005) Multidrug resistance in yeast *Candida*. Int Rev Cytol 242:215–248
20. Cannon RD, Lamping E, Holmes AR, Niimi K, Tanabe K, Niimi M, Monk BC (2007) *Candida albicans* drug resistance another way to cope with stress. Microbiology 153:3211–3217
21. Ramirez E, Garcia-Rodriguez J, Borobia AM, Ortega JM, Lei S, Barrios-Fernandez A, Sanchez M, Carcas AJ, Herrero A, de la Puente JM, Frias J (2012) Use of antifungal agents in pediatric and adult high-risk areas. Eur J Clin Microbiol Infect Dis 31:337–347
22. Kinsky SC (1970) Antibiotic interaction with model membranes. Annu Rev Pharmacol 10:119–142
23. Lanternier F, Lortholary O (2008) Liposomal amphotericin B: what is its role in 2008? Clin Microbiol Infect 14:71–83
24. Georgopapadakou NH, Walsh TJ (1994) Human mycoses: drugs and targets for emerging pathogens. Science 264:371–373
25. Hancock RE (2001) Cationic peptides: effectors in innate immunity and novel antimicrobials. Lancet Infect Dis 1:156–164
26. Boman HG (2003) Antibacterial peptides: basic facts and emerging concepts. J Intern Med 254:197–215
27. Beisswenger C, Bals R (2005) Functions of antimicrobial peptides in host defense and immunity. Curr Protein Pept Sci 6:255–264
28. Mangoni ML, Saugar JM, Dellisanti M, Barra D, Simmaco M, Rivas L (2005) Temporins, small antimicrobial peptides with leishmanicidal activity. J Biol Chem 280:984–990
29. Mookherjee N, Rehaume LM, Hancock RE (2007) Cathelicidins and functional analogues as antisepsis molecules. Expert Opin Ther Targets 11:993–1004
30. Mookherjee N, Hancock RE (2007) Cationic host defence peptides: innate immune regulatory peptides as a novel approach for treating infections. Cell Mol Life Sci 64:922–933
31. Yeung AT, Gellatly SL, Hancock RE (2011) Multifunctional cationic host defence peptides and their clinical applications. Cell Mol Life Sci 68:2161–2176
32. Shai Y (2002) Mode of action of membrane active antimicrobial peptides. Biopolymers 66:236–248
33. Mangoni ML (2011) Host-defense peptides: from biology to therapeutic strategies. Cell Mol Life Sci 68:2157–2159
34. Mangoni ML, Fiocco D, Mignogna G, Barra D, Simmaco M (2003) Functional characterisation of the 1–18 fragment of esculentin-1b, an antimicrobial peptide from *Rana esculenta*. Peptides 24:1771–1777
35. Simmaco M, Mignogna G, Barra D, Bossa F (1994) Antimicrobial peptides from skin secretions of *Rana esculenta.* Molecular cloning of cDNAs encoding esculentin and brevinins and isolation of new active peptides. J Biol Chem 269:11956–11961
36. Ponti D, Mignogna G, Mangoni ML, De Biase D, Simmaco M, Barra D (1999) Expression and activity of cyclic and linear analogues of esculentin-1, an anti-microbial peptide from amphibian skin. Eur J Biochem 263:921–927
37. Avrahami D, Shai Y (2004) A new group of antifungal and antibacterial lipopeptides derived from non-membrane active peptides conjugated to palmitic acid. J Biol Chem 279:12277–12285
38. Marcellini L, Borro M, Gentile G, Rinaldi AC, Stella L, Aimola P, Barra D, Mangoni ML (2009) Esculentin-1b(1–18)–a membrane-active antimicrobial peptide that synergizes with antibiotics and modifies the expression level of a limited number of proteins in *Escherichia coli*. FEBS J 276:5647–5664
39. Uccelletti D, Zanni E, Marcellini L, Palleschi C, Barra D, Mangoni ML (2010) Anti-Pseudomonas activity of frog skin antimicrobial peptides in a *Caenorhabditis elegans* infection model: a plausible mode of action in vitro and in vivo. Antimicrob Agents Chemother 54:3853–3860
40. Marsh EK, May RC (2012) *Caenorhabditis elegans,* a model organism for investigating immunity. Appl Environ Microbiol 78:2075–2081
41. Stiernagel T (2006) Maintenance of *C. elegans*, Wormbook, ed. The *C. elegans* Research Community, Wormbook. doi:10.895/wormbook.1.101.1. http://www.wormbook.org 11 Feb 2006
42. Grieco P, Carotenuto A, Auriemma L, Saviello MR, Campiglia P, Gomez-Monterrey IM, Marcellini L, Luca V, Barra D, Novellino E, Mangoni ML (2013) The effect of d-amino acid substitution on the selectivity of temporin L towards target cells: identification of a potent anti-*Candida* peptide. Biochim Biophys Acta 1828:652–660
43. Hawser S, Francolini M, Islam K (1996) The effects of antifungal agents on the morphogenetic transformation by *Candida albicans* in vitro. J Antimicrob Chemother 38:579–587
44. Cleary IA, Reinhard SM, Miller CL, Murdoch C, Thornhill MH, Lazzell AL, Monteagudo C, Thomas DP, Saville SP (2011) *Candida albicans* adhesin Als3p is dispensable for virulence in the mouse model of disseminated candidiasis. Microbiology 157:1806–1815
45. Valenti P, Visca P, Antonini G, Orsi N (1985) Antifungal activity of ovotransferrin towards genus *Candida*. Mycopathologia 89:169–175
46. Luca V, Stringaro A, Colone M, Pini A, Mangoni ML (2013) Esculentin(1–21), an amphibian skin membrane-active peptide with potent activity on both planktonic and biofilm cells of the bacterial pathogen *Pseudomonas aeruginosa*. Cell Mol Life Sci 70:2773–2786
47. Mangoni ML, Papo N, Barra D, Simmaco M, Bozzi A, Di Giulio A, Rinaldi AC (2004) Effects of the antimicrobial peptide temporin L on cell morphology, membrane permeability and viability of *Escherichia coli*. Biochem J 380:859–865
48. Breger J, Fuchs BB, Aperis G, Moy TI, Ausubel FM, Mylonakis E (2007) Antifungal chemical compounds identified using a *C. elegans* pathogenicity assay. PLoS Pathog 3:e18
49. Moy TI, Ball AR, Anklesaria Z, Casadei G, Lewis K, Ausubel FM (2006) Identification of novel antimicrobials using a live-animal infection model. Proc Natl Acad Sci USA 103:10414–10419
50. Chevalier M, Medioni E, Precheur I (2012) Inhibition of *Candida albicans* yeast-hyphal transition and biofilm formation by *Solidago virgaurea* water extracts. J Med Microbiol 61:1016–1022
51. Douglas LJ (2003) *Candida* biofilms and their role in infection. Trends Microbiol 11:30–36
52. Jabra-Rizk MA, Falkler WA, Meiller TF (2004) Fungal biofilms and drug resistance. Emerg Infect Dis 10:14–19
53. Canton E, Peman J, Gobernado M, Viudes A, Espinel-Ingroff A (2004) Patterns of amphotericin B killing kinetics against seven *Candida* species. Antimicrob Agents Chemother 48:2477–2482
54. Hong SY, Oh JE, Lee KH (1999) In vitro antifungal activity and cytotoxicity of a novel membrane-active peptide. Antimicrob Agents Chemother 43:1704–1707
55. Younsi M, Ramanandraibe E, Bonaly R, Donner M, Coulon J (2000) Amphotericin B resistance and membrane fluidity in *Kluyveromyces lactis* strains. Antimicrob Agents Chemother 44:1911–1916

56. Mayer FL, Wilson D, Hube B (2013) Candida albicans pathogenicity mechanisms. Virulence 4:119–128
57. Kuriyama T, Williams DW, Bagg J, Coulter WA, Ready D, Lewis MA (2005) In vitro susceptibility of oral *Candida* to seven antifungal agents. Oral Microbiol Immunol 20:349–353
58. Pfaller MA, Boyken L, Hollis RJ, Messer SA, Tendolkar S, Diekema DJ (2005) In vitro activities of anidulafungin against more than 2,500 clinical isolates of *Candida* spp., including 315 isolates resistant to fluconazole. J Clin Microbiol 43:5425–5427
59. Kontoyiannis DP, Lewis RE (2002) Antifungal drug resistance of pathogenic fungi. Lancet 359:1135–1144
60. Benincasa M, Scocchi M, Pacor S, Tossi A, Nobili D, Basaglia G, Busetti M, Gennaro R (2006) Fungicidal activity of five cathelicidin peptides against clinically isolated yeasts. J Antimicrob Chemother 58:950–959
61. Sung WS, Lee J, Lee DG (2008) Fungicidal effect and the mode of action of piscidin 2 derived from hybrid striped bass. Biochem Biophys Res Commun 371:551–555
62. den Hertog AL, van Marle J, van Veen HA, Van't Hof W, Bolscher JG, Veerman EC, Nieuw Amerongen AV (2005) Candidacidal effects of two antimicrobial peptides: histatin 5 causes small membrane defects, but LL-37 causes massive disruption of the cell membrane. Biochem J 388:689–695
63. Makovitzki A, Avrahami D, Shai Y (2006) Ultrashort antibacterial and antifungal lipopeptides. Proc Natl Acad Sci USA 103:15997–16002
64. Wang P, Nan YH, Shin SY (2010) Candidacidal mechanism of a Leu/Lys-rich alpha-helical amphipathic model antimicrobial peptide and its diastereomer composed of D, L-amino acids. J Pept Sci 16:601–606
65. Aerts AM, Francois IE, Meert EM, Li QT, Cammue BP, Thevissen K (2007) The antifungal activity of RsAFP2, a plant defensin from raphanus sativus, involves the induction of reactive oxygen species in *Candida albicans*. J Mol Microbiol Biotechnol 13:243–247
66. Thevissen K, de Mello Tavares P, Xu D, Blankenship J, Vandenbosch D, Idkowiak-Baldys J, Govaert G, Bink A, Rozental S, de Groot PW, Davis TR, Kumamoto CA, Vargas G, Nimrichter L, Coenye T, Mitchell A, Roemer T, Hannun YA, Cammue BP (2012) The plant defensin RsAFP2 induces cell wall stress, septin mislocalization and accumulation of ceramides in *Candida albicans*. Mol Microbiol 84:166–180
67. Choi H, Lee DG (2013) The influence of the N-terminal region of antimicrobial peptide pleurocidin on fungal apoptosis. J Microbiol Biotechnol [Epub ahead of print]
68. Maurya IK, Thota CK, Sharma J, Tupe SG, Chaudhary P, Singh MK, Thakur IS, Deshpande M, Prasad R, Chauhan VS (2013) Mechanism of action of novel synthetic dodecapeptides against *Candida albicans*. Biochim Biophys Acta 1830:5193–5203
69. Gow NA, van de Veerdonk FL, Brown AJ, Netea MG (2011) *Candida albicans* morphogenesis and host defence: discriminating invasion from colonization. Nat Rev Microbiol 10:112–122
70. Baillie GS, Douglas LJ (2000) Matrix polymers of *Candida* biofilms and their possible role in biofilm resistance to antifungal agents. J Antimicrob Chemother 46:397–403
71. Ghannoum MA, Janini G, Khamis L, Radwan SS (1986) Dimorphism-associated variations in the lipid composition of *Candida albicans*. J Gen Microbiol 132:2367–2375
72. Hitchcock CA, Barrett-Bee KJ, Russell NJ (1989) The lipid composition and permeability to the triazole antifungal antibiotic ICI 153066 of serum-grown mycelial cultures of *Candida albicans*. J Gen Microbiol 135:1949–1955
73. Thevissen K, Osborn RW, Acland DP, Broekaert WF (1997) Specific, high affinity binding sites for an antifungal plant defensin on *Neurospora crassa* hyphae and microsomal membranes. J Biol Chem 272:32176–32181
74. Thevissen K, Terras FR, Broekaert WF (1999) Permeabilization of fungal membranes by plant defensins inhibits fungal growth. Appl Environ Microbiol 65:5451–5458
75. Wong JH, Ng TB, Legowska A, Rolka K, Hui M, Cho CH (2011) Antifungal action of human cathelicidin fragment (LL13–37) on *Candida albicans*. Peptides 32:1996–2002
76. Ewbank JJ, Zugasti O (2011) *C. elegans:* model host and tool for antimicrobial drug discovery. Dis Model Mech 4:300–304
77. Pukkila-Worley R, Peleg AY, Tampakakis E, Mylonakis E (2009) *Candida albicans* hyphal formation and virulence assessed using a *Caenorhabditis elegans* infection model. Eukaryot Cell 8:1750–1758
78. Pukkila-Worley R, Ausubel FM, Mylonakis E (2011) *Candida albicans* infection of *Caenorhabditis elegans* induces antifungal immune defenses. PLoS Pathog 7:e1002074
79. Coleman JJ, Ghosh S, Okoli I, Mylonakis E (2011) Antifungal activity of microbial secondary metabolites. PLoS One 6:e25321